

12-2017

Multi-Hazard Resilience of Steel MRF Buildings

Rachel A. Chicchi
Purdue University

Follow this and additional works at: https://docs.lib.purdue.edu/open_access_dissertations

Recommended Citation

Chicchi, Rachel A., "Multi-Hazard Resilience of Steel MRF Buildings" (2017). *Open Access Dissertations*. 1536.
https://docs.lib.purdue.edu/open_access_dissertations/1536

This document has been made available through Purdue e-Pubs, a service of the Purdue University Libraries.
Please contact epubs@purdue.edu for additional information.

MULTI-HAZARD RESILIENCE OF STEEL MRF BUILDINGS

by

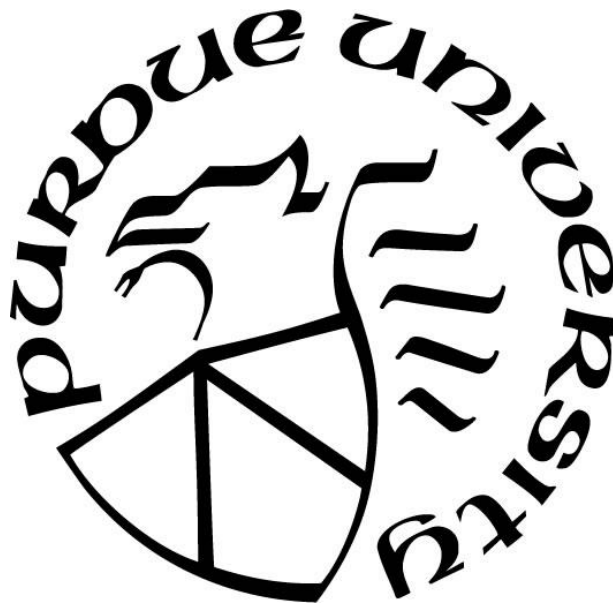
Rachel A. Chicchi

A Dissertation

Submitted to the Faculty of Purdue University

In Partial Fulfillment of the Requirements for the degree of

Doctor of Philosophy



Lyles School of Civil Engineering

West Lafayette, Indiana

December 2017

**THE PURDUE UNIVERSITY GRADUATE SCHOOL
STATEMENT OF COMMITTEE APPROVAL**

Dr. Amit H. Varma, Chair

Lyles School of Civil Engineering

Dr. Mark D. Bowman

Lyles School of Civil Engineering

Dr. Robert J. Connor

Lyles School of Civil Engineering

Dr. Erica C. Fischer

Civil and Construction Engineering, Oregon State University

Dr. Judy Liu

Civil and Construction Engineering, Oregon State University

Approved by:

Dr. Dulcy M. Abraham

Head of the Graduate Program

*Dedicated to my Pop Pop,
who truly appreciated the value of a good education
and was one of my biggest supporters.*

ACKNOWLEDGMENTS

This work would not have been possible without the help and support from a wonderful network of people. I must first thank my advisor, Dr. Varma, for his guidance and encouragement over these past four years. I am so grateful that you gave me the freedom to learn and struggle on my own, while also providing support when needed. I will be forever indebted to you for your mentorship and for the opportunities that you provided for me. Thank you also to my committee members: Drs Mark Bowman, Robert Connor, Judy Liu and Erica Fischer. I was lucky to learn from and work with each of you in different capacities. I admire you all and I am very grateful for your mentorship. Thank you especially to Dr. Liu for being one of my biggest advocates in my early years at Purdue. I will always look up to you for the way in which you prioritize and care for your students. And special thanks to Erica: thank you for passing along your experiences and lessons learned throughout graduate school. You have a proactive, go-getter attitude and you encouraged me to do the same.

I am also very grateful to Dr. Robert Jacko, who funded two years of my studies as his teaching assistant for the Senior Design course. You are a truly fascinating man and I feel very privileged that I was able to work with you. I will carry many of your stories and life lessons with me always. Thank you also to Yi (Cici) Li, an undergraduate research student, who helped to complete my analyses. I hope this work inspired you to pursue research. You have a bright future in structural engineering!

To all of the amazing friends I have made while at Purdue: pursuing a PhD is full of ups and downs, and I am so grateful to have had a wonderful support system of friends who recognized the challenges and victories that come along with pursuing this degree. It was humbling to get to know and work with so many talented people from all over the world. Special thanks to Amy Getchell, my dearest friend at Purdue. Thank you for always being there for me, and for being my ‘family’ away from home.

Love and thanks always to my family. My parents, Ann and Gary, raised three daughters to be strong, independent women. Thank you for supporting us with unconditional love, and for always believing in me far beyond the ability that I had to believe in myself. To my sisters, Sarah and Laura: you both know how much you mean to me. You have never quite understood what my job

entails, but you could always get a good laugh by pretending to! Thank you for your humor, your love, and your never-ending support.

This work was not funded. Thank you to the College of Engineering and Lyles School of Civil Engineering for providing fellowship funding, which allowed me the flexibility to pursue the work that I was most passionate about.

TABLE OF CONTENTS

LIST OF TABLES	xi
LIST OF FIGURES	xiii
ABSTRACT	xix
CHAPTER 1. INTRODUCTION	1
1.1 Building Resilience	1
1.2 Multi-hazard Approach	2
1.2.1 Probabilistic vs. Deterministic Approaches	3
1.2.2 Prescriptive vs. Performance-Based Approaches	3
1.2.3 Life Cycle Cost Analysis	3
1.2.4 Calculating Risk	4
1.3 Current Design Practices and Limitations	5
1.3.1 Fire Design	5
1.3.2 Seismic Design	6
1.3.3 Wind Design	7
1.4 Research Needs	8
1.5 Research Objectives	9
1.6 Thesis Overview	10
CHAPTER 2. STATE OF THE ART AND LITERATURE REVIEW	13
2.1 Seismic Analysis and Design	13
2.1.1 Determining Seismic Hazard	13
2.1.2 Incremental Dynamic Analyses	15
2.1.3 Literature Review	15
2.1.4 Gravity Frame Contributions to Lateral Stiffness of Building	16
2.2 Fire Analysis and Design	18
2.2.1 Determining Fire Loads	18
2.2.1.1 CFD Models	18
2.2.1.2 Time-temperature Curves	19
2.2.1.2.1 Implications of firefighting measures on fire load density	21
2.2.1.3 Comparison of Fire Load Methods	22

2.2.2	Incremental Fire Analyses	22
2.2.3	Heat Transfer Analyses.....	23
2.2.4	Literature Review	24
2.3	Post-Earthquake Fire Analyses and Design.....	26
2.3.1	Literature Review	27
2.3.2	Impact of Nonstructural Damage on Fire Resilience	29
CHAPTER 3. PROPOSED METHODOLOGY FOR ASSESSING POST-EARTHQUAKE FIRE RESILIENCE		35
3.1	Outline of PEF Methodology.....	35
3.2	Fire Damaged Building Assessment.....	38
3.2.1	Failure Modes and Limits for Fire Assessment.....	39
CHAPTER 4. BUILDING DESIGN AND HAZARD SELECTION.....		49
4.1	Structural Design of Ten Story Office Buildings	49
4.1.1	Gravity Load Design.....	49
4.1.2	Lateral Design for Chicago building	50
4.1.3	Lateral Design for Los Angeles building.....	51
4.1.4	Prescriptive Fire Design	51
4.2	Determination of Hazards for Performance-Based Analyses	52
4.2.1	Selection of Seismic Hazard.....	52
4.2.1.1	Chicago, IL Seismic Hazards	52
4.2.1.2	Los Angeles, CA Seismic Hazards.....	53
4.2.2	Selection of Fire Hazard	53
4.2.2.1	Location of Fire	53
4.2.2.2	Fire Time-Temperature Curves	54
4.2.3	Selection of Wind Hazard.....	55
4.2.3.1	Chicago, IL Wind Hazards	55
4.2.3.2	Los Angeles, CA Wind Hazards.....	56
CHAPTER 5. BUILDING MODELING AND ANALYSIS APPROACH		79
5.1	Modelled Elements	79
5.2	Modelled Connections	80
5.3	Material Models	81

5.4	Damping Considerations.....	82
5.5	Seismic Model vs. Fire Model.....	84
5.6	Application of Seismic Hazard.....	84
5.7	Application of Fire Hazard.....	85
5.8	Application of Wind Hazard.....	86
CHAPTER 6. CHICAGO BUILDING SIMULATION RESULTS.....		95
6.1	Seismic Response.....	95
6.2	Fifth Story Fires.....	97
6.2.1	Fire 1.....	97
6.2.1.1	Corner Compartment Fire.....	97
6.2.1.2	Edge Compartment Fire.....	98
6.2.1.3	Interior Compartment Fire.....	100
6.2.1.4	Full Story Fire.....	101
6.2.1.5	Gravity Column Capacity Check.....	101
6.2.2	Fire 2.....	103
6.2.2.1	Corner Compartment Fire.....	104
6.2.2.2	Edge Compartment Fire.....	104
6.2.2.3	Interior Compartment Fire.....	104
6.2.2.4	Full Story Fire.....	105
6.2.3	Fire 3.....	105
6.2.3.1	Corner Compartment Fire.....	105
6.2.3.2	Edge Compartment Fire.....	105
6.2.3.3	Interior Compartment Fire.....	106
6.2.3.4	Full Story Fire.....	106
6.3	Ninth Story Fires.....	106
6.3.1	Fire 1.....	107
6.3.1.1	Corner Compartment Fire.....	107
6.3.1.2	Edge Compartment Fire.....	108
6.3.1.3	Interior Compartment Fire.....	109
6.3.1.4	Gravity Column Capacity Check.....	109
6.3.2	Fire 2.....	110

6.3.2.1	Corner Compartment Fire.....	110
6.3.3	Fire 3.....	110
6.3.3.1	Corner Compartment Fire.....	111
6.3.3.2	Edge Compartment Fire.....	111
6.3.3.3	Interior Compartment Fire.....	112
6.4	Wind Response.....	112
6.4.1	Fire Following Wind Considerations.....	113
6.5	Summary and Conclusions.....	113
CHAPTER 7. LOS ANGELES BUILDING SIMULATION RESULTS.....		145
7.1	Seismic Response.....	145
7.2	Fifth Story Fires.....	147
7.3	Ninth Story Fires.....	148
7.3.1	Fire 1.....	149
7.3.1.1	Corner Compartment Fire.....	149
7.3.1.2	Edge Compartment Fire.....	150
7.3.2	Fire 3.....	150
7.3.2.1	Corner Compartment Fire.....	150
7.3.2.2	Edge Compartment Fire.....	151
7.4	First Story Fires.....	151
7.4.1	Fire 1.....	152
7.4.1.1	Corner Compartment Fire.....	152
7.4.1.2	Edge Compartment Fire.....	153
7.4.1.3	Interior Compartment Fire.....	153
7.4.1.4	Gravity Column Capacity Check.....	153
7.4.2	Fire 3.....	154
7.4.2.1	Corner Compartment Fire.....	154
7.4.2.2	Edge Compartment Fire.....	154
7.4.2.3	Interior Compartment Fire.....	154
7.4.3	Fires in Structures with Beam Fracture.....	155
7.5	Wind Response.....	157
7.6	Summary and Conclusions.....	158

CHAPTER 8. PILOT STUDY RESULTS.....	182
8.1 Gravity Columns with 2 hr FRR.....	182
8.1.1 Fifth Story Corner Compartment Fire	182
8.1.2 Ninth Story Corner Compartment Fire	184
8.1.3 Cost Comparison for Increased Fireproofing	185
8.2 Increased Gravity Column Sizes.....	186
8.2.1 Fifth Story Corner Compartment Fire	187
8.2.2 Ninth Story Corner Compartment Fire	187
8.2.3 Cost Comparison for Increased Gravity Column Sizes	188
8.3 Including Rebar Mat in Composite Slab.....	189
8.4 Incorporating Fireproofing Damage	190
8.4.1 Chicago Building.....	191
8.4.2 Los Angeles Building	194
8.5 Travelling Fires.....	197
8.6 Aftershocks	199
8.7 Fragility Curves	201
8.7.1 State of the Art.....	201
8.7.2 Application to Case Study Buildings.....	202
CHAPTER 9. SUMMARY AND CONCLUSIONS	223
9.1 Research Summary	223
9.2 Conclusions.....	226
9.3 Future Work.....	228
REFERENCES	231
VITA.....	242

LIST OF TABLES

Table 1.1 Qualitative assessment of hazard interactions for buildings [4]	12
Table 3.1 Failure mechanisms and acceptance criteria.....	47
Table 4.1 Design location and hazard scenarios in parametric study	57
Table 4.2 Seismic loads for case study buildings	60
Table 4.3 SFRM thicknesses per prescriptive approach.....	66
Table 4.4 Design locations and hazard scenarios in parametric study	69
Table 4.5 Eurocode fire parameters to generate time-temperature curves	74
Table 4.6 Eurocode fire parameters to generate time-temperature curves	76
Table 4.7 Mean wind speeds at each story for Chicago building	76
Table 4.8 Mean wind speeds at each story for Los Angeles building	77
Table 6.1 Results of IFA analyses for non-fractured Chicago building at the 5 th story	133
Table 6.2 Results of IFA analyses for non-fractured Chicago building at the 9 th story	143
Table 7.1 Beam fracture locations in Los Angeles building designated by story level.....	162
Table 7.2 Results of IFA analyses for non-fractured Los Angeles building at the 5 th story.....	164
Table 7.3 Results of IFA analyses for non-fractured Los Angeles building at the 9 th story.....	166
Table 7.4 Results of IFA analyses for non-fractured Los Angeles building at the 1 st story.....	168
Table 7.5 First story fire results for compartments with beam fracture: failure modes and times for Fire 1	179
Table 7.6 First story fire results for compartments with beam fracture: failure modes and times for Fire 3	180
Table 8.1 Cost comparison for structures with 1 hr FRR on all members versus 2 hr FRR on gravity columns and 1 hr FRR on all other members.....	209
Table 8.2 Original and revised gravity column sizes used in pilot study	209
Table 8.3 Failure type, time, and deflection for original versus revised gravity columns.....	209
Table 8.4 Utilization ratios for original gravity columns	210
Table 8.5 Utilization ratios for revised gravity columns	210
Table 8.6 Utilization ratios for Chicago moment frame columns	210
Table 8.7 Utilization ratios for Los Angeles moment frame columns.....	211

Table 8.8 Cost comparison of steel framing for entire building using original column sizes and revised column sizes	211
Table 8.9 Story drift ratios of upper levels of Chicago building with aftershocks	220

LIST OF FIGURES

Figure 2.1 Pushover analyses: base shear vs. roof drift response [23]	31
Figure 2.2 Base shear vs. drift angle: modeling comparison for 20-story building [24]	31
Figure 2.3 Design fires using ISO834, ASTM E119, and Eurocode	32
Figure 2.4 Effect of thermal enclosure factor on fire time-temperature curve	32
Figure 2.5 Effect of opening factor on fire time-temperature curve	33
Figure 2.6 Effect of fire load density factor on fire time-temperature curve	33
Figure 2.7 Result of a 2D heat transfer analysis of a wide flange beam with SFRM and a composite slab, showing temperature gradient (using ABAQUS software)	34
Figure 3.1 Overview of proposed methodology	41
Figure 3.2 Case study building: layout, member sizes, and design loads	42
Figure 3.3 Summary of ABAQUS modeling approach	43
Figure 3.4 Flow chart for conducting incremental dynamic analyses	44
Figure 3.5 Flow chart for conducting incremental fire analyses (Part 1)	45
Figure 3.6 Flow chart for conducting incremental fire analyses (Part 2)	46
Figure 4.1 First floor plan of Chicago building	58
Figure 4.2 Gravity frames in Chicago and Los Angeles building at gridlines 2 and 3	59
Figure 4.3 Moment frames in Chicago building at gridlines 1 and 4	61
Figure 4.4 Moment frames in Chicago building at gridlines A and F	62
Figure 4.5 First floor plan of Los Angeles building	63
Figure 4.6 Moment frames in Los Angeles building at gridlines 1 and 4	64
Figure 4.7 Moment frames in Los Angeles building at gridlines A and F	65
Figure 4.8 Seven ground motion acceleration time histories for Chicago building	67
Figure 4.9 Orientations of ground motions to determine orthogonal components	68
Figure 4.10 Chicago building design response spectrum with ground motions overlaid	68
Figure 4.11 Seven selected ground motion acceleration time histories used for Los Angeles building (Longitudinal building direction)	70
Figure 4.12 Seven selected ground motion acceleration time histories used for Los Angeles building (Transverse building direction)	71
Figure 4.13 Los Angeles building design response spectrum with ground motions overlaid	72

Figure 4.14 Compartment fire designations and locations	73
Figure 4.15 Parametric time-temperature curves selected for analyses.....	73
Figure 4.16 Final 3 parametric time-temperature curves used in analyses.....	74
Figure 4.17 Parametric time-temperature curves used in analyses with scaled Fire 1	75
Figure 4.18 Parametric time-temperature curves used in analyses with scaled Fire 2	75
Figure 4.19 Parametric time-temperature curves used in analyses with scaled Fire 3	76
Figure 4.20 Fluctuating wind speed time histories at each story for Chicago building.....	77
Figure 4.21 Fluctuating wind speed time histories at each story for Los Angeles building.....	78
Figure 5.1 Schematic of modeling approach for composite floor system [15].....	88
Figure 5.2 Schematic of gravity connection macro model for equivalent gravity connector [15]	88
Figure 5.3 Young's modulus vs. temperature relationship	89
Figure 5.4 Steel true yield stress vs. plastic strain relationship	89
Figure 5.5 Concrete true stress vs. inelastic strain relationship with temperature changes (°C) ..	90
Figure 5.6 Rayleigh damping based on structural frequency (Los Angeles).....	90
Figure 5.7 Interpolation of temperatures in ABAQUS for a wide-flange cross-section	91
Figure 5.8 Temperature gradation and integration points [15].....	91
Figure 5.9 Time-temperature response of W14x22 composite beam with 1 hr FRR exposed to Fire 1	92
Figure 5.10 Time-temperature response of W14x22 composite beam with 1 hr FRR exposed to Fire 2.....	93
Figure 5.11 Time-temperature response of W14x22 composite beam with 1 hr FRR exposed to Fire 3.....	94
Figure 6.1 Modal shapes and periods for Chicago building	116
Figure 6.2 Maximum story drift ratios (not incorporating fracture) for Chicago building.....	116
Figure 6.3 Plastic hinge locations observed in Chicago building (EQ4-3).....	117
Figure 6.4 Plastic hinge locations observed in Chicago building (EQ5-4).....	117
Figure 6.5 Results of IDA for Chicago building: PGA vs. maximum story drift ratio	118
Figure 6.6 Initiation of soft story collapse of Chicago building	119
Figure 6.7 Response of Chicago building exposed to 5 th story corner compartment Fire 1-1 ...	120
Figure 6.8 Axial loads of fifth story columns in Chicago building exposed to 5 th story corner compartment Fire 1-1.....	121

Figure 6.9 Graphical representation of interior gravity column load (red circle) redistributed to adjacent columns (blue circles) for corner compartment Fire 1-1 at 5 th story	122
Figure 6.10 Response of Chicago building exposed to 5 th story	122
Figure 6.11 Response of Chicago building exposed to 5 th story edge compartment Fire 1-1	123
Figure 6.12 Axial loads of fifth story columns in Chicago building exposed to 5 th story edge compartment Fire 1-1	124
Figure 6.13 Graphical representation of interior gravity column loads (red circles) redistributed to adjacent columns (blue circles) for edge compartment Fire 1-1 at 5 th story	125
Figure 6.14 Response of Chicago building exposed to 5 th story interior compartment Fire 1-1	126
Figure 6.15 Axial loads of fifth story columns in Chicago building exposed to 5 th story interior compartment Fire 1-1	127
Figure 6.16 Response of Chicago building exposed to 5 th story full story Fire 1-1.5	128
Figure 6.17 Fifth story W12x58 gravity column capacity versus temperature: comparison of ABAQUS results and calculated values	129
Figure 6.18 Response of Chicago building exposed to 5 th story corner compartment Fire 3-1 .	130
Figure 6.19 Response of Chicago building exposed to 5 th story edge compartment Fire 3-1	131
Figure 6.20 Response of Chicago building exposed to 5 th story interior compartment Fire 3-1	132
Figure 6.21 Response of Chicago building exposed to 9 th story corner compartment Fire 1-1 .	134
Figure 6.22 Response of Chicago building exposed to 9 th story corner compartment Fire 1-1.5	135
Figure 6.23 Response of Chicago building exposed to 9 th story edge compartment Fire 1-1	136
Figure 6.24 Response of Chicago building exposed to 9 th story edge compartment Fire 1-1.5 .	137
Figure 6.25 Response of Chicago building exposed to 9 th story interior compartment Fire 1-1	138
Figure 6.26 Ninth story W8x24 gravity column capacity versus temperature: comparison of ABAQUS results and calculated values	139
Figure 6.27 Response of Chicago building exposed to 9 th story corner compartment Fire 3-1 .	140
Figure 6.28 Response of Chicago building exposed to 9 th story edge compartment Fire 3-1	141

Figure 6.29 Response of Chicago building exposed to 9 th story interior compartment Fire 3-1	142
Figure 6.30 Lateral response of Chicago building subjected to wind time history	144
Figure 7.1 Modal shapes and periods for Los Angeles building	160
Figure 7.2 Maximum Story Drift Ratios for Los Angeles building.....	160
Figure 7.3 Fracture locations observed in Los Angeles building due to EQ1-1.25.....	161
Figure 7.4 Results of IDA for Los Angeles building: PGA vs. maximum story drift ratio.....	163
Figure 7.5 Results of IDA for Los Angeles building: S_a vs. maximum story drift ratio	163
Figure 7.6 Response of Los Angeles building exposed to 5 th story edge compartment Fire 1-1 after EQ7-0.75.....	165
Figure 7.7 Response of Los Angeles building exposed to 9 th story.....	167
Figure 7.8 Response of Los Angeles building exposed to 1 st story corner compartment Fire 1-1	169
Figure 7.9 Response of Los Angeles building exposed to 1 st story	170
Figure 7.10 First story W14x90 gravity column capacity versus temperature: comparison of ABAQUS results and calculated values	171
Figure 7.11 Axial load and temperature versus time for the failed interior gravity column in Los Angeles building exposed to 1 st story corner compartment Fire 3-1	172
Figure 7.12 Axial load and temperature versus time for the failed interior gravity column in Los Angeles building exposed to 1 st story corner compartment Fire 3-1.25	172
Figure 7.13 Progression of failure for 1 st story corner compartment fire with fractured moment frame beams in Los Angeles building (EQ2-1.25 and Fire 1-1A)	173
Figure 7.14 Progression of failure for 1 st story corner compartment fire with fractured moment frame beams in Los Angeles building (EQ7-1 and Fire 1-1A).....	174
Figure 7.15 Progression of failure for 1 st story corner compartment fire with fractured moment frame beams in Los Angeles building (EQ1-0.75 and Fire 3-1A)	175
Figure 7.16 Progression of failure for 1 st story edge compartment fire with fractured moment frame beams in Los Angeles building (EQ3-1.25 and Fire 3-1B2)	176
Figure 7.17 Progression of failure for 1 st story edge compartment fire with fractured moment frame beams in Los Angeles building (EQ4-1 and Fire 1-1B)	177
Figure 7.18 Plan view of vertical deformations (mm) in the Los Angeles building subjected to EQ1-1.25 and Fire 3-1B	178

Figure 7.19 Lateral response of Los Angeles building subjected to wind time history.....	181
Figure 8.1 Compartment failures observed with 2 hr FRR on gravity columns.....	206
Figure 8.2 Peak steel temperature and time determined from heat transfer for W12x58 column.....	207
Figure 8.3 Peak steel temperature and time determined from heat transfer for W8x24 column.....	208
Figure 8.4 Bay failure for interior compartment Fire 3-1 using #5 @ 12” rebar mat.....	211
Figure 8.5 Influence of fireproofing damage on column axial load and temperature over time (Fire 1-1 in compartment 5A after EQ4-3).....	212
Figure 8.6 Influence of fireproofing damage on column axial load and temperature over time (Fire 1-1 in compartment 9A after EQ4-3).....	213
Figure 8.7 Influence of fireproofing damage on column axial load and temperature over time (Fire 1-1 in compartment 9B after EQ4-3).....	214
Figure 8.8 Influence of fireproofing damage on column axial load and temperature over time (Fire 1-1 in compartment 5B after EQ4-3).....	215
Figure 8.9 Comparison of beam compressive load and midspan vertical deflection of W30x124 subjected to Fire 1-1 in compartment 1B2, with and without fireproofing damage (EQ 2-1).....	216
Figure 8.10 Comparison of beam compressive load and midspan vertical deflection of W27x94 subjected to Fire 1-1 in compartment 5B, with and without fireproofing damage (EQ1-1.25).....	216
Figure 8.11 Moving fire: Scenario D_M1	217
Figure 8.12 Moving fire: Scenario D_M2	217
Figure 8.13 Column axial load and temperature versus time relationship for Chicago building (EQ4-3) with Fire 1-1 as travelling fire D_M1 at 9 th story.....	218
Figure 8.14 Results of Fire 1-1 as travelling fire D_M1 at 5 th story of Los Angeles building (EQ7-0.75).....	219
Figure 8.15 Column axial load and temperature versus time relationship for Los Angeles building (EQ4-3) with Fire 1-1 as travelling fire D_M2 at first story	220
Figure 8.16 Deflected shape of Chicago building subjected to EQ3-3, Fire 6-0.75 at 9D and EQ3-3 aftershock.....	221

Figure 8.17 Seismic fragility curves for Chicago and Los Angeles buildings: Probability of exceeding specified story drift ratios (SDRs) vs. spectral accelerations.....	221
Figure 8.18 Fire fragility curve for Chicago and Los Angeles buildings: Probability of exceeding L/20 deflection vs. Ingberg's Fire Area	222
Figure 8.19 Fire fragility curve for Chicago and Los Angeles buildings: Probability of gravity column failure vs. gravity column internal temperature	222

ABSTRACT

Author: Chicchi, Rachel, A. PhD
Institution: Purdue University
Degree Received: December 2017
Title: Multi-Hazard Resilience of Steel MRF Buildings
Committee Chair: Amit H. Varma

Multi-hazard analyses can be used to create more sustainable and resilient structural designs by considering cascading hazards and the overall system performance of structures exposed to multiple hazard types. This dissertation develops a methodology to assess building resilience for seismic, wind, fire, and post-earthquake fire scenarios. Special emphasis is placed on understanding the interdependencies and relationships between earthquake and fire damage in the assessment of structures for post-earthquake fire.

The proposed methodology includes designing a building structure according to the latest building codes, developing a three-dimensional (3D) finite element method (FEM) computer model to represent building behavior, and conducting incremental dynamic and incremental fire analyses as a means to assess building performance to multiple cascading hazards. The approach is articulated by analyzing two 10-story steel structures. These structures were designed for hazard levels in Chicago, IL and Los Angeles, CA. The buildings have the same geometry and gravity framing, but vary in the design of the perimeter moment resisting frames (MRFs).

Detailed 3D FEM building models were developed in ABAQUS in order to more adequately simulate real-building behavior. The framing members are modeled using beam elements and the composite floor slabs are modeled as shell elements. This model provides building level response to earthquakes, wind, fires, and fires following earthquakes. It permits redistribution of loading through catenary action during column failure in a fire event and can simulate connection and member failures. In order to simulate seismic hazards, nonlinear time history ground displacement records were applied to the base of the building and Rayleigh damping was implemented. Because ABAQUS is not traditionally used to simulate seismic building behavior, the seismic response was validated using another computer program. Fire loads were modeled using parametric time-temperature curves from Eurocode to simulate compartment fires at the first, fifth and ninth stories of the buildings. Damage from the seismic structural model was imported into the fire structural

model in order to capture post-earthquake fire behavior. The level of modeling within each model varied as necessary in order to adequately capture building behavior for each hazard, while maintaining computational efficiency.

The findings of this study show that post-earthquake fire resilience for structures in high and low seismic areas are the same regardless of seismic damage, as long as moment frame connections have not fractured. For compartment fires where there is no seismic damage (no plastic hinging or fracture of members), the system responds the same as a fire-only scenario. Gravity columns are the most vulnerable components because of their high utilization ratio. Buckling of gravity columns can cause column, bay or system failures in the corner, edge and interior compartments, respectively. The perimeter moment frame system can help to prevent system collapse due to gravity column failure, but it cannot prevent the gravity column failure from occurring. In some cases, moment frame connection fractures may result in additional, subsequent failure modes (such as system collapse) that occur after gravity column failure initiates.

Pilot studies show that increasing gravity column sizes or its fireproofing can increase the multi-hazard resilience of the system. These modifications can prevent gravity column failure from occurring and, in turn, any subsequent failures that may occur in response. In addition, implementing a rebar mat within the composite slab can help to redistribute loads and prevent progressive collapse in interior compartments. Studies were also performed to examine the effect of fireproofing damage on the fire resilience of the structure.

CHAPTER 1. INTRODUCTION

The built environment is susceptible to both natural and manmade hazards. Some natural hazards include earthquakes, wind storms (hurricanes, typhoons), tsunamis, snow storms, wild-fires, and flooding. Manmade hazards can include fires, blasts, and impact, among others. Researchers and practitioners have traditionally analyzed building hazards independently; however, with the recent focus on resilience, a multi-hazard analysis approach has emerged. Improving system resilience against one hazard could in turn benefit or hinder system resilience when subjected to a different hazard type, so a holistic approach is taken to leverage resources to design the optimal structure to resist multiple different hazards. This multi-hazard approach requires understanding the interrelationship between the different hazards, the probabilities and consequences of each occurrence, and each hazard's effect on the structural response.

Cascading hazards are a type of multiple hazard scenario in which a hazard event occurs and then (a) secondary event(s) follow(s). These scenarios are particularly dangerous because the initial damage from the first event may be further exacerbated by subsequent events. Examples of cascading hazards include post-earthquake fires, earthquake and tsunami, and fire following blast. This project focuses on a methodology for evaluating steel structures with perimeter moment resisting frames subjected to multiple hazards (namely, wind, seismic, fire and post-earthquake fires) in order to assess building resilience.

1.1 Building Resilience

Resilience means quick recovery from disasters. From a structural context, this entails designing structural systems so that there is minimal structural damage and, thus, minimal disruption to the regular operations within the building. Consideration of nonstructural damage, such as fire and water damage to the building interior and its contents, is beyond the scope of this work. Only structural resilience will be considered.

The building industry has introduced a number of recent initiatives that recognize the importance of resilient communities and structures, and the possibility of multi-hazard events occurring. For instance, the U.S. Green Building Council (USGBC) recently approved three new credits for Leadership in Energy and Environmental Design (LEED) certification. This certification program

rates buildings based on how environmentally friendly they are. These new credits are awarded for resilient design in the case of extreme events, such as emergency preparedness and “passive survivability and functionality during emergencies” [1]. Another initiative with a similar goal is the U.S. Resiliency Council (USRC), which brings together professionals in industry and academia to develop building ratings for various manmade and natural hazards. This council recently launched the earthquake building rating, which rates the potential damage, safety and recovery of buildings [2]. These actions demonstrate that resilience after an extreme event is important not only for human safety but also sustainability. In an effort to prevent widespread damage from occurring, steps can be taken to mitigate at a community level and also at an individual building level [3]. Emergency preparedness, quick action from first responders, and back up water resources are just some of the actions to help to mitigate damage at a community level. At a building level, resilient structural and nonstructural system multi-hazard designs are necessary.

1.2 Multi-hazard Approach

Standard structural engineering practice consists of analyzing and designing buildings to resist hazards applied independently of one another. This approach is an envelope method where the structure is designed for each individual load combination and the controlling case is implemented. A multi-hazard approach, however, accounts for the realization that there is “inherent multi-hazard resiliency within the system” [4]. It recognizes that there are interrelationships between the analysis and performance of structures subjected to different hazards. Sometimes this interrelationship can be synergistic, while other times the relationship can be antagonistic. By assessing the interrelationships of multiple hazards, a more resilient, optimized built environment will result. Table 1.1 provides a qualitative comparison of certain hazard interactions, indicating the level of importance of each interaction [4]. As illustrated in the table, wind and seismic are highly interdependent, as well as seismic and fire, seismic and blast, and fire and blast.

Multi-hazard physical theory (MPT) is the concept that assumes inherent multi-hazard resiliency of structural systems. It recognizes that improving a component or system’s performance under one hazard could in turn improve its performance when subjected to a different hazard. An example of this synergistic interaction is wind and progressive collapse. If a system is designed for wind and progressive collapse separately, the building may be overdesigned. However, if the progressive collapse resistance system is integrated into the lateral force-resisting system,

performance of both hazards would be improved by increased strength and stiffness of members. Blast and seismic, however, have contradicting influence because they are affected in opposite ways by mass. As the mass of a building is increased, its seismic forces increase which would require stronger members; however, in a blast scenario increased mass is beneficial to dissipate the blast forces. In short, bolstering of a system to withstand potential blast threats could greatly decrease the seismic resilience of the system. This work will aim to further understand these interactions between wind, seismic and fire, and the implications of changes to specific components that could improve or compromise multi-hazard resilience.

There are other important differences in hazard performance that must be considered. For instance, seismic and blast hazards cause inelastic behavior, while structures subjected to wind are assumed to remain elastic. Additionally, the extent of the hazard applied to the system can vary greatly by hazard. For instance, blast would result in local hazards affecting fewer components, while wind and earthquakes would affect global response.

1.2.1 Probabilistic vs. Deterministic Approaches

Structure systems have traditionally been designed in a deterministic manner, which uses safety factors to compare demand and capacity of structural members. More recently, however, researchers have acknowledged that there are a number of uncertainties in design: loads, strength and modeling techniques. Thus, a more probabilistic approach has emerged. This includes risk analyses, fragility curves and life-cycle performance studies.

1.2.2 Prescriptive vs. Performance-Based Approaches

Structural engineering is also moving away from the prescriptive-based approach, which is a reliability based method that specifies a specific solution. With this prescriptive method, codes and standards dictate designs without regard to specific performance criteria. With a performance-based approach, structural engineers have more freedom to use alternative methods to assess if the building meets performance objectives. It allows the engineer to assess performance levels based on the owner, stakeholder, and code officials' expectations.

1.2.3 Life Cycle Cost Analysis

Another consideration is the variation in frequency and amplitude of the different hazards. Hazards have different mean recurrence intervals with distinct probabilities of exceedance. According to

ASCE 7-10 [5], for a design basis earthquake, there is a 10% probability of exceedance in 50 years with a mean recurrence interval (MRI) = 476 years. For a design wind event, the probability of exceedance is 7% in 50 years with a MRI= 700 years. Life cycle cost analysis is used to inform design decisions to determine the most monetarily efficient structure. It accounts for the frequency of each hazard. For the i th hazard, the life cycle cost, C_i , is:

$$C_i = \sum_{j=1}^{j=N} p_{ij} c_{ij} \quad \text{Equation 1-1}$$

In this equation, p_{ij} is the probability of occurrence of the i th hazard with j th intensity where the sum of the probabilities of the N hazard levels is equal to 1. c_{ij} is the cost of the i th hazard with j th intensity [4]. This approach allows for comparison of costs when considering hazards individually versus the multi-hazard approach.

1.2.4 Calculating Risk

Ultimately, the goal of multi-hazard design and assessment is to achieve predetermined performance levels at optimal cost, while minimizing risk. Risk is defined as the balance between degradation of a structure due to a hazard and the consequences of this damage [4]. The equation for risk is:

$$R_i = C * T * V \quad \text{Equation 1-2}$$

where R_i is the risk, C is the consequences, T is the threat (hazard), and V is the vulnerability. Each of these factors are determined by experts based on a 1-10 rating system. Vulnerability can be interpreted as the inverse of capacity. It is a measure of how susceptible the component or system is to degradation from a hazard. FEMA 452 [6] provides vulnerability rating guidelines, but it is very subjective.

Risk can be reduced by reducing threat (frequency or amplitude), vulnerability or consequence. Vulnerability and consequence can be reduced through resilient design. Threat is often dependent on the location of the structure and can be difficult to minimize. One example of reducing a threat such as blast is implementation of bollards and other security measures to minimize the potential for the threat to occur. Resilient design is a method of reducing risk and can be achieved through improved robustness, redundancy, resourcefulness, and recovery/rapidity [4]. In particular,

increased robustness and redundancy can be achieved through structural design; resourcefulness and recovery are responses to the hazard and are addressed at a global, community level. Community level measures can include emergency preparedness, quick action from first responders, and having adequate back up resources (such as water).

1.3 Current Design Practices and Limitations

This section will discuss the current design practices and limitations of fire, seismic and wind design currently used in the United States.

1.3.1 Fire Design

Structural engineers in the United States do not usually conduct fire analyses or design; instead, architects are typically responsible to specify the fire-resistance rating requirements and determine the fire protection necessary to achieve that rating. The International Building Code (IBC) [7] specifies fire-resistance ratings for structural components and assemblies based on the building use, size, and combustibility of building materials. This rating is the time (in hours) that an element or system can be exposed to a standard fire before failure would likely occur. Table 601 in IBC provides these hourly resistance ratings which vary for primary members, floor and floor secondary beams, roof and roof secondary beams, bearing walls, and nonbearing walls [7]. Primary members are defined as columns and members with direct connections to columns, as well as bracing members necessary for stability. There is no distinction between gravity and lateral frames. The strength and stiffness of steel is greatly reduced at elevated temperatures, which may require passive fire protection measures to increase the fire-resistance rating. Spray-applied fire-resistive materials (SFRM) are commonly applied to steel structures. Fire tests can be conducted using ASTM E119 to determine the required thickness of SFRM [8]. However, a more common, alternative approach, is to reference a database of tests that have been conducted on a limited variety of steel shapes and assemblies. Underwriters Laboratory's database is commonly used for this approach [9]. Each wide flange beam has a W/D value, where W is the weight per linear foot and D is the perimeter of the member exposed to the fire. The W/D for the tested beam is divided by the W/D for the beam being designed and the thickness of the fireproofing is scaled by that amount. The AISC Design Guide 19 also contains fire test results and example problems for determining fireproofing thicknesses [10].

1.3.2 Seismic Design

Moment-resisting frames (often referred to as moment frames or MRFs) are the focus of this study. These frames consist of beams and column members connected with rigid beam-to-column connections that are designed to resist the lateral loads on the structure. The lateral stiffness of the frame is provided through the fixed connections and bending rigidity of the framing members. This system is appealing to architects as it allows for a more open floor plan that is not inhibited by braces or walls. However, because the stiffness is dependent on bending rigidity, it tends to result in larger building drifts than braced frame or shear wall systems. Depending on the seismicity of the building location, moment frames are classified as ordinary, intermediate and special. Each type has specific detailing and design requirements outlined in AISC 341 [11].

The seismic-force-resisting system dissipates energy generated by the ground motion through inelastic behavior. Steel moment frames are designed to form plastic hinges at beam ends, acting as fuses to minimize additional damage to the remainder of the structure. Depending upon the post-yield capacity of the members, these fuses may need to be replaced after an earthquake. Locating the hinges in the beams and preventing hinging in the columns is called the strong column-weak beam philosophy, which is required for special moment frame systems in the seismic provisions of AISC [11]. This philosophy provides a more efficient way to dissipate energy but it also minimizes the potential of collapse due to a soft-story mechanism [12].

Reduced beam sections are sometimes employed to ensure the strong column-weak beam concept. Essentially, the flanges of the beam section near the ends are reduced to a dog-bone shape, which enables the fuse (hinge) to form in this location. Haunched connections and flange rib connections are other approaches to move the hinge away from the column and connection. Lately, there has been a push to further limit damage and increase resilience by using self-centering, rocking frames; with this design, post-tensioning strands are anchored at the beam-to-column connections to pull the frame back to plumb without causing inelastic damage [13].

The Northridge Earthquake of 1994 brought to light some potential issues with moment frame connections. Fractures were found at or near the beam flange groove welds, proving that moment frames were not as ductile as researchers and practitioners originally believed. Though these failures did not result in collapse, extensive retrofitting of the connections was required. There were a number of contributing factors to these failures which include low fracture toughness of the weld metal in the beam flange to column connection, poor quality of welding due to limited

access, and stress concentrations from the backing bar/weld tab [12]. Following Northridge, minimum toughness requirements for weld metal were improved and quality control was more closely monitored, among other improvements. The Kobe Earthquake, which occurred in Japan one year after Northridge, also resulted in severely damaged buildings due to brittle fractures of beam-to-column connections [12]. These earthquakes represented a milestone for the improvement of steel seismic resistant structures.

As the damage from Kobe and Northridge illustrated, the beam-to-column connections of the moment frames are critical to the performance of the structure. The panel zone, which is the area of the column web where the beam frames in, can experience very high shear forces and must be designed to prevent column web yielding or crippling and flange distortion. Recognizing the importance of connection design, AISC developed a list of prequalified moment connections that have been tested [14]. These include standard connections, such as welded unreinforced flange-welded web connections, but also some proprietary connections using untraditional methods, such as SidePlate, that have been extensively tested and certified. Newly proposed connection types must undergo rigorous testing.

Seismic drift may also control the lateral system design. ASCE 7 [5] specifies allowable story drift limits based on the type of the structure and its corresponding risk category. These limits, which are a function of the story height, are compared with the inelastic drifts observed in the building analyses. For analyses conducted using linear elastic methods, the computed deflections must be scaled by a deflection amplification factor and importance factor to represent inelastic deformations.

1.3.3 Wind Design

In addition to seismic design, the lateral system of the building must be evaluated for resistance to design wind loads. Moment frames are designed to remain elastic when subjected to a wind event. The lateral stiffness of moment frames is provided through the fixed connections and bending rigidity of the framing members and, thus, is typically more flexible than alternative systems such as shear walls or braces. Because of their inherent flexibility, moment frame designs to resist wind loads are typically controlled by lateral deflection limits, not strength requirements. ASCE 7 recommends drift limits of $L/600$ to $L/400$, where L is the building height. These limits are suggested in order to limit damage to cladding and nonstructural walls and partitions [5]. Because

the lateral system is designed to remain elastic, structural damage from wind loading is far less likely than seismic damage. Also, unlike seismic design, moment frames designed for wind do not require any special detailing for ductility.

Per ASCE 7 [5], wind loads are typically determined from either the main wind-force resisting system method, components and cladding method, or wind tunnel testing. Loading from the main wind-force resisting system is used to analyze the lateral force resisting system while components and cladding loading is calculated for elements of the building envelope that may experience higher pressures across a smaller area. Based on the building location, a basic wind speed is determined from weather station data, which corresponds to a 3-sec gust speed. The equivalent static wind pressure is then calculated through an equation involving wind speed, exposure, directionality, topographic factors, gust effects and other parameters. This statically loaded procedure is used for most regular structures.

Wind speeds for an Occupancy Category II building in ASCE 7 represent a 7% probability of exceedance in 50 years, which corresponds to a mean recurrence interval (MRI) of 700 years. According to the Commentary of Appendix C in ASCE 7, using the 700 year MRI to check serviceability is overly conservative. The commentary recommends using serviceability wind speed. Engineering judgement allows determination of 10, 25, 50 or 100-year MRI for wind drift serviceability. For this project, a 100-year MRI was used to evaluate serviceability.

When the structure is not regular or it is susceptible to torsional effects, vortex shedding, galloping or flutter, wind-tunnel test models must be used. Through wind tunnel testing or computational fluid dynamic (CFD) simulations, pressure time histories can be determined and applied to computational models using nonlinear time history analyses.

1.4 Research Needs

Research of steel buildings exposed to multiple hazards has traditionally been approached from an individual, or component, level. Furthermore, structural design is often conducted with two-dimensional (2D), simplified frames. Actual system level performance of steel moment frame buildings, including the effects of gravity connections and frames, and the composite slab, is not usually analyzed, as it requires sophisticated modeling. This dissertation explores a methodology

for assessing building resilience to multiple hazards while using more realistic, 3D building models.

A performance-based method for evaluating fire resilience of structures is called incremental fire analysis (IFA). It follows the same methodology used in incremental dynamic analysis, a well-established and documented procedure for seismic analyses. This work explores the most indicative intensity measures and engineering damage parameters necessary to conduct IFA and understand building behavior to fire hazards. IFA performed thus far has focused on individual components, such as beams and columns. Additional research is needed to study IFA at a building system level.

The results of this work can be used to identify vulnerabilities in steel structural components and assemblies for different hazards.

1.5 Research Objectives

The primary goals of this study are to: (1) identify vulnerabilities in steel moment frame buildings subjected to multiple hazards and (2) make recommendations for improvements to specific building components that could increase the overall system performance and resilience. This project will focus on system-level behavior.

The research objectives of this project are as follows:

- (1) Establish a methodology for analysis of a building exposed to multiple hazards.
- (2) Develop numerical models to simulate building behavior when subjected to seismic, wind, fire, and fire following earthquake hazards.
- (3) Develop fragility curves from the numerical models to identify building vulnerability.
- (4) Provide recommendations to improve multi-hazard resilience of steel moment frame buildings.

To obtain these objectives, this project consisted of the following tasks:

- **TASK I – Development of 3D Finite Element Method Building Models:** ABAQUS, a commercially available finite element method software, was used to develop 3D finite

element method (FEM) models of a ten-story steel-frame building. A detailed description of the model is provided by Agarwal [15]. Agarwal created the model to analyze the structure when subjected to compartment fires. Modifications and simplifications to the model were necessary to produce reasonable results when subjected to ground accelerations.

- **TASK II – Parametric Study:** The multi-hazard resilience of buildings in a high and low seismic region are compared to one another to determine the impact of seismicity on the multi-hazard resilience. Comparisons are made between the building behavior results of fire-only analyses and post-earthquake fires with the same parametric time-temperature curve. Failure mechanisms and rates of failure are compared. The purpose of this study is to realize the effect that earthquake ground motions can have on fire resistance. Finally, building components were chosen and modified strategically to determine the effect on the building behavior. For instance, the impact of changing gravity column sizes was studied.
- **TASK III – Development of Fragility Curves through IDA and IFA:** Incremental dynamic analyses (IDA) and incremental fire analyses (IFA) were conducted in order to develop fragility curves. This provides the probability that the damage measure occurs given a corresponding engineering demand parameter. This procedure can be an effective means for assessing building resilience; however, for this project, the fragility curves were not as useful as originally expected and, thus, did not encompass the vast scope of work that was originally intended. Still, this work provides the procedure and recommendations for implementation with other building structures. Refer to Section 8.7 for further explanation.
- **TASK IV – Recommendations for Multi-hazard Building Resilience:** Results of the parametric studies help to inform recommendations for multi-hazard building resilience. By determining the vulnerable elements for each of the hazards, improvements can be recommended.

1.6 Thesis Overview

Chapter 2 will include a literature review and current state of the art procedures for fire, seismic and post-earthquake fire analysis and design. In Chapter 3, the proposed methodology for assessment of post-earthquake fire building resilience is explained. The case study building and

its design, as well as the selection of each hazard scenario, is discussed in Chapter 4. Chapter 5 includes the modeling technique and analysis approach for the finite element method building model. Chapter 6 covers results of the incremental dynamic analyses and incremental fire analyses for the Chicago case study building. Chapter 7 presents the building analysis results for the Los Angeles building. Pilot studies, which cover a wide range of topics, are explained in Chapter 8. Chapter 9 contains conclusions and recommendations for future work.

Table 1.1 Qualitative assessment of hazard interactions for buildings [4]

Interaction levels: H=High, M=Medium, L=Low interaction

	Wind	Seismic	Fire	Blast	Flood
Wind	-	H	M	H	M
Seismic	-	-	H	H	M
Fire	-	-	-	H	M
Blast	-	-	-	-	L
Flood	-	-	-	-	-

CHAPTER 2. STATE OF THE ART AND LITERATURE REVIEW

This chapter presents the current state of the art of analysis and design in structural fire engineering and post-earthquake fire engineering. It includes a literature review of relevant research in the area of steel buildings exposed to seismic, fire and fire following earthquakes. This work focuses on building-level research and response, and only briefly touches on component-level studies.

2.1 Seismic Analysis and Design

As outlined in ASCE 41 [16], there are four primary procedures to analyze buildings subjected to seismic loads: Linear Static, Nonlinear Static, Linear Dynamic, and Nonlinear Dynamic. Static procedures do not consider dynamic effects so they should only be used with regular structures and when higher mode effects are considered insignificant. Linear Static Procedure (LSP) applies pseudo seismic forces to each story through the equivalent lateral force procedure developed in ASCE 7 [5]. Nonlinear response is then accounted for through the use of R and C_d factors, also provided in the code and varying based on the type of lateral system. Nonlinear Static Procedure (NSP) incorporates nonlinearity in the analysis itself. An example of this is static pushover, which involves incrementally applying a static force to the building and observing the lateral force versus displacement. Linear Dynamic Procedure (LDP) assumes elastic properties of the material and applies the loads dynamically, accounting for higher modes. An example of this is response spectrum analysis, which uses the equations of motion to develop mode shapes and spectral accelerations. Nonlinear Dynamic Procedure (NDP) incorporates both the nonlinearity of the material and the dynamic effects of the building response through a time history record. This procedure is more computationally expensive, but it can be used for all building types and most closely represents true building behavior. While many designers in industry may choose not to use NDP, it is the most accurate representation of the building behavior and will be used in this project to best inform building performance.

2.1.1 Determining Seismic Hazard

In order to perform advanced analyses using the nonlinear dynamic procedure, it is critical to understand the seismic hazard through adequate selection and scaling of ground motion records.

Chapter 16 of ASCE 7-10 [5] requires three or more appropriate ground motion records. When using three-dimensional analysis, each individual record should have orthogonal pairs of horizontal ground motion accelerations. These records must be selected from events with similar “magnitudes, fault distance, and source mechanisms” as the maximum considered earthquake (MCE) [5]. Online databases, such as PEER [17] and COSMOS [18], provide earthquake records based on station readings from actual events. Synthetic ground motions can also be created but are discouraged in favor of actual records.

Each component of the ground motion record can be converted into a 5% damped response spectrum. The orthogonal components must result in a square root of the sum of the squares (SRSS) with a mean value of the records that must be greater than the design response spectrum in the range of $0.2T$ to $1.5T$, where T is the period of the fundamental mode of the structure. If at least seven records are used, design forces and drifts can be averaged. With less than seven records, the worst case controls.

The Applied Technology Council (ATC) conducted studies of ground motion selection and scaling through the ATC-82 project [19]. The goal of the project was to provide improved and clearer guidance on ground motion selection and scaling, as there seems to be a lack of general consensus in the earthquake engineering community. They provide recommendations for updates to the ASCE 7 approach outlined above. The updated approach requires knowing the type of assessment to be conducted (intensity-based, scenario-based, etc.), the level of ground motion (MCE or design basis earthquake, DBE), and the seismic region (near-fault versus far-field), among others. ATC-82 recommends using a range of $0.2T$ to $3T$ for moment frames as opposed to the $1.5T$ upper bound indicated in ASCE 7. Far-field records can be oriented randomly to determine the orthogonal components. Near-fault records must be in the fault normal/fault parallel orientation. The council recommends scaling to meet 110% of the target spectrum in order to be conservative. NIST provides its own guidelines as well, through work with ATC [20]. It supports ground motion selection based on the conditional spectrum, which is a computational method for selecting a ground motion spectrum that has properties of a naturally occurring ground motion at the site. Other approaches are uniform hazard spectra and conditional mean spectra. FEMA P-58 [21] also provides ground motion scaling guidance.

2.1.2 Incremental Dynamic Analyses

The nonlinear dynamic procedure can be used to design and analyze structures for specific ground motion records; however, this does not give an adequate picture of the progression of behavior. Therefore, incremental dynamic analysis (IDA) is commonly used in conjunction with NDP to create a parametric analysis of building behavior to seismic loads. This method is similar to the nonlinear static pushover approach previously mentioned, which scales the force to develop a force-displacement curve. In the IDA approach, each ground motion record can be scaled using an intensity measure (IM) to generate response curves. According to Vamvatsikos et al. [22], some possible IM variables are Peak Ground Acceleration (PGA), Peak Ground Velocity (PGV), the $\zeta=5\%$ damped spectral acceleration, and the R-factor. Once the demand is determined through scaling of the IM, the capacity must be evaluated through a damage measure (DM). This is the output from the analysis which is used to determine the suitability of the structure. Examples of the DM can be maximum base shear, node rotations, peak roof drift, interstory drift ratios, etc. [22]. This procedure of incrementally scaling multiple ground motions aims to capture the variability in amplitude and frequency of the building response, providing smaller dispersion and, thus, increased confidence in the range of results. PGA is the selected IM for this project.

2.1.3 Literature Review

Chi et al. [23] explored different modeling techniques for steel moment frame buildings subjected to ground motions. Figure 2.1 shows pushover results of a 17-story building when comparing 2D frames (with and without second order effects) and three-dimensional (3D) buildings. 3D-B is a basic 3D model which includes all lateral frames and gravity columns which are connected rigidly through kinematic restraints. The 3D-F model is the full model which includes the gravity beams and shear connections. These shear connections have a flexural capacity of about 10% of the plastic moment capacity of the beam. As the figure shows, the 3D models produced more improved building response. It was found that the stiffness contribution due to the gravity frames could be attributed primarily to the gravity columns, which provided additional lateral strength to critical stories in the lower region of the building. When a time history analysis was performed, the maximum story drift ratio was about 0.025 for 2D, 0.023 for the 3D-B model and 0.016 for the 3D-F model. Refer to Section 2.1.4 for additional discussion about the gravity frame contribution to the lateral stiffness of the building.

Foutch and Yun [24] compared modeling techniques for steel moment frames subjected to seismic loads. The report considered elastic (linear centerline models) as well as nonlinear centerline models, with and without panel zones modeled. Panel zones were idealized as a scissors model using the approach developed by Krawinkler [25]. Figure 2.2 shows results of the different modeling techniques for a pushover analysis. M1 represents a centerline model that allows nonlinearity in the beams and columns. M2 represents the actual length of the beams and columns with panel zones.

Earthquake engineering has been transitioning from the traditional prescriptive approach to a performance-based approach of analysis and design that compares designated damage measures to the anticipated level of damage for a given hazard level as a method for evaluating seismic risk. These analyses require nonlinear models that are reliable and calibrated based on experimental data that properly captures the deterioration of strength and stiffness in the structural components. Work by Lignos and Krawinkler [26] explains the approach and calibration of such models. A number of agencies provide guidelines for the performance-based seismic design approach: Pacific Earthquake Engineering Research Center Tall Building Initiative [27], FEMA 445 [28], and the Los Angeles Tall Buildings Structural Design Council [29].

2.1.4 Gravity Frame Contributions to Lateral Stiffness of Building

Traditionally, the gravity system is neglected in lateral-force-resisting system design; however, studies have shown that gravity frames can offer additional stiffness and energy dissipation to the building system that is not negligible [24, 30]. Because gravity frames experience essentially the same drift as the lateral frames, gravity frames can be subjected to large interstory drifts that result in simple, pinned connections with large rotations. Also, gravity frames typically constitute a significant portion of a building, as moment frames are more costly and usually limited to the exterior. Tests of simple shear connections were conducted with and without the floor slabs [31]. Findings showed that large rotations of 0.14 radians could be achieved and that roughly 15-20% of the beam plastic moment capacity could be transferred in the connection. With the floor slab contribution, the maximum lateral load resistance increased by nearly two. The shear tab connections achieved rotations between 0.09 and 0.15 radians.

Flores et al. [30] studied 2, 4, and 8 story buildings with and without the gravity framing. The gravity connections were modeled as partially restrained assuming either 0, 35, 50 or 70% of the

plastic moment capacity of the beam. When subjected to DBE and MCE loading, residual deformations reduced as the percentage of gravity connection resistance increased. In fact, for the 8 story building, soft-story collapse of the building was prevented by including the gravity framing contribution. This influence was also reflected in the reduced interstory drift ratios.

In seismic analyses, even if the stiffness contributions of the gravity system are ignored, the engineer cannot ignore the inherent P-delta effects. This P-delta effect is often modeled with a leaning column rigidly attached to the lateral-force-resisting system that has gravity loading applied so as to simulate the destabilizing load of gravity frame imperfections [23, 24]. When the lateral contribution of gravity framing is not included in the design, the leaning column is assigned zero flexural stiffness. When its contribution is to be included, the equivalent lateral stiffness of the columns can be modeled through an equivalent bay that is rigidly attached to the lateral frame. Similarly, gravity beam stiffnesses are modeled as the equivalent stiffness of all of the gravity frame beams in that direction. Rotational springs can be used to model equivalent strength and stiffness of the gravity connections [30], using assumptions for elastic rotation based on connection tests by Liu and Astaneh-Asl [31]. A similar procedure is outlined by Foutch and Yun [24]. The equivalent gravity frame reduced maximum interstory drifts, though the contribution could sometimes be considered negligible. In the 20-story building, these effects were more pronounced due to the greater P-delta effects.

Gupta and Krawinkler [32] accounted for gravity contributions in their work by using an equivalent bay rigidly attached to the lateral load resisting frame. Each of the two equivalent gravity columns had a moment of inertia equal to half of the gravity columns at that level. The out of plane resistance of the orthogonal moment resisting frame columns was also considered. It was determined that the lateral stiffness contribution of the gravity frame was most influenced by the gravity columns and a smaller influence was had with the gravity connections.

Judd et al. [33] suggested implementation of the dual system design concept for integrating the response of lateral and gravity frames. This approach is similar to the dual systems already specified in ASCE 7-10 [5] but would require that 10% of the seismic forces would need to be resisted by the gravity framing system. Work funded through the National Science Foundation is currently ongoing to further explore the role of gravity framing on the seismic performance [34].

2.2 Fire Analysis and Design

The prescriptive approach of fire-resistance ratings per IBC [7], which is based on standard furnace tests of short span members, does not necessarily translate well into real building behavior. Following the World Trade Center collapse in 2001, this approach has been further scrutinized with many professionals calling for a change to performance-based fire resistance design and for the structural engineer to take over the responsibility of fire resistance design of the structure through conducting fire analyses [35]. This transition within the design industry has been slow to develop; nevertheless, within the realm of research, various fire analyses have been conducted. The following sections will highlight the typical procedure for conducting these state of the art analyses using the following models: fire, heat transfer, and structural.

2.2.1 Determining Fire Loads

In the performance-based approach, the fire hazard is considered a thermal load applied to the structure and is referred to as a design-basis fire [35]. Design-basis fires are typically classified as either localized or compartment fires. Localized fires do not cause flashover because of the low rate of released heat. Because this study focuses on global response, only compartment and full story fires, which are both large, post-flashover fires, will be considered.

Determination of fire loads can be approached in a number of different ways: computational fluid dynamic (CFD) or two-zone models can be developed, time-temperature curves from a standard can be used, or actual fire tests can be conducted.

2.2.1.1 *CFD Models*

CFD models involve modeling the growth and behavior of the fire by dividing the compartment into many different zones to reflect the different temperatures throughout the space. These models are highly complex and require a number of detailed assumptions of materials and properties within the compartment. The National Institute of Standards and Technology (NIST) provides software called FDS (Fire Dynamics Simulator) which can be used to conduct CFD analyses. Other programs exist that also specifically focus on CFD for fires.

2.2.1.2 Time-temperature Curves

Time-temperature curves commonly used for design fires are provided in ASTM E119 [8], ISO 834 [36], and Eurocode 1 [37], as shown in Figure 2.3. The ASTM and ISO curves are commonly used for fire furnace testing. These curves only have a heating phase and the formulation of the curves do not have any variables other than time. An approximation for the ASTM E119 curve is used to calculate fire temperature, T [38]:

$$T=750[1-e^{-3.79533\sqrt{t_h}}]+170.41\sqrt{t_h}+T_0 \quad \text{Equation 2-1}$$

where t_h is the time in hours and T_0 is the ambient temperature ($^{\circ}\text{C}$). For all calculations and models used in this work, the ambient temperature is assumed to be 20°C .

The ISO 834 curve, which is quite similar to the ASTM E119 curve, is given by the following equation where t is the time in minutes:

$$T=20+345\log(8t+1) \quad \text{Equation 2-2}$$

In contrast, Eurocode parametric curves include both a heating and cooling phase, and vary depending on the thermal inertia of the enclosure (b), opening factor (O), and fire load density ($q_{f,d}$). The equation for the heating phase is as follows:

$$\theta_g = 20+1325(1-0.324e^{-0.2t^*}-0.204e^{-1.7t^*}-0.472e^{-19t^*}) \quad \text{Equation 2-3}$$

where θ_g is the gas temperature in the fire compartment, and t^* is calculated as:

$$t^* = t \left(\frac{O}{b} \right)^2 / \left(\frac{0.04}{1160} \right)^2 \quad \text{Equation 2-4}$$

t is the time in hours. The units of O and b are $\text{m}^{1/2}$ and $\text{J}/\text{m}^2\text{s}^{1/2}\text{K}$, respectively. The cooling phase is calculated as:

$$\theta_g = \theta_{\max} - 250 (t^* - t_{\max}^* x) \quad \text{Equation 2-5}$$

when t_{\max}^* is greater than 2. t_{\max}^* is a function of the opening factor and the fire load density. x is usually 1, but varies depending on the fire growth rate, t_{lim} . θ_{\max} is the maximum fire temperature. Refer to Eurocode [37] for more detailed calculations of these parameters.

The cooling phase is important as it results in thermal contraction, which can produce large tensile forces. The Eurocode parametric time-temperature curves are used for room fires in the post-flashover phase with the following limitations: rectangular enclosures, floor area less than 500 m², ceiling heights less than 4 m and no ceiling openings. It is assumed that the room contains a fully developed fire with uniform temperature throughout the compartment, which is called a one zone approach.

The thermal properties of the walls, ceiling and floor are calculated using the following equation:

$$b = \sqrt{\rho c \lambda} \quad \text{Equation 2-6}$$

where ρ is the material density, c is the specific heat, and λ is the thermal conductivity. The opening factor is calculated based on the ratio of opening area to wall area:

$$O = A_v \sqrt{h_{eq} / A_t} \quad \text{Equation 2-7}$$

A_v is the total area of openings on the walls, h_{eq} is the weighted average of the window heights, and A_t is the total area of the enclosure, including walls, floor and ceiling. The fire load density, $q_{t,d}$, must be between 50 and 1,000 MJ/m² and it is determined by $q_{f,d}$ (the fire load density at the floor surface, A_f) relative to the total area of the enclosure, as shown in the equation below. The fire load density, $q_{f,d}$, varies based on building occupancy. Refer to Section 2.2.1.2.1 to see how $q_{f,d}$ is affected by various additional parameters.

$$q_{t,d} = q_{f,d} * A_f / A_t \quad \text{Equation 2-8}$$

A parametric study of the Eurocode time-temperature curve was conducted to show how varying the factors affects the design fire and, in particular, the peak temperature and heating durations. Results of this study are shown in Figure 2.4, Figure 2.5 and Figure 2.6. Varying the thermal inertia of the enclosure (b) affects both the peak temperature and the decay rate. Enclosures with a low thermal inertia result in rapidly increasing surface temperatures because they are not well insulated. Because materials with low thermal inertia store less heat, less heat is transfer back into the compartment as the fire decays, resulting in a rapid decay rate. The opposite is true of materials with high thermal inertia. As the fuel load density increases, the peak temperature and fire duration both increase. Changes to the opening factor affects the peak temperature, fire duration and decay rate, making it an especially useful parameter to emulate different fire scenarios. Fires that are well

ventilated (with a higher O factor) will burn at higher temperatures but for a shorter duration. Large openings produce rapid heat loss through convection and radiation, while smaller openings keep the heat trapped for a longer period of time, resulting in slower decay rates.

While Eurocode assumes a one zone approach, designers recognize that there are actually at least two zones: an upper, hot zone and a lower, cooler zone. Structural members in the lower zone (such as the floor slab below the fire) are not usually subjected to elevated temperatures, as the change in internal temperatures in those members are expected to be insignificant [39].

2.2.1.2.1 Implications of firefighting measures on fire load density

The fire load density factor used in the Eurocode time-temperature curves is dependent on many different factors. It is through this variable that fire-fighting measures and active fire suppression system can be incorporated into the development the fire time-temperature curve. Fire load density is generated by the following equation [37]:

$$q_{f,d} = q_{f,k} * m * \delta_{q1} * \delta_{q2} * \delta_n \quad \text{Equation 2-9}$$

$q_{f,k}$ is a value for fire load density that varies based on occupancy of the space. For a residence, $q_{f,k}$ is 780 MJ/m², while an office is 420 MJ/m². A library is 1500 MJ/m², which is a high value due to books which can be fuel for the fire. m is the combustion factor, which can be assumed as 0.8 for cellulosic materials. δ_{q1} is a factor that accounts for fire activation risk due to compartment size, while δ_{q2} accounts for fire activation risk due to occupancy type. The larger the compartment area, the higher the δ_{q1} factor (ranging from 1.1 – 2.13). The δ_{q2} factor varies from 0.78 (for low risk occupancies such as swimming pools) up to 1.66 (for high risk occupancies such as manufacturing factories of fireworks or paints). Offices are specified a δ_{q2} factor equal to 1.0.

Determination of active fire protection, such as sprinklers, detectors and smoke exhaust systems, must be considered as well. δ_n accounts for different active firefighting measures. Eurocode, for example, allows a reduction in the fire severity if sprinklers are installed. The equation is:

$$\delta_n = \prod_{i=1}^{10} \delta_{ni} \quad \text{Equation 2-10}$$

where δ_{ni} is defined in Table E.2 of Eurocode [37]. It states that $\delta_{ni} = 1$ can be used for “normal firefighting measures” where there are safe access routes and fire devices and systems working

properly. If these systems are presumed to not be in place (such as due to potential damage from an earthquake event), δ_{ni} should equal 1.5. In other words, the fire load density is highly dependent on firefighting assumptions.

2.2.1.3 Comparison of Fire Load Methods

Pope and Bailey conducted comparisons amongst CFD models, Eurocode, and fire tests and determined that Eurocode provides reasonable predictions for average compartment temperatures, though it over predicts the growth phase of the fire and should include a nonlinear decay rate [40]. Additionally, CFD analysis results can be too complex to apply to the heat transfer structural models. For these reasons and due to its simplicity, standard fire curves are commonly used in favor of CFD analyses [41].

2.2.2 Incremental Fire Analyses

The incremental dynamic analysis model used in earthquake engineering is being replicated to apply to fire scenarios. The three domains of the model: intensity measure, engineering demand parameters and estimating damage [22, 42] are applied to fire engineering. This concept is articulated by Moss et al. [43]. They named the approach Incremental Fire Analysis and performed preliminary studies to validate the process. Unlike IDA which commonly uses PGA or S_a as the intensity measure, there does not seem to be a consensus among researchers on the most indicative intensity measure to use for fire.

Moss et al. studied a two-span concrete beam using both peak room temperature and the total radiant heat energy (RHE) as the intensity measures. The total radiant heat energy is the calculated area under the radiant heat flux versus time curve. In this study, sixteen fires were chosen by using four different ventilation factors and four different fuel load densities. These were then scaled by the intensity measures to constants of peak temperatures = 800°C and radiant heat energy = 30 MJ/m². The maximum displacement in the beam was recorded as the engineering damage parameter. Through calculating the dispersion of the IFA curves, it was clear that RHE had less dispersion of values, meaning that it is a more efficient IM than the peak temperature. RHE is not a simple value to calculate, however, as it involves radiant heat transferring back and forth between the enclosure and the members inside. There does not seem to be a simplified method for calculating the total RHE, similar to the calculation of the room temperature in the parametric

time-temperature curve. Instead, using a computer model to represent the computational fluid dynamics of the enclosure is necessary.

Devaney [44] considered different intensity measures for a performance-based fire study. He considered Ingberg's equal area concept from 1928 [45], which is a rough method for measuring fire severity. It calculated the area under a temperature-time curve, which constitutes no numerical significance in terms of units. It also does not consider heat transfer or the difference between a fast hot fire and a slow cool one. Other suggested intensity measures included maximum steel temperature (but this does not account for varying fire protection levels), rate of temperature increase (but this does not consider fire peak or duration), and peak compartment gas temperature, which was the chosen IM. Devaney used Monte Carlo simulation to determine the range of realistic results. The engineering demand parameter for the beam was midspan deflection. In another study, Lange [42] also used peak compartment temperature as the IM.

A concrete column study was conducted which used the maximum temperature within the column cross-section as the intensity measure. However, this is not plausible for the building being modeled because of the variation of fire protection for the different components. Twenty-seven fire scenarios were studied by varying the compartment size, fuel load and ventilation. A clear correlation between opening factor and the residual strength index of the column was found, as the column capacity was affected by both the peak temperature and the duration of the fire [46].

In another study, fire load in a compartment (MJ/m^2) was used as the IM [47]. At least one compartment was studied per story. The damage states used were flexural resistance of beams (local failure) and maximum resistance of columns (could lead to collapse).

2.2.3 Heat Transfer Analyses

Once the fire time-temperature curve has been selected, finite element method (FEM) models can be used to conduct heat transfer analyses to determine the temperature of each structural component throughout its cross-section. Two-dimensional (2D) heat transfer analyses are commonly used because the time-temperature curves assume that the room contains a fully-developed fire with uniform temperature throughout the compartment; thus, there is no need to use more computationally expensive 3D modeling. When using a CFD fire hazard, this assumption no longer applies and 3D FEM models are necessary to conduct heat transfer analyses.

In FEM heat transfer models, the structural member and its corresponding fireproofing is modeled and exposed to the predetermined fire hazard. Thermal expansion, specific heat, thermal conductivity, and density are defined for each of material to model the thermal transfer of heat from the gas to the structural component. These models perform conduction, convection and radiation calculations to determine the internal temperatures of the structural member along its cross-section, as shown in Figure 2.7. These internal temperatures are determined at specific nodes, which are then applied to the structural building model.

More simplified analytical methods, such as the “lumped mass method” can also be employed, which assumes that the entire member cross-section has the same temperature. This can be a valid assumption for steel member thicknesses less than 100 mm (4 in) and when exposed to a sudden rise in temperature [41]. The AISC Specification for Structural Steel Buildings [48] allows designers to use this assumption.

2.2.4 Literature Review

Many researchers have focused on studying individual structural components to observe behavior when subjected to a fire. In particular, beam-to-column connections have been studied at length [49-59]. Beams, columns and floors have also been studied in isolation [60-70]. The test procedures for individual structural elements are outlined in standards such as ISO 834 [36], ASTM E119 [8] and Eurocode [71]. While the above-mentioned research informs modeling decisions, this paper will focus on studies of system-level behavior.

Very few full-scale fire tests have been conducted due to the high expense. One of most familiar series of experiments is the Cardington fire tests, which consisted of six full-scale fire tests on an 8-story structure in Bedfordshire, UK [72]. The observations of these large-scale tests helped to inform and benchmark computational modeling of fires. Beams experienced significant deflection (600+ mm, or 24 in), which led to catenary action but no instability or collapse. The bottom flange of beams were often distorted due to thermal expansion and deflection when pushed against the column. Fracture in the end-plate beam-to-column connection occurred during cooling, due to thermal contraction causing high tensile forces in the connection. The top of columns, near connections where fireproofing was not present, resulted in localized buckling failure.

Agarwal and Varma [70] studied the system-level performance of a steel moment frame building using 3D FEM models. They found that, if all structural components were designed for the same

level of fire safety, gravity columns would likely fail first. Upon failure of the columns, catenary and flexural action redistribute load to the adjacent columns. Fang et al. [73] found that, depending on the loading, it is even possible for loads to be redistributed to upper, ambient temperature floors. Fischer [74] expanded upon Agarwal's work by studying full-story fires and varying the fire resistance ratings on the structural members. Again, gravity columns were the first component to fail. When these members were protected with excess fire protection, significant deflections occurred in the beams and slab but failure did not occur. She also considered moving fires but found that full-story fires were an appropriate conservative approach in place of moving fires.

Memari and Mahmoud [75] explored moment frames with reduced beam section connections for 3, 9 and 20-story frames using 2D modeling. Gravity frames were idealized as a leaning column. They found that the global stability of the structure was not compromised by only a one compartment fire. At a local level, beams experienced residual axial tensile forces and deflections. Jiang et al. [76] conducted 2D frame analyses to observe various collapse mechanisms: heated bay collapse, column buckling, local lateral drift of heated floor, and global lateral collapse. This study also compared the influence of beam sizes on the structural response. Additionally, the magnitude of gravity loading was varied. They determined that local lateral drift occurred at low loading levels; with increased loading, column buckling occurred. As the beam sections increase, this affects the location of the plastic hinge, causing column failure mechanisms instead of beam mechanisms. Additionally, edge bays were more susceptible to progressive collapse because these bays were not able to develop adequate catenary action. Similar analyses and findings were determined by Sun et al. [77].

Some studies have shown that thermal expansion (bowing) usually controls the behavior over that of material degradation due to the elevated temperatures. Flint et al. [78] and Usmani et al. [79] studied the World Trade Center collapse using 2D FEM models. They found that, as the floor deflected due to thermal expansion, tensile membrane action occurred. The exterior columns were pulled inward, forming plastic hinges in these columns at the floor levels. Similar responses were found when using 3D models. However, redistribution of loads throughout the structure was observed with the 3D models, making it a more robust model and slower to fail than the 2D models [80]. It is important to note that the truss system of the World Trade Center is different than that of traditional floor framing with conventional hot rolled steel shapes.

Quiel and Garlock [81] studied 2D versus 3D modeling for structures exposed to fires and concluded that the moment frame members were relatively unaffected by the modeling approach; however, the deflection of the filler beams in the 3D model was noticeably less due to the stiffness of the continuous slab.

In another study, vertically traveling fires were simulated to account for the time that it takes for actual fires to move between floors (between 6 and 30 minutes based on observations of actual buildings) [82]. This is different than the approach of modeling multiple floor fires at once, because it accounts for the heating and cooling response of the floors relative to each other. The rate of the moving fires greatly affected the global response of the structure.

2.3 Post-Earthquake Fire Analyses and Design

The 1906 San Francisco earthquake and the 1923 Tokyo earthquake are classic examples that brought to light the potential damage of fire following earthquakes. The San Francisco earthquake resulted in 80% of the total damage occurring due to post-earthquake fires [83]. The Tokyo earthquake resulted in 77% of the total losses due to the fire, causing 140,000 lives lost and 447,000 homes destroyed [3]. This has continued to be a problem in more recent years, as the Kobe earthquake in 1995 resulted in 108 fires. Because of its dense urban setting and due to thousands of breaks in the underground water distribution system caused by the earthquake, fires spread following the Kobe earthquake [84].

Scawthorn et al. [85] and Botting [86] summarized the historical cases of fires following earthquakes and the community level impacts to utilities, communications, roadways, and buildings. Most conflagrations are in low or mid-rise timber buildings. Although the threat to high-rise steel buildings is unlikely, the risk would be very great, as adequate time would be needed to allow for safe evacuation of inhabitants [87].

Earthquakes can cause structural damage and residual drifts, potentially preventing people from safely exiting the building during a fire. In addition, nonstructural components, such as sprinklers and pipelines, may be damaged, which could increase the duration and intensity of the fire. Additionally, first responders may be slow to react to fires because they are already preoccupied responding to earthquake-related issues. Ground motion from earthquakes has been known to

ignite fires through short circuiting, abrasions, chemical reactions, among other causes [85]. These issues together inflame the potential for damage due to post-earthquake fires (PEF).

2.3.1 Literature Review

Della Corte et al. [88] classified earthquake damage as ‘geometrical’ and ‘mechanical’. Geometrical damage is defined as residual deformations caused by plasticity in the structure. Mechanical damage is “degradation of mechanical properties” due to plastic deformation. A simple single-bay, single-story portal frame was studied to show that the buckling critical load of the column frames was significantly lower than the Euler buckling load when considering the effects of seismic damage. Multi-bay, multi-story 2D frames were then analyzed. The study found a 10% reduction in fire resistance for a design level seismic event but for very rare earthquakes, the contribution of earthquake damage to fire resistance was much more significant.

Pantousa and Mistakidis [89] conducted analyses of post-earthquake fires by considering the non-structural damage caused by the earthquake, namely the functionality of the sprinkler system and the breakage of windows. As the seismic loads increase, so did the assumed nonstructural damage. Computational fluid dynamics was used to study scenarios where broken windows affect the ventilation. The structural system was found to fail at the heated beams where restrained thermal expansion and catenary action occurred. They found a 14% reduction in fire-resistance time for the design earthquake when nonstructural damage was assumed.

Behnam and Ronagh [90] analyzed a 10-story moment frame building using 2D frame analyses and accounted for earthquake effects through stiffness degradation and residual deformations. Three different fire scenarios were used: fire at the first, fourth and seventh floors respectively, with both 5 minute and 25 minute delays before spreading the fires between floors. The application of the fire (time delay and story level) changed both the fire resistance time and failure shape of the building. In some cases, one level was in the cooling phase while the upper level was heating. For fast moving vertical fires, collapse occurred during heating but for slower spreading fires, collapse occurred during the cooling phase. Sway mechanisms were observed for fast moving fires but beam mechanisms were observed for slower moving fires.

Khorasani et al. [91] compared a fire-only and post-earthquake fire scenario using OpenSees, an open source analysis software from UC Berkeley. They found that the earthquake decreases the time to form a plastic hinge due to fire at the beam to perimeter column interface. Column drifts

of 1.7% were achieved in fire following earthquake, due to thermal expansion and the residual drift of the earthquake.

Memari et al. [92] studied moment resisting frames with reduced beam section connections in low, medium and high-rise structures, using 2D frame analyses. The leaning column approach was used to represent P-delta effects and stiffness of the gravity columns. Panel zones in the beam-to-column connections are modeled using the scissor model, with rigid links and a rotational spring to capture the moment-rotation of the connection. Life safety performance was determined in 80% of the analyses, while collapse prevention consisted of the remaining 20%. These performance criteria levels are explained in more detail in Section 3.2. Post-earthquake fires tended to produce lower interstory drift ratios than the earthquake scenarios and system-level collapse was not imminent. Large tensile forces were developed in the beams during the cooling phase, while axial compressive force-bending (caused during heating because of thermal expansion and restraint) tended to control the beam design.

Zaharia and Pintea [93] used pushover frame analysis and both ISO 834 and natural fire curves to compare three different frames. The frames that were designed for higher seismicity levels appeared to have reserve fire resistance. Also, the fire resistance time of the structure was affected by its level of damage, with undamaged structures resisting fire loads for longer prior to collapse; however, in some cases, this difference is very minimal (roughly one minute). Two primary methods of collapse were observed: a global (structural) sway mechanism and a beam mechanism. Typically, the same mode of collapse was observed in the frames, whether or not the structure was damaged in the earthquake.

Behnam and Ronagh [94] proposed a post-earthquake factor to be applied to the equivalent static equation for calculating base shear due to seismic loads. In this, $V_{PEF} = C_{PEF(t)} C_s * W$. This $C_{PEF(t)}$ value would be evaluated iteratively through redesign of the frame until it achieves a satisfactory performance level when subjected to the post-earthquake fire.

Quiel and Marjanishvili [95] studied the effect of damage on the fire resistance of steel buildings, focusing on fire following blast or impact scenarios. They found that the structure was very susceptible to global instabilities and that further studies would be needed to compare the effects of fire intensity and fireproofing with the acceptance criteria and collapse time. A performance-based design approach was suggested.

2.3.2 Impact of Nonstructural Damage on Fire Resilience

Nonstructural damage can occur as a result of large drifts and accelerations due to wind and seismic loads. This damage can greatly limit the functionality of the building following a hazardous event. While nonstructural damage will not be explored in depth in this study, some potential implications of this damage on subsequent fire hazards will be considered.

For instance, when steel yields during an earthquake, the adherence of the spray-applied fire-resistive material (SFRM) can be affected. This was studied by Braxtan and Pessiki [96] who acknowledged that large deformations of 20 times the yield strain of steel in beams near the steel moment frame connections is possible and that this could affect the bond performance of the SFRM. Steel plates were tension yielded and adhesive and cohesive strengths of the SFRM were tested. Keller and Pessiki found that debonding, cracking and spalling were all possible failure mechanisms of SFRM in cyclicly loaded beam-to-column moment connections [97]. At an interstory drift ratio of 3%, debonding and cracking of the insulation occurred. Detachment was more frequent for dry-mix (DM) than wet-mix (WM) fireproofing while cracking was more likely in WM than DM. Using computer modeling, they found a 20-30% reduction in flexural capacity of these connections when the fireproofing was spalled and the steel was exposed to elevated temperatures.

Sprinkler systems may also be damaged in an earthquake event, which would increase the duration of a subsequent fire. Fragility curves were developed based on physical tests conducted at the University of Buffalo. These curves shows the likelihood of leaking for different components of the sprinkler system when subjected to peak floor accelerations [98]. Interstory drift can also affect piping performance. In another study [99], hospital piping was tested for seismic loading and it was found that restrained welded assemblies could withstand interstory drift ratios of 4.34% without any damage or leaking; however, threaded assemblies could only withstand drifts of 2.2% before leaking occurred. Unrestrained piping fared worse with only 1.08% drift causing leakage. Cladding failures could also occur. It is possible that large suction forces could occur on the cladding during a wind event, causing it to detach from the building. Another possibility is that excessive drifts could lead to breakage of windows. Both of these scenarios would in turn affect the opening factor of exterior compartment fires. However, studies have shown that if the cladding

and its connections are properly detailed, façade damage is unlikely, even with drifts up to 0.04 radians [100, 101].

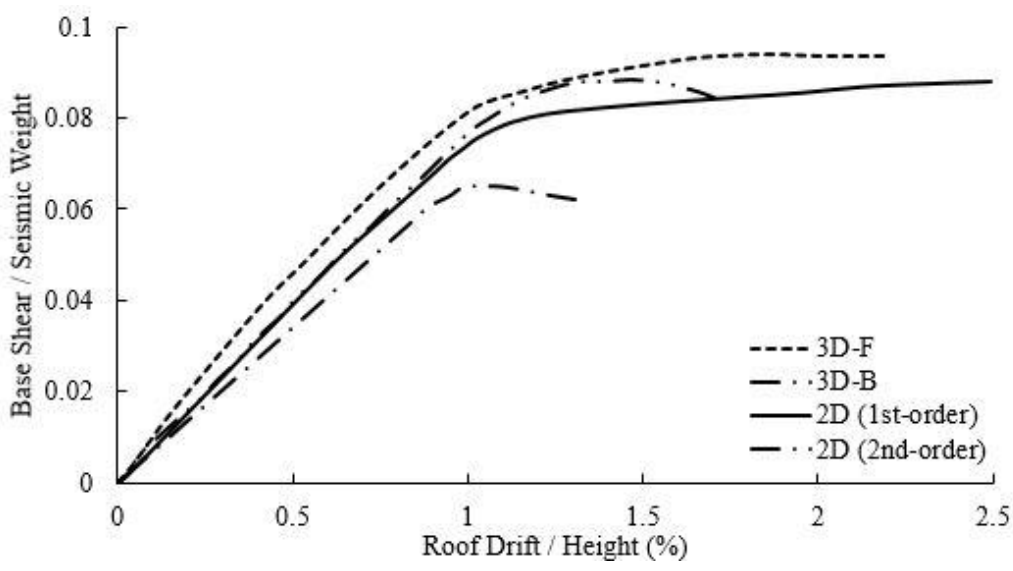


Figure 2.1 Pushover analyses: base shear vs. roof drift response [23]

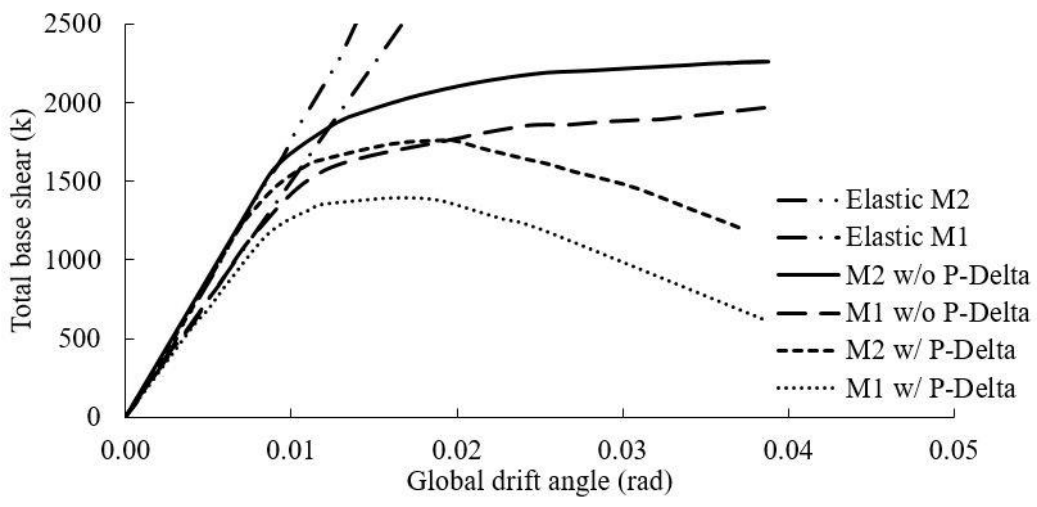


Figure 2.2 Base shear vs. drift angle: modeling comparison for 20-story building [24]

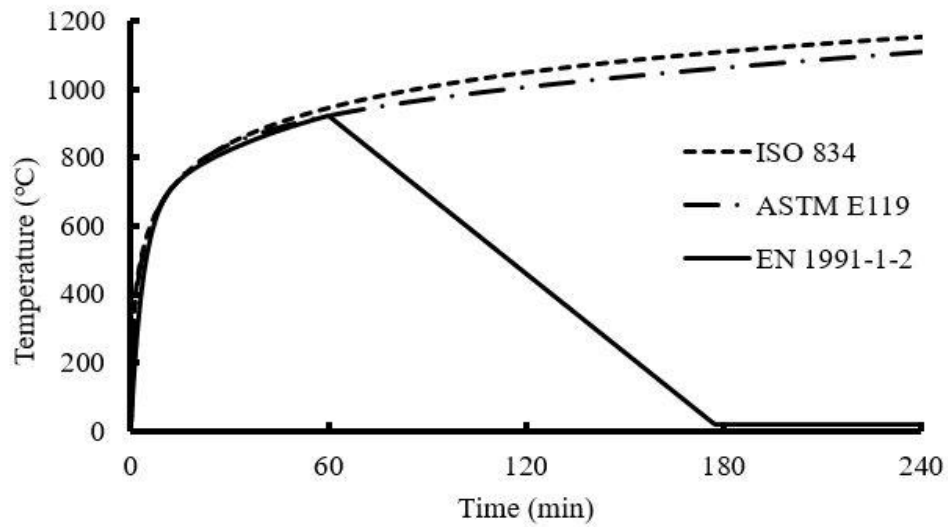


Figure 2.3 Design fires using ISO834, ASTM E119, and Eurocode

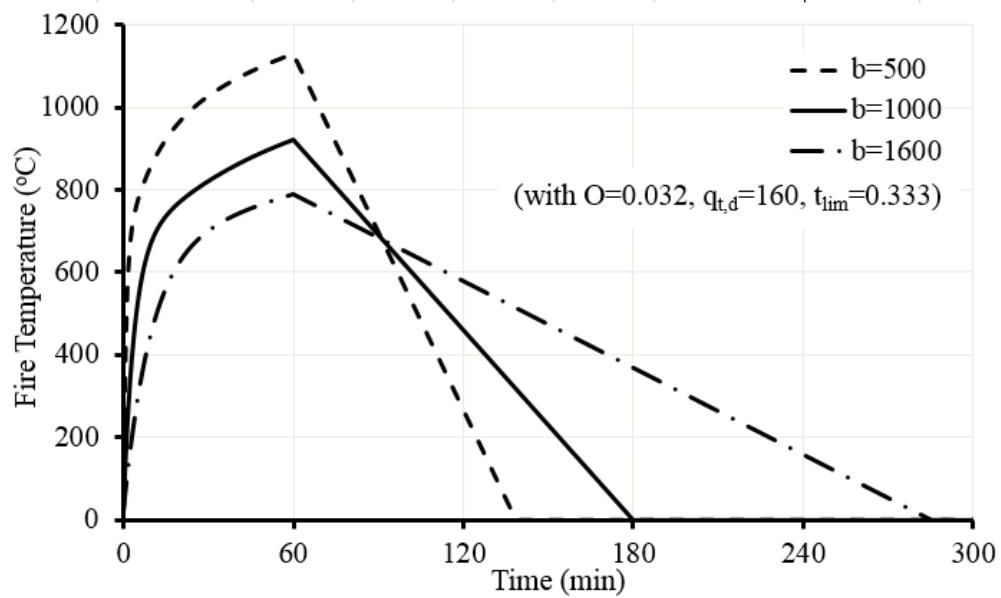


Figure 2.4 Effect of thermal enclosure factor on fire time-temperature curve

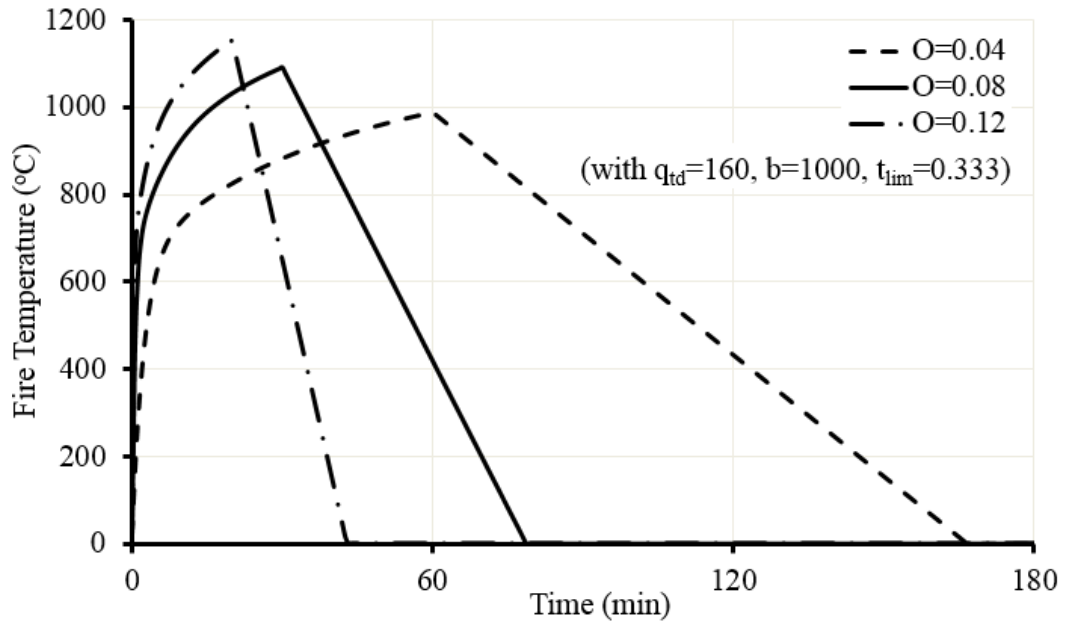


Figure 2.5 Effect of opening factor on fire time-temperature curve

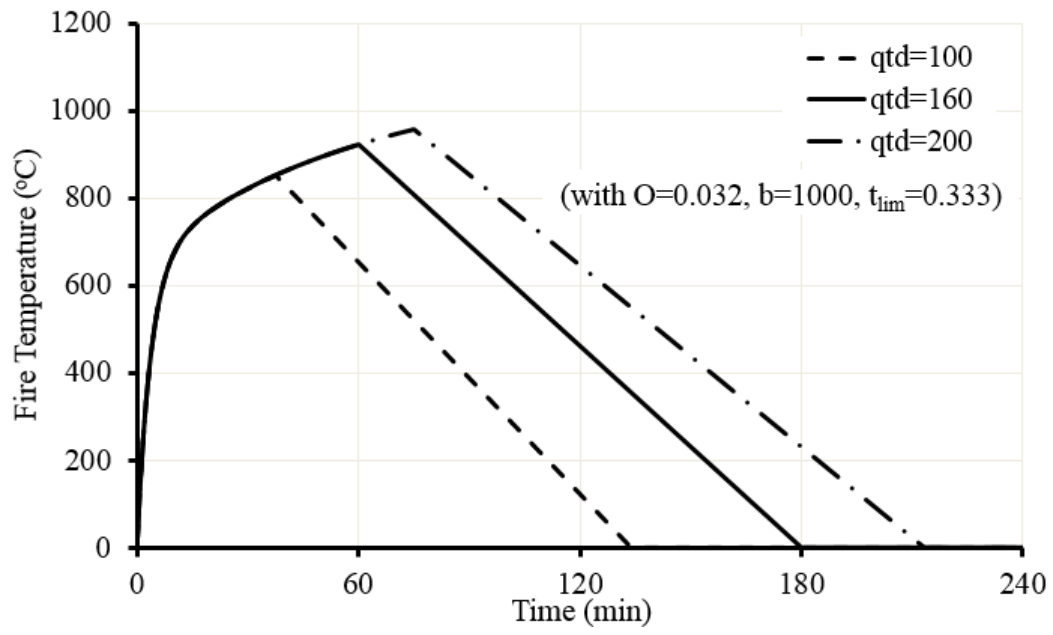


Figure 2.6 Effect of fire load density factor on fire time-temperature curve

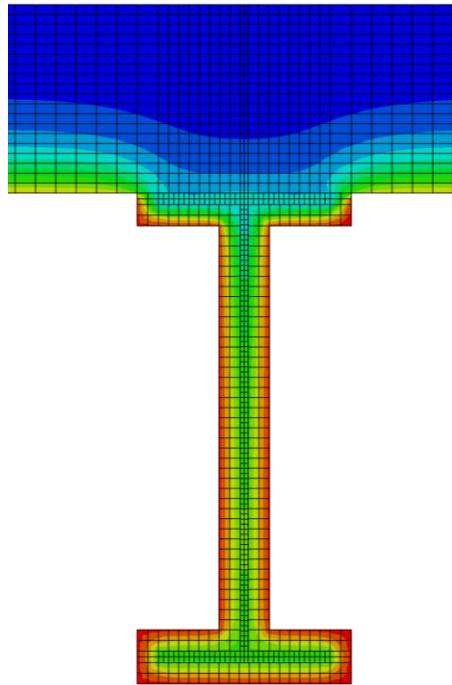


Figure 2.7 Result of a 2D heat transfer analysis of a wide flange beam with SFRM and a composite slab, showing temperature gradient (using ABAQUS software)

CHAPTER 3. PROPOSED METHODOLOGY FOR ASSESSING POST-EARTHQUAKE FIRE RESILIENCE

This chapter presents the proposed methodology for how to assess a building for post-earthquake fire resilience. It includes a step by step procedure including recommendations for modeling, selection of hazards and selection of parameters for incremental analyses. This chapter also explains the post-earthquake fire failure modes that could occur, as well as the proposed acceptance criteria.

Faggiano and Mazzolani [102] made notable strides towards assessing resilience. In their study, 2D frame analyses were conducted using pushover analysis. Fire loads were applied to two bays in each of the two stories. Seismic performance levels were benchmarked by interstory drift ratios and plastic hinge rotations according to FEMA 356 [103]. Similar criteria was established for fire: Operational Fire, Life Safety Fire, Local Collapse Fire, Section Collapse Fire and Global Collapse Fire, based on yielding, plastic hinging, beam mechanisms, failure of the cross-section and a global mechanism respectively. A performance chart was generated which compared seismic performance levels, fire performance levels, and fire resistance in a 3D bar chart [102]. This approach can be further advanced by developing 3D fragility curves to determine the probability of collapse for various hazard severities. These 3D surface plots can be used to show the interrelationship between the level of each hazard and the corresponding probability of collapse. The process for creating these plots are outlined in the methodology below.

3.1 Outline of PEF Methodology

Based on the current state of the art, the following methodology is proposed for evaluating steel buildings exposed to post-earthquake fires (PEF). The methodology is outlined in Figure 3.1. Included in the methodology are the steps described in more detail below, including the design of the structure, selection of the seismic hazard, and implementation of incremental dynamic analyses and incremental fire analyses.

- (i) Design of the structure using applicable building codes (Figure 3.2) – Standard design procedures should be used to determine the structural framing members, connection details, and fireproofing requirements. Structures that are regular and symmetric in

- shape are usually designed using 2D linear static procedures outlined in ASCE 7 [5] for seismic and wind analyses. These analyses provide a qualitative estimate of building performance, which can more accurately be estimated with more sophisticated analyses.
- (ii) Development of a 3D FEM Model (Figure 3.3) – A detailed nonlinear, inelastic 3D finite element model of the complete building structure should be developed. This includes consideration of the gravity framing contribution, such as the composite slab and gravity connections. The model should account for inelastic deformations, instability failures, and connection damage at elevated temperatures. It should also incorporate the effect of temperature on material properties. Separate seismic and fire models may need to be developed, with the ability to import the results of the seismic analyses into the fire model.
 - (iii) Selection of ground motions (Figure 3.4) – Ground motions may be selected using the ASCE 7 procedure explained previously, or by other means. This includes selection of at least 7 ground motions which are scaled to fit the design response spectrum of the building. Ground motion records scaled from actual seismic events should be used.
 - (iv) Apply ground motion to base of building (Figure 3.4) – The selected time histories should be applied to the building base using either acceleration or displacement records. Ground motions should be applied in both orthogonal directions.
 - (v) Incrementally scale ground motion (Figure 3.4) – Ground motions must be scaled by a selected intensity measure, which can include PGA, PGV or S_a , among others. The procedure suggests scaling PGA after each analysis, though spectral acceleration may be a better IM in some instances.
 - (vi) Generate IDA response curve (Figure 3.4) – After each analysis is run, the maximum story drift ratio for each intensity measure (PGA) should be recorded, and used to develop a plot of PGA vs. story drift ratio. This will show a progression of the building response as the intensity of the seismic event increases.
 - (vii) Select fire locations (Figure 3.5) – Fires should be considered at strategic locations throughout the building. At a minimum, fire analyses should be conducted at a lower, mid and upper level. Corner, exterior, and interior compartments should be studied as

- well. Each bay of the structure could be considered one compartment. Full story fires may also be considered.
- (viii) Select fire time-temperature curves (Figure 3.5) – Eurocode parametric time-temperature curves can be used to represent compartment fires. A minimum of three curves are recommended to accompany the seven seismic time histories required by ASCE 7. Opening factor, thermal inertia of the enclosure, and fire load density should be varied to produce seven distinct curves, which vary in peak fire temperature and rate of heating and cooling.
 - (ix) Conduct 2D heat transfer (Figure 3.5) – 2D heat transfer is necessary to determine the internal temperatures of all of the structural members exposed to the fire. This should be performed using FEM or other numerical analysis software. The fireproofing should be modeled at the design thickness, or the thickness determined using the prescriptive approach. Thermal properties for each material should be taken as per Eurocode where applicable.
 - (x) Apply temperatures to building model (Figure 3.5) – The internal temperatures, which are determined through heat transfer analyses, should be assigned to the members in the building model that are exposed to the compartment fire. Five minute increments are recommended.
 - (xi) Incrementally scale fire time-temperature curves (Figure 3.6) – The fire time-temperature curves should be scaled in a manner similar to the scaling of PGA used in IDA. The curves may be scaled by peak fire temperature, as shown in Figure 5, or other parameters such as those discussed in Section 2.2.2.
 - (xii) Generate IFA response curve (Figure 3.6) – The recommended damage parameter for IFA of building systems is the story deflection ratio, which measures the maximum vertical deflection divided by the span. This damage parameter, or another representative value should be recorded at each IM using the results of the incremental analyses conducted in the previous step.
 - (xiii) Develop fragility curves (Figure 3.1) –The IDA and IFA results should be used to generate fragility curves, which identify the probability of failure to occur. Fragility curves have been used extensively in seismic analyses to calculate the probability of

collapse or failure of a structure at different intensity measures. Fragility curves are determined using the following equation:

$$P(C|x) = \Phi\left(\frac{\ln\left(\frac{x}{\theta}\right)}{\beta}\right) \quad \text{Equation 3-1}$$

where $P(C|x)$ is the probability of collapse or failure at an intensity measure of x . $\Phi(\cdot)$ indicates a normal cumulative distribution function. θ is the mean of the fragility function and β is the standard deviation. The results from IDA and IFA should be plotted relative to one another to create a 3D surface plot. This plot will indicate the probability of collapse of the structure with varying severities of earthquake and cascading fire hazards. This will evaluate the vulnerability of steel moment-frame buildings subjected to fire following earthquake hazards.

3.2 Fire Damaged Building Assessment

Life safety of building occupants is the foremost priority for structural engineers. However, as the industry continues to push towards more resilient and sustainable structures, there is pressure by owners and officials to meet higher levels of performance. FEMA 356 [103] and ASCE 41 [16] summarize performance objectives for building behavior subjected to earthquakes as follows: collapse prevention, life safety, immediate occupancy and operational. Collapse prevention is when the building undergoes extensive damage but it remains standing. In these cases, demolition of the structure after the event is most likely. Life safety ensures that the occupants of the building can exit, despite significant damage. Immediate occupancy entails only minor repair of the structure and the building can quickly return to its normal operations. This keeps businesses running, which is in the interest of many building owners. Operational means that essentially no damage has occurred and the building continues to be operational throughout the earthquake event. The same concept of performance levels can be applied to structural design for fire safety. The fire resistance ratings specified in the building code are intended to ensure that life safety is maintained, by requiring a minimum designated timeframe for which the structure must remain stable, allowing occupants to egress. Beyond this timeframe, however, there is little guidance of performance levels. Performance-based fire engineering allows the designer to understand the scope of damage

that will occur and the repairs that may be necessary. The following discussion explores the factors to consider when evaluating damage after a fire. It is important to note that only structural damage is being considered. It is not uncommon that a building will undergo demolition after a fire due to the extensive damage of the nonstructural components, while the structure remains relatively intact.

Fire exposure can alter the material properties of steel. Steel properties such as yield stress, ultimate stress, and modulus of elasticity all vary with increasing steel temperature, as shown in Figure 5.3 and Figure 5.4. These changes can lead to bent or damaged members that may or may not affect global stability of the structure. Even when stability is maintained, it is still important to consider the material properties of the steel once the structure has cooled in order to evaluate any repairs or replacements that would be needed to maintain structural integrity throughout the life of the structure.

Steel structures that have been exposed to fires can be classified in three categories: 1) virtually straight; 2) noticeably deformed but repairable; and 3) severely deformed beyond repair. Members in categories 1 and 2 do not usually undergo metallurgical property changes. For temperature rises less than 870°C, it is generally accepted that there will be minimal impact on metallurgical and physical properties once the steel has cooled to ambient temperatures [104]. Members that are nearly straight can be considered unaffected by the high temperatures. Buckling and large deformations commonly occur at around 650°C; thus, even when category 2 deformations occur, it is unlikely that material property degradation has taken place. For category 3 members, these deformations are typically so extreme that repair of the members is very unlikely. In these cases, repair is cost prohibitive and, instead, replacement or demolition is the most common approach. While each member is assessed individually, the severity and extent of damage depends greatly on the failure mode.

3.2.1 Failure Modes and Limits for Fire Assessment

Table 3.1 shows the primary failure modes observed during the building analyses subjected to compartment fires. These failure modes are: column failure, bay failure, compartment failure, connection failure, and system collapse. Column failure occurs when a column is no longer able to support axial loads, or when it deforms enough to cause deflections greater than the vertical deflection criteria stated below. Bay failure is when multiple columns fail, resulting in

deformations across the bay. Compartment failures are when the beams and slab within the compartment deflect beyond the deflection criteria. Connection failures typically occur due to large tensile forces or rotations caused by thermal expansion of the steel framing members. In many cases, connection failure also occurred after column failure resulted in large beam rotations. System collapse is defined as member failures that result in collapse of more than one bay of the structure.

A compartment failure is limited primarily to the structural and nonstructural components within that compartment. For this reason, it is plausible to make repairs to the compartment framing (through heat straightening and/or replacement of structural members) without compromising the remainder of the structure. Column failures cause more widespread damage, also affecting the stories above. Minimizing the likelihood of column failures, bay failures, and system collapse would result in a more resilient structure.

The vertical deflections of four different types of failures are shown in the last column of Table 3.1: (a) column failure due to Fire 1, (b) bay failure due to Fire 1, (c) compartment failure due to Fire 2, and (d) connection failure due to Fire 1. The location of the compartment fire is shown using a dashed line. For compartment failure, deflections are limited primarily to the compartment where the fire took place. The beams and girders at the periphery of the compartment fire are also subjected to the fire, resulting in deformations which cause some additional deformation in the adjacent compartments. Table 3.1 shows a column failure which occurs where the deflection is at its maximum. This leads to significant deformations in the beams and slabs of the four bays surrounding this column. Bay failures are similar to column failures but they affect additional bays. In Table 3.1, two columns have failed at the locations of maximum deflection. These failures create significant deformations in the beams and slabs of the six adjacent bays. For both column and bay failures, these deformations are also seen at all stories above the failed columns. Compartment failures are only observed at the story that has been subjected to fire.

Deflection criteria for failures due to fire were determined from the British Standard 476-20:1987 [105], which provides limits for deflection and rate of deflection. Deflections must be less than $L/20$ and the rate of deflection (in order to prevent run-away deflections) must be limited to $L^2/(9000d)$ (in mm/min), where L is the length of the span and d is the distance from the top of the structural section to the bottom of the design tension zone. The length, L , used to calculate deflection limits for each failure mode is shown in Table 3.1.

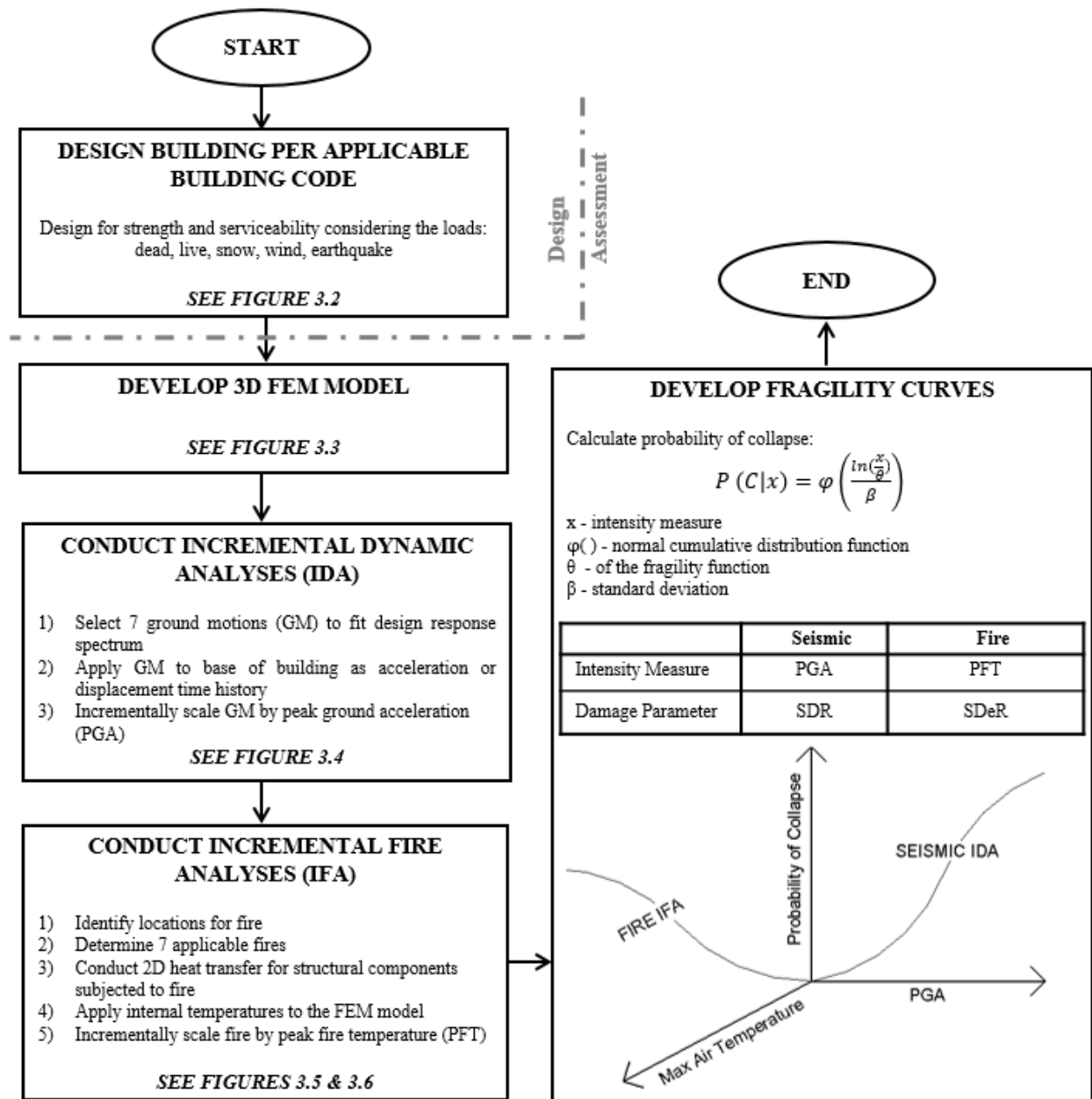
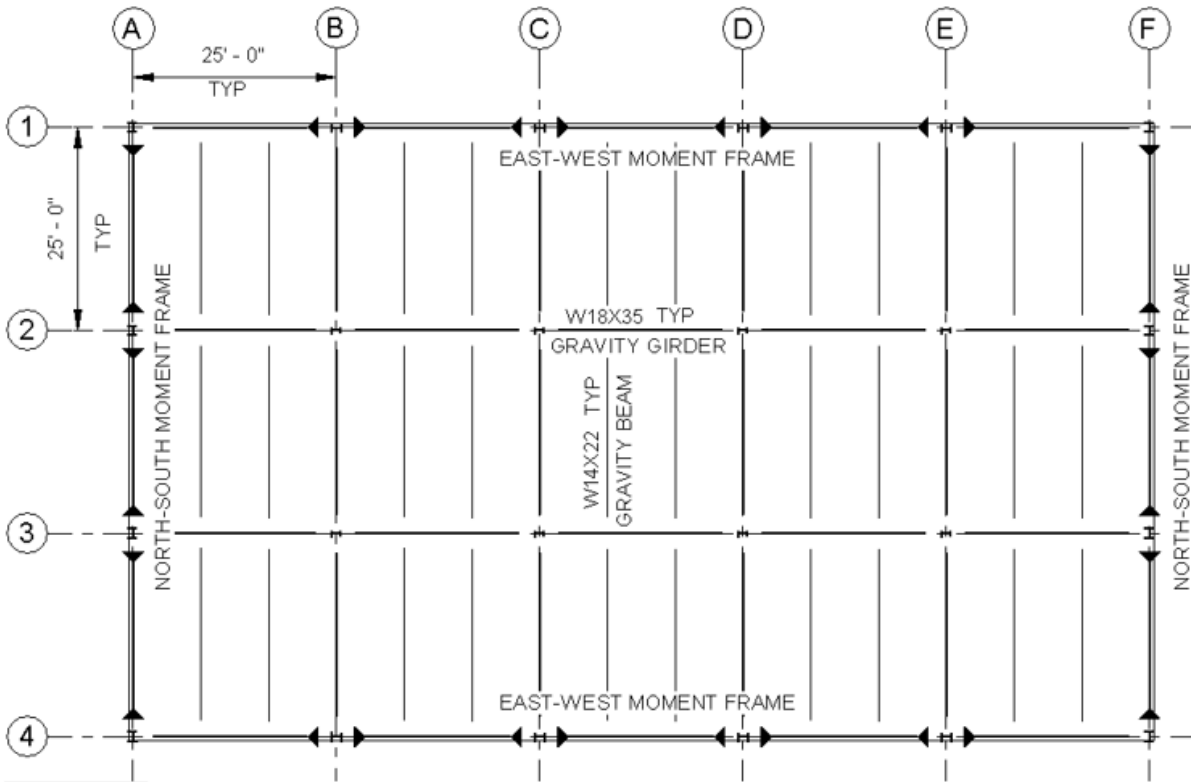


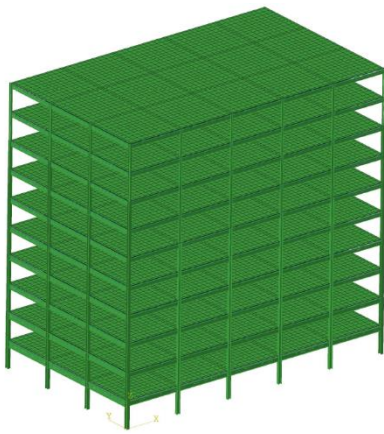
Figure 3.1 Overview of proposed methodology



	N-S MF Frames		E-W MF Frames		Gravity Frames
	Columns	Beams	Columns	Beams	Columns
10	W14x53	W18x50	W12x45	W18x35	W8x24
9	W14x53	W18x50	W12x45	W18x35	W8x24
8	W14x90	W21x83	W14x53	W18x50	W8x40
7	W14x90	W21x83	W14x53	W18x50	W8x40
6	W14x109	W21x93	W14x99	W18x60	W12x58
5	W14x109	W21x93	W14x99	W18x60	W12x58
4	W14x159	W21x111	W14x145	W18x71	W14x74
3	W14x159	W21x111	W14x145	W18x71	W14x74
2	W14x311	W27x217	W14x283	W21x132	W14x90
1	W14x311	W27x217	W14x283	W21x132	W14x90

Design Loads for Chicago, IL office building				
Risk Category	II			
Dead Load	65 psf			
Live Load	50 psf			
Wind	Basic Wind Speed		115 mph	
	Wind Exposure Category		B	
Seismic	Seismic Design Category		B	
	S _{Ds}	0.14 g	S _{D1}	0.098 g

Figure 3.2 Case study building: layout, member sizes, and design loads



Structural Element	ABAQUS FEM element
Beams & Columns	B31 beam elements
Composite slab	S4R shell elements
Shear Studs ^[1]	Rigid connectors
Moment connections ^[2]	Welded connector
Gravity connections ^[3]	Equivalent connector element

Notes: [1] Incorporation of force-slip behavior of studs is preferred
 [2] Development of more detailed moment connectors which capture moment-rotation behavior & failure modes is ongoing
 [3] Refer to Agarwal and Varma (2014) for details

Figure 3.3 Summary of ABAQUS modeling approach

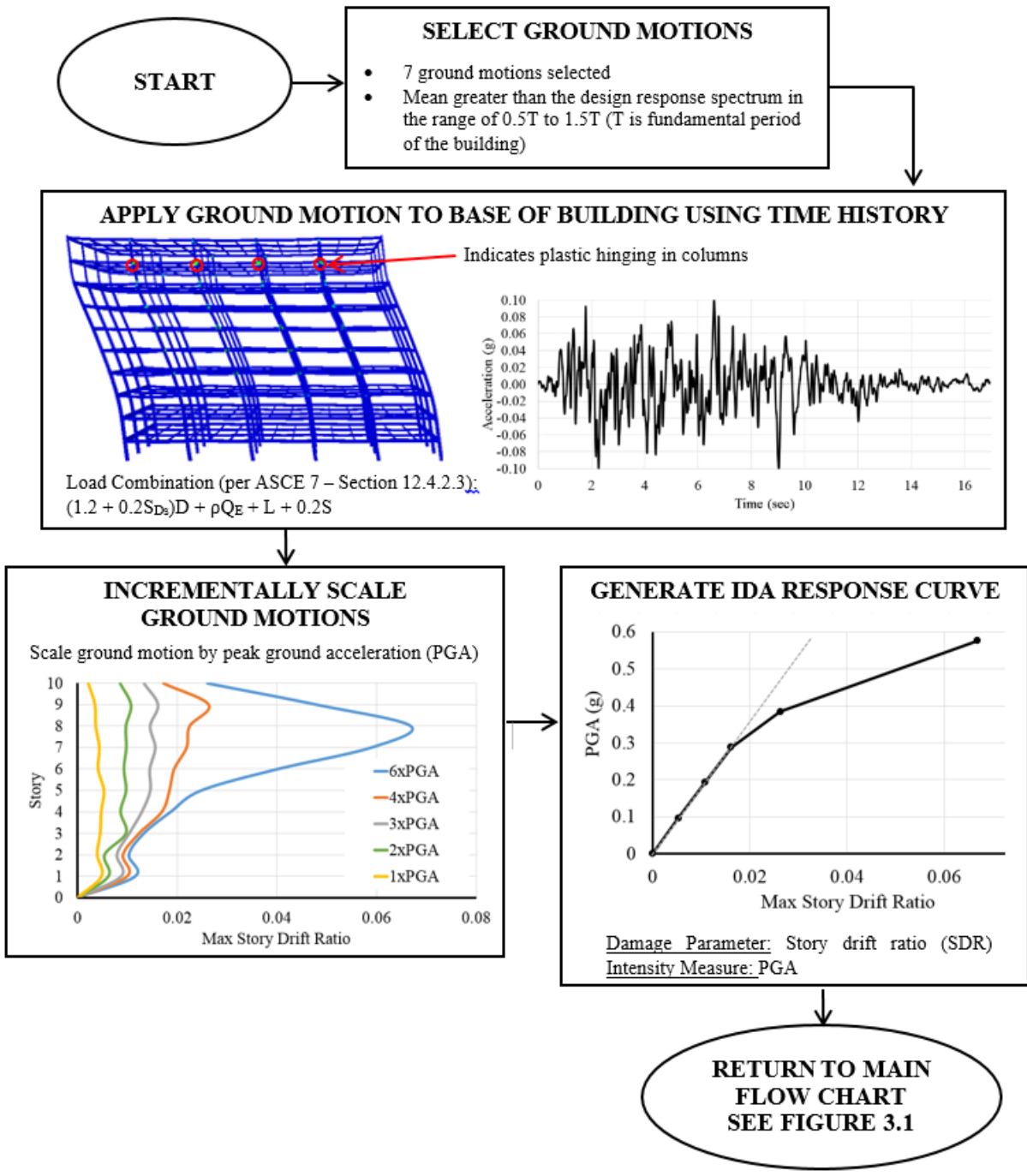


Figure 3.4 Flow chart for conducting incremental dynamic analyses

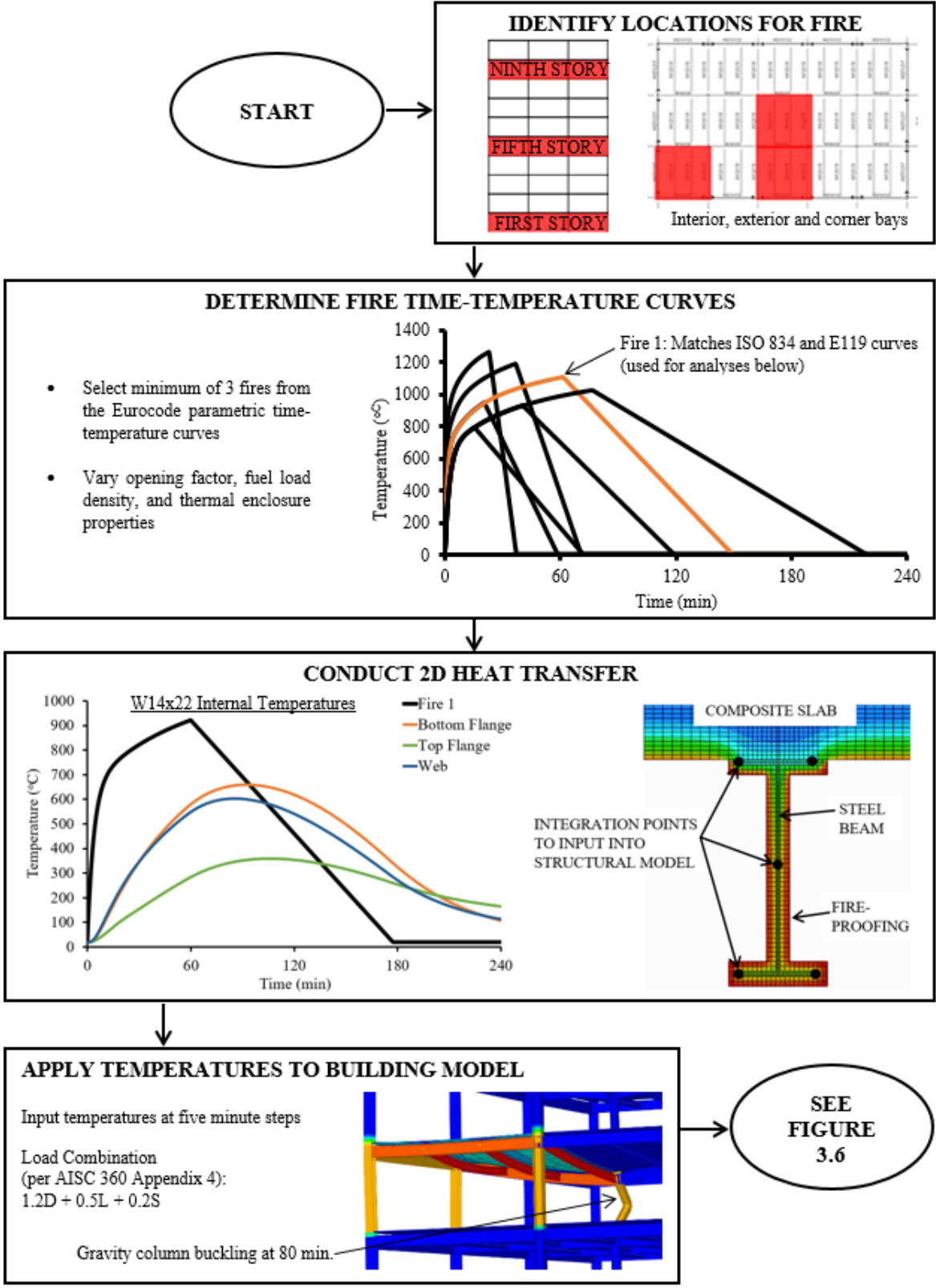


Figure 3.5 Flow chart for conducting incremental fire analyses (Part 1)

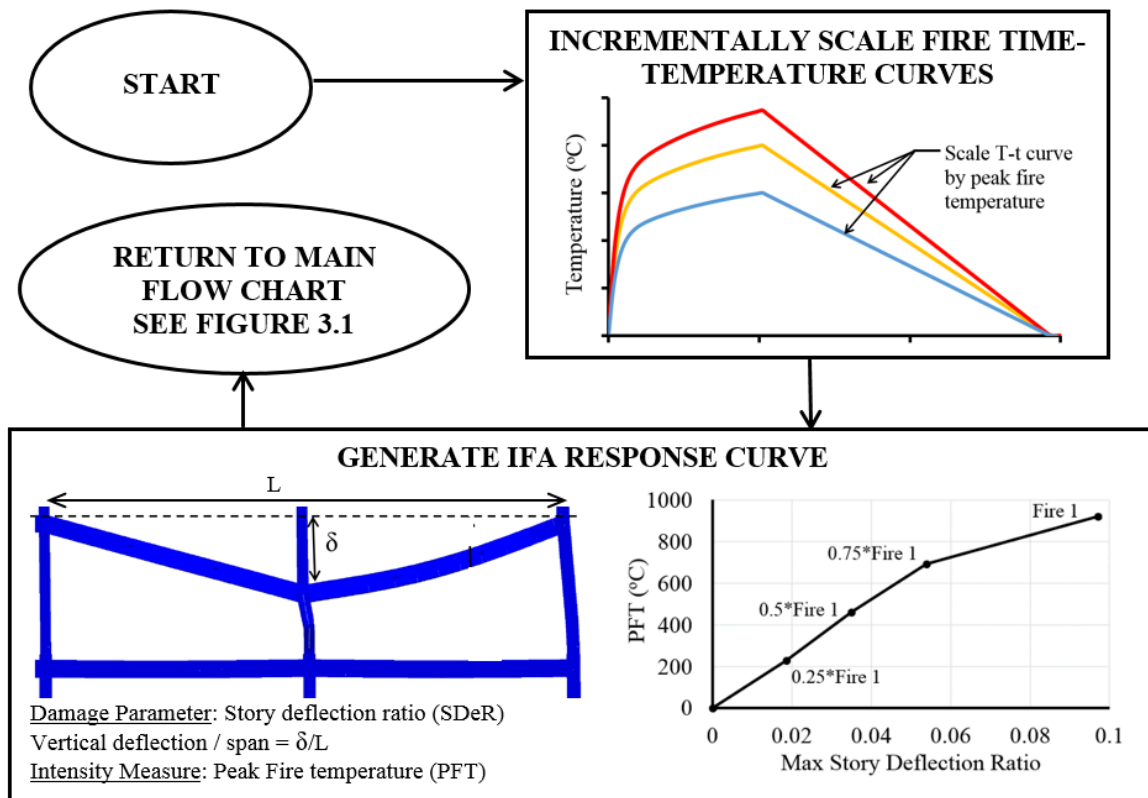


Figure 3.6 Flow chart for conducting incremental fire analyses (Part 2)

Table 3.1 Failure mechanisms and acceptance criteria

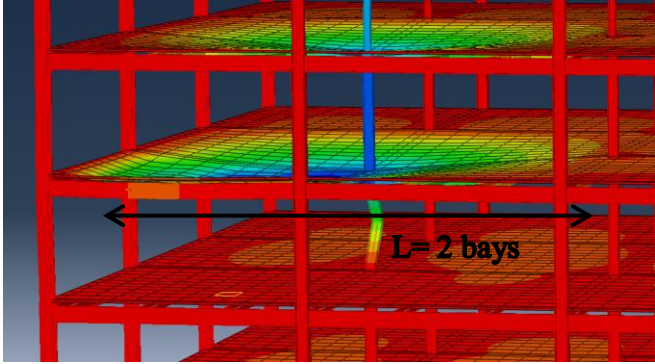
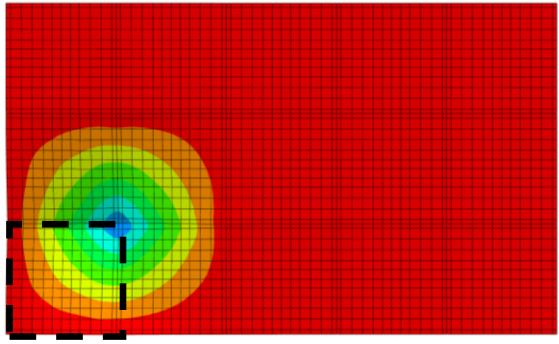
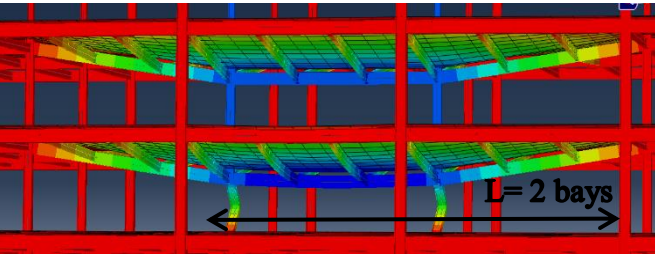
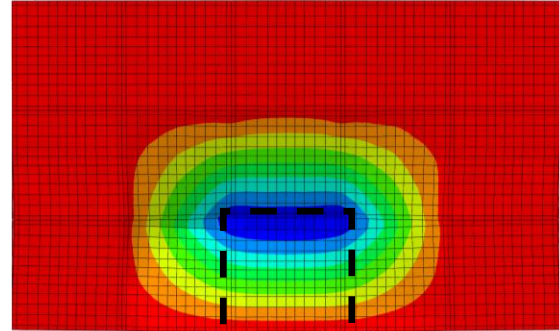
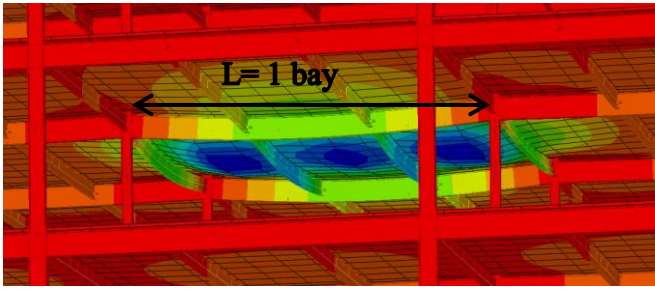
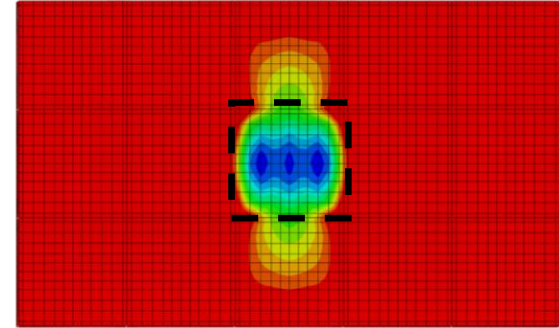
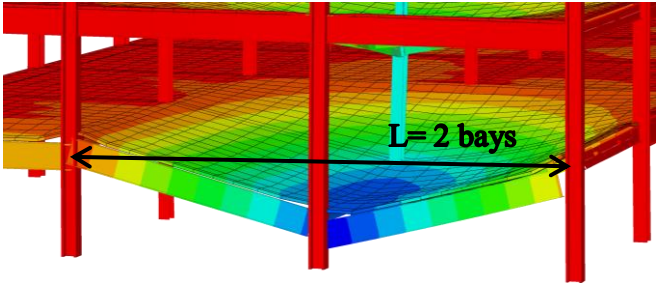
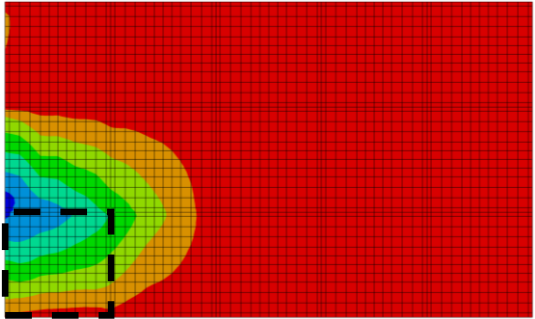
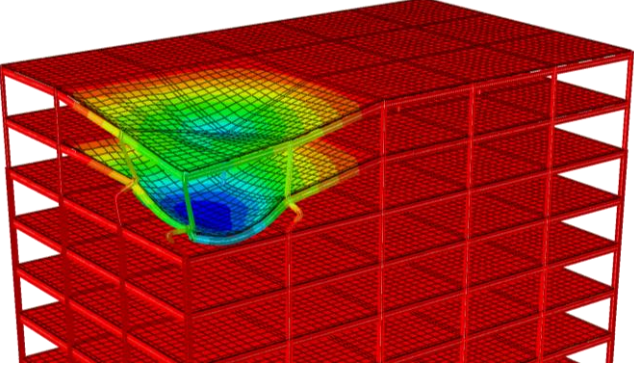
Failure Type	Failure Mode Simulation	Acceptance Criteria	Plan View (showing extent of deflection)
Column Failure		Deflection Limit: 762 mm	
		Deflection Rate Limit: 47mm/min	
Bay Failure		Deflection Limit: 762 mm	
		Deflection Rate Limit: 47mm/min	
Compartment Failure		Deflection Limit: 381 mm	
Deflection Rate Limit: 12mm/min			

Table 3.1 continued

Failure Type	Failure Mode Simulation	Acceptance Criteria	Plan View (showing extent of deflection)
<i>Connection failure</i>		<p><i>Deflection Limit:</i> 762 mm</p> <p><i>Deflection Rate Limit:</i> 47mm/min</p>	
<i>System failure</i>		<p><i>Collapse:</i> <i>No acceptance criteria</i></p>	<p><i>Varies depending on where collapse occurs.</i></p>

CHAPTER 4. BUILDING DESIGN AND HAZARD SELECTION

Two ten-story office buildings have been designed using traditional methods in order to later analyze using more sophisticated, performance-based methods. Both buildings were designed using U.S. building codes and standards: IBC [7], ASCE 7 [5], and AISC 360 [48]. It is generally believed that a building designed to resist higher seismic loads will inherently improve multi-hazard resilience. This hypothesis is tested by analyzing two buildings, which have the same building configuration but were designed for different levels of seismicity and wind loads. One building was designed for a hazard level in Chicago, IL and the other was designed for a hazard level in Los Angeles, CA. The different hazard scenarios that have been evaluated are shown in Table 4.1. This chapter will explain the design procedure, final structural design, and hazard selection for both the Chicago and Los Angeles buildings.

4.1 Structural Design of Ten Story Office Buildings

The two case study buildings have the same geometry and gravity framing; the structures vary only in the member sizes of the lateral-force resisting system. Both structures utilize perimeter moment frames as the lateral system. There is a three bay by five bay layout with each bay measuring 25 ft (7.63 m) x 25 ft (7.63 m). Each story height is 12 ft (3.66 m). Figure 4.1 and Figure 4.5 show first floor plans of the Chicago and Los Angeles buildings, respectively. Openings for stairs, elevators and utilities have been omitted for simplicity of the model. Future studies could be conducted to explore the impact of large openings on multi-hazard resilience. The Chicago building was originally designed by Agarwal [15] and was reanalyzed to ensure compliance with current building codes.

4.1.1 Gravity Load Design

Each floor system was designed for a 65 pounds per square foot (psf) dead load and 50 psf live load. Snow loads at each location were also evaluated. Gravity beams are W14x22 and the interior girders are W18x35. In the initial design by Agarwal [15], the building had W12x19 beams. These beams were redesigned to comply with more typical serviceability limit states and standard practice. Each floor slab is a 3"-20 gauge (75 mm) composite deck with 2 ½" (65 mm) light-weight

concrete topping. This composite deck was chosen because it can achieve a 1-hour fire rating per UL Design D904 [9]. The studs used to develop composite action between the steel and the deck are $\frac{3}{4}$ " diameter and $4\frac{1}{2}$ " long. Each beam was designed to achieve a minimum of 25% composite action. Welded wire reinforcement (152mmx152mm MW10) is embedded in the concrete slab. The gravity framing for the roof is the same as the typical floors. See Figure 4.2 for the gravity column sizes.

4.1.2 Lateral Design for Chicago building

The structure was initially designed by Agarwal [15] per ASCE 7-05 to withstand hazard levels located in Chicago, IL. The moment frames were designed as ordinary moment resisting frames and the seismic design category was B. The equivalent lateral force procedure, which is a linear static procedure outlined in ASCE 7, was used for the seismic design. The parameters used to determine seismic forces are provided in Table 4.2. RAM Structural System [106], commercially available software, was used for the design. The structure complied with ASCE 7-10 [5] and AISC 360-10 [48].

Because ordinary moment resisting frames were used, the moment frame connections did not need to comply with the prequalified connection specified for special and intermediate steel moment frames in AISC 358 [14]. Thus, a welded unreinforced flange, bolted web (WUF-B) connection was specified.

Wind loads were calculated using the Main Wind Force Resisting System Directional Procedure (Chapter 27) in ASCE 7-10 [5]. This procedure calculates an equivalent static pressure for the windward, leeward, and side walls for different elevations of the building. The basic wind speed is 115 mph and the exposure category is B. Due to the low seismicity of the area, the lateral system was controlled by wind drift of $L/400$, where L is the building height. This is a recommended limit set by industry standards. The calculated base shear for the building due to wind is 447 kips and 125 kips due to seismic. The member sizes for the moment frames are shown in Figure 4.3 and Figure 4.4.

The fundamental period of the structure is 2.9 seconds. It should be noted that this is a longer period than is usually typical of frame buildings. For instance, a commonly used rule of thumb is 0.1 times the number of stories, which would result in a 1 sec period for this 10 story building. Since the building was controlled by wind drift, the period of the building must not have been

considered in depth. Seismic forces were calculated using the approximate fundamental period (T_a) times the coefficient for upper limit on calculated period (C_u), as restricted in ASCE 7 [11]. For this structure, $T_{max}=2.19$ sec.

4.1.3 Lateral Design for Los Angeles building

The same analysis approaches were used for the Los Angeles building: equivalent lateral force procedure for seismic loads and main wind force resisting system directional procedure for wind loads. However, because the structure was classified as a seismic design category D, the moment frames needed to be designed as Special Moment Resisting Frames. This means that the frames must comply with the AISC Seismic Provisions [11], which requires adherence to the strong column-weak beam philosophy, stability bracing, and ductility requirements. Ultimately, the design of the moment frame members was controlled by seismic strength requirements and provisions.

Welded unreinforced flange-welded web (WUF-W) moment connections were selected from AISC 358 [14] to be used in the special moment resisting frames. This type of connection includes prequalification limits for the beam depth, weight, flange thickness, etc. The moment frame design for the Los Angeles building adhered to these limitations. In addition, the connection designates a protected zone from the column face to a distance d (beam depth) away. Within this zone, no bracing, connections, or shear studs can be used.

Wind forces were also applied, though it did not control the design. Portions of Los Angeles fall within a special wind region where higher wind speeds may be specified by the local jurisdiction. Because the building was designed using ASCE and not the California or Los Angeles building codes, this special wind speed was not used. The basic wind speed of 110 mph was used and the exposure category is B. The building base shear due to wind is 388 kips and 805 kips due to seismic. The fundamental period of the structure is 2.1 seconds. T_{max} of 1.8 sec was used for the calculation of seismic forces. The member sizes for the moment frames are shown in Figure 4.6 and Figure 4.7.

4.1.4 Prescriptive Fire Design

The fire resistance rating for the structural members is determined from the International Building Code (IBC) [7]. Both office structures are defined as building occupancy B, which corresponds to

a Type IB building. This building type requires a 2-hour fire rating on all framing members; however, the building type can be reduced to Type IIA if the building has a sprinkler system and proper control valves and initiating devices. Type IIA buildings require only a 1-hour fire rating for all structural members. Thus, for each structural member within both buildings, a 1-hour fire resistance rating was used.

The thickness of fireproofing required for each structural member was determined using the W/D approach outlined in Ruddy [10] based on fire tests conducted by Underwriters Laboratory [9]. Table 4.3 provides a summary of member sizes and SFRM thicknesses for many of the structural members analyzed in this project. The composite deck is not fire protected, as it can already achieve the performance rating without fireproofing.

4.2 Determination of Hazards for Performance-Based Analyses

4.2.1 Selection of Seismic Hazard

4.2.1.1 *Chicago, IL Seismic Hazards*

Because Chicago is in an area of low seismicity, adequate records of actual earthquakes in the vicinity were not available on the COSMOS [18] or PEER [17] databases. Most of the recording stations were beyond the Joyner Boore distance of 74 km and there were not even seven records available to use. Relocating the building to the New Madrid fault was briefly considered, but this area also did not have good readings. Therefore, synthetic ground motions were created using the software, SeismoArtif [107]. This software generated synthetic accelerograms using an algorithm by Halldorsson and Papageorgiou [108].

The seven selected ground motions for the building in Chicago are shown in Figure 4.8. Because of the 3D analysis of the structure, accelerations needed to be identified in orthogonal directions. This was accomplished by assigning angles to the ground motion so that the orthogonal directions could be determined from the one accelerogram record, as illustrated in Figure 4.9. It was decided that three ground motions would be predominantly in each of the orthogonal directions (i.e., $\Theta=5^\circ$ and 85°) and that the final orientation would be at 45° . As required by ASCE 7 [5], the mean value of the records is greater than the design response spectrum in the range of 0.2T to 1.5T, as shown in Figure 4.10. The maximum considered earthquake is used for the design response spectrum.

4.2.1.2 Los Angeles, CA Seismic Hazards

Ground motions for the Los Angeles building were selected based on actual earthquake records obtained from the online PEER database [17]. Seven notable earthquakes in the Los Angeles, CA vicinity were selected, as shown in Table 4.4. Each record was scaled in order for the mean value of the records to be greater than the design response spectrum in the range of 0.2T to 1.5T. The acceleration time histories in each orthogonal direction are shown in Figure 4.11 and Figure 4.12. Figure 4.13 displays each of the ground motions relative to the design response spectrum for the design basis earthquake.

4.2.2 Selection of Fire Hazard

The same fire hazards are assigned to each building. While these locations could potentially experience different hazards (due to differences in fire-responders or issues with water supply), it was decided to use the same fire hazards scenarios for ease of comparison.

4.2.2.1 Location of Fire

There is a lot of uncertainty in defining and locating the fire hazard. Many possible scenarios exist: interior and exterior compartment fires at different building levels, full story fires, horizontally and/or vertically moving fires. These factors will all affect the fire hazard and the building response. Engineering judgement must be used to determine the critical locations for analysis while remaining realistic about the likelihood of each fire event.

For the purposes of this study, only compartment fires will be studied in order to control the variables more closely. Each compartment represents one bay of the structure. Compartment fires will be explored at a mid and upper level of the building, studying both interior and exterior compartments. Three compartments were studied. These compartments are classified as Case A (corner compartment), B (exterior compartment in third bay of long size of building), and C (interior, center compartment), as shown in Figure 4.14. When the ground motion was prominent in the transverse direction, compartment B2 was studied instead of compartment B. Case D considers a full story fire scenario. Case D_M1 and Case D_M2 are full story moving fire scenarios, as described in Section 8.5.

Fires are analyzed at the fifth and ninth stories to represent both a mid-story level and upper-story level. Lower levels are not usually considered because firefighting measures are very effective at

lower levels where trucks and hoses can easily reach; however, it is possible that an earthquake event could hinder firefighting of a lower level fire. For this reason, a first-story fire was considered in the Los Angeles building.

4.2.2.2 Fire Time-Temperature Curves

As explained previously, to determine the fire model, time-temperature curves from a standard can be used or computational fluid dynamic (CFD) models can be created. These CFD models are highly complex and require a lot of assumptions of materials and properties within the compartment; for these reasons, it was decided to use standard fire curves instead. For this project, parametric time-temperature curves were developed using Annex A of Eurocode 1 [37] for compartment fires. These parametric curves are preferable to the ASTM and ISO curves because they include a cooling phase and vary depending on the previously defined factors: thermal inertia of the enclosure (b), opening factor (O), and fire load density ($q_{t,d}$).

Because the goal of the project is to cover a range of fire scenarios to better understand overall system behavior due to post-earthquake fires, seven different fire scenarios were initially selected which vary the $q_{t,d}$ and O factors. These parameters affect the peak fire temperature, total heat release, and the fire duration, all of which can be used as intensity measures. The b factor was kept constant at $1000 \text{ J/m}^2\text{s}^{1/2}\text{K}$ because there is less likelihood of variability with this factor. The seven proposed fire scenarios are shown in Figure 4.15 and the parameters for these fires are given in Table 4.5.

Incrementally scaling each of the seven fires and varying their locations within the building would be extremely computationally intensive. It also became evident that when scaling the fires by peak fire temperature for the incremental fire analyses (explained further in Section 2.2.2), many of the fires would be very similar to one another in terms of peak temperature and duration. Thus, the initial seven fires were reduced to only three, as shown in Figure 4.16. These three fires represent short, mid and long duration fires. Figure 4.17 through Figure 4.19 show that many of the seven fires shared similar properties when compared with scaled versions of Fires 1 and 2. The areas under the curves in each of the figures were also calculated (shown in Table 4.6) and found to be nearly equal. This is a method of assessing fire intensity known as Ingberg's concept [45] and helps to validate the decision to use fewer fire curves.

4.2.3 Selection of Wind Hazard

Pressure time histories are used to capture dynamic behavior from a wind event. Because the case study structures were designed to behave elastically in a wind event, only one wind time history has been used for each building as a means to validate the approach. More time histories could be studied at varying intensities if desired.

The NatHaz On-line Wind Simulator (NOWS), which is an open source program created by researchers at the University of Notre Dame, was used to generate wind velocity time histories [109]. The program uses ASCE 7 mean wind speeds to simulate stationary Gaussian multivariate wind fields. The building frequency, exposure category, and 3 sec gust wind speed are input into the program. Building heights are specified at each of the ten stories in order to generate velocity time histories at each story level.

NOWS outputs mean wind speeds and fluctuating wind speeds at each of the story levels. These represent horizontal wind velocities acting perpendicular to the building surface, which create a buffeting drag force. Vertical wind pressure time histories and crosswinds are not considered.

The buffeting drag force can be calculated by summing the mean and fluctuating wind velocities and then converting to a force [110]. The drag force, q , is calculated using the drag equation shown below:

$$q = \frac{1}{2} \rho U(t)^2 C_D A \quad \text{Equation 4-1}$$

ρ is the air density (1.225 kg/m³). $U(t)$ is the summation of mean and fluctuating wind velocities over time, t . C_D is the drag coefficient and A is the tributary area. The drag coefficient varies depending on the building's shape. $C_D=2.03$ was used [110].

4.2.3.1 Chicago, IL Wind Hazards

Wind time histories were generated at each story for wind hazards levels in Chicago, IL. Because the NOWS program generates time histories based on ASCE 7-98 basic wind speeds, the basic wind speed of 90 mph was used and multiplied by the wind factor of 1.6 from the former load combination. Table 4.7 shows the mean wind speeds at each story as provided by NOWS. Figure 4.20 displays the fluctuating wind speeds at each story. This data is converted into an along-wind drag force using Equation 4-1.

4.2.3.2 *Los Angeles, CA Wind Hazards*

The same approach was used to generate the wind time history in Los Angeles. The ASCE 7-98 basic wind speed for Los Angeles is 85 mph; however, because it falls within a Special Wind Region, 100 mph was used at the direction of the County of Los Angeles Building Code Manual [111]. Table 4.8 provides the mean wind speeds at each story level, while Figure 4.21 shows the fluctuating wind time history for each story. These wind speeds are added together and converted into a drag force using Equation 4-1.

Table 4.1 Design location and hazard scenarios in parametric study

	Chicago	Los Angeles
Controlling Lateral Design	Wind	Seismic
Hazard Scenarios	Seismic	Seismic
	Fire	Fire
	Seismic + Fire	Seismic + Fire
	Wind + Fire	Wind + Fire

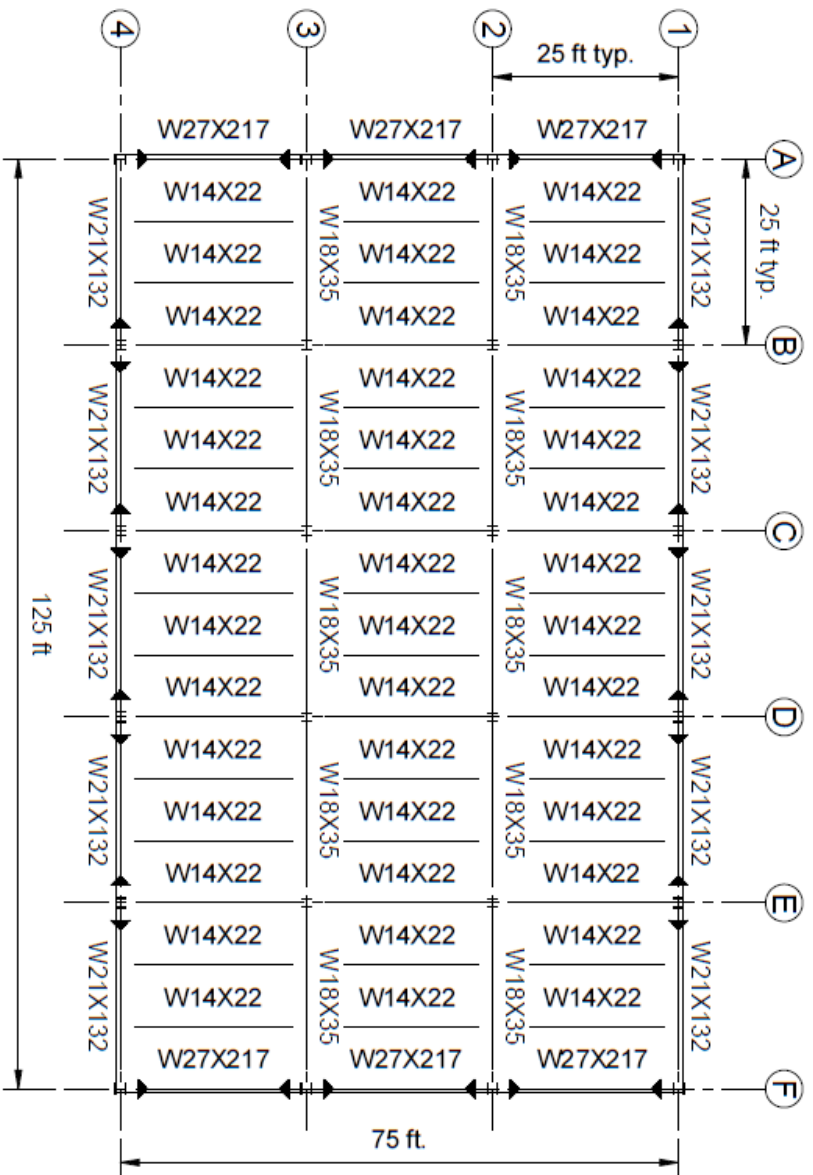


Figure 4.1 First floor plan of Chicago building

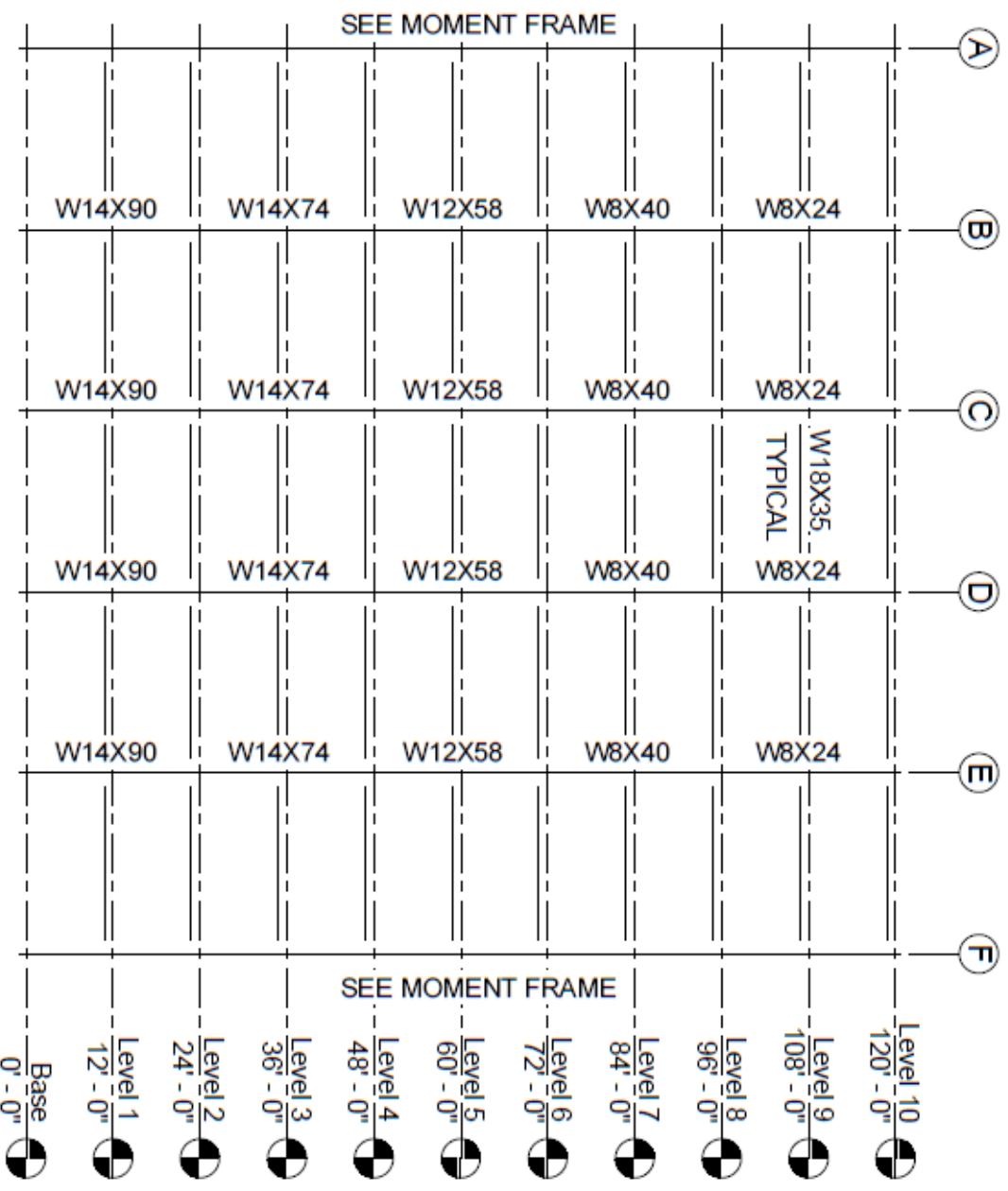


Figure 4.2 Gravity frames in Chicago and Los Angeles building at gridlines 2 and 3

Table 4.2 Seismic loads for case study buildings

	Chicago	Los Angeles
Seismic Importance Factor	1.0	1.0
Site Classification	D	D
Spectral Response Accelerations	$S_s=0.131g$ $S_1=.061g$	$S_s=2.431g$ $S_1=0.852g$
Seismic Design Category	B	D

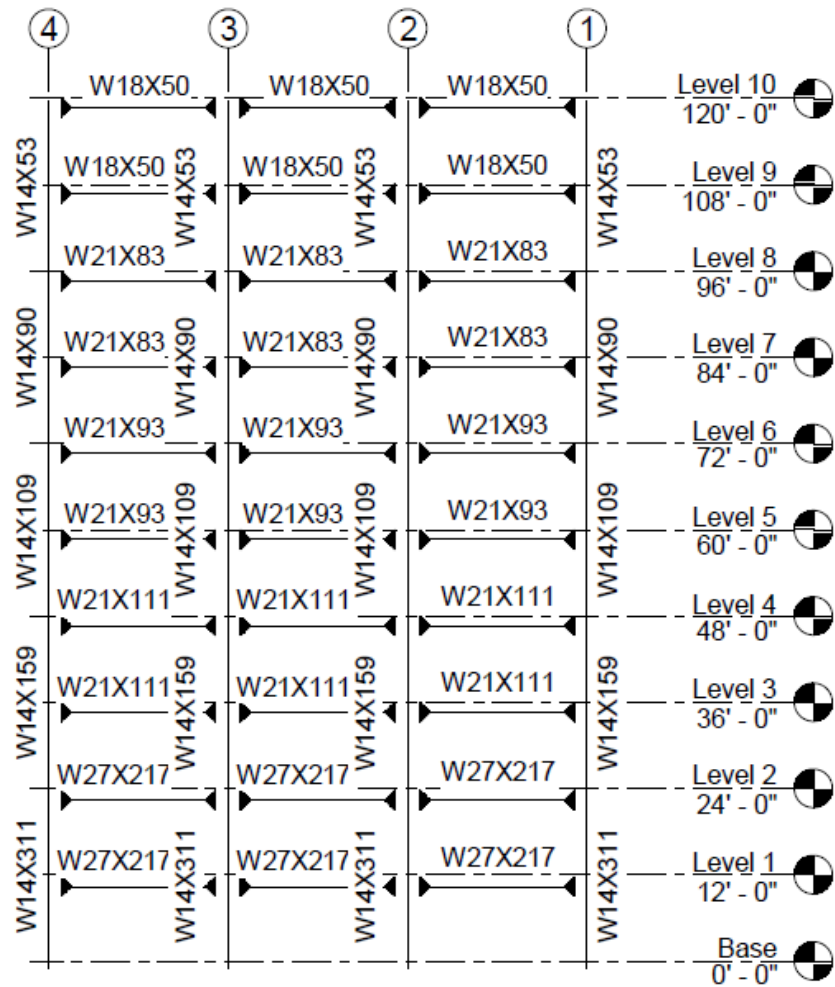


Figure 4.4 Moment frames in Chicago building at gridlines A and F

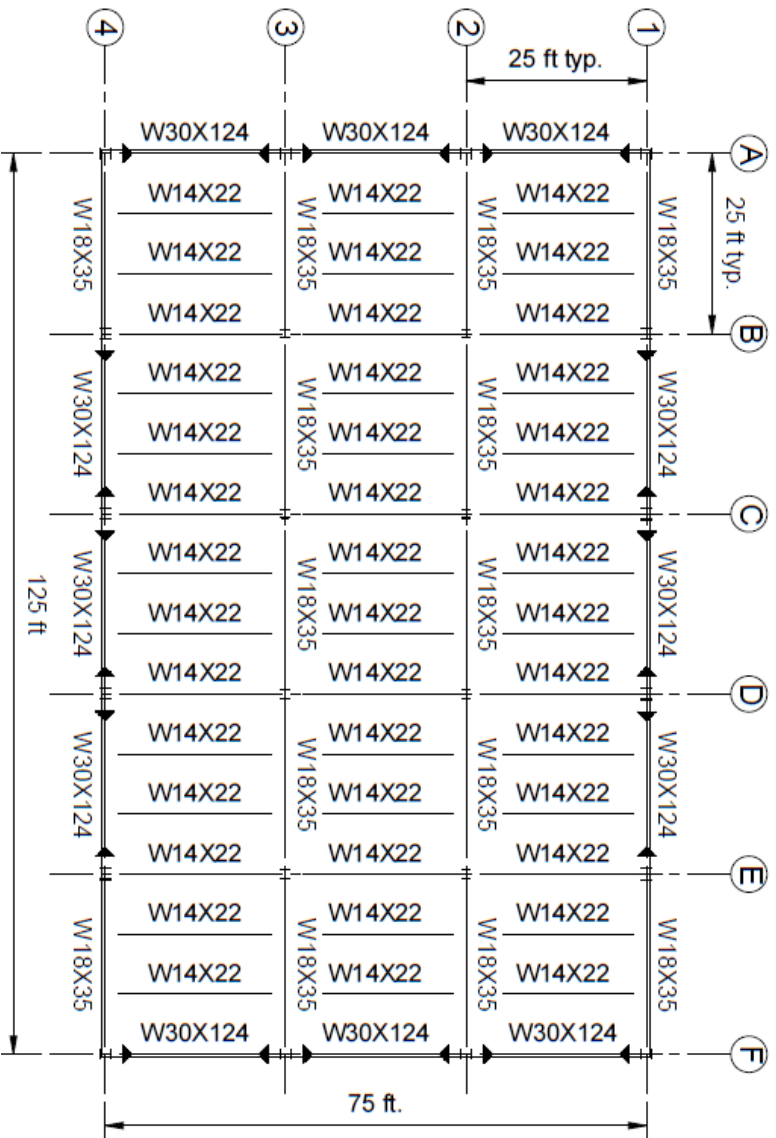


Figure 4.5 First floor plan of Los Angeles building

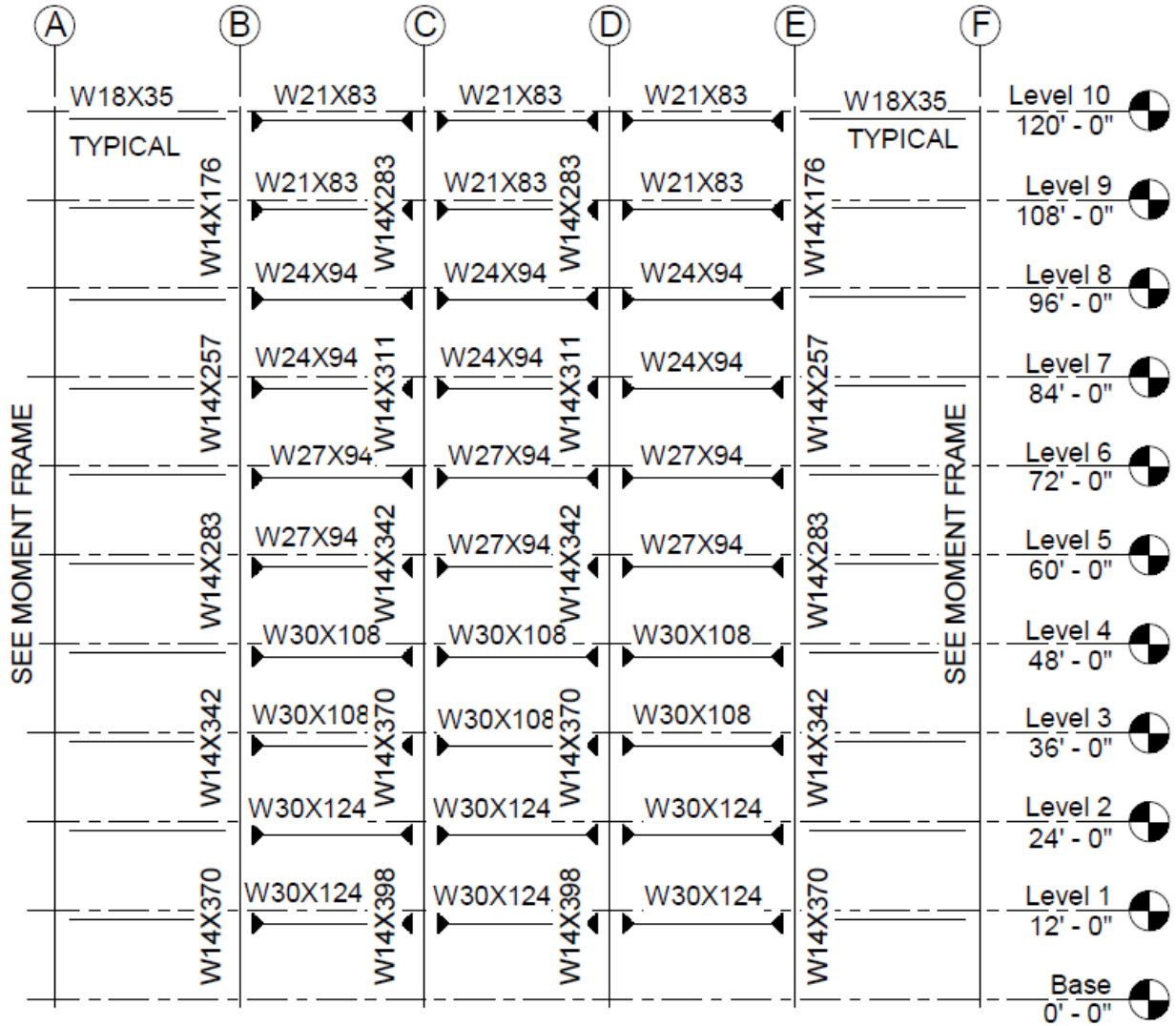


Figure 4.6 Moment frames in Los Angeles building at gridlines 1 and 4

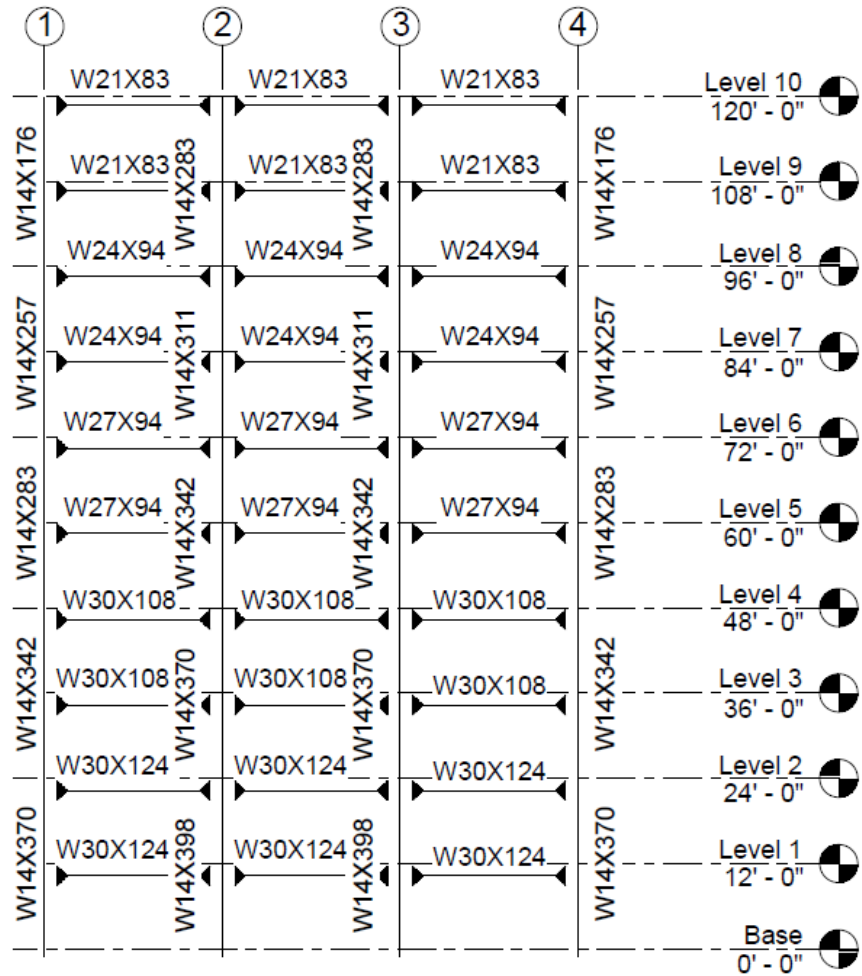


Figure 4.7 Moment frames in Los Angeles building at gridlines A and F

Table 4.3 SFRM thicknesses per prescriptive approach

	Member Size	W/D2 (actual)	Test Designation	W/D1 (test)	Test Thickness, in	SFRM Thickness Required, in (mm)
Beams	W14x22	0.534	D902	0.82	0.38	1/2 (12)
	W18x35	0.672	D902	0.82	0.38	3/8 (10)
	W18x50	0.880	D902	0.82	0.38	3/8 (10)
	W18x60	1.04	D902	0.82	0.38	3/8 (10)
	W21x93	1.40	D902	0.82	0.38	3/8 (10)
Columns	W8x24	0.591	X772	R-equation		13/16 (21)
	W12x45	0.83	X772	R-equation		11/16 (18)
	W12x58	0.925	X772	R-equation		11/16 (18)
	W14x53	0.92	X772	R-equation		11/16 (18)
	W14x99	1.181	X772	R-equation		9/16 (15)
	W14x109	1.29	X772	R-equation		9/16 (15)

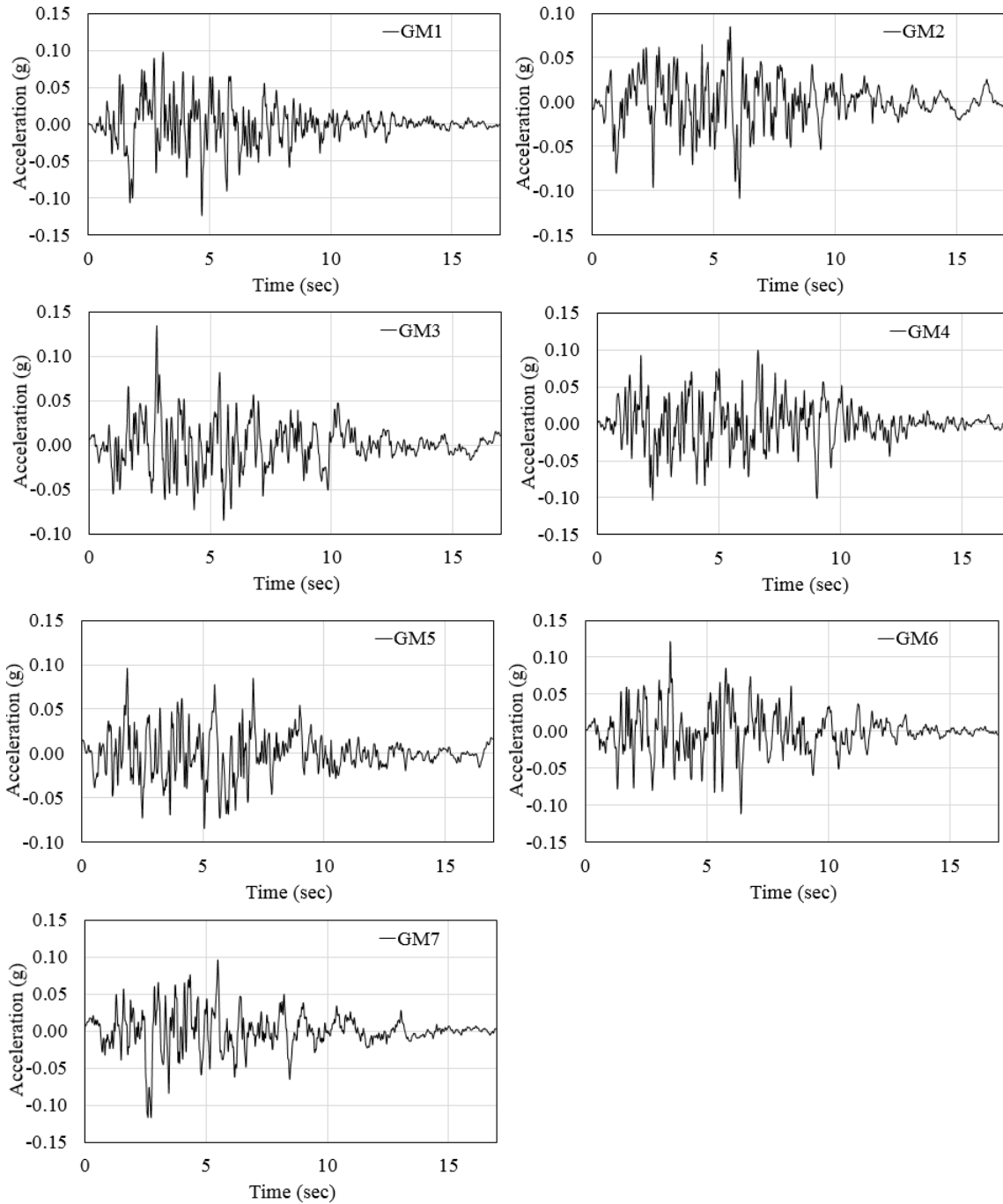


Figure 4.8 Seven ground motion acceleration time histories for Chicago building

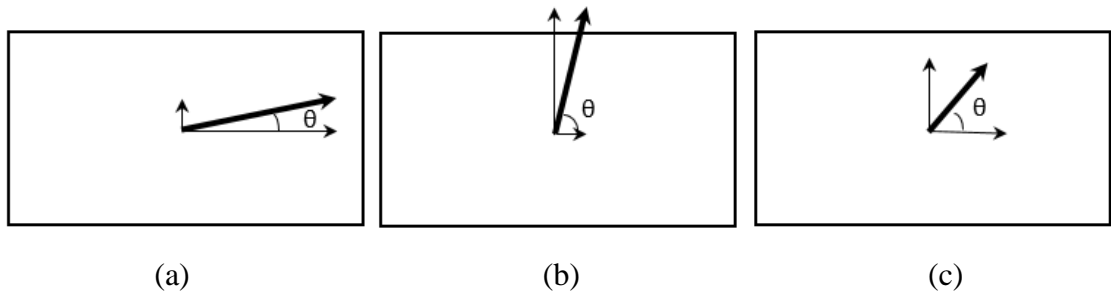


Figure 4.9 Orientations of ground motions to determine orthogonal components
(a) $\theta = 5^\circ$, (b) $\theta = 85^\circ$, (c) $\theta = 45^\circ$

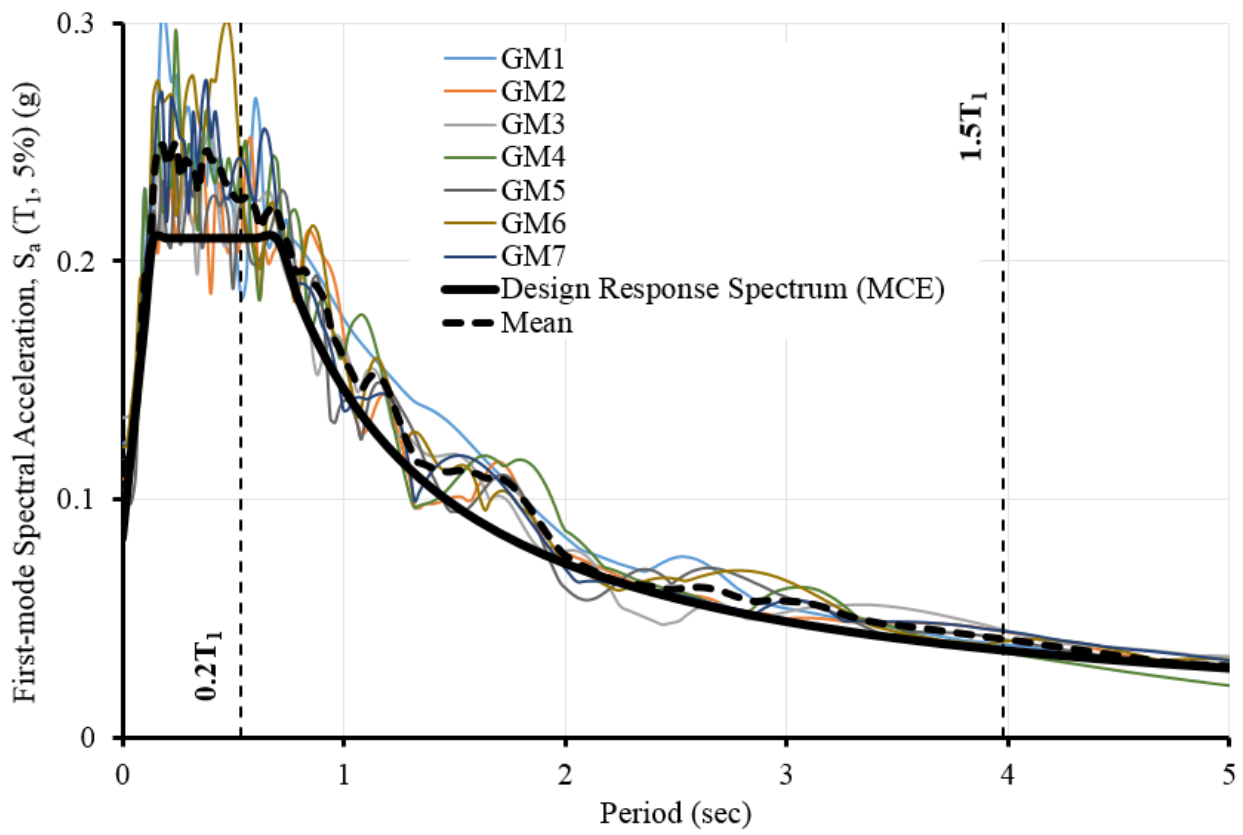


Figure 4.10 Chicago building design response spectrum with ground motions overlaid

Table 4.4 Design locations and hazard scenarios in parametric study

Record #	Event Name	Station Name	Year	Magnitude	Scale Factor
1	Imperial Valley-02	El Centro Array #9	1940	6.95	2.1
2	Kern County	Taft Lincoln School	1979	7.36	3.0
3	San Fernando	Castaic – Old Ridge Route	1971	6.61	3.3
4	Imperial Valley-06	Aeropuerto Mexicali	1989	6.53	2.5
5	Mammoth Lakes-02	Mammoth Lakes H.S.	1994	5.69	3.8
6	Loma Prieta	Palo Alto – SLAC Lab	1952	6.93	2.0
7	Northridge	Santa Monica City Hall	1980	6.69	2.4

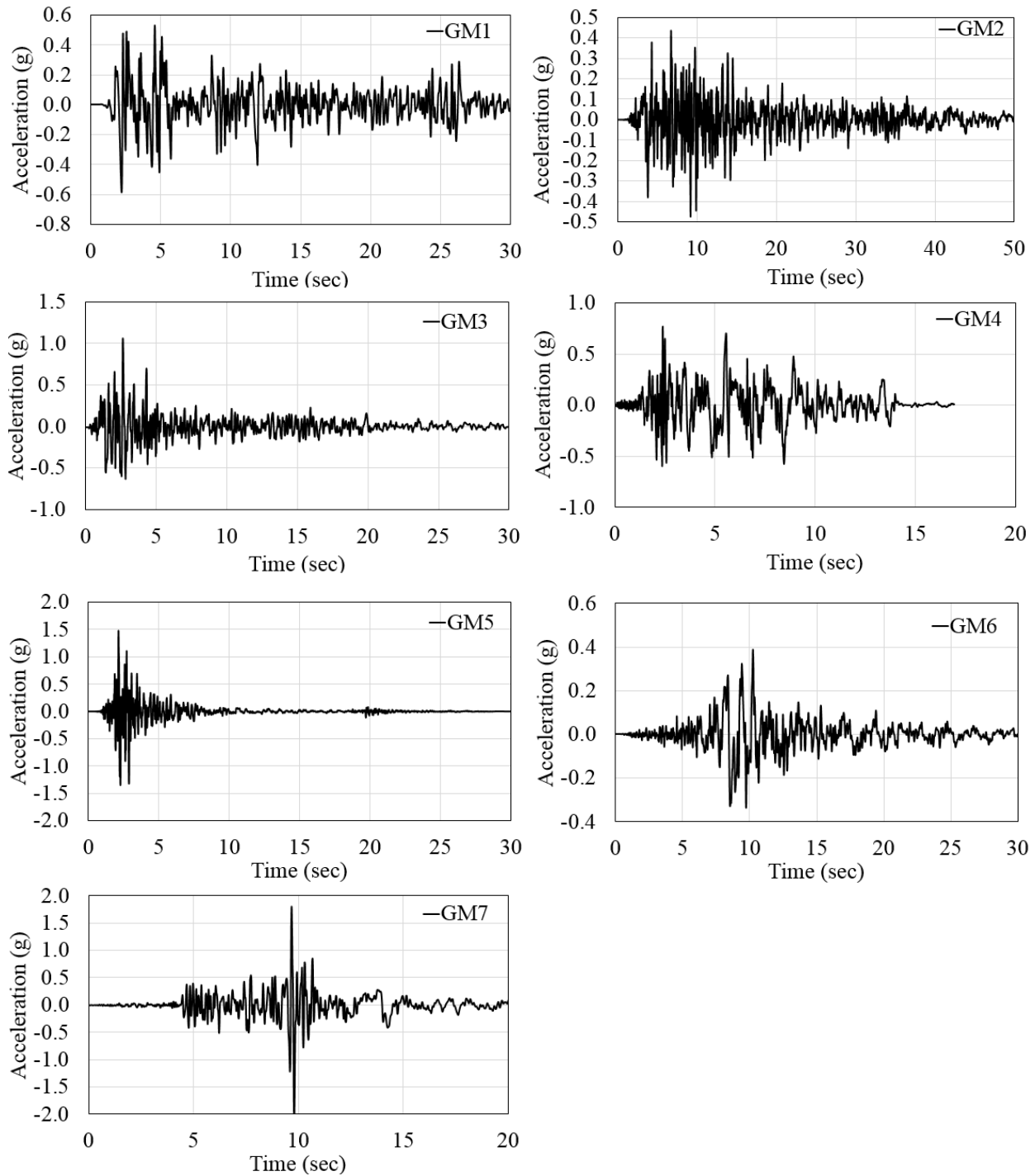


Figure 4.11 Seven selected ground motion acceleration time histories used for Los Angeles building (Longitudinal building direction)

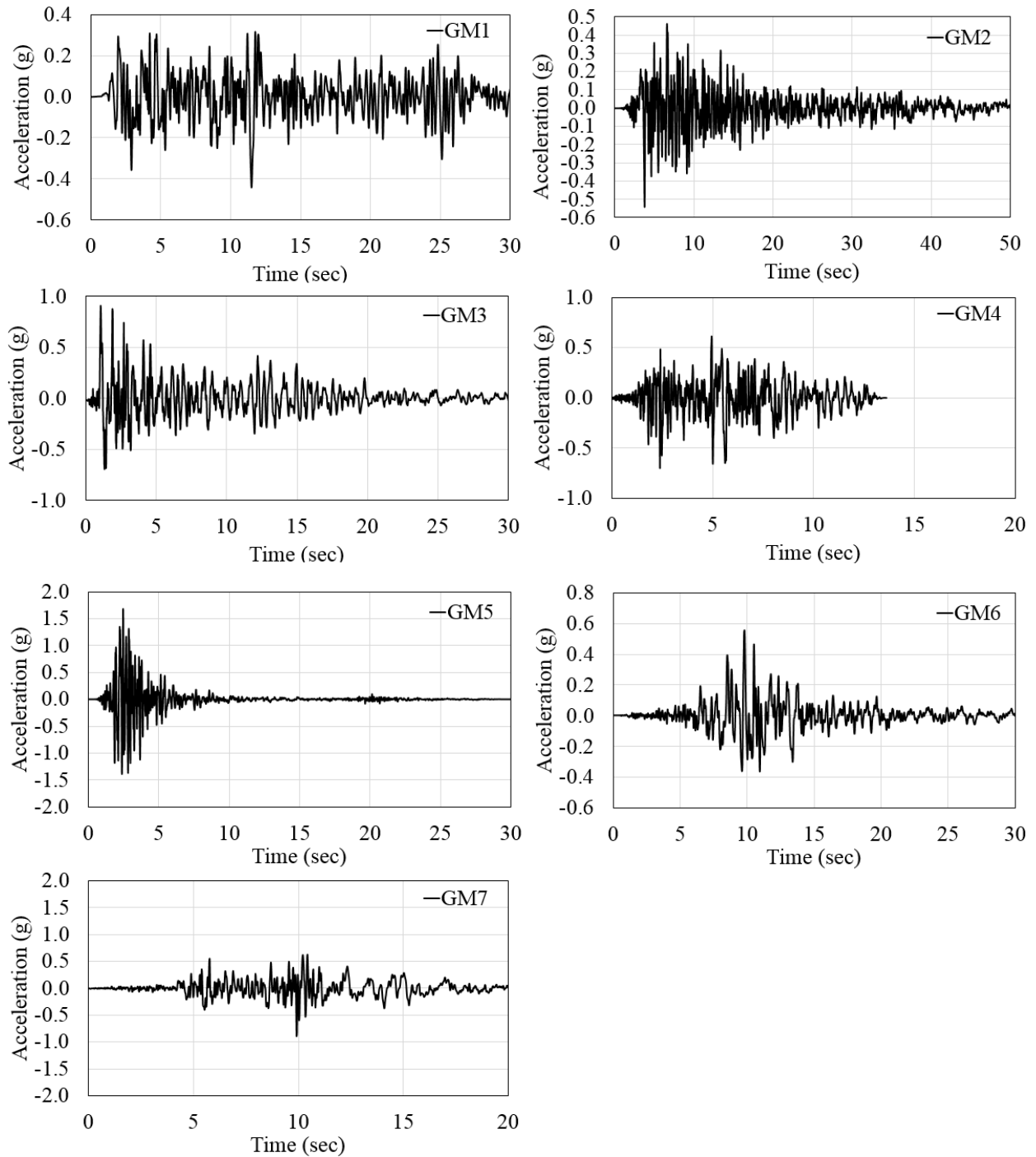


Figure 4.12 Seven selected ground motion acceleration time histories used for Los Angeles building (Transverse building direction)

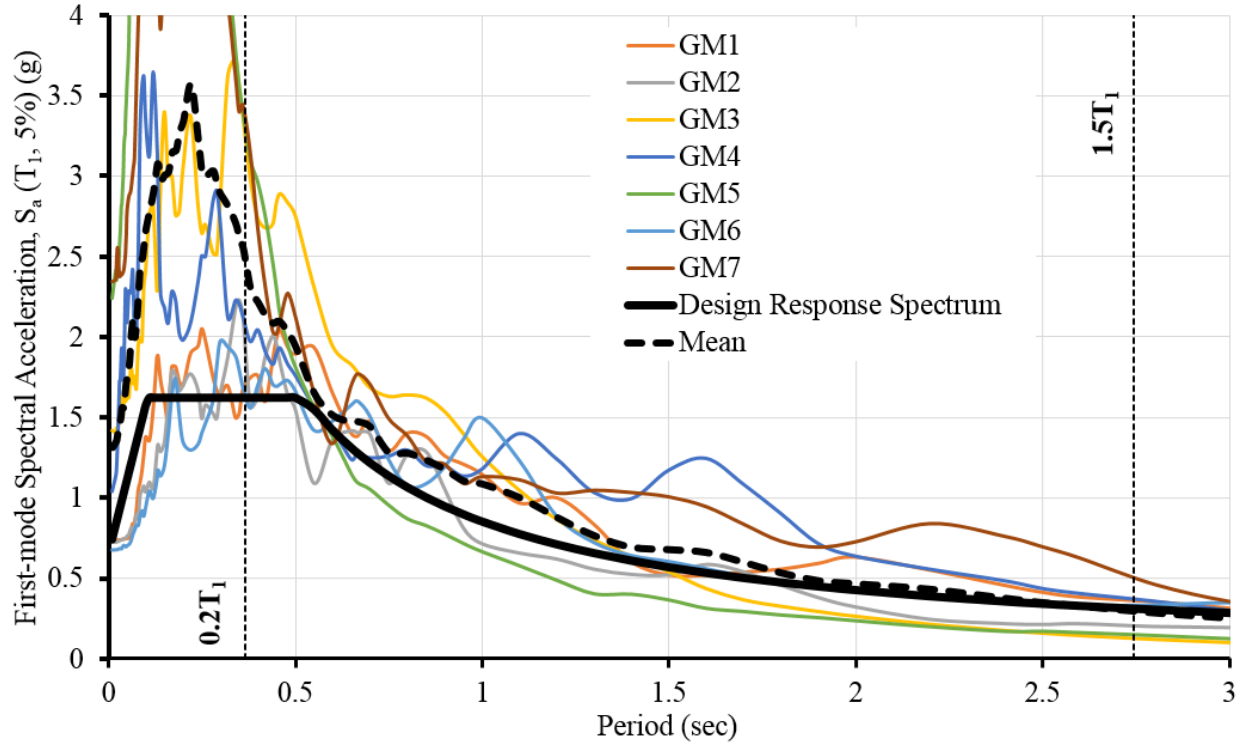


Figure 4.13 Los Angeles building design response spectrum with ground motions overlaid

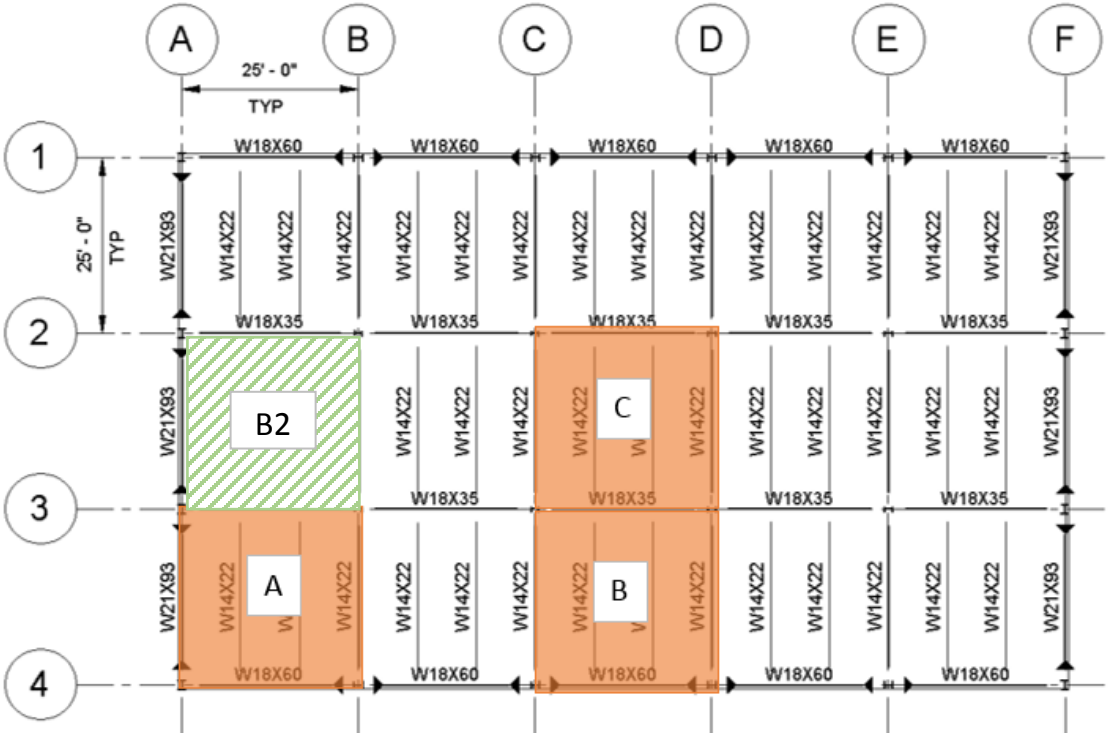


Figure 4.14 Compartment fire designations and locations

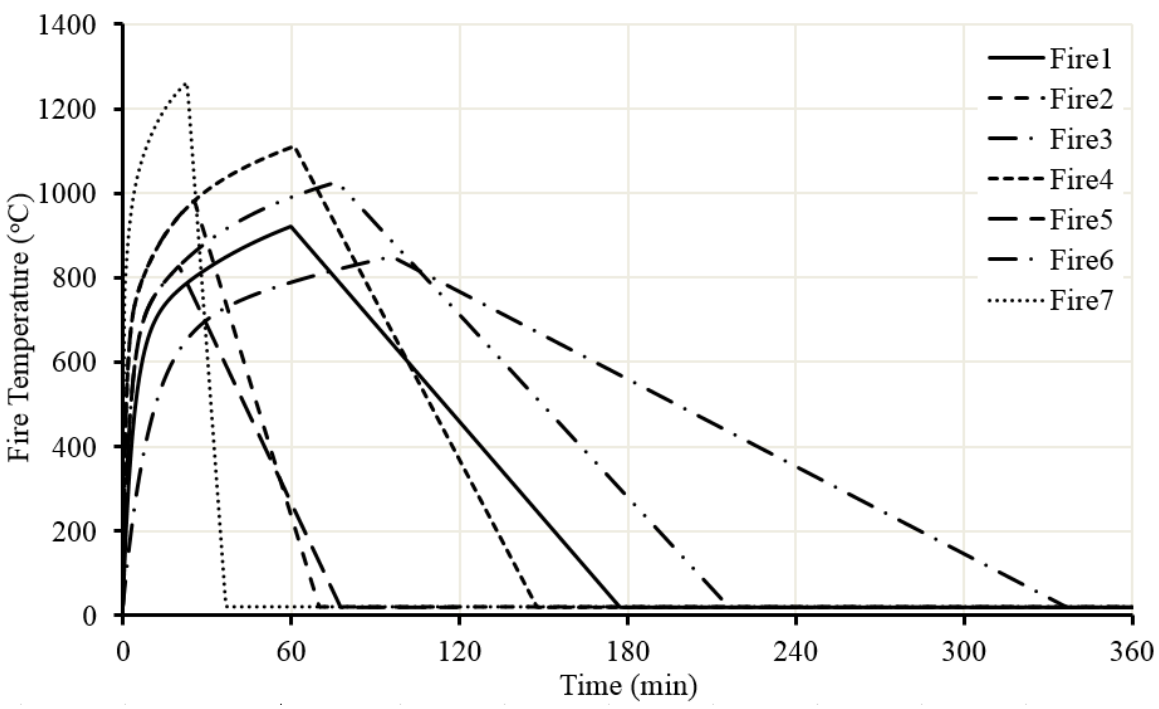


Figure 4.15 Parametric time-temperature curves selected for analyses

Table 4.5 Eurocode fire parameters to generate time-temperature curves

Fire #	Opening Factor, O	Thermal property of enclosure, b	Fire growth rate, t_{im}	Fire load density at floor, q_{fd}	Fire load density, q_{td}
1	0.032	1000	0.333	627	160
2	0.06	1000	0.333	500	128
3	0.02	1000	0.333	627	160
4	0.06	1000	0.333	1200	306
5	0.04	1000	0.333	200	51
6	0.04	1000	0.333	1000	255
7	0.16	1000	0.333	1200	306

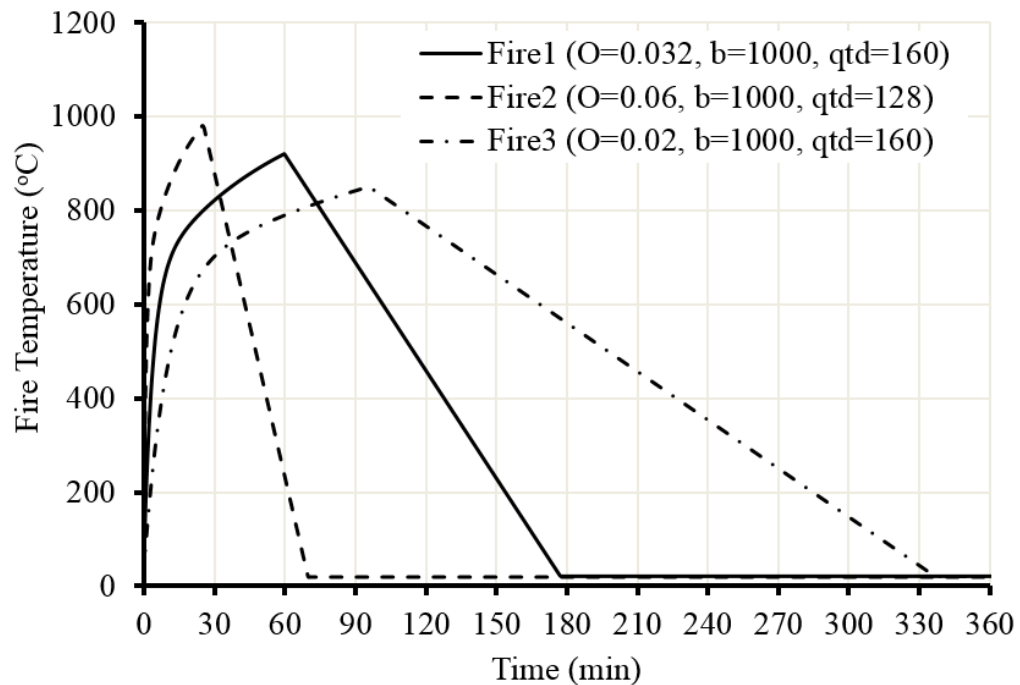


Figure 4.16 Final 3 parametric time-temperature curves used in analyses

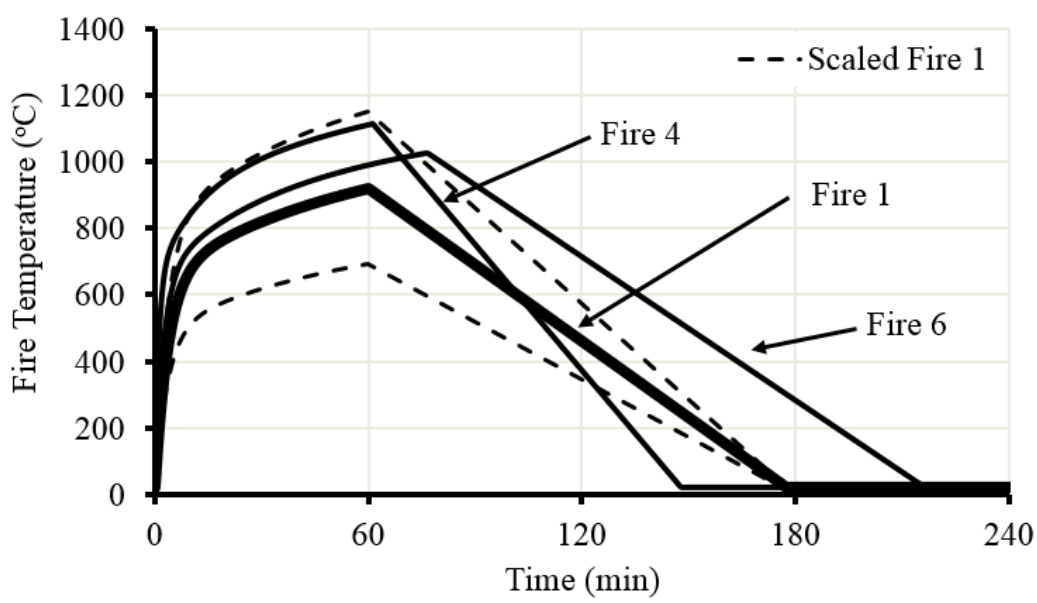


Figure 4.17 Parametric time-temperature curves used in analyses with scaled Fire 1

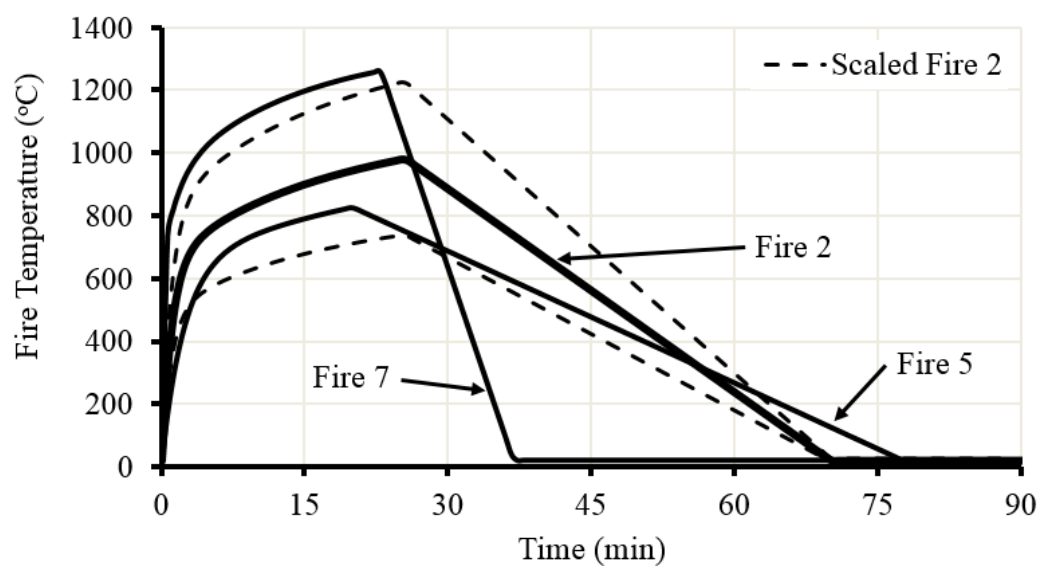


Figure 4.18 Parametric time-temperature curves used in analyses with scaled Fire 2

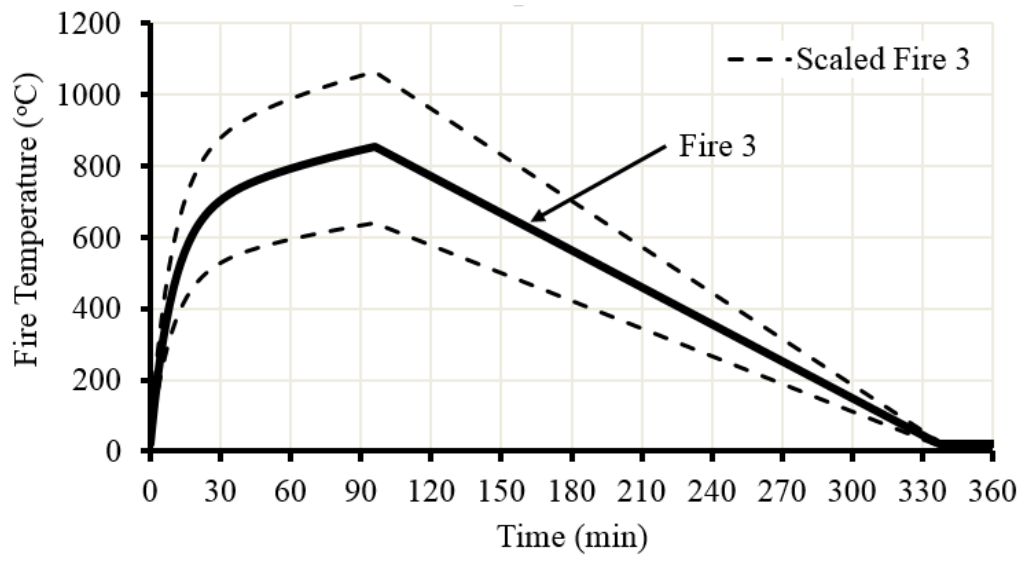


Figure 4.19 Parametric time-temperature curves used in analyses with scaled Fire 3

Table 4.6 Eurocode fire parameters to generate time-temperature curves

Fire #	Peak Fire Temperature (°C)	Area under the curve (min °C)
1	921	101,435
4	1112	107,938
6	1025	137,161
2	980	43,520
5	825	33,532
7	1261	34,272
3	851	172,064

Table 4.7 Mean wind speeds at each story for Chicago building

Story	1	2	3	4	5	6	7	8	9	10
Mean Wind Speed (m/s)	14.1	16.7	18.5	19.9	21.1	22.0	22.9	23.7	24.4	25.0

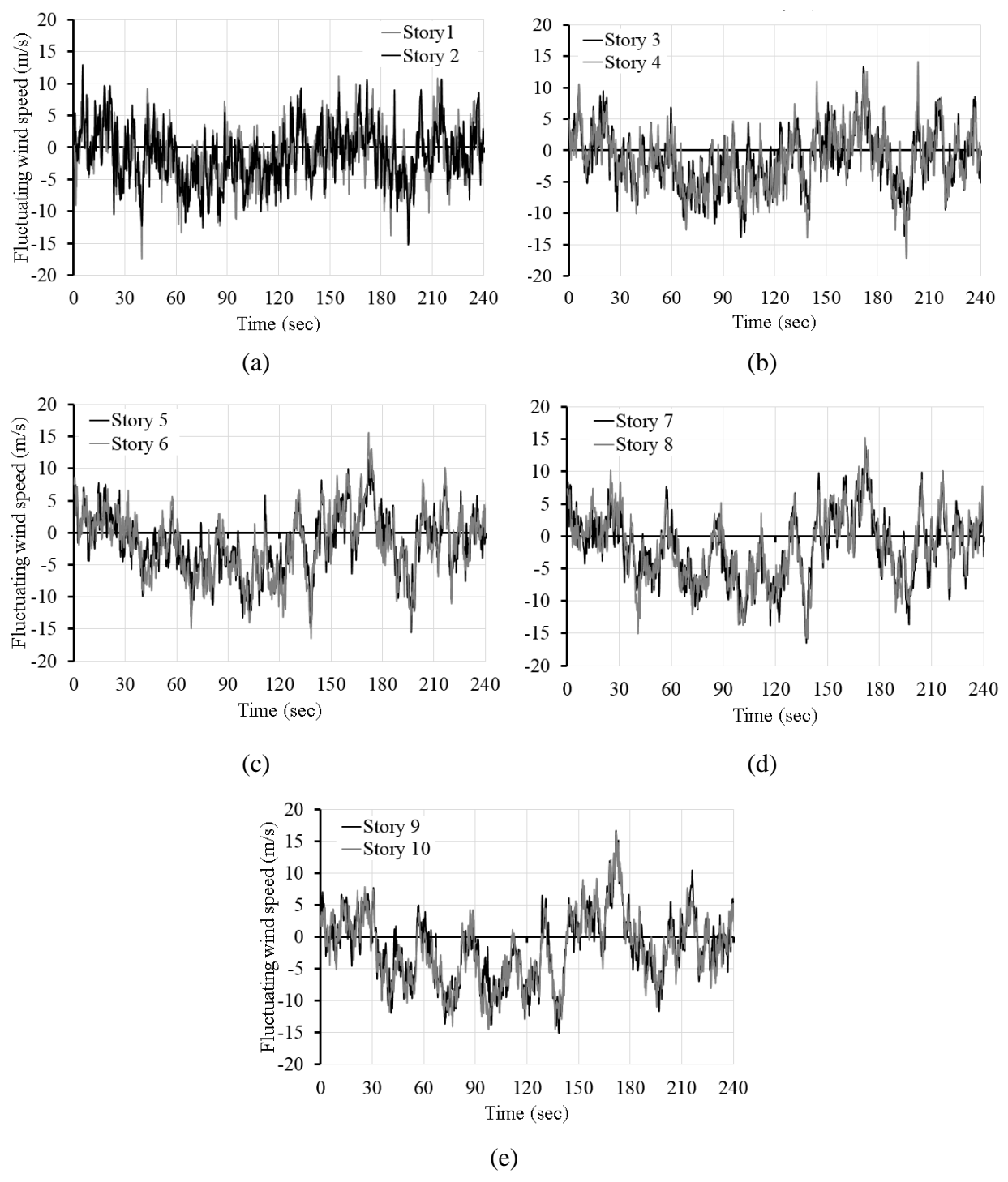


Figure 4.20 Fluctuating wind speed time histories at each story for Chicago building

Table 4.8 Mean wind speeds at each story for Los Angeles building

Story	1	2	3	4	5	6	7	8	9	10
Mean Wind Speed (m/s)	15.6	18.6	20.6	22.1	23.4	24.5	25.4	26.3	27.1	27.8

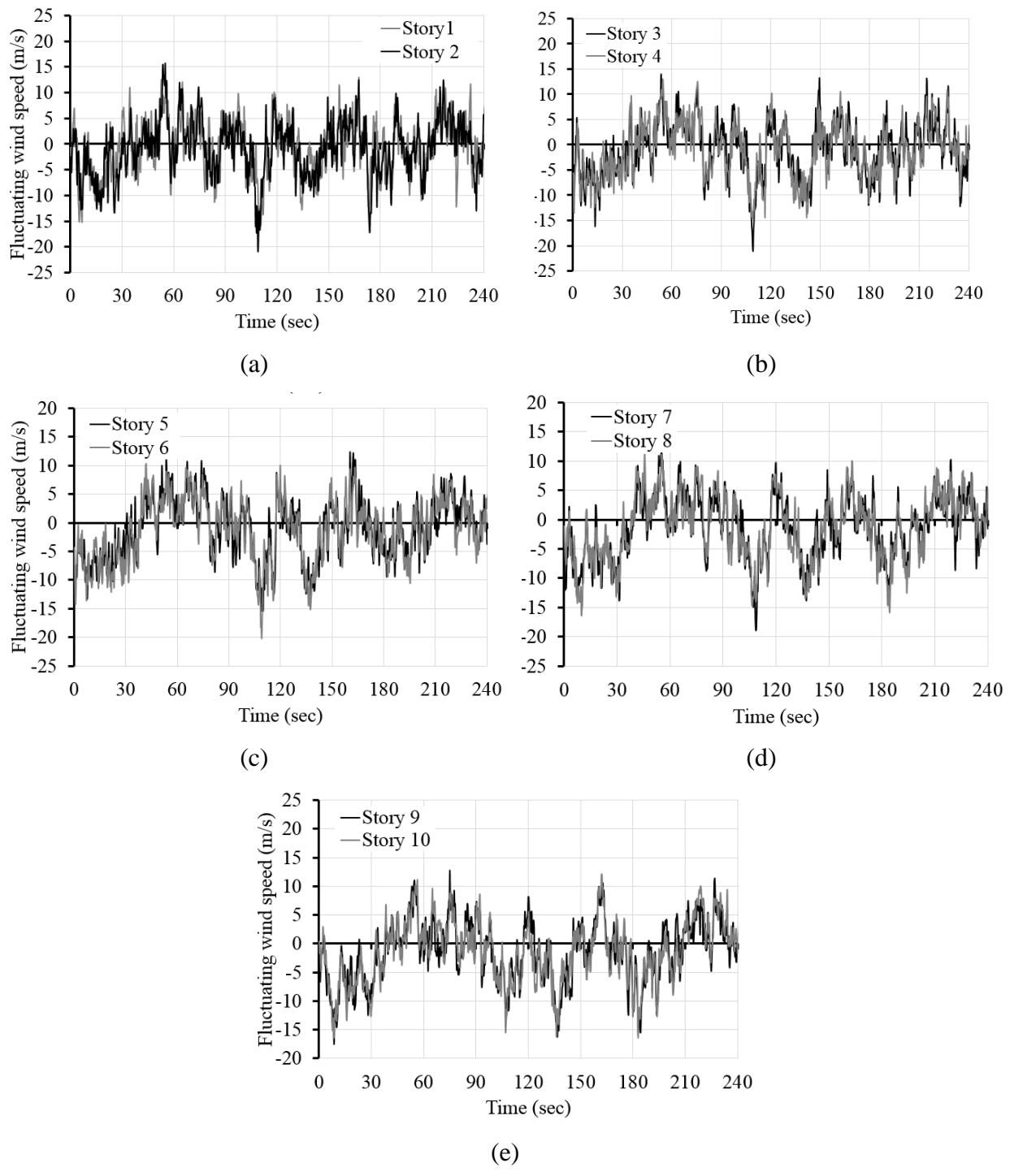


Figure 4.21 Fluctuating wind speed time histories at each story for Los Angeles building

CHAPTER 5. BUILDING MODELING AND ANALYSIS APPROACH

ABAQUS [112], a commercially available finite element method software, was used to develop three-dimensional (3D) models of the two case study building structures. These nonlinear inelastic models were created in order to simulate inelastic deformations, instability failures, connection damage at elevated temperatures, and the effect of temperature on material strength and stiffness. These models provide a way to assign time history records and temperature changes directly to the model in order to analyze the effects of seismic and fire hazards in a more sophisticated manner than traditional, simplified methods.

The modeling approach was adapted from Agarwal [15], who created the building model to analyze the structure subjected to compartment fires. Modifications were made to the original model in order to avoid over-constraints and produce reasonable results when subjected to ground motions. This chapter summarizes the various aspects of the model.

5.1 Modelled Elements

The beams and columns are modeled using 2-node B31 beam elements. This is a one-dimensional line element that is an approximation of a 3D solid element using Timoshenko beam theory. This approximation was beneficial in place of 3D solid elements because of the simplicity and efficiency of beam elements and the complexity and size of the model. However, there are limitations to using this type of element. Local buckling and lateral torsional buckling, as well as distortion of the shape, cannot be captured through this modeling approach. Because this project attempts to understand overall building behavior from multiple hazards, it was deemed acceptable to use beam elements.

The composite slab was modeled using S4R shell elements, which is a 4-node, reduced integration shell element commonly used for general-purpose applications. The composite slab is conservatively modeled as 2 1/2" thick light-weight concrete, to match the concrete above the deck flutes. The steel deck is idealized as rebar embedded in the slab, using the built-in embedded rebar option in ABAQUS. The rebar area matches the area of the steel deck and is applied only in the strong direction of the deck. The welded wire fabric in the slab, used to prevent cracking, was also idealized as embedded rebar.

When analyzing building response to high seismic events, large plastic strains were observed at the slab edges, resulting in slab failure. This was due to diaphragm failure. The diaphragm design was checked and found to be sufficient. However, because of the simplifying assumption of modeling only the topping slab, diaphragm failure was observed during some of the high intensity seismic events. To remedy this issue, a 3 ½” slab was assigned to the perimeter at a distance of 30” from the slab edge. Three #5 steel reinforcing bars were also assigned along the perimeter to assist with transferring diaphragm forces, a method commonly used in engineering practice.

The shear studs, which transfer forces between the slab and beams, are modeled using rigid connectors and spaced at about 30” intervals. A schematic of the modeling approach for the composite floor system is shown in Figure 5.1. It is acknowledged that studs do not actually behave as rigid connectors; instead, studs may deform and concrete may crush, causing slip. Ideally, this force-slip behavior should be captured through a user-defined connector element especially since this behavior is highly temperature-dependent [65]. The author explored implementing force-slip behavior into the shear connector model; however, with the current modeling approach, the connector length is not accurate because it connects from the beam centerline to the center of the shell element, as shown in Figure 5.1. In order to accurately model the shear stud length, a number of rigid offsets would be needed which could cause instabilities in the model. It was decided that this level of complexity is not necessary for this project, which focuses on better understanding global response. The rigid connectors were removed within the protected zones of the Special Moment Frame connections of the Los Angeles building.

Initial imperfections and notional loads were not applied to the model to simulate P-Δ effects. The notional load approach (Direct Analysis Method) in Appendix 7 of the AISC Specification [48] is intended for linear static procedures as a way to account for nonlinearity in the structure. It is not applicable to this model.

5.2 Modelled Connections

The simple (shear) connections in the building were modeled as shear-tab connections using wire connector elements that include the axial force-axial displacement-moment-rotation-temperature behavior, based on work by Sarraj [113] and Agarwal [15]. One equivalent connector element was determined for each gravity connection through detailed finite element modeling subjected to a variety of displacement-rotations. No modifications were made to the connection models by

Agarwal. A schematic of the connection is shown in Figure 5.2. For more details about these connections, refer to Agarwal [69].

The perimeter of the building consists of moment frames with fixed beam-to-column connections. These connections were modeled as rigid connectors (which cannot fail) in the Agarwal [15] model, which only considered fire hazards. This simplification was justified based on work by Yang et al. [49] which found through experimental testing that the tested moment connections maintained design strength up to 650°C and stiffness decreased by only 25%.

As the Northridge and Kobe earthquakes showed, moment framed buildings can often experience moment connection failures due to seismic events. Following these events, however, more stringent detailing requirements were implemented to prevent these types of failures. The author explored incorporating rotational springs at beam-to-column moment connections in order to capture nonlinear behavior and potential failure of connections. However, ABAQUS connectors seem to be limited in cyclic capabilities. These connectors do not load and unload in a traditional hysteresis loop. The connector options currently available in ABAQUS do not appear to have a way to properly simulate the cyclic behavior of moment frame connections. For this reason, the moment connections are modeled as rigid connectors. It is presumed that the connections were designed with adequate strength and ductility to withstand failure up to the rotation limits specified in AISC 341 [11]. With this assumption, the rotations at the joints are tracked to assess connection failure. Fracture is incorporated into the material model to represent connection failure at large rotations, as described in the following section. To simulate connection failure from an earthquake event, welded connectors were removed in the fire model at locations where fracture had occurred.

5.3 Material Models

ABAQUS has an extensive library of material models, which account for temperature changes. The structural framing members are ASTM A992 steel. Reduction factors provided in Table 3.1 of Eurocode 3 [114] were used to scale steel properties by temperature level. Both elastic behavior (Young's Modulus) and inelastic behavior with isotropic hardening are temperature dependent. Coefficients of expansion were also input at different temperatures. Figure 5.3 illustrates the degradation of stiffness for steel and concrete as temperatures increase. Figure 5.4 shows the true stress-plastic strain curves for the steel as temperatures change.

Ductile damage is incorporated into the steel material model in order to capture fracture at high interstory drift ratios. The Seismic Provisions for Structural Steel Buildings (AISC 341) [11] indicate that beam-to-column connections in Special Moment Frames must accommodate a story drift ratio of at least 0.04 radians. Thus, for the Los Angeles building, which was designed with Special Moment Frames, fracture strain is specified as 0.02 mm/mm with the presumption that fracture will occur at a drift ratio of 0.04. This is determined based on the geometric relationship between drift and curvature:

$$\varepsilon_p = \theta_p / 2 \quad \text{Equation 5-1}$$

where ε_p is the plastic strain and θ_p is the plastic rotation causing a hinge mechanism. AISC 341 [11] does not specify story drift angle requirements for connections in Ordinary Moment Frames. A drift ratio limit of 0.02 was selected for the Chicago building. This is the allowable drift limit for design per ASCE 7 [5]. FEMA 355D shows a range of plastic rotations before failure for moment frame connection tests. For post-Northridge type connections, failures tended to occur in the range of 0.01 to 0.04 radians.

The material model for concrete is based on two failure mechanisms: tensile cracking and compressive crushing. ABAQUS provides a built-in concrete damaged plasticity model which predicts this behavior. Figure 3.2 in Eurocode 4 [115] provides the stress-strain relationship of concrete subjected to compression at temperatures 20°C to 1200°C. This relationship is shown in Figure 5.5.

5.4 Damping Considerations

Understanding the damping of building structures is very complex because of all of the factors that influence the structural response (i.e.: stiffness assumptions, nonstructural elements, energy dissipation from steel connections or opening and closing of cracks in concrete, etc.). Forced harmonic vibration tests can be used on building structures to better understand damping behavior but these tests are relatively infrequent [116]. Instead, simplified methods are typically employed. Rayleigh damping is a commonly used approach for estimating the damping behavior of building structures, which uses mass-proportional and stiffness-proportional damping coefficients:

$$c = a_0 m + a_1 k \quad \text{Equation 5-2}$$

where c = viscous damping coefficient, a_0 = mass-proportional damping coefficient, m =mass matrix, a_1 =stiffness-proportional damping coefficient, k =stiffness matrix.

This results in the following equation using the damping ratio, ζ_n for the n th mode:

$$\zeta_n = \frac{a_0}{2} \frac{1}{\omega_n} + \frac{a_1}{2} \omega_n \quad \text{Equation 5-3}$$

Using only the modes that contribute to 90% modal participation, a_0 and a_1 can be calculated. Figure 5.6 illustrates Rayleigh damping for the Los Angeles building, where $a_0=0.255$ and $a_1=0.0075$. Between the first and fifth mode, damping is conservatively approximated, as it falls below the specified damping ratio. Beyond the fifth mode, however, the damping approximation is not conservative. Rayleigh damping is based on the initial linear stiffness of the structure; thus, when nonlinearity occurs, it is possible that damping is unrealistically large [117].

It is important to note that work by others [118] has shown that Rayleigh damping is not a realistic approximation. Instead, using effective damping ratios based on the dynamic response of actual building structures is more realistic. However, because Rayleigh damping is the industry accepted approach for estimating damping, it is used for this project. The following work incorporated Rayleigh damping with these assumptions:

[119] 12-story SCBF with 2% damping ratio used at 1st and 5th modes

[120] 20-story MRF building with 2.3% damping ratio used at 1st and 5th modes

[13] 4-story SC-MRF 2% and 5% damping ratio used at 1st and 3rd modes

[121] 3-story MRF at 4.3%, 9-story MRF at 3.6%, and 20-story MRF at 2.3% damping ratios

When determining the beta factor necessary for Rayleigh damping of 5%, this value caused a very small stable time increment in the explicit analyses, making it impossible for the model to converge. For this reason, a smaller beta factor was assigned (at 1/1000th of the initial beta factor) in order to scale up the stable time increment to a computable value. This causes the damping to behave more closely to the “Mass Contribution” line in Figure 5.6. This results in damping of the analytical structure that is less than the specified damping ratio of 5%. However, this was deemed acceptable because 2% damping is used often. For this project, 5% was chosen based on the earthquake forces and design spectrum per ASCE 7-10 [5]. A similar approach is explained in Chen et al. [122, 123], which uses Rayleigh damping with a very small beta factor to keep the time

increment at a reasonable value to be able to analyze a ten-story concrete structure subjected to ground motions. Damping is defined within ABAQUS as a material property.

5.5 Seismic Model vs. Fire Model

The previously mentioned gravity connector elements caused strange behavior in the fire following seismic loading step. It appears that the connectors remained excited even after the structure had stopped moving and subsequent steps caused excessive deformations of these connectors. To remedy this issue, during the seismic loading step, idealized pinned connections were used instead of the previously mentioned equivalent gravity connectors. Again, this is due to the uncertainty in cyclic behavior of these connectors. Work by Chi et al. [23] showed that the gravity frame contribution to the lateral stiffness of the structure was primarily attributed to the gravity columns themselves and not the gravity connections and, thus, this was viewed as an adequate simplification to the model. The results of this seismic model were then imported into a new fire model which introduced the gravity connectors. Mass scaling could also be introduced in the fire model to make the analyses run more efficiently.

As shown previously in Figure 5.1, rigid connectors were necessary to account for the difference in centerline elevation of beams framing into girders. This resulted in a large number of connectors throughout the building. For the purposes of model simplicity and efficiency, these elevation variations were only modeled at the level exposed to fire. At the other levels, the gravity framing members were all modeled at the elevation of the moment frame members.

5.6 Application of Seismic Hazard

Ground motion was applied as a displacement time history by assigning horizontal displacement constraints to the bases of all of the columns. The author could not determine a way to assign an acceleration while also restraining the column bases in place, so the column bases move. This means that displacements must be subtracted by the base displacement to obtain the relative displacements. Most of the earthquake records being used in this project are less than 20 seconds long; however, the model would often have to run for 1.5 to 3 times the record length in order to allow ample time for the building to become stationary again. This can be a time-intensive procedure. The time step was, therefore, minimized as much as possible.

The load combination used to simulate the seismic hazard is:

$$(1.2+0.2S_{DS})D+\rho Q_e+0.5L+0.2S \quad \text{Equation 5-4}$$

S_{DS} is defined and calculated in ASCE 7 [5] as the design 5 percent damped spectral response acceleration parameter at short periods. ρ is the building redundancy, which is assumed to be 1.0. Q_e is the earthquake load, L is the live load, and S is the snow load. Due to an absence of vertical ground motion information, the effect of vertical accelerations is applied through the $0.2S_{DS}$ portion of the load combination. Live load reduction was not applied to the ABAQUS model due to the variability in reduction factors for different elements and locations throughout the structure.

5.7 Application of Fire Hazard

Three previously described parametric time-temperature curves (Figure 4.16) are used to represent a short, medium, and long duration fire. These curves provide the air temperatures within the affected compartment over time. In order to determine the internal temperatures of the structural members throughout each cross-section, ABAQUS was used to conduct 2D heat transfer analyses. The cross-section of each member in the fire compartment was modeled as a 2D part and exposed to each parametric time-temperature curve. Fireproofing was modeled at the thickness required to achieve the designated fire resistance rating, as described in Section 4.1.4. The following material properties were defined for each of the material types (steel, concrete and insulation) in order to model the thermal transfer of heat from the gas to the structural component: thermal expansion, specific heat, thermal conductivity, and density.

Figure 5.8(a) shows an example of the heat transfer analyses. Nodal temperatures are recorded at five locations along the wide-flange section (flange edges and center of web). These nodal temperatures are then input into the building model at five minute intervals. Figure 5.7 shows the distribution of temperatures along a wide flange cross-section using the 5 integration points shown. There is a linear interpolation along the beam flanges between points 1 and 2, and between points 4 and 5. Temperatures along the web are parabolically interpolated temperatures along the slab. Heat transfer for the composite slab is recorded at 5 locations along the thickness of the slab. Because only the top 2½” of slab is modeled in the building model, only temperatures within the top 2½” of the cross-section are recorded. These 5 integration points (shown in Figure 5.8(b)) are input into the building model and are linearly interpolated between points. At locations where there

is a beam directly below the deck (as illustrated in Figure 5.8(a)), the temperatures are recorded at 5 equally spaced points as shown. At locations where there is not a beam located directly below the deck (as illustrated in Figure 5.8(b)), temperatures are recorded at both a location with the flute and one without the flute. These temperatures are then averaged together to represent the temperature variations across the slab thickness.

Some results of heat transfer analyses conducted on a W14x22 composite beam section with fire protection (1 hr FRR) are shown in Figure 5.9 through Figure 5.11. Figure 5.9 shows the time-temperature relationship when exposed to Fire 1. Figure 5.10 and Figure 5.11 show the response when subjected to Fire 2 and Fire 3, respectively. As can be seen by the graphs, the fireproofing delays the rise in steel temperature. The composite slab heats even more slowly, due to the low thermal conductivity of concrete. In all cases, the bottom flange reaches the highest temperature. The top flange reaches significantly lower temperatures because it releases heat to the adjacent composite slab. Though Fire 2 has the highest peak temperature, the steel beam and concrete slab do not reach internal temperatures as high as Fire 1 and Fire 3. This is because Fire 2 heats very quickly and then cools quickly. The slow heating rate of Fire 3 causes the highest temperatures in the structural members.

After the temperatures are recorded at 5 minute intervals for each integration point, these temperatures are input into the building model. The load combination for the fire analysis is taken from the AISC Specification, Appendix 4 (Section 4.1.4) [48]. It also corresponds with the load combination for extraordinary events in ASCE 7 [5]. The load combination is:

$$1.2D+A_T+0.5L+0.2S \quad \text{Equation 5-5}$$

A_T is defined as the nominal forces and deformations due to the design-basis fire. These forces and deformations are captured by assigning temperatures and temperature-dependent properties to each of the affected members.

5.8 Application of Wind Hazard

Wind load was applied as a force time history to each story. It was presumed that the structural system (i.e. – girts, exterior façade details) was detailed properly to adequately distribute loads from the façade to the building diaphragm at each level. With this assumption, the drag force at each story was distributed across the diaphragm as a body force. The wind pressure at each story

was converted into the drag force by multiplying by the tributary area. This is calculated as the length of the building face that is perpendicular to the wind direction times the tributary height of that story. Tributary height is one half of the story height above and below the story. For this study, wind was applied perpendicular to the long side of the building. The load combination for ASCE 7-10 is given by:

$$1.2D+1.0W+L+ 0.5L_r \quad \text{Equation 5-6}$$

where D is the dead load, W is wind load calculated from a strength based wind approach, L is live load and L_r is roof live load. Because the NatHaz On-line Wind Simulator [109] used values from ASCE 7-98, the load combination from ASCE 7-98 was used instead:

$$1.2D+1.6W+0.5L+ 0.5L_r \quad \text{Equation 5-7}$$

W in this equation is based on a basic wind speed that is serviceability-based and, thus, a lower value than provided in the wind maps of ASCE 7-10.

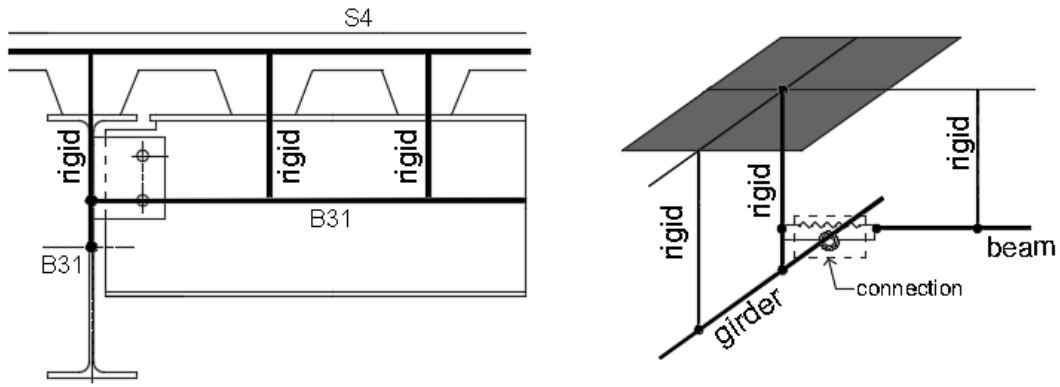


Figure 5.1 Schematic of modeling approach for composite floor system [15]

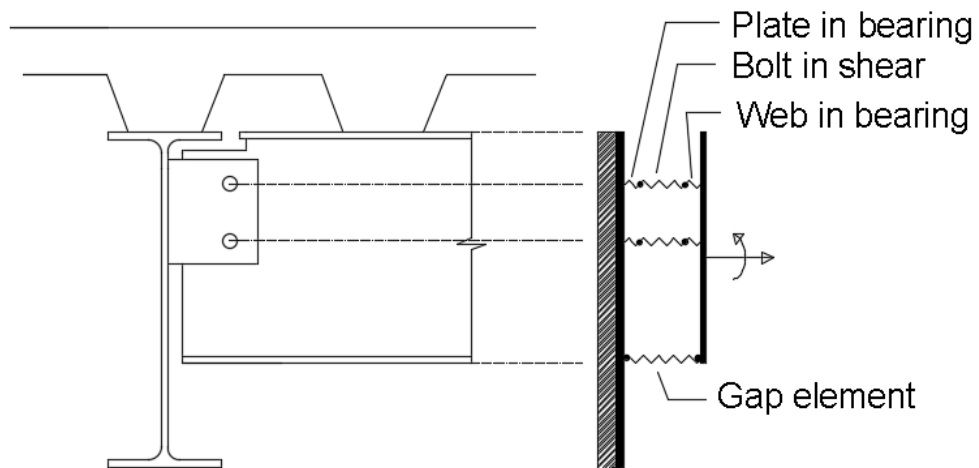


Figure 5.2 Schematic of gravity connection macro model for equivalent gravity connector [15]

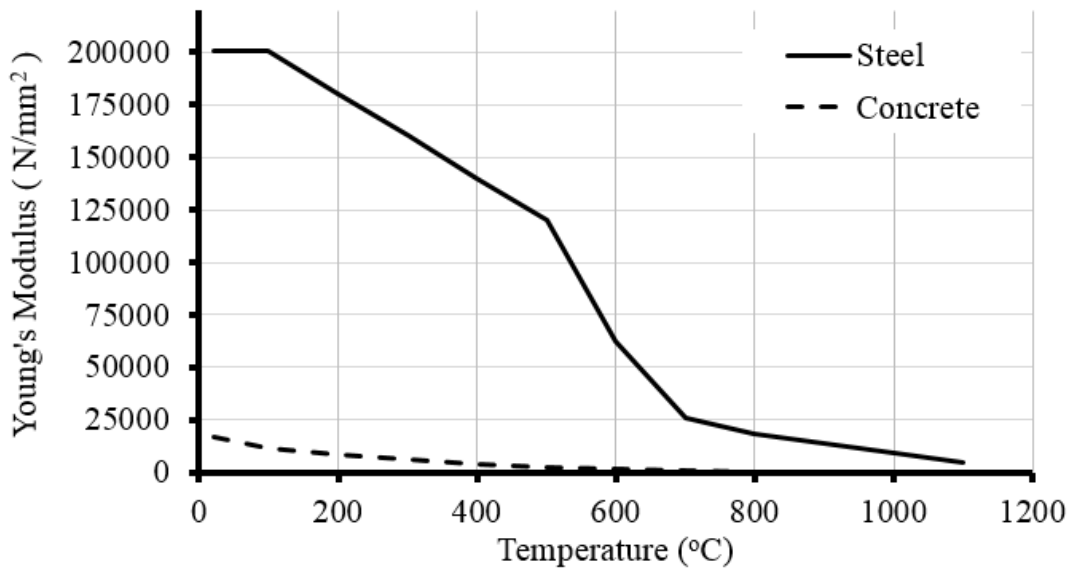


Figure 5.3 Young's modulus vs. temperature relationship

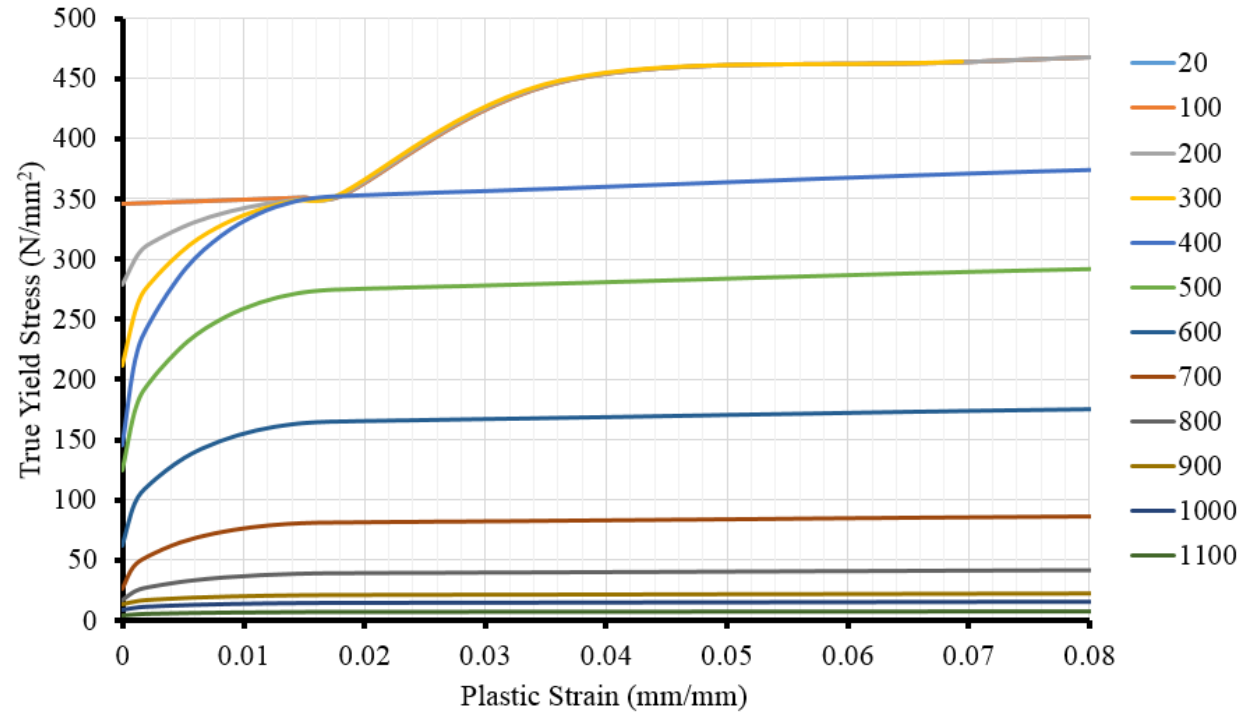


Figure 5.4 Steel true yield stress vs. plastic strain relationship

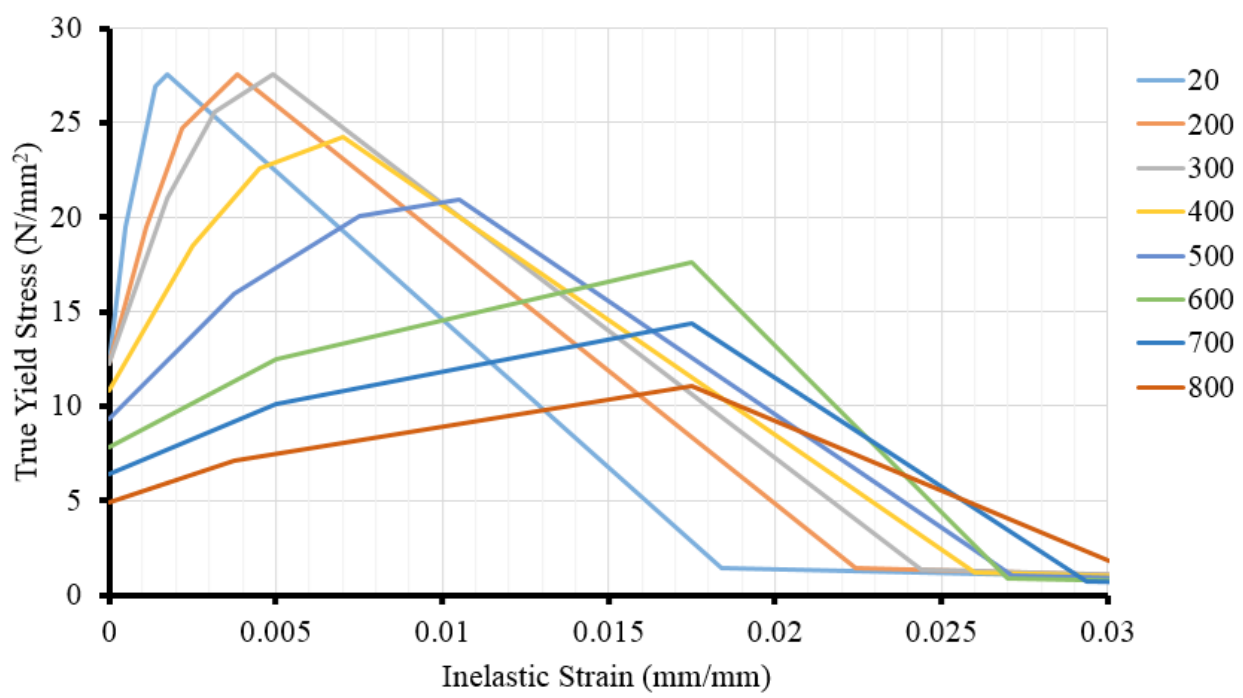


Figure 5.5 Concrete true stress vs. inelastic strain relationship with temperature changes (°C)

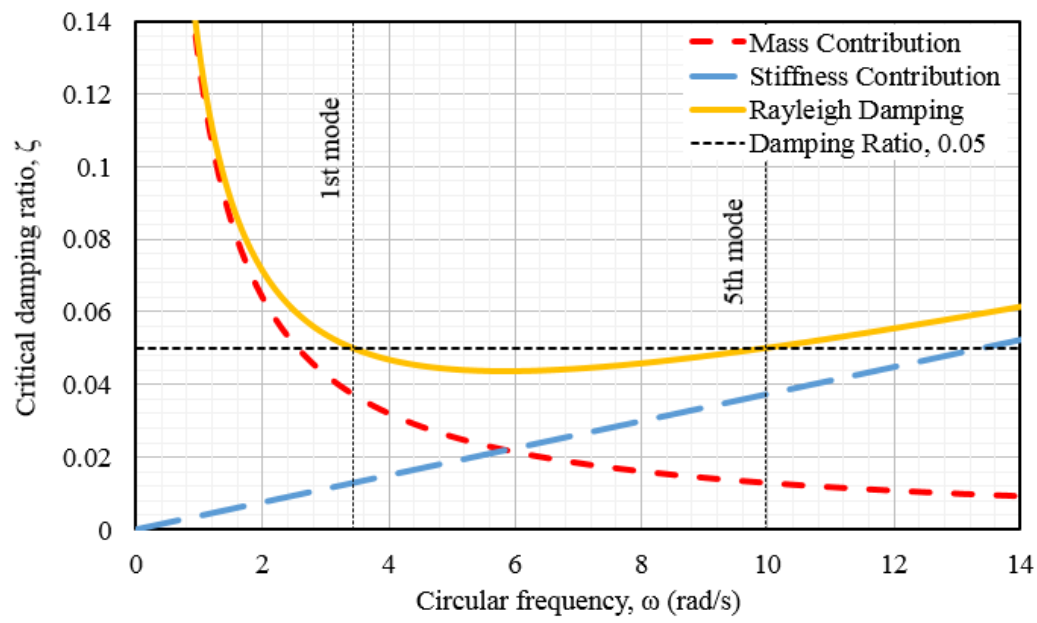


Figure 5.6 Rayleigh damping based on structural frequency (Los Angeles)

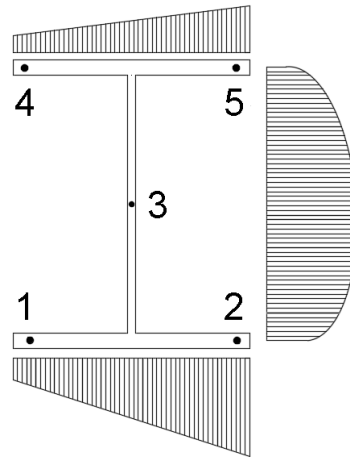


Figure 5.7 Interpolation of temperatures in ABAQUS for a wide-flange cross-section

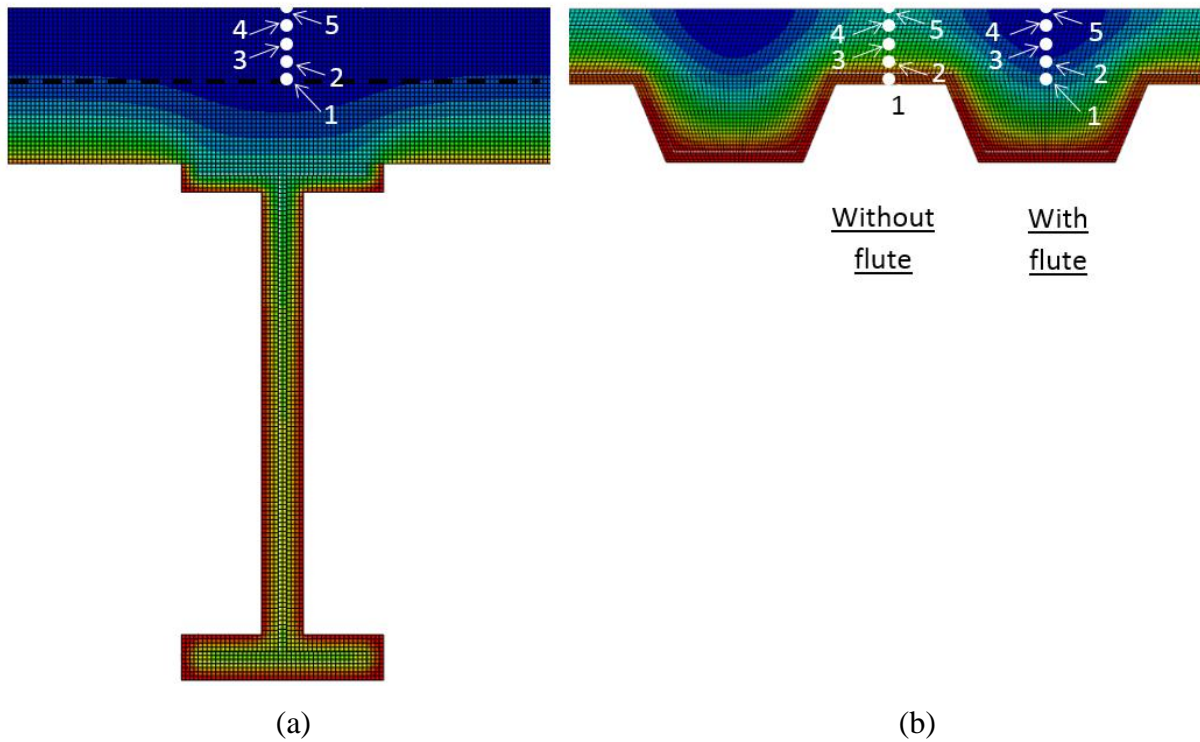


Figure 5.8 Temperature gradation and integration points [15]

(a) At composite slab with beam below

(b) At composite slab without beam directly below

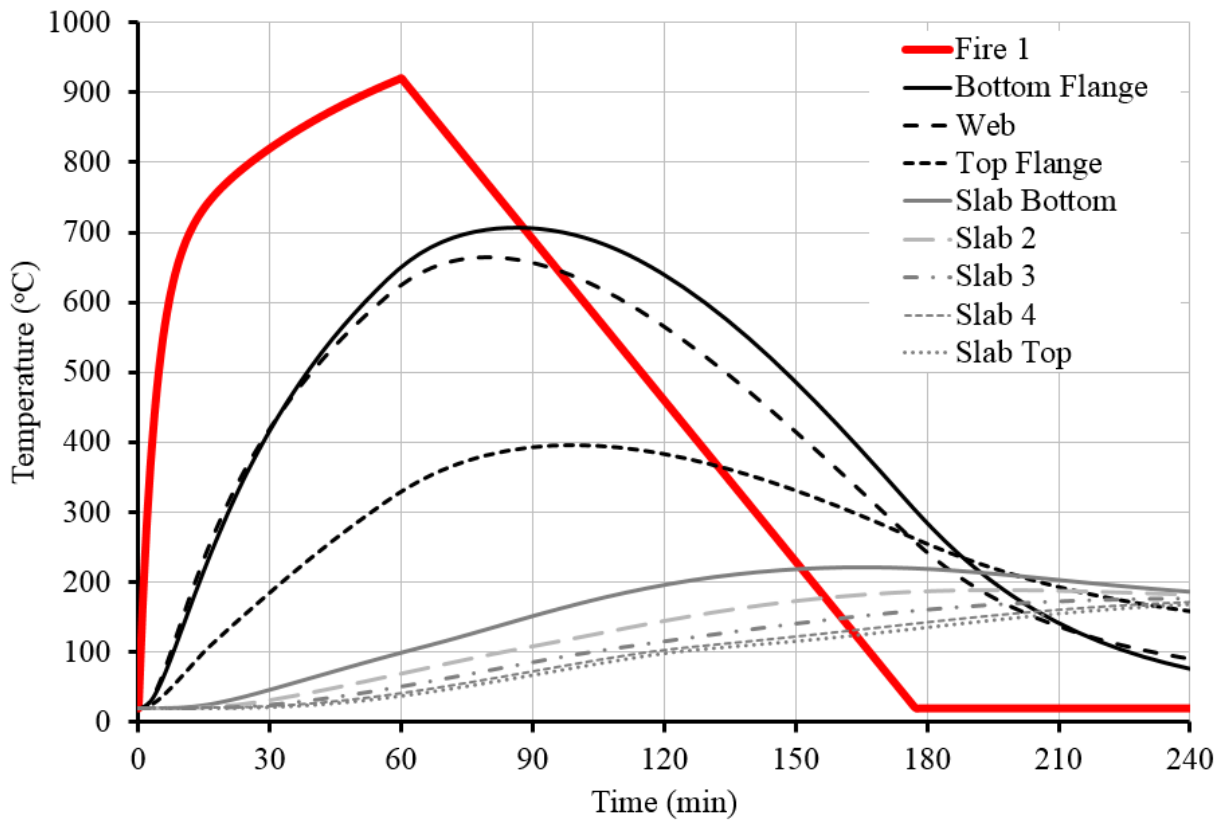


Figure 5.9 Time-temperature response of W14x22 composite beam with 1 hr FRR exposed to Fire 1

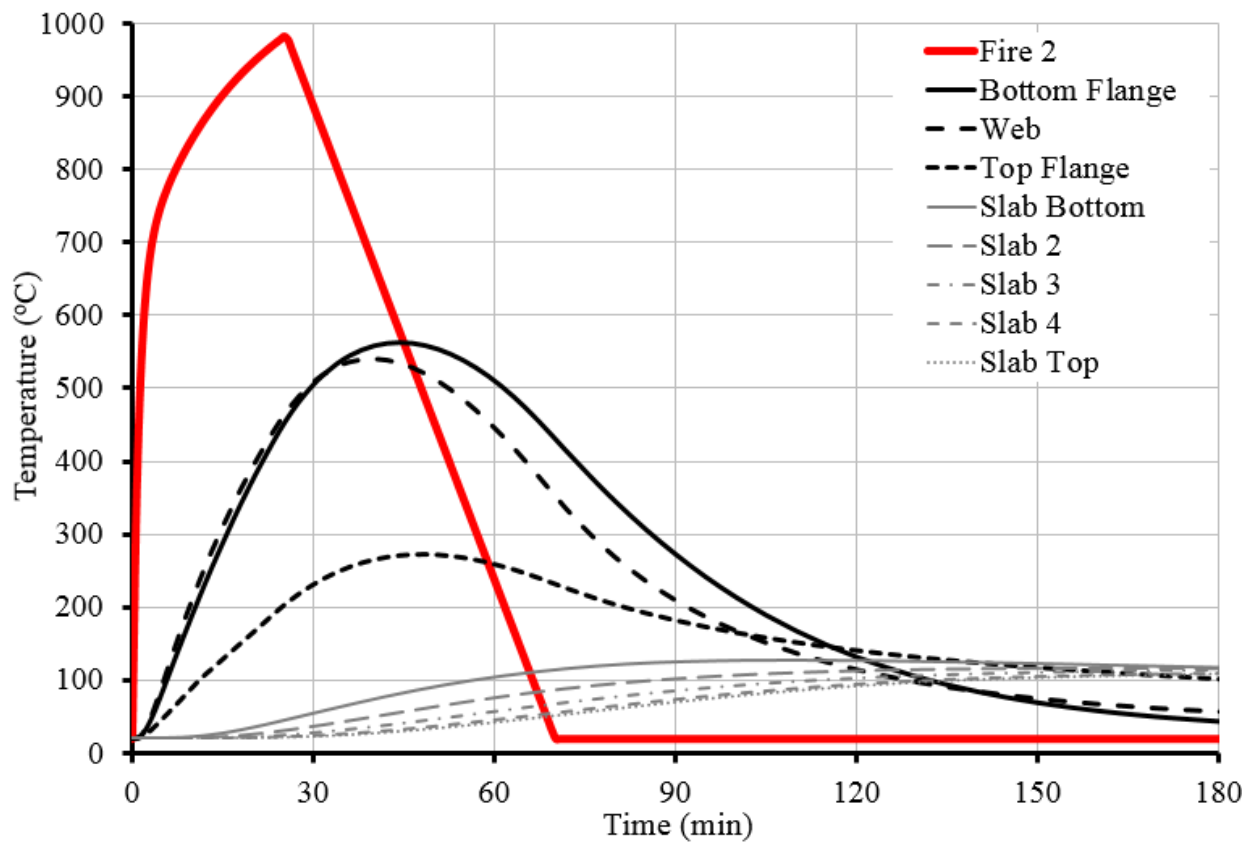


Figure 5.10 Time-temperature response of W14x22 composite beam with 1 hr FRR exposed to Fire 2

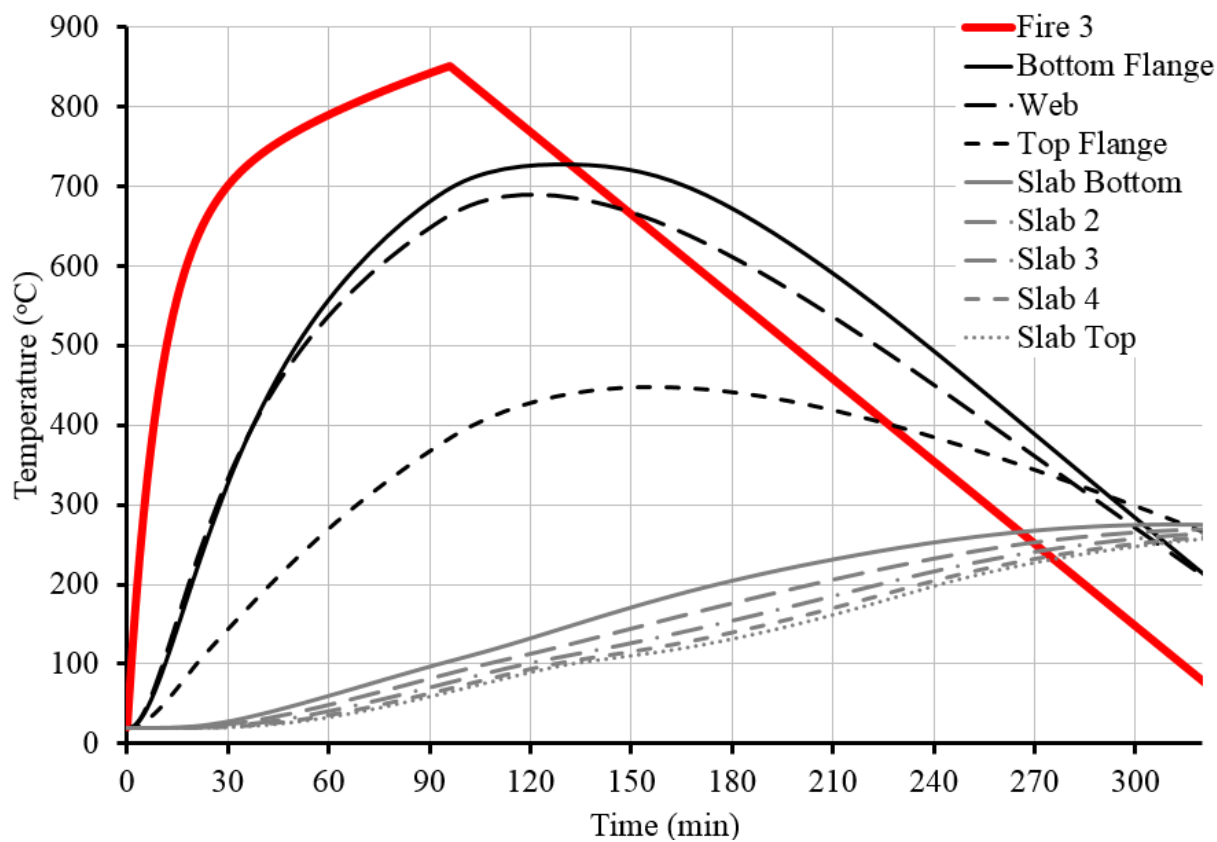


Figure 5.11 Time-temperature response of W14x22 composite beam with 1 hr FRR exposed to Fire 3

CHAPTER 6. CHICAGO BUILDING SIMULATION RESULTS

A variety of seismic and fire simulations were conducted for the Chicago building in order to determine vulnerabilities. This chapter will present the results of these studies conducted using the finite element method. These include results from: (1) incremental dynamic analyses, (2) incremental fire analyses, and (3) wind hazard analyses.

6.1 Seismic Response

The Chicago building was subjected to the seven ground motions explained in Chapter 4. However, before seismic analyses could be conducted, the fundamental period of the building needed to be determined from frequency analysis. Figure 6.1 shows the modal shapes and corresponding period for each of the first three modes. The fundamental mode is lateral translation in the longitudinal direction with a period of 2.65 sec. The second mode is lateral translation in the transverse building direction with a 2.26 sec period. The third mode is a torsional mode with a 1.38 sec period. These modes were used to determine the coefficients for Rayleigh damping, as explained in Section 5.4.

Each of the seven ground motions were scaled per incremental dynamic analyses by the intensity measure, PGA. Ground motion intensities of 1, 2, 3, 4 and 6 times the PGA for each earthquake were studied. The designation EQ4-6, for example, indicates that the fourth earthquake ground motion was scaled by 6 times its PGA. Figure 6.2 shows the maximum story drift ratios that were recorded at each level for the seven different earthquakes scaled by different PGAs. The results from this figure do not incorporate fracture. Fracture is presumed to occur at a maximum story drift ratio of 0.02, designated with a dotted red line in the figure. Fracture was omitted from the analyses in this figure in order to show where the maximum story drift ratios occur and what levels are most prone to damage or even soft story collapse. In general, for intensities of 4 and 6 times the PGA, the upper stories (7-9) are the most prone to failure.

As shown in Figure 6.2(a), story drift ratios at 1 times the PGA are well below the fracture limit and the corresponding life safety performance category of ASCE 41 [16]. This is because the seismicity level in Chicago is relatively low and the structure was controlled by wind drift instead

of seismic strength or seismic drift serviceability. All ground motions at this intensity remain elastic without any residual drifts.

Figure 6.2(b) shows results for ground motion intensities at 3 times the PGA. At this intensity, story drift ratios begin to approach the fracture limit. In addition, plastic hinges begin to form in the moment frames. Figure 6.3 shows where plastic hinging has formed (circled in red for the columns and green for the beams) within the moment frame columns along the longitudinal direction of the building for EQ4 scaled by 3 times PGA. No inelasticity was observed in the transverse direction or in any of the gravity frames. A residual drift of only 18 mm (3/4 in) is observed at the roof of this structure. The building was designed as an ordinary moment frame and, therefore, it did not need to comply with the strong column – weak beam design outlined in the AISC Seismic Design Manual [11]. The preferred location for plastic hinging is in the beams just outside of the beam-to-column connections. Instead, plastic hinging is observed in the moment frame columns. Hinging in columns is dangerous, as it can lead to a story mechanism collapse.

Figure 6.2(c) and (d) display results for ground motion intensities at 4 and 6 times the PGA, respectively. At these intensities, the story drift ratios are well beyond the fracture limit. Figure 6.4 shows where plastic hinging has formed within the transverse moment frames for EQ5 scaled by 4 times the PGA. Green circles indicate locations of plastic hinging in the beams while red circles indicate column plastic hinging. A residual drift of 38 mm (1.5 in) is observed at the roof. The results of these analyses are summarized in Figure 6.5, which shows the PGA versus maximum story drift ratio for each earthquake ground motion. With the exception of EQ1, ground motions with PGA greater than 0.3g resulted in story drift ratios greater than 0.02. Ground motions beyond 0.02 story drift ratio resulted in a story mechanism collapse of the structure, as shown in Figure 6.6. Fires were not analyzed following these scenarios because the system had already collapsed due to the earthquake.

Structures exposed to earthquake intensities less than or equal to 3xPGA, which did not result in system collapse, were then exposed to compartment fires. The following sections explore the structural response of the building subjected to corner, edge, interior, and full story compartment fires at the fifth and ninth stories. The fifth story was selected because it is beyond the reach of firefighting ladders while also supporting multiple stories above. The ninth story was studied because many of the seismic analyses resulted in plastic hinging of framing members at this level.

6.2 Fifth Story Fires

Fifth story fires were simulated at a corner, edge, and interior compartment, as well as a full story fire. Fires 1, 2 and 3 as shown in Figure 4.16 were each scaled at 0.75, 1 and 1.25 or 1.5 times the peak fire temperature (PFT). The scaled factor of 1.5 was used for Fires 1 and 2. Only 1.25 was used for Fire 3 because using 1.5 would have resulted in an unrealistic fire scenario. These three scaled fires represent short, medium, and long duration fires with varying peak fire temperatures. The designation Fire 1-1.5 indicates Fire 1 that is scaled by 1.5 times the peak fire temperature. The compartment fires were simulated after different earthquakes and earthquake levels had been analyzed. These earthquakes caused varying levels of plastic hinging within the structural members and residual drifts. As explained previously, seismic damage was minimal at the fifth story, and was more prevalent at upper levels. Regardless of the level of seismic damage, the same failure mode occurred for all earthquake scenarios subjected to the fifth story compartment fires. The findings below represent failure modes determined from all previously conducted earthquake scenarios that did not cause fracture. Table 6.1 summarizes the results of the findings explained in the following sections.

6.2.1 Fire 1

6.2.1.1 *Corner Compartment Fire*

Failure of the interior gravity column occurs when the corner compartment is subjected to Fire 1-1. A rendering of this failure is shown in Figure 6.7(a). The failed column is a W12x58. Figure 6.7(b) represents the column axial force and column flange temperature versus time for this fire intensity. Note that the column flange and web temperatures were nearly equal over time and the larger temperature was used. As steel temperature increases, the gravity column maintains and only slightly increases its axial load until failure occurs at 544°C. At this temperature, the column loses all load carrying capacity and buckles at 95 minutes. The loads are then redistributed to the adjacent columns, thereby maintaining stability and preventing global system collapse.

The gravity column, located at column lines B-3 in Figure 6.8(a), is the failed interior column, designated as INT. Each of the adjacent columns are also labeled in Figure 6.8(a) by cardinal directions. The column axial loads for each of the adjacent columns over time are shown in Figure 6.8(b). The gravity columns not subjected to fire (N, NE and E) maintain the same axial load as the compartment is heated. The INT column that is subjected to temperature changes experiences

a slight increase in axial load. The moment frame columns within the compartment fire (W and S) experience axial load increases as the temperature of the members increase. This is because, as heated, the members want to expand but are constrained by the moment connections at the stories above and below, causing an increase in axial compression in these members. This in turn causes the axial loads in the adjacent, ambient moment frame columns (NW and SE) to decrease. The corner column (SW) also is subjected to a decrease in axial load. This is due to the continuity of the cantilevered beam in the E-W moment frame imposing a tensile force on the corner column. When the INT column fails, the beam-to-column connections fail at the buckled column. The failed column loads are primarily redistributed to columns E, N and W through the composite slab. Figure 6.9 shows the interior column load (represented by a red circle). The blue circles represent the relative percentage (shown graphically by area) of the interior column load that is redistributed to the adjacent columns. Column E receives the largest percentage of load because load can be transferred in the strong direction of the slab that is not subjected to elevated temperatures. While Column W also has loads transferred to it, the load is less because the framing system is subjected to the elevated temperatures. The same principle is true for the N versus S columns. Column N received more load because the W14x22 beam and slab along the column line was not subjected to elevated temperatures, unlike the framing and slab adjacent to Column S.

Fire 1-1.5 results in column failure and a deflected shape very similar to the Fire 1-1 case. The time of failure, however, is much earlier at 50 minutes. This is because the scaled fire time-temperature curve causes the column to reach the critical, failure temperature of 544°C more quickly, as shown in Figure 6.10.

When the peak fire temperature of Fire 1 is scaled by 0.75, the compartment does not undergo failure. The beams and girders deflect in a similar shape to a compartment failure but the deflection is only 208 mm (8 in), which is within the acceptance criteria and, thus, no failure occurs.

A summary of the failure modes, maximum vertical deflections, and time of failure is given in Table 6.1.

6.2.1.2 Edge Compartment Fire

The fifth story edge compartment, designated in Figure 4.14 as Compartment B, was subjected to Fire 1 as shown in Figure 4.16. Again, this fire was scaled at 0.75, 1 and 1.5 times the peak fire temperature. The interior gravity columns in this compartment are W12x58. Figure 6.11 shows the

failure mode of Fires 1-1 applied to the edge compartment. The interior gravity columns fail at roughly 544°C, at the same times as those observed in the corner compartment fire scenarios. However, because two gravity columns are now exposed to the fire in this compartment, two column failures occur at once, resulting in more widespread deflections than the corner compartment, which is being referred to as a bay failure per Section 3.2.1.

The failed gravity columns are designated as INT1 and INT2 in Figure 6.12(a) and the adjacent columns are designated by cardinal directions. The failed columns are located at column lines C-3 and D-3. Figure 6.12(b) illustrates the redistribution of axial load over time for each of the columns adjacent to the failed gravity columns. The failed columns (INT1 and INT2) slightly increase in axial load as exposed to increasing temperature. The interior gravity columns not exposed to the compartment fire (NW, N1, N2, NE, E, and W) all maintain the same axial temperature until 98 minutes, when the INT1 and INT2 columns fail. At this point, loads are redistributed to these columns. Most of the load is distributed to columns W and E through the composite slab. Loads to N1 and N2 are lesser because loads must be transferred through a less stiff beam, a W14x22, and load must transfer in the weak direction of the composite slab. Columns NW and NE attract even less load, as they are diagonal from the failed columns and require load transfer through the slab. The adjacent moment frame columns subjected to temperature increases (S1 and S2) vary in axial load over time. These columns are restrained by the moment frame connections above and below and, thus, when subjected to temperature increases that cause the columns to want to expand, they are subjected to additional axial compression. The opposite is true for the SW and SE columns which balance these forces while not being subjected to any temperature fluctuations on its members. The columns are exposed to tensile forces which reduce the axial compression on these members.

Figure 6.13 displays the relative distribution of axial loads to each of the adjacent columns. The red circles show the axial load in the columns prior to failure. The blue circles show how much of the initial axial load is redistributed to each column, as shown as a portion of the area of the red circle. As explained previously, most load is distributed to columns E and W, following by columns N1 and N2. Through adequate redistribution of column loads, the structure, while severely damaged with significant deflections, does not completely collapse.

Fire 1-1.5 results in bay failure that looks very similar to the Fire 1-1 case. The interior gravity columns fail at 50 minutes. This occurs when the columns reach the 544°C failure temperature that

has been previously identified. Table 6.1 summarizes the failure modes, maximum vertical deflection and time of failure for each of the scaled fire scenarios.

Fire 1-0.75 does not result in any type of failure. The floor system reaches a maximum of 208 mm (8 in) of deflection during the fire, which is within the compartment failure acceptance limits of 381 mm (15 in) given in Table 3.1.

6.2.1.3 Interior Compartment Fire

The fifth story interior compartment is designated as Compartment C in Figure 4.14 and referred to as 5C for the fifth story. Figure 6.14(a) shows the deflected shape of the building when exposed to Fire 1-1 in compartment 5C. All four of the interior columns (W12x58) within the compartment failed and caused system collapse of the structure. Figure 6.14(b) shows the vertical deformation of those columns as they buckle due to elevated temperatures. The system experiences run away deflections and the analysis was ended when the floor system of compartment 5C reached the floor system below. The large deformations that occur in compartment 5C cause significant leaning of other columns within that story. This shows that the adjacent columns are not rigid enough to act as a support to resist the large tensile forces that would need to be carried through catenary action from the failed compartment to the adjacent compartments. In addition, when the columns fail and experience significant deformations, this causes connection failure in the beam-to-column connections framing into those columns, which makes load redistribution to adjacent columns very unlikely.

Figure 6.15(a) circles the columns that have failed and are designated as INT1-4. The axial force in those columns over time is shown in Figure 6.15(b). The failed columns experience only a slight increase in load as fire temperatures increase. At approximately 91 minutes, the columns reach the critical temperature to cause column buckling. Loads are shed primarily to the adjacent gravity columns (W1, W2, E1, and E2). The adjacent columns are already leaning and unable to withstand the additional loads, causing collapse of these columns as well. The moment frame columns to the north and south of the compartment (N1, N2, S1, and S2) attract very little load when the initial gravity column failures occur because the beam-to-column connections have failed and the slab is weak in this direction. A more robust diaphragm with the ability to transfer loads in two directions could help prevent this type of system failure from occurring, as will be shown in Section 8.3.

Fire 1-1.5 experiences the same failure mechanism as Fire 1-1. It occurs at 50 minutes, when the interior gravity columns fail. Again, the adjacent columns are incapable of providing proper anchorage to resist the tensile forces that would be necessary to distribute loads through catenary action.

Fire 1-0.75 resulted in only 242 mm (9.5 in) of maximum vertical deflection in the compartment floor system. Once the fire had cooled, only 53 mm (2 in) of residual deflection resulted due to the fire in addition to the initial gravity load deflections.

6.2.1.4 Full Story Fire

Fire 1-1 and 1-1.5 were applied simultaneously to all of the bays in the fifth story of the Chicago building. Fire 1-1 caused simultaneous column failure of the interior gravity columns at 100 minutes, resulting in system collapse of that story. Fire 1-1.5 resulted in the same failure mechanism at 51 minutes. Figure 6.16(a) shows the deflected shape of the structure when the interior gravity columns begin to collapse after exposure to Fire 1-1.5. The columns experience the same buckling failure observed in the individual compartment studies at a temperature of approximately 548°C.

The previous compartment studies have shown that gravity columns only experience a very slight increase in axial load as they are heated because they are relatively unrestrained against expansion. In full story fires, the composite slabs and beams in the bays adjacent to the column being studied are also exposed to elevated temperatures and, thus, lack the stiffness of an unheated compartment. For this reason, there is even less axial restraint in a full story fire and, thus, the increase in axial load is even less for the interior gravity columns subjected to full story fires than what was observed for the individual compartment fires. This causes a slightly longer extended failure time, though it does not prevent the failure mechanism from occurring.

6.2.1.5 Gravity Column Capacity Check

Gravity column failure has precipitated all of the observed failure modes discussed thus far. Therefore, it is important to understand this failure mechanism and validate that the results are reasonable. These results are validated in this section, which compares the ABAQUS failure temperatures and axial loads with the AISC capacity equations designated for gravity columns subjected to elevated temperatures.

The utilization ratio is defined as the demand divided by the capacity of the column. This value is 0.64 for the W12x58 columns at the fifth floor. This considers the capacity of the column at ambient conditions with the demand determined from the load combination for fire of $1.2D+0.5L+A_T$. This utilization ratio provides some reserve capacity for the column at ambient conditions. The capacity at elevated temperatures must be considered as well.

Appendix 4 of AISC 360-16 provides criteria to aid structural engineers in structural design for fire conditions [48]. It includes a simple method of analysis that can be used to design individual structural components subjected to fire conditions. This appendix provides equations to determine member capacities at elevated temperatures. In this section, the compressive capacity of the interior gravity column supporting the fifth story will be calculated using the simple method of analysis from AISC 360. The column strength equations are based on work by Takagi and Deierlein [69].

Chapter E in the specification covers design of compression members under ambient conditions. Appendix 4 incorporates material property reduction factors and modifications to the design equations in Chapter E in order to calculate compressive capacity of a column subjected to elevated temperatures. For instance, in lieu of Equation E3-2 in Chapter E, Appendix 4 provides an alternative flexural buckling equation (Equation A-4-2 in Appendix 4) which is:

$$F_{cr}(T) = \left[0.42 \sqrt{\frac{F_y(T)}{F_e(T)}} \right] F_y(T) \quad \text{Equation 6-1}$$

$F_y(T)$ is the yield stress at temperature, T . The critical elastic buckling stress, $F_e(T)$, is calculated using Equation E3-4 for ambient conditions, which is modified to incorporate the modulus of elasticity at elevated temperature, T . This material property is calculated using reduction coefficients in Table A-4.2.1 of Appendix 4 to capture the stiffness reduction of steel with increasing temperatures. The modified equation of E3-4 for critical elastic buckling stress at temperature T is:

$$F_e(T) = \frac{\pi^2 E(T)}{(L_c/r)^2} \quad \text{Equation 6-2}$$

where $E(T)$ is the modulus of elasticity at temperature T , L_c is the effective length of the member (KL), and r is the radius of gyration of the member.

The nominal compressive strength, P_n , can then be calculated using the following equation, where A_g is the gross cross-sectional area of the member:

$$P_n(T) = F_{cr}(T)A_g \quad \text{Equation 6-3}$$

Figure 6.17 shows the axial capacity versus temperature relationship of the W12x58 column with a length of 12 ft, which is the typical story height. The gray line, designated as “Capacity-Simply Supported”, provides the capacity equation for a simply supported column where K , the effective length factor, is 1.0. This is an overly conservative design equation because it does not account for the rotational restraints provided by the cooler columns above and below the compartment fire. The designer may choose to use a modified slenderness (L/r) value. Consideration must be made, however, about the likelihood of multi-story fires or vertically moving fires that would compromise this assumption of rotational restraints. If deemed applicable, the calculated column capacity can be significantly improved using the modified slenderness. The modified L/r value, referred to as L_c/r , is defined in the Commentary of Appendix 4 as:

$$\left(\frac{L_c}{r}\right)_T = \left(1 - \frac{T-32}{n(3,600)}\right) \left(\frac{L_c}{r}\right) - \frac{35}{n(3,600)}(T-32) \geq 0 \quad \text{Equation 6-4}$$

n is a constant used to indicate if there are one or two cooler columns (above and/or below) the analyzed column. $n=1$ is used if there are cooler columns both above and below and $n=2$ is used for columns with a cooler column either above or below. T is the lumped mass temperature of the analyzed column in degrees Fahrenheit.

The solid black line designated as “Capacity-Rotational Restraint” in Figure 6.17 shows the axial capacity using the modified L/r factor. The axial demand on the column based on the load combination $1.2D+0.5L+A_T$ is 1850 kN (416 kips) and is denoted by the red dotted line. As mentioned previously, the W12x58 column failed at 544°C in ABAQUS. The red circle in Figure 6.17 shows the intersection of demand and capacity. This occurs at 514°C. Thus, the design equation is slightly more conservative than the results from ABAQUS, but both produce comparable failure temperatures.

6.2.2 Fire 2

Fire 2 is a fire with a large opening factor. This means that the fire quickly reaches a high fire temperature but also that it cools quickly. Because the steel members are fireproofed, there is a

delay in the time it takes for the steel to heat up and also a reduction in the peak steel temperature as compared to the peak fire temperature. This can be seen in Figure 5.10 for a W14x22 beam exposed to Fire 2-1. For these reasons, very few failures occurred for Fire 2. This suggests that very quick burning, but also quick to cool fires (i.e. – a compartment with a high opening factor) will not likely lead to failure if fireproofing is designed for a fire resistance rating beyond the duration of the fire. Still, the findings of Fire 2 simulations at the fifth floor are explained in more detail below.

6.2.2.1 Corner Compartment Fire

Fires 2-0.75 and 2-1 did not result in any failures. The floors experienced sagging and expansion of the floor system in compartment 5A due to the elevated temperatures but these deflections were less than the limit of 381 mm (15 in) specified in Table 3.1 for compartment failures. Fire 2-0.75 caused only 169 mm (7 in) of maximum deflection and Fire 2-1 caused 235 (9 in) mm of deflection. Fire 2-1.5, however, caused compartment failure with a maximum vertical deflection of 471 mm (18.5 in). No other member failures were observed and the system remained stable.

6.2.2.2 Edge Compartment Fire

The deflections vary slightly from the corner to the edge compartment but the general findings are the same. Fires 2-0.75 and 2-1 did not result in any failures. Fire 2-0.75 led to 159 mm (6 in) of maximum deflection and Fire 2-1 resulted in 219 mm (8.5 in) of deflection. Fire 2-1.5 caused compartment failure with a maximum vertical deflection of 442 mm (17.5 in). As with the corner compartment scenario, no other member failures were observed and the system remained stable.

6.2.2.3 Interior Compartment Fire

The interior fifth story compartment experienced the same behavior as the corner and edge compartments when subjected to Fire 2. The only difference is that it experiences larger deflections. This is because the exterior moment frame was part of the corner and edge compartments and these members are stiffer than the gravity framing members.

Fire 2-0.75 and 2-1 again did not result in any type of failure. The maximum vertical deflections due to these fires were 187 and 288 mm (7 and 11 in), respectively. Fire 2-1.5 caused compartment failure with 542 mm (21 in) of maximum vertical deflection occurring at 55 minutes.

6.2.2.4 Full Story Fire

Fire 2-1.5 was applied to the entire fifth story framing system. This resulted in compartment failure with a maximum deflection of 465 mm (18 in). This fire only caused sagging of the floor framing and did not result in any type of member or connection strength failures. The structure exposed to the full story fire of Fire 2-1.5 experienced the same failure modes as the compartment studies.

6.2.3 Fire 3

Fire 3 was selected to represent a long duration fire. The results of analyses for fifth story fires at the corner, edge and interior compartments, as well as full story fires, is described in the following sections. Fire 3 was scaled at 0.75, 1, and 1.25 times the peak fire temperature.

6.2.3.1 Corner Compartment Fire

The fifth story corner compartment subjected to Fire 3-1 results in an interior gravity column failure, as shown in Figure 6.18. The axial load-time relationship is similar to Fire 1-1 results, where the column essentially maintains its axial load as the temperatures increase until finally buckling at the failure temperature. Because Fire 3-1 is a longer duration fire that heats more gradually, the failure time of the column is delayed. It fails at approximately 544°C but this occurs after 100 minutes. Loads are redistributed in a similar fashion to the Fire 1-1 results, maintaining global stability of the system. The same response is observed for Fire 3-1.5. Column failure again occurs, but at 77 minutes.

When Fire 3-0.75 is analyzed, no failures are observed. The floor system deflects in a shape similar to compartment failure, shown in Table 3.1. Failure does not occur because the maximum deflection is only 228 mm (9 in).

6.2.3.2 Edge Compartment Fire

Figure 6.19 shows the failure mode for Fire 3-1 subjected to the edge compartment, 5B. Yet again, the interior gravity columns fail at approximately 544°C, at the same times as those observed in the corner compartment fire scenarios. However, because two gravity columns are now exposed to the fire in this compartment, two column failures occur at once, resulting in more widespread deflections than the corner compartment, which is being referred to as a bay failure per Table 3.1. Because Fire 3-1 heats up gradually over 90 minutes, the column reaches its failure temperature

of 544°C more slowly than Fire 1-1. This allows 100 mins before collapse, which is significantly better than the 1 hr fire rating for which the system was designed.

Fire 3-1.25 results in a similar failure mode: interior gravity column failures resulting in a bay failure. This occurs at 76 mins and results in 2122 mm (84 in) of deformation.

6.2.3.3 Interior Compartment Fire

Figure 6.20(a) shows the response of the Chicago building exposed to Fire 3-1 in the fifth story interior compartment (5C). The analysis was ended when the framing's maximum deflection was equal to the story height. The four interior gravity columns collapse when they reach their failure temperature of 544°C. When this happens, significant runaway deflections occur, as can be seen in the vertical deflection and temperature versus time plot in Figure 6.20(b). The other columns within the fifth story are bent towards the failed compartment. This is because the slab and framing system must try to span three bays when the columns fail. This creates large tensile forces that develop in an attempt to redistribute loads through catenary action.

As with the previous compartment studies, Fire 3-0.75 does not cause any type of failure and Fire 3-1.25 results in the same failure mechanism as Fire 3-1. A summary of the failure modes, deflections and times of failure is given in Table 6.1.

6.2.3.4 Full Story Fire

Fires 3-1 and 3-1.25 were applied to the entire fifth story of the Chicago building. As with the Fire 1 full story fire scenario, both of these fires resulted in system collapse. The interior gravity columns in the fifth story buckled simultaneously, causing collapse. This occurred at 103 minutes for Fire 3-1 and 77 minutes for Fire 3-1.25. These failure times are slightly longer than the compartment fire scenarios previously studied because having every bay of the story heated resulted in even less restraint of the gravity columns and, thus, essentially no increase in column axial force in this scenario. This is in contrast to the slight axial load increase observed in the other compartment failures.

6.3 Ninth Story Fires

Ninth story fires were simulated at a corner, edge, and interior compartment, as well as a full story fire. Fires 1, 2 and 3, as shown in Figure 4.16, were each scaled at 0.75, 1, and 1.25 or 1.5 times

the peak fire temperature. The scalar factor of 1.5 was used for Fires 1 and 2. Only 1.25 was used for Fire 3 because using 1.5 would have resulted in an unrealistic fire scenario.

The compartment fires were applied after earthquake damage had already occurred. When fracture occurred in the moment frame columns, the structural system collapsed and, thus, fire analyses were not conducted. The results discussed in the subsequent sections represents failure modes that occurred after seismic events where fracture had not occurred. Moment frame columns experienced plastic hinging due to many of the seismic analyses (see Figure 6.3 and Figure 6.4). Despite this damage, the same failure modes occur for the ninth story compartment fires.

6.3.1 Fire 1

6.3.1.1 Corner Compartment Fire

Compartment 9A is subjected to Fires 1-1, 1-1.5 and 1-0.75. When exposed to Fire 1-1, interior gravity column failure occurs, as shown in Figure 6.21. The interior gravity columns at the ninth story are W8x24. The axial load in the interior gravity column increases slightly as steel temperature increases. The initial load is 602.7 kN (135 kips) and increases to 650 kN (145 kips). At 70 minutes, when the column reaches an internal temperature of 499°C, the column buckles and loses all load carrying capacity. Loads are redistributed to the adjacent columns. As shown in Figure 6.21(a), the adjacent moment frame columns have been pulled in and are leaning. This was not observed at compartment 5A because the moment frame columns at the fifth story were heavier sections that had excess stiffness and capacity. The moment frame columns at the ninth story are W12x45 and W14x53, which are not particularly heavy sections. Despite leaning, the columns sufficiently carry the transferred loads to prevent system collapse.

Fire 1-1.5 in compartment 9A initiates failure at 46 minutes, when the interior gravity column fails. However, instead of redistributing the loads as was achieved when Fire 1-1 occurred, the moment frame columns are weakened by their elevated temperatures and unable to withstand the tensile forces pulling inward on the columns. Figure 6.22(a) shows the deflected shape of the system when the interior gravity column initially collapses. Figure 6.22(b) shows the deflected shape of the adjacent, exterior moment frame columns prior to their eventual collapse at about 60 minutes.

Fire 1-0.75 causes a maximum of 248 mm (10 in) of vertical deflection within the framing system but no failure modes occur.

6.3.1.2 Edge Compartment Fire

Fire 1-1, when simulated at compartment 9B, results in interior gravity column failures of the two interior columns exposed to elevated temperatures within the compartment. This resulted in a bay failure with 2144 mm (84 in) of vertical deflection. The gravity columns failed 69 minutes after the fire began. Figure 6.23(a) shows the final deflected shape of the system. Figure 6.23(b) plots the column axial load and internal steel temperature versus time. As the graph shows, the column loses load carrying capacity at 69 minutes when the column reaches 499°C.

Fire 1-1.5 results in system collapse of the structure when the fire occurs in the edge compartment. The two interior gravity columns collapse at 45 minutes, when the internal temperature of the column reaches 499°C. This is shown in Figure 6.24(a). The columns continue to deflect but the system maintains stability for another 55 minutes until the exterior moment frames within the edge compartment exposed to the fire fail. A rendering of this failure is provided in Figure 6.24(b). Once all four columns within the fire compartment have failed, the adjacent columns begin to fail as well, resulting in progressive system collapse. Figure 6.24(c) show the compartment which was exposed to the fire and denotes the designations for the adjacent columns. Figure 6.24(d) displays the column axial load over time for each of the columns within the compartment, as well as the adjacent columns. The graph shows that the interior gravity columns, INT1 and INT2, lose load carrying capacity at 45 minutes. The loads from this column are through the composite slab to the adjacent columns. In particular, the east and west columns (E and W) carry the largest portion of the collapsed column loads. Next, columns to the north (N1 and N2) and then columns NE and NW and the SE and SW columns. Columns S1 and S2 do not increase in axial load when the interior gravity columns fail. This is because the beams and slab connecting the columns are being heated and have very little stiffness, and this is in the weak direction of the composite slab. Additionally, the W14x22 beam-to-column connections framing into the failed columns fractured when the columns failed due to significant rotations and deformations, requiring the loads to be transferred through the slab. As columns S1 and S2 continue to be heated by Fire 1-1.5, they progressively lose strength and stiffness. At 100 minutes, these columns collapse, resulting in system collapse of the structure. This did not occur in Fire 1-1 because the moment frame columns had enough reserve capacity to withstand the effects of strength and stiffness reductions caused by Fire 1-1. The internal temperatures reached due to Fire 1-1.5 were too great for these columns to withstand. Fire 1-0.75 did not result in any failures.

6.3.1.3 Interior Compartment Fire

When the interior compartment on the ninth story was exposed to Fire 1-1, system failure of the structure occurred. This compartment consists of only interior gravity columns and gravity framing. These columns began to fail when they reached 499°C, which occurred 67 minutes after the fire initiated. When the columns fail and the system deflects dramatically, the connections to those columns fracture, making it difficult for loads to be successfully transferred to adjacent columns, ensuring system stability. As shown in Figure 6.25(a), the ninth story columns outside of the fire compartment begin to lean toward the interior compartment. This is because of the large deflections resulting from the failed columns and the attempt of the framing and slab to transfer these forces using catenary action. The columns are being pulled inward by the tensile forces within the diaphragm. These columns are unable to withstand these forces and the adjacent columns collapse, leading to system collapse. Figure 6.25(b) displays the vertical displacement of the column over time. Run away deflection has occurred and the adjacent system is not robust enough to prevent this from occurring. The model was stopped when the floor system deflected to the story below.

Fire 1-1.5 in the ninth story interior compartment also resulted in system failure of the structure. The four interior gravity columns fail at 499°C, which occurred at approximately 45 mins. This caused large, runaway deflections which cannot be resolved by the adjacent columns. The interior gravity columns to the east and west of the compartment fire are bent inward in an attempt to withstand the tensile forces resulting from the deflected framing system. This lead to failure of the adjacent interior gravity columns which propagated the collapse to the other bays of the story.

Fire 1-0.75 did not result in any failures.

6.3.1.4 Gravity Column Capacity Check

The utilization ratio for the W8x24 columns at the ninth story is 0.73. This considers the capacity of the column at ambient conditions with the demand determined from the load combination of 1.2D+0.5L. This utilization ratio provides some reserve capacity for the column, but is less conservatively designed than the W12x58 columns studied on the fifth floor, which had a utilization ratio of 0.64.

The design of the failed W8x24 gravity column was checked using the same procedure described in Section 6.2.1.5. Figure 6.26 shows the axial capacity versus temperature relationship of the

W8x24 column. The solid black line designated as “Capacity-Rotational Restraint” shows the axial capacity using the modified L/r factor, which accounts for rotational restraints due to the cooler columns above and below the fire. The gray line shows the column capacity for the simply support case, not accounting for the rotational restraint of the cooler columns above and below. The axial demand on the column based on the load combination $1.2D+0.5L+A_T$ is 587 kN (129 kips), as designated by the red dotted line. As mentioned previously, the W8x24 column failed at 499°C in ABAQUS. The red circle in Figure 6.26 shows the intersection of demand and calculated capacity. This occurs very near to the observed failure temperature from ABAQUS of 499°C. Thus, the design equation closely predicts the failure temperature and column capacity when using the modified L/r factor for rotational restraint.

6.3.2 Fire 2

Previous studies have shown that Fire 2 does not cause significant damage to the structure. For these reasons, only the corner compartment and full story fire scenarios were considered, and priority was given to other scenarios that are more likely to cause failure modes.

6.3.2.1 Corner Compartment Fire

Neither Fire 2-0.75 nor Fire 2-1 resulted in any type of failure for a corner compartment fire. The framing system deflected a maximum of 208 and 275 mm (8 and 11 in), respectively. This deflection appeared similar to compartment failure, as defined in Table 3.1. However, the deflections are less than the acceptance criteria of 381 mm (15 in). No connections or members failures occur.

Fire 2-1.5 in the ninth story corner compartment caused column failure, resulting in 1297 mm (51 in) of vertical deflection when the structure was able to stabilize itself. This occurred 37 minutes after the fire started, when the column temperature reached approximately 500°C.

6.3.3 Fire 3

When Fire 3 is subjected to the various compartments on the ninth floor, these scenarios result in the same failure modes at the Fire 1, except with different failure times and total deflections. The results of these findings will be briefly summarized below, as well as in Table 6.2.

6.3.3.1 Corner Compartment Fire

Fire 3-1 simulated in the ninth story corner compartment causes column failure at 88 minutes, when the column flange reaches its failure temperature. This is shown in Figure 6.27(a) and (b), which shows the final deflected shape of the building and failed column axial load and temperature versus time relationship.

Fire 3-1.25 causes system collapse of the structure at 66 minutes. The same interior gravity column that failed in the Fire 3-1 scenario also failed when subjected to Fire 3-1.25. However, the system redistributes the loads and prevents collapse for only an additional 52 minutes before the other three columns within this compartment fail. These columns are part of the moment frame system; however, because they were designed to resist lateral drifts near the roof, the columns did not need to be as stiff and strong as columns at the lower levels that need to resist greater shear forces. The moment frame columns in this compartment are W12x45 and W14x53.

Fire 3-0.75 results in a maximum floor deflection of 254 mm (10 in), but this does not cause compartment failure or any type of connection or member failure.

6.3.3.2 Edge Compartment Fire

Failure at the ninth story edge compartment exposed to Fire 3-1 is observed at the two interior gravity columns, as depicted in Figure 6.28(a). Figure 6.28(b) shows the axial load in each of the two failed gravity columns over time. The columns lose their load carrying capacity at 82 minutes, which leads to bay failure. The system is robust enough to stabilize itself, redistribute loads, and prevent system collapse. The maximum vertical deflection that results is 1940 mm (76 in).

Fire 3-1.25 in the ninth story edge compartment initiates column collapse of the two interior gravity columns. This occurs at 66 minutes when the W8x24 columns reach their failure temperature. However, instead of resulting in only bay failure, as was the case with Fire 3-1, the exterior moment frame columns (W12x45) in that compartment also began to buckle, in a similar manner to Figure 6.24(b). The time at which this progressive collapse occurs depends on the level of plasticity in the moment frame columns. For EQ2-2, where no plastic hinging occurs in the columns within the compartment, these columns fail 82 minutes after the initial gravity column failures, when the W12x45 columns reach 720°C. EQ2-3 causes plastic hinging at the top and bottom of the edge moment frame columns in this compartment. This leads to collapse of the exterior columns only 52 minutes after the interior gravity columns fail. Thus, while the initial

failure is not affected by earthquake damage, the time it takes for progressive collapse to occur is dependent on seismic damage.

Fire 3-0.75 does not cause any type of failure in compartment 9B. It results in a maximum deflection of the floor system of only 249 mm (10 in).

6.3.3.3 Interior Compartment Fire

As was the case with fifth story interior compartment fires, as well as the ninth story interior compartment, Fire 3-1 and 3-1.25 exposed to the interior compartment of the ninth story both cause system failure. The four interior gravity columns (W8x24s) within the compartment fail at 85 and 65 minutes, respectively. This failure creates run away deflections (see Figure 6.29(b)) and connection failures for all of the beams framing into those columns. Load redistribution is difficult without having the connections to help transfer the failed column loads. In addition, the slab must now span three bays, resulting in very large tensile forces. Figure 6.29(a) shows the deflected shape of the building exposed to Fire 3-1. Note that analyses were ceased when the floor system deflected the full story height. The figure shows how the other columns at the ninth story are pulled inward by the tensile forces of the floor system, in an attempt to restabilize. These loads are too high for the relatively light column sections used at the ninth story, resulting in progressive collapse.

Again, Fire 3-0.75 does not result in failure of any type. The system merely deflects a maximum of 303 mm (12 in) as it is heated.

6.4 Wind Response

Wind time histories (Figure 4.20) were applied at each level of the Chicago building using the procedure explained in Section 5.8. The wind was applied as a strength-level wind case and, thus, the deflections reported are 60% higher than the deflections typically reported for serviceability checks. Figure 6.30(a) shows the lateral displacement of the roof when subjected to the wind time history and Figure 6.30(b) shows the deflected shape at the maximum deflection, scaled by 10. The maximum deflection is 213 mm (8 in). When divided by 1.6, the maximum deflection for the serviceability check is 133 mm (5 in). This deflection is greater than the suggested allowable limit of $L/400=91$ mm (4 in). This increase is likely due to the flexibility of the structure and its dynamic response. Despite these larger deflections, the structure remains elastic throughout the duration of the wind event. Fire events following this wind scenario remain the same as the failure modes,

deflections, and times summarized in Table 6.1 and Table 6.2, which were compiled from post-earthquake fire scenarios that did not cause fracture.

There are not currently provisions that specify detailing and design for ductility due to wind in the same way that it is applied to seismic design. If the building had been designed for higher intensity wind events (such as hurricane loads), the structure would still need to be designed to remain elastic. For these reasons, a fire event after a wind event should always result in the same behavior as a fire-only event.

6.4.1 Fire Following Wind Considerations

As mentioned previously, structures are designed to remain elastic when subjected to wind hazard. However, structural damage has occasionally been observed, in high wind storms such as hurricanes and tornados. The damage typically observed in design level wind hazards is nonstructural. Windborne debris can damage glazing, which is why IBC mandates glazing protection for buildings in hurricane-prone regions [7]. In addition, large suction forces on the cladding and roof can lead to breaching of the building envelope [124]. This can affect the fire hazard levels as it introduces high opening factors for exterior compartment fires. Wind can also spread the fire between structures which can lead to conflagration, as observed in California wild fires.

Failure of the cladding system could potentially lead to a large opening factor. Results have shown that Fire 2, which is a short duration fire with a large opening, does not cause failure within the system. This fire assumes a fire load density of 500 MJ/m^2 and opening factor of 0.06. Thus, for buildings with an opening factor greater than or equal to 0.06 and a fire load density less than or equal to 500 MJ/m^2 , fire is unlikely to cause damage because of the short duration of the fire. The presumed fire load density for an office is 420 MJ/m^2 so a fire load density value less than 500 MJ/m^2 is likely for this type of commercial building.

6.5 Summary and Conclusions

In this chapter, the Chicago building was subjected to earthquake time histories, various fire scenarios and a wind time history. Seven earthquake records were applied to the base of the building and were scaled at 1, 2, 3, 4 and 6 times the PGA. At 1 times the PGA, the ground motions all remained elastic and did not experience any damage. Because Chicago is in a low seismic area,

the ground motions needed to be scaled by at least 3 times the PGA in order to experience fracture of any of the framing elements. Plastic hinging and fracture of the steel members occurred in the perimeter moment frame columns, primarily at the upper levels of the building. Fracture in the columns during earthquakes would result in collapse of the structure. For cases where fracture did not occur, fire following earthquake scenarios were examined.

Fires 1, 2, and 3 were exposed to the Chicago building at the fifth and ninth stories. These compartment fires were analyzed at a corner, edge, and interior compartment, as well as the full story. Each fire was scaled by 0.75, 1, and 1.5 or 1.25 of the peak fire temperature. Fires scaled by 0.75 did not experience any failure modes. Fire 2 only experienced failure when scaled by 1.5 times the peak fire temperature. This is because Fire 2 is a very quick fire that heats quickly but also cools quickly, not allowing enough time for the steel sections to reach internal temperatures of any significance. It was decided that fires of this short duration need not be considered in future studies.

Fires 1-1, 1-1.5, 3-1, and 3-1.25 all resulted in column failures. As the interior gravity columns within the fire compartment were heated, they would experience a very slight, nearly negligible axial load increase due to thermal expansion. These columns buckled when they reached their critical temperature. The corner compartment experienced column collapse and then restabilized as the loads from the failed column were redistributed to adjacent columns. Edge compartments resulted in two gravity column failures, which caused bay failure. Again, the system restabilized. Four columns collapse at the interior compartment, resulting in system collapse. The full story fires also result in columns collapses that lead to system collapse.

For Fires 1-1.5 and 3-1.25 at the ninth story, system collapse occurred at the corner and edge compartments as well. After the gravity columns buckle, the moment frame columns exposed to the fire at this level also collapsed. These columns had a lower excess capacity than the moment frame columns at the fifth story.

Column capacity equations provided in Appendix 4 of AISC 360 [48] were found to closely predict the critical failure temperature of the columns at both the fifth and ninth stories when using the modified unbraced length factor that accounts for rotational restraint of the cooler columns above and below the compartment fire.

The wind time history analysis did not cause any damage or residual deformations of the structure. Thus, the wind event has no impact on the fire resilience of the structure in a fire following wind

scenario, unless it is determined that cladding damage has occurred, resulting a change in the opening factor and, thus, a different fire time-temperature curve.

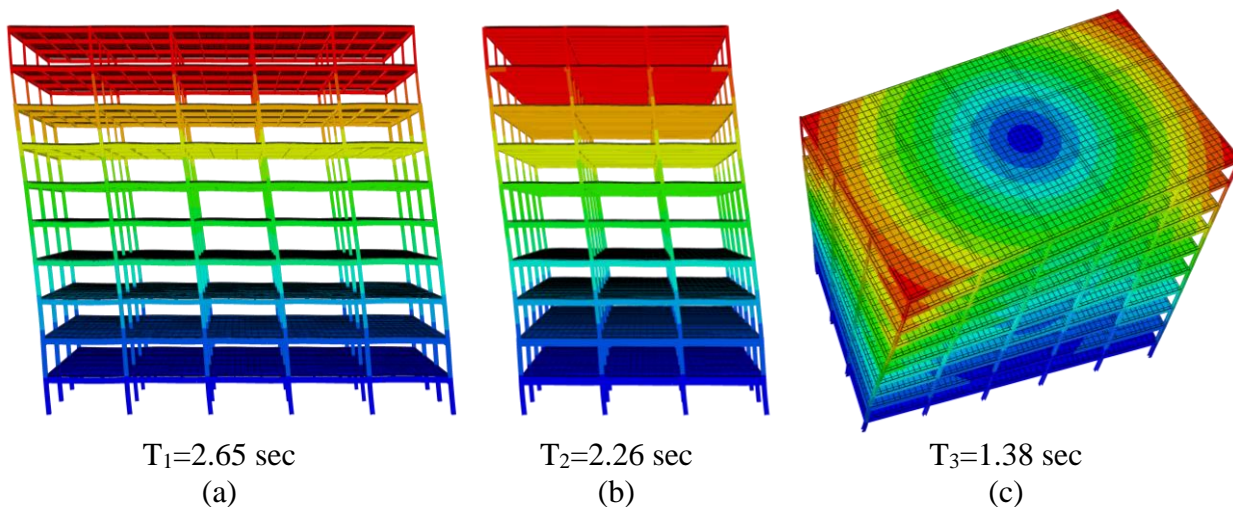


Figure 6.1 Modal shapes and periods for Chicago building
(a) first, (b) second, and (c) third modes

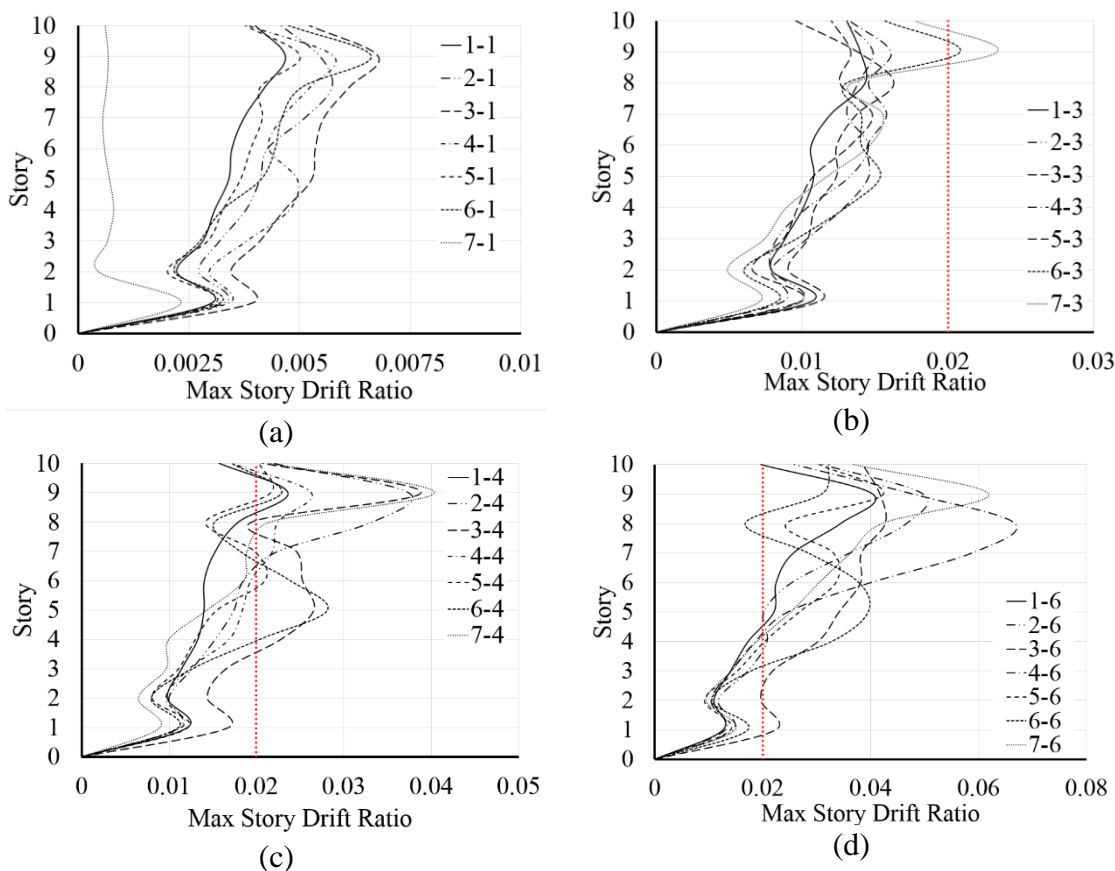


Figure 6.2 Maximum story drift ratios (not incorporating fracture) for Chicago building
(a) 1*PGA (b) 3*PGA (c) 4*PGA (d) 6*PGA

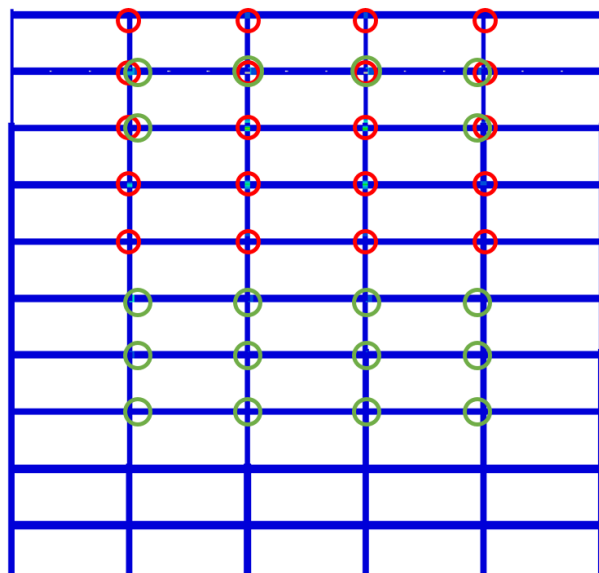


Figure 6.3 Plastic hinge locations observed in Chicago building (EQ4-3)

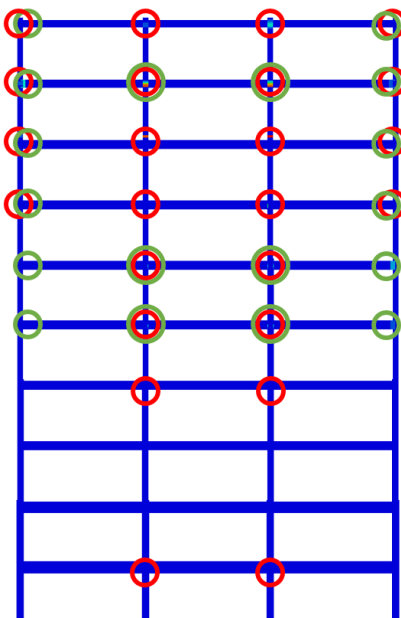


Figure 6.4 Plastic hinge locations observed in Chicago building (EQ5-4)

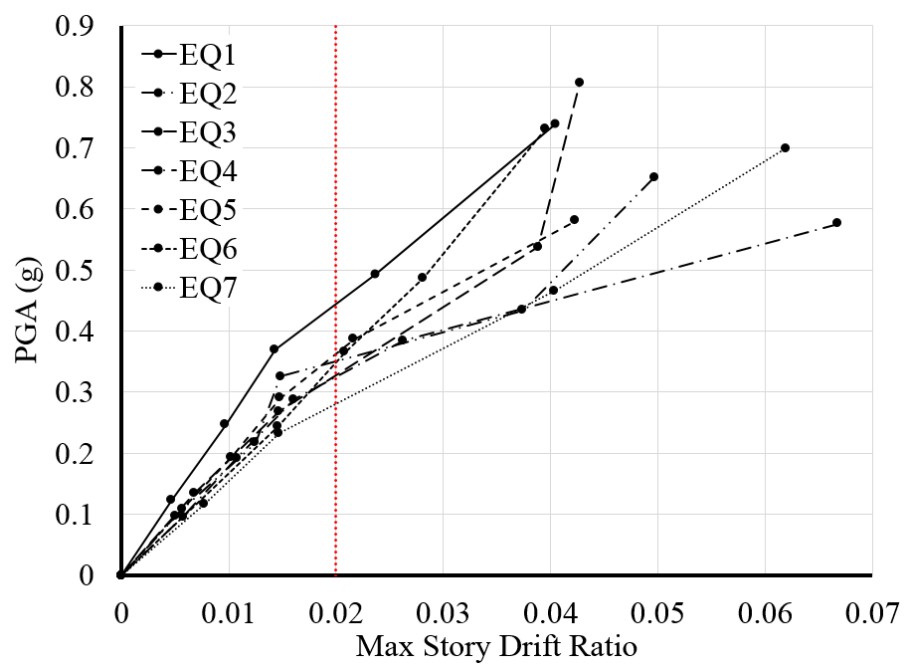


Figure 6.5 Results of IDA for Chicago building: PGA vs. maximum story drift ratio

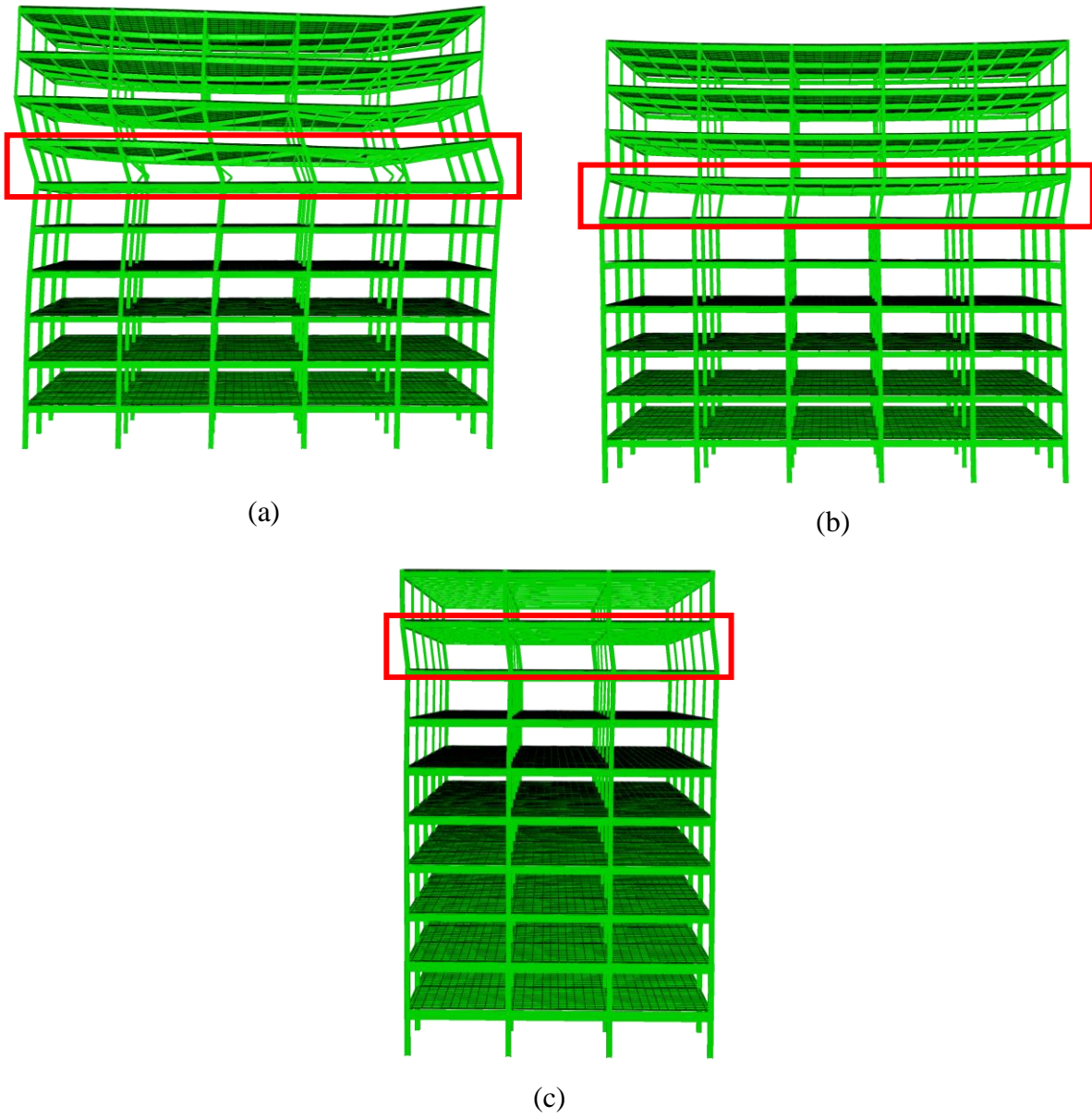
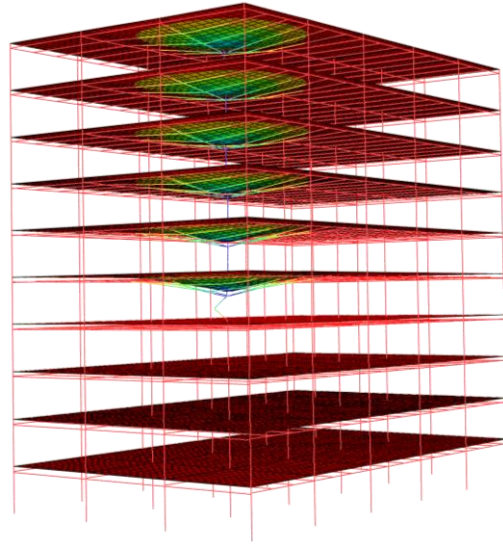
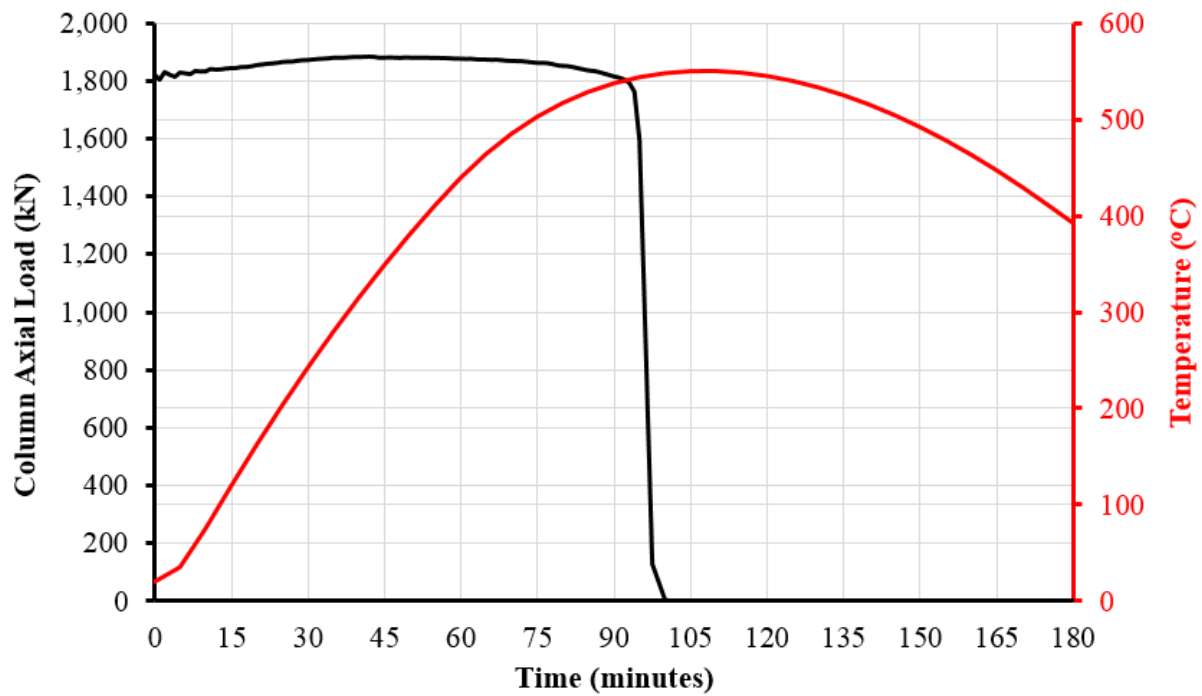


Figure 6.6 Initiation of soft story collapse of Chicago building
(a) EQ2-6, (b) EQ4-6, and (c) EQ5-6



(a)



(b)

Figure 6.7 Response of Chicago building exposed to 5th story corner compartment Fire 1-1
 (a) rendering of interior gravity column failure
 (b) axial load and temperature versus time for the failed interior gravity column

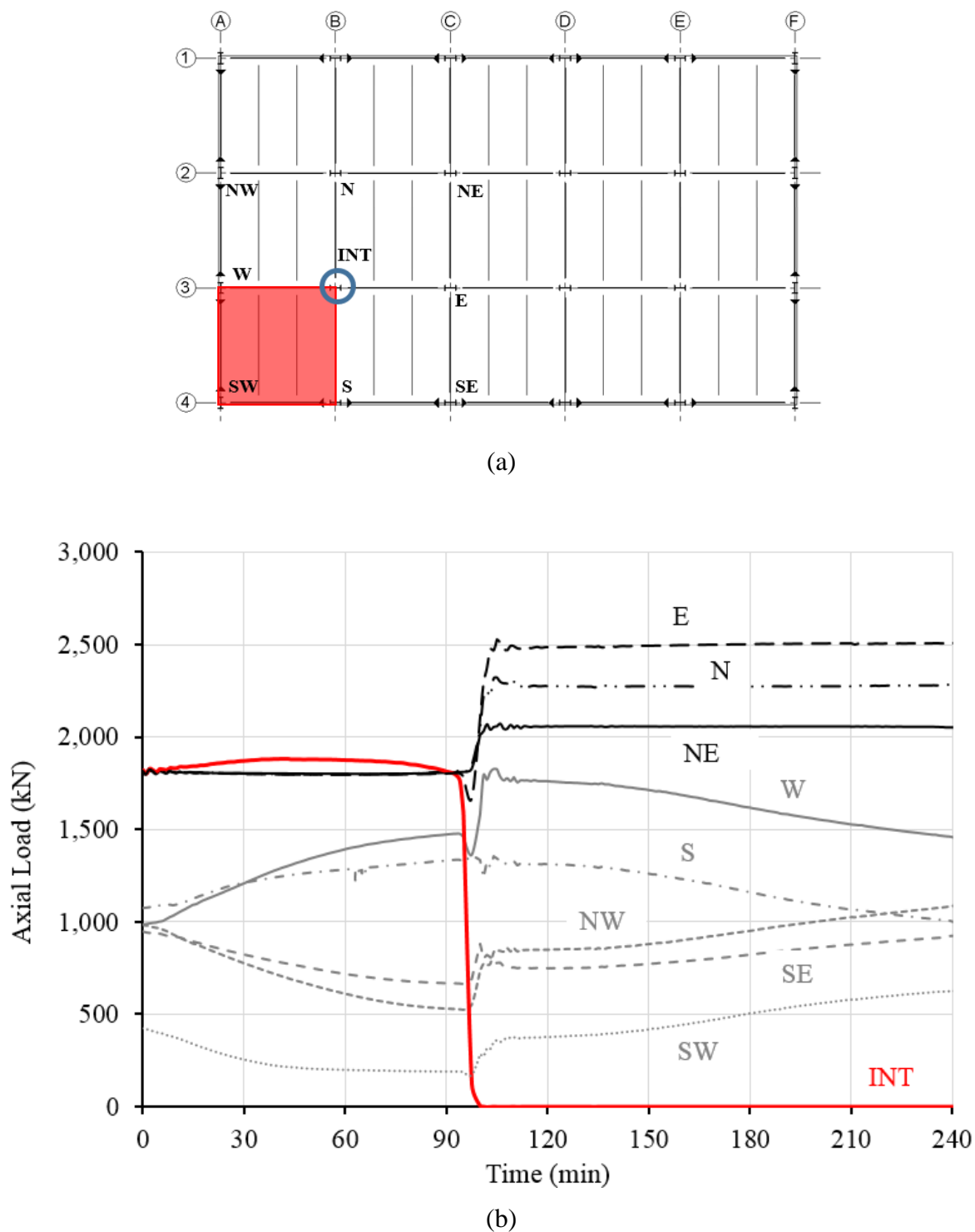


Figure 6.8 Axial loads of fifth story columns in Chicago building exposed to 5th story corner compartment Fire 1-1

(a) column designations

(b) axial load versus time of columns adjacent to failed interior gravity column, INT

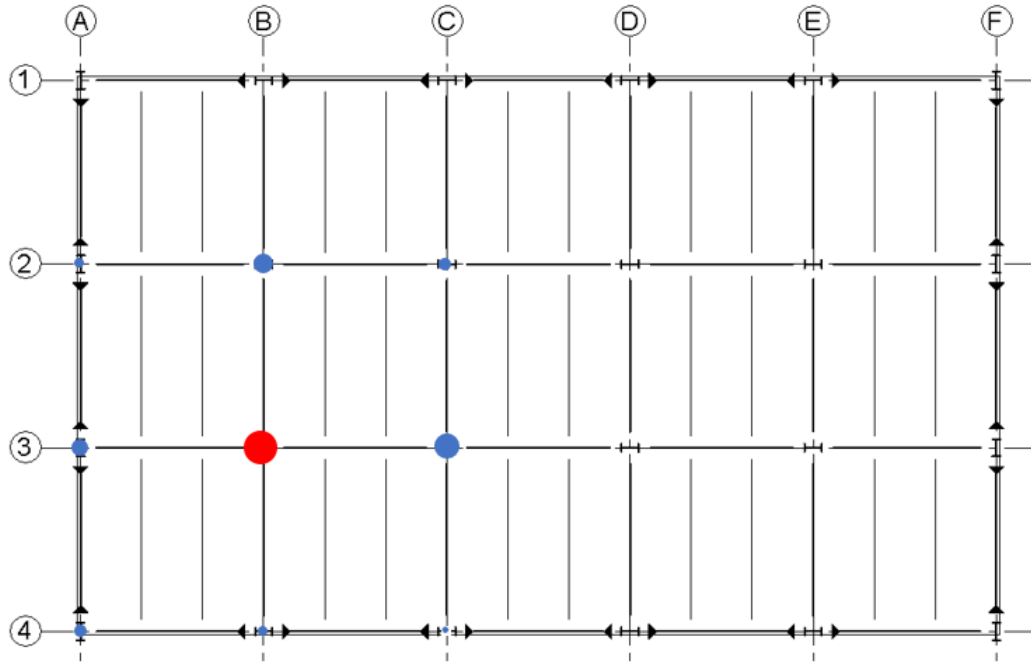


Figure 6.9 Graphical representation of interior gravity column load (red circle) redistributed to adjacent columns (blue circles) for corner compartment Fire 1-1 at 5th story

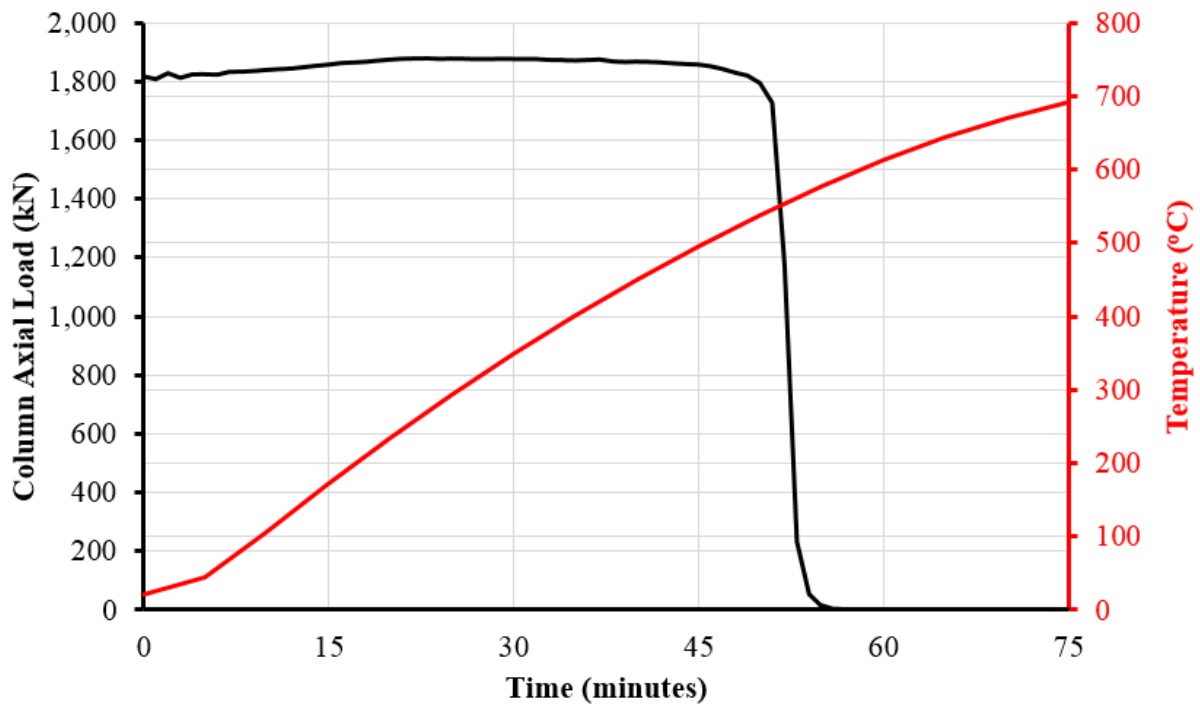
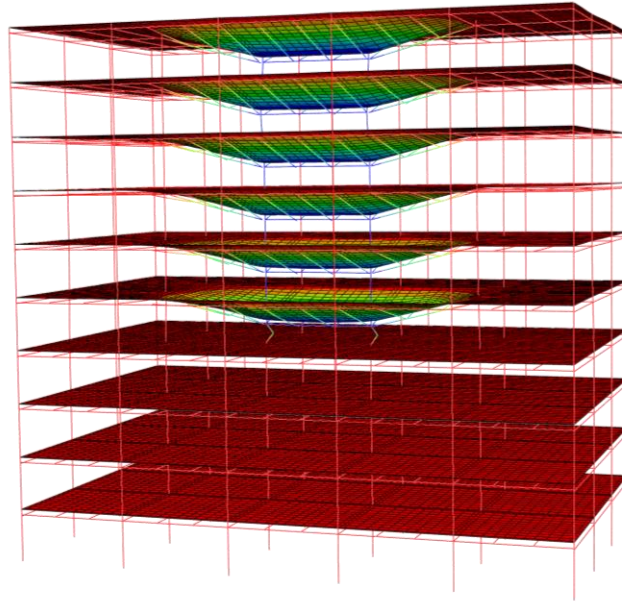
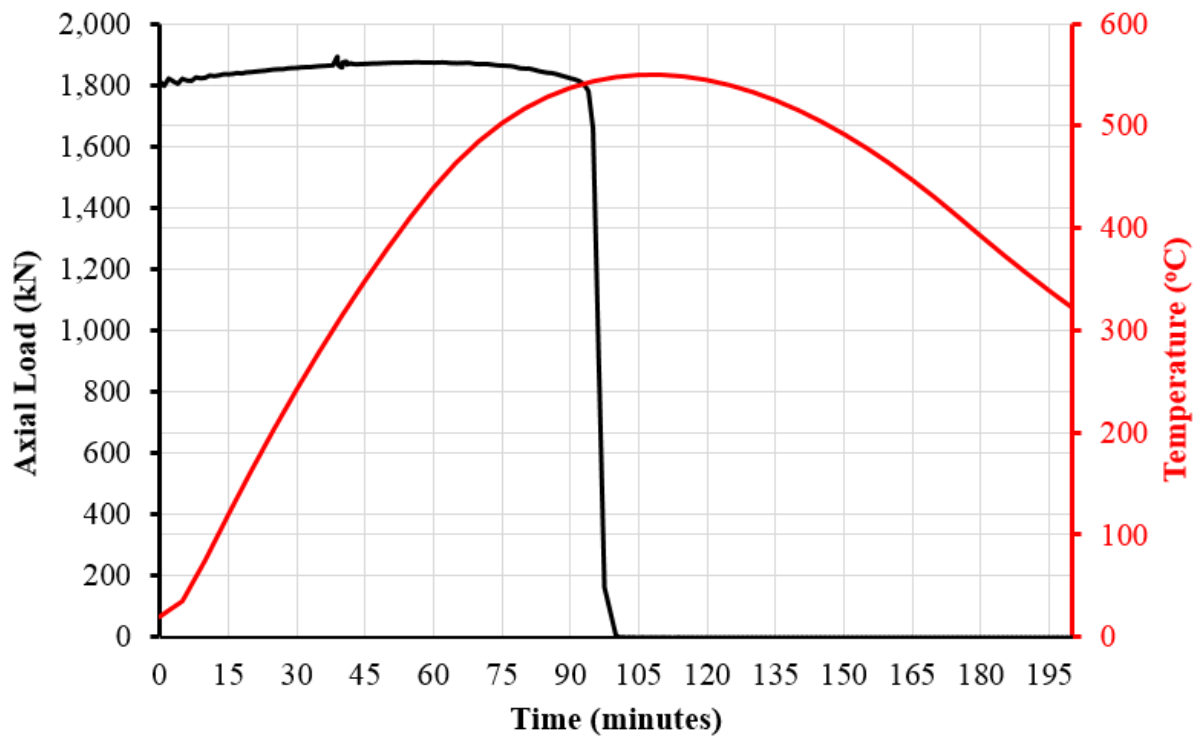


Figure 6.10 Response of Chicago building exposed to 5th story corner compartment Fire 1-1.5



(a)

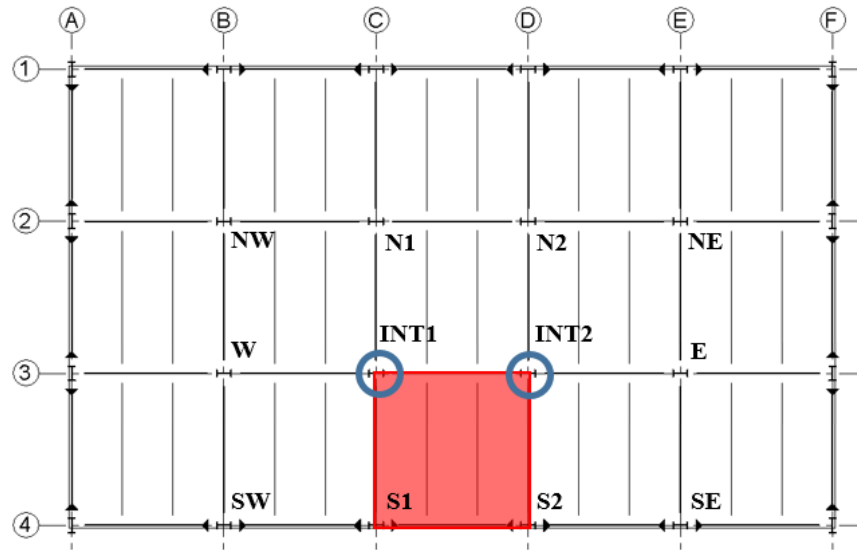


(b)

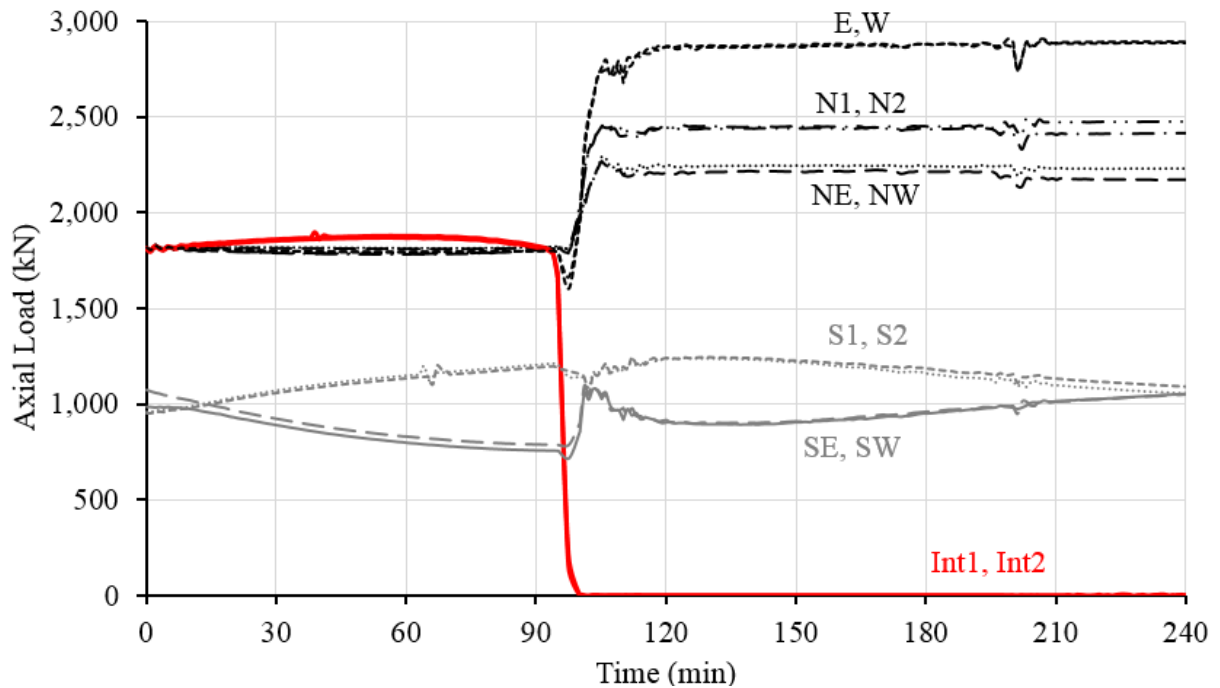
Figure 6.11 Response of Chicago building exposed to 5th story edge compartment Fire 1-1

(a) rendering of interior gravity column failures

(b) axial load and temperature versus time for the failed interior gravity columns



(a)



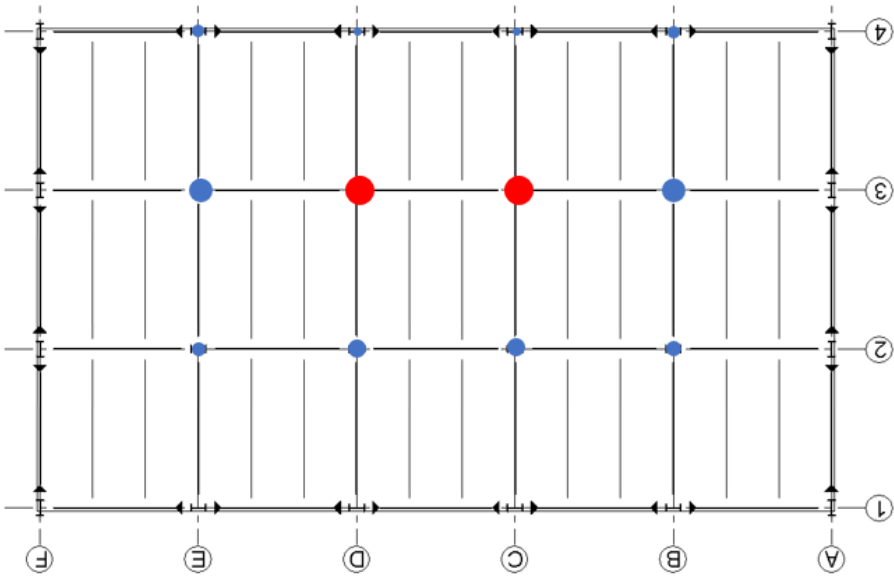
(b)

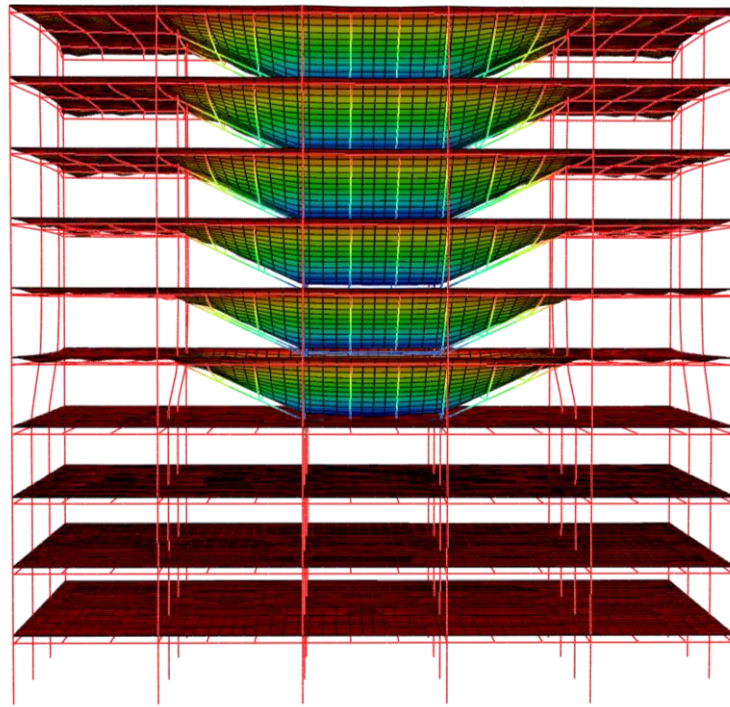
Figure 6.12 Axial loads of fifth story columns in Chicago building exposed to 5th story edge compartment Fire 1-1

(a) column designations

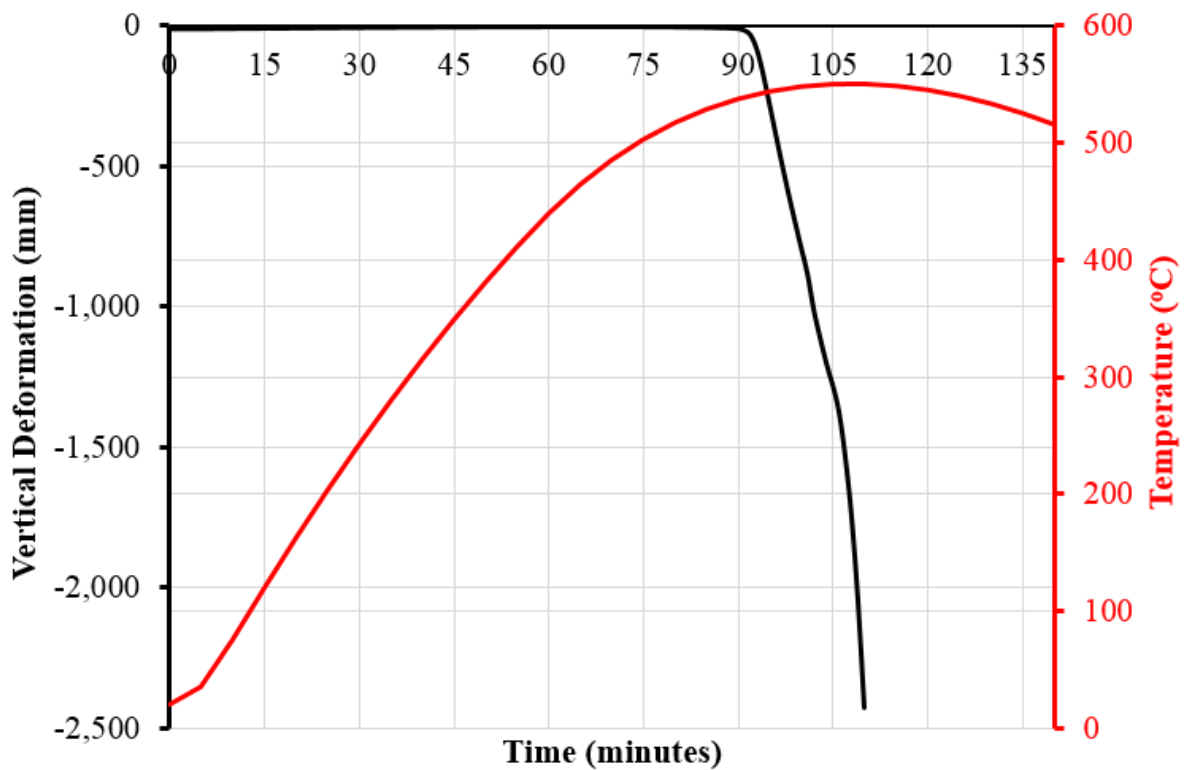
(b) axial load versus time of columns adjacent to failed interior gravity columns, INT1 and INT2

Figure 6.13 Graphical representation of interior gravity column loads (red circles) redistributed to adjacent columns (blue circles) for edge compartment Fire 1-1 at 5th story



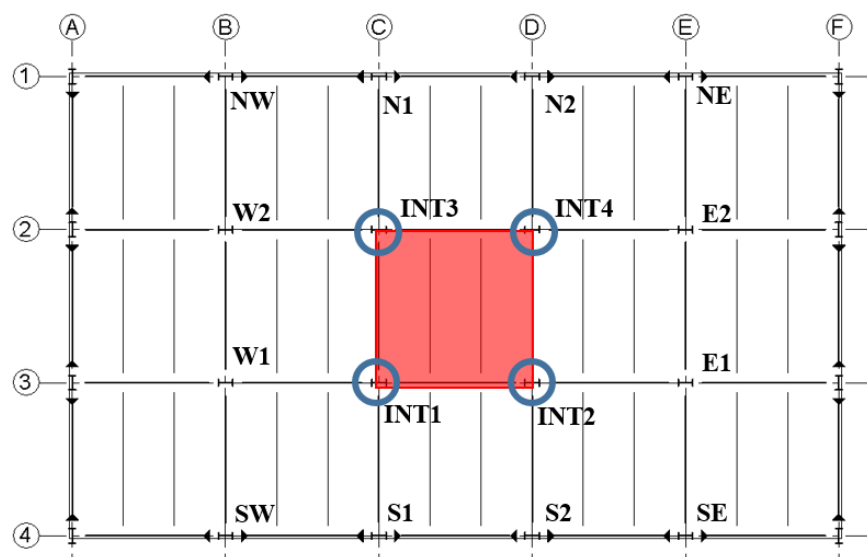


(a)

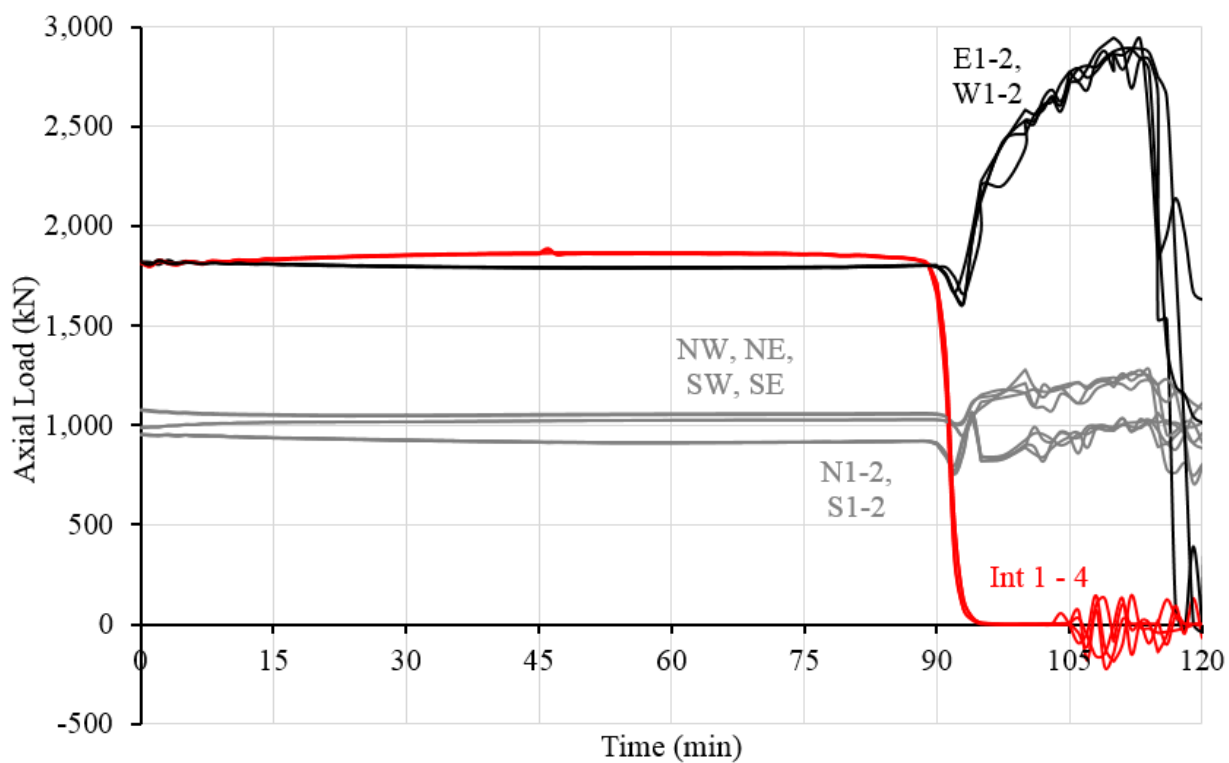


(b)

Figure 6.14 Response of Chicago building exposed to 5th story interior compartment Fire 1-1
 (a) rendering of interior gravity columns resulting in system collapse
 (b) vertical deflection and temperature versus time for the failed interior gravity columns



(a)

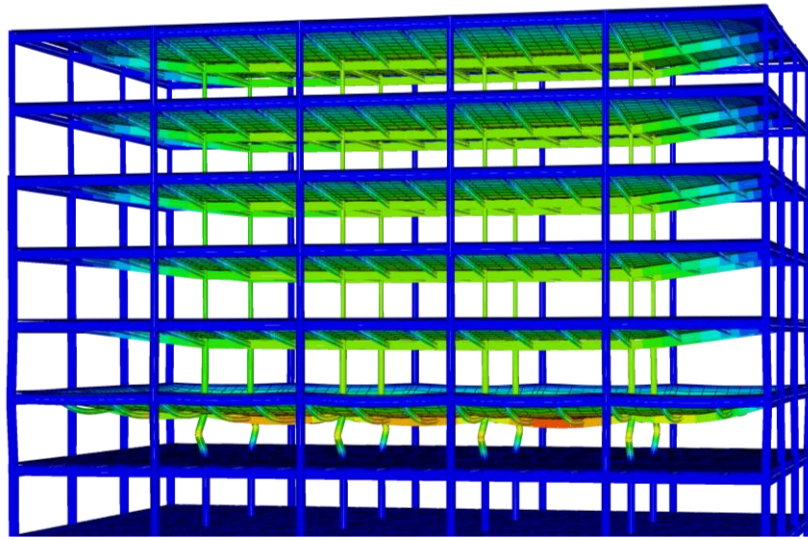


(b)

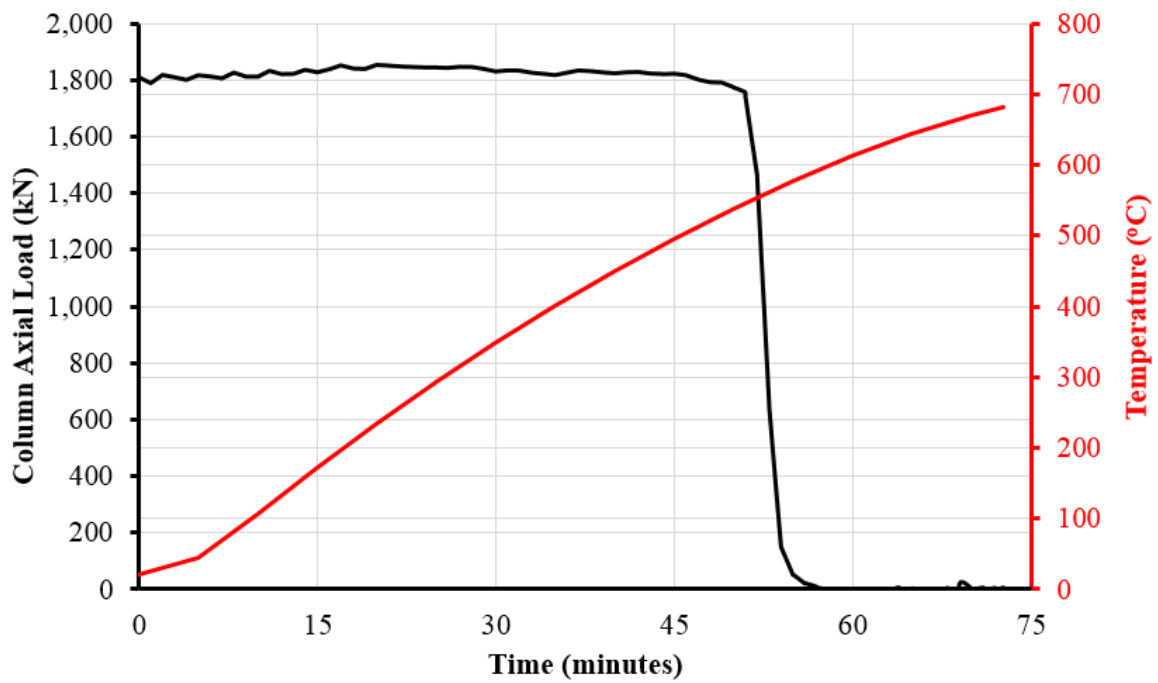
Figure 6.15 Axial loads of fifth story columns in Chicago building exposed to 5th story interior compartment Fire 1-1

(a) column designations

(b) axial load versus time of columns adjacent to failed interior gravity columns, INT1-4



(a)



(b)

Figure 6.16 Response of Chicago building exposed to 5th story full story Fire 1-1.5
 (a) rendering of interior gravity columns' failure initiation resulting in system collapse
 (b) vertical deflection and temperature versus time for the failed interior gravity columns

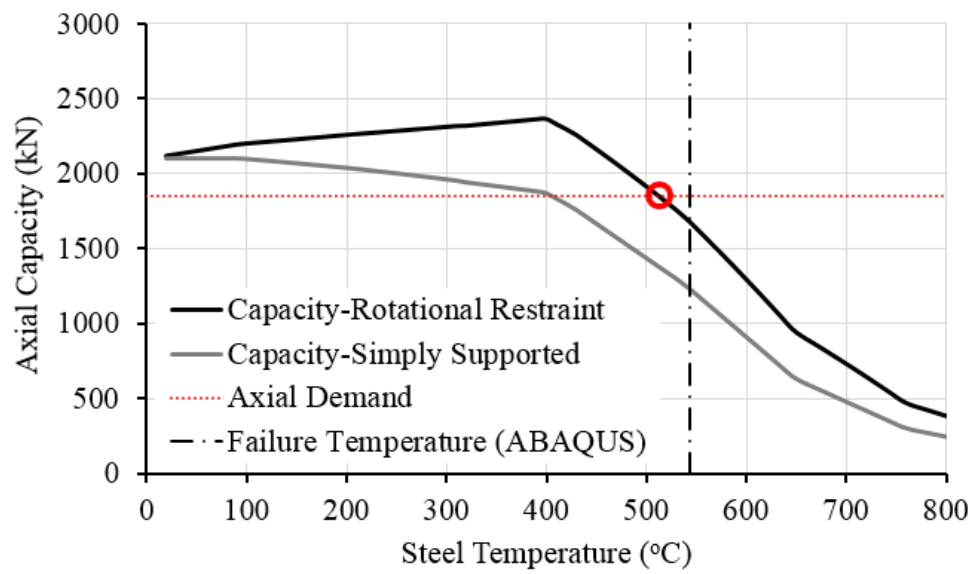
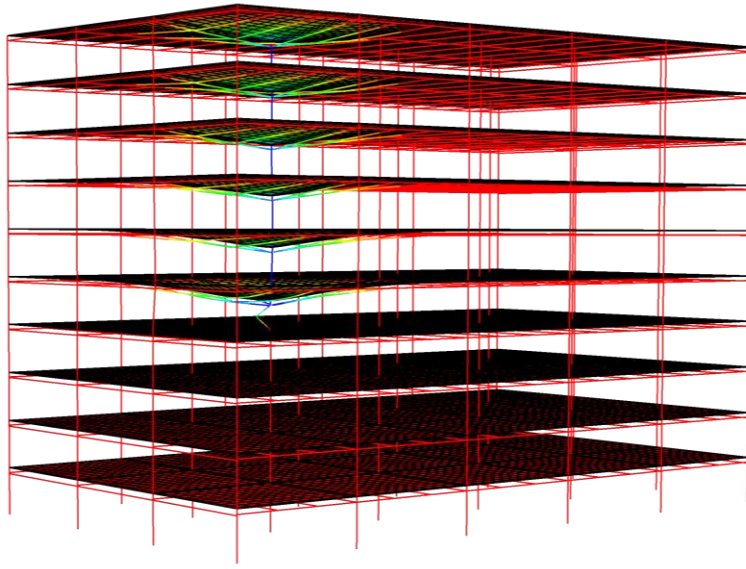
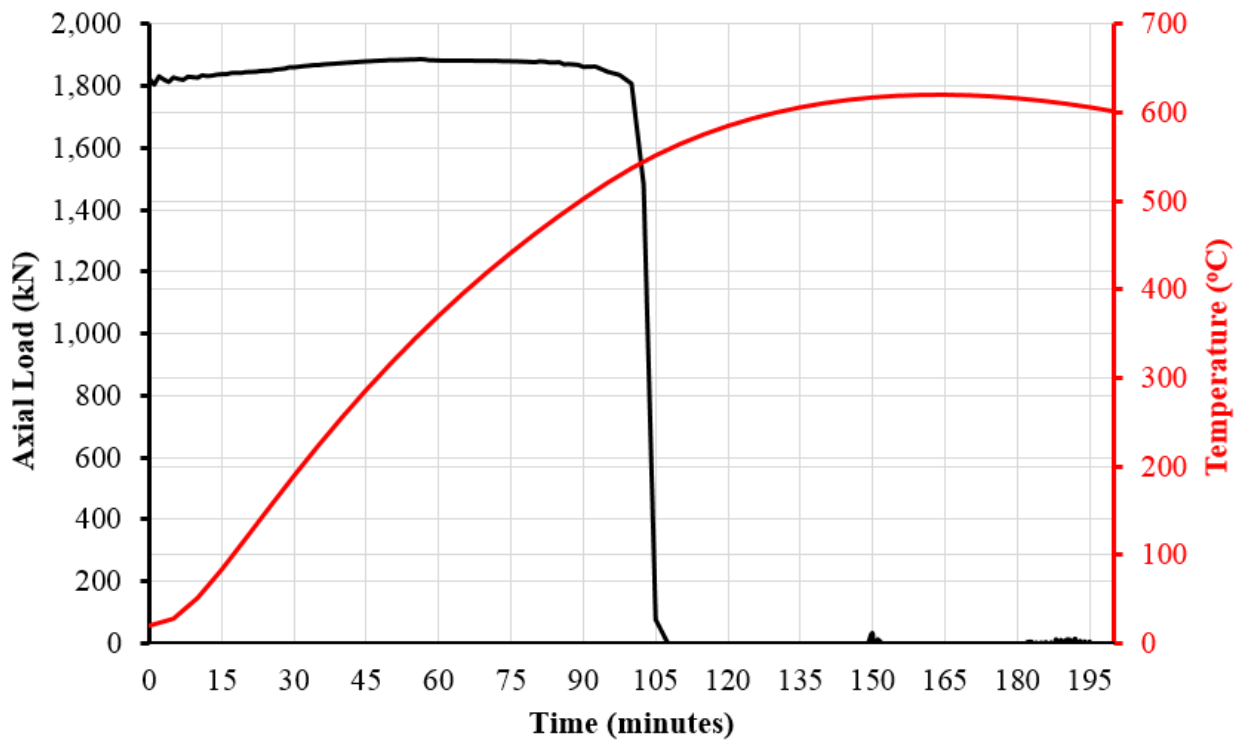


Figure 6.17 Fifth story W12x58 gravity column capacity versus temperature: comparison of ABAQUS results and calculated values



(a)



(b)

Figure 6.18 Response of Chicago building exposed to 5th story corner compartment Fire 3-1

(a) rendering of interior gravity column failure

(b) axial load and temperature versus time for the failed interior gravity column

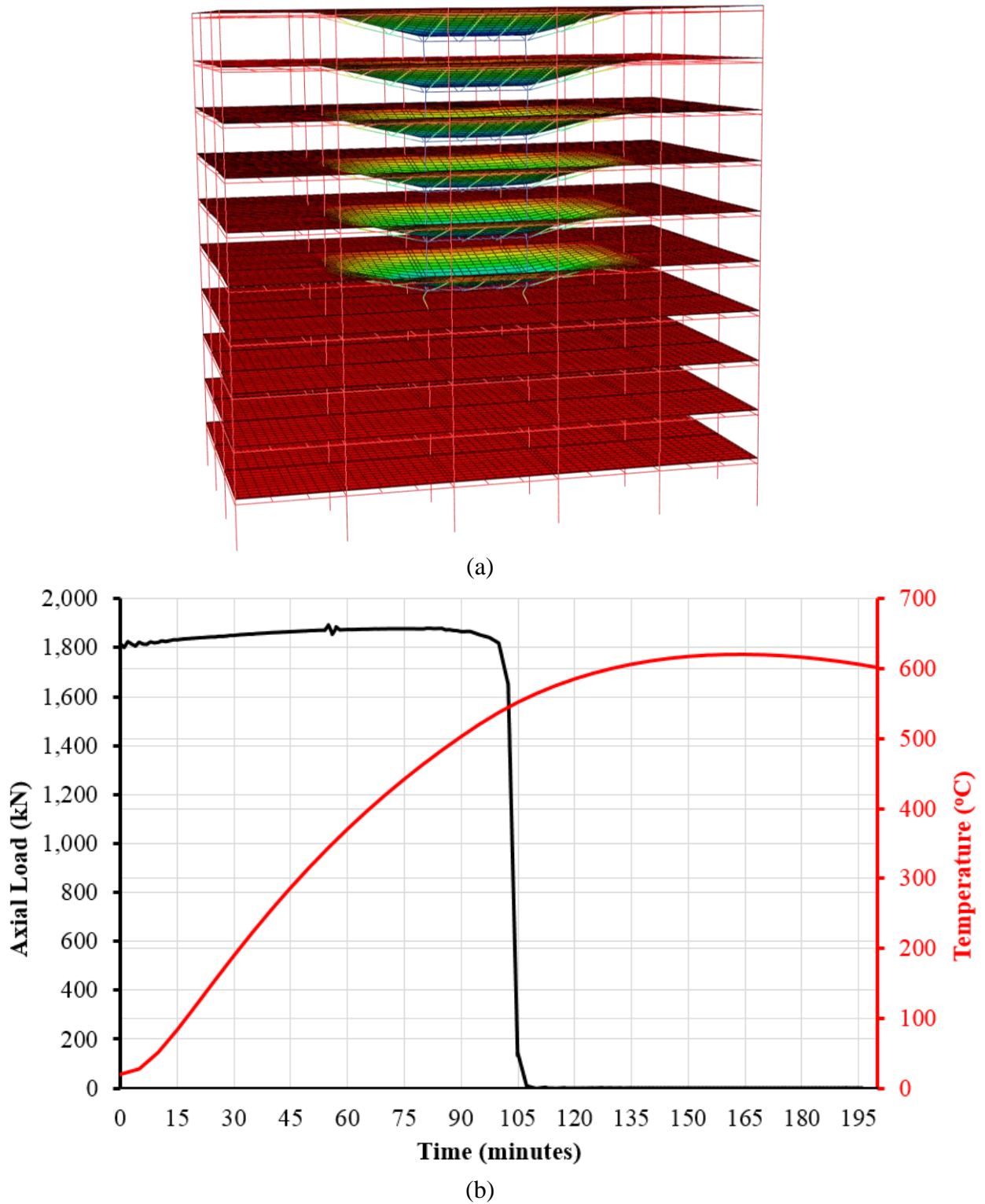


Figure 6.19 Response of Chicago building exposed to 5th story edge compartment Fire 3-1
 (a) rendering of interior gravity column failures
 (b) axial load and temperature versus time for the failed interior gravity columns

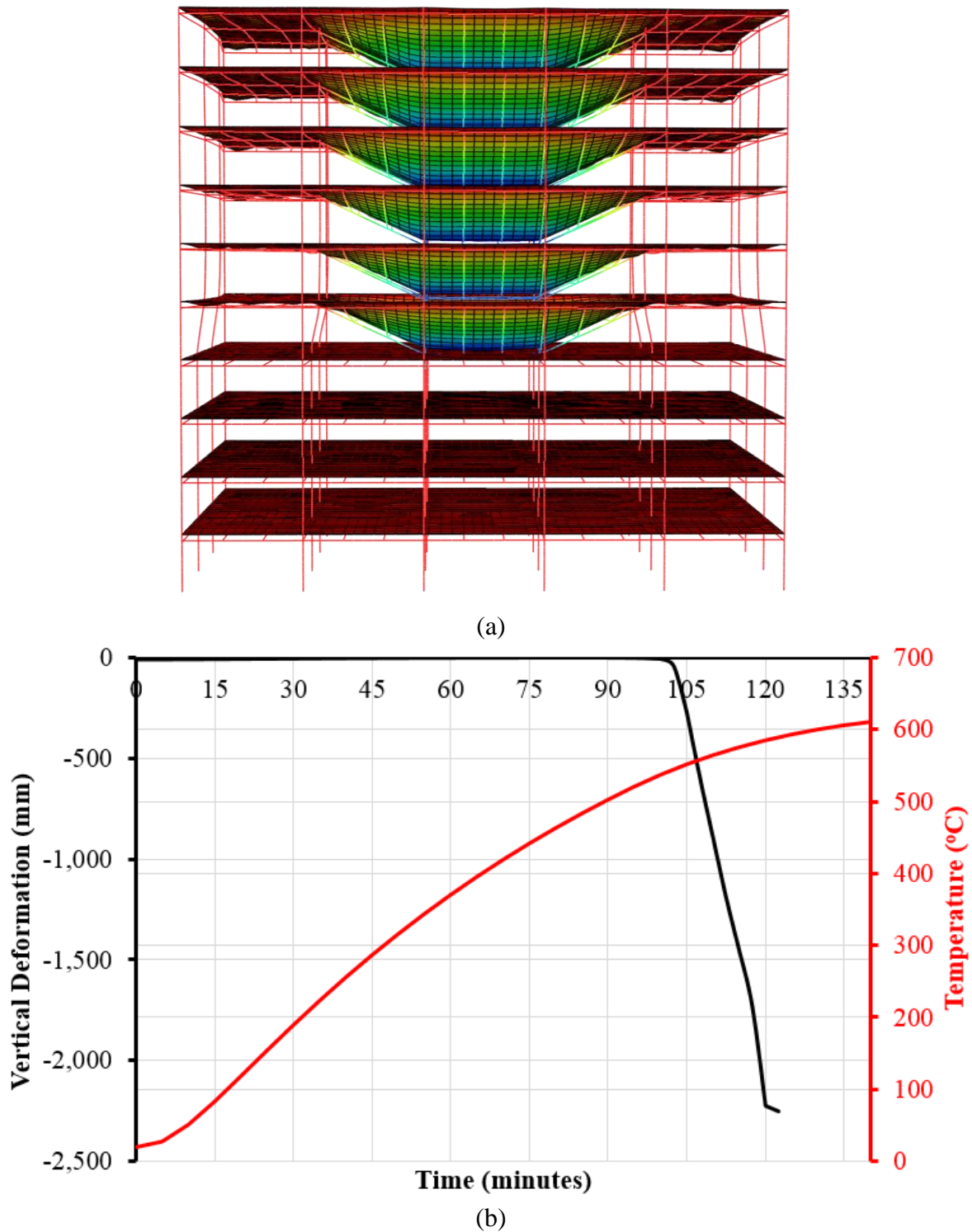
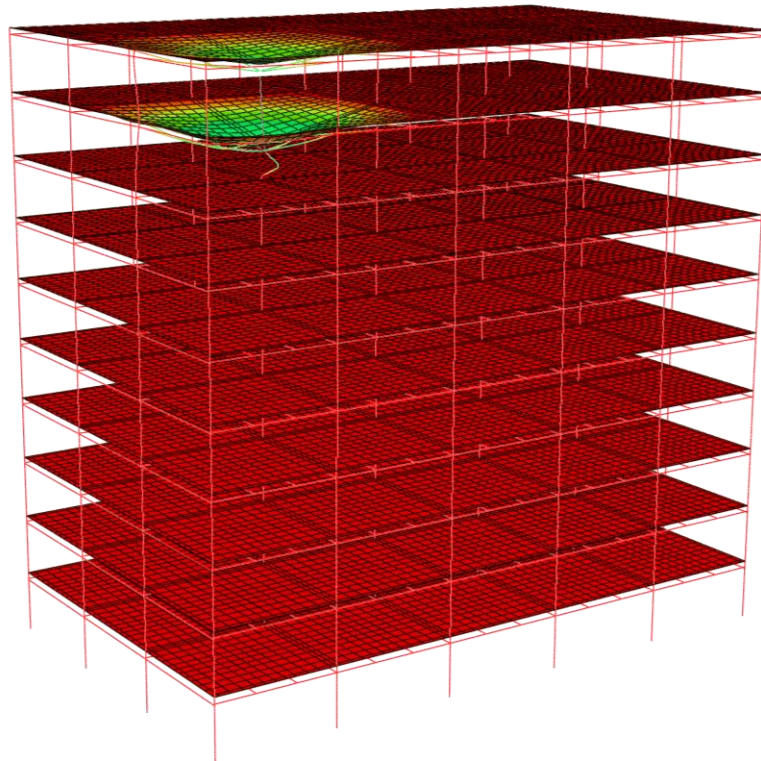


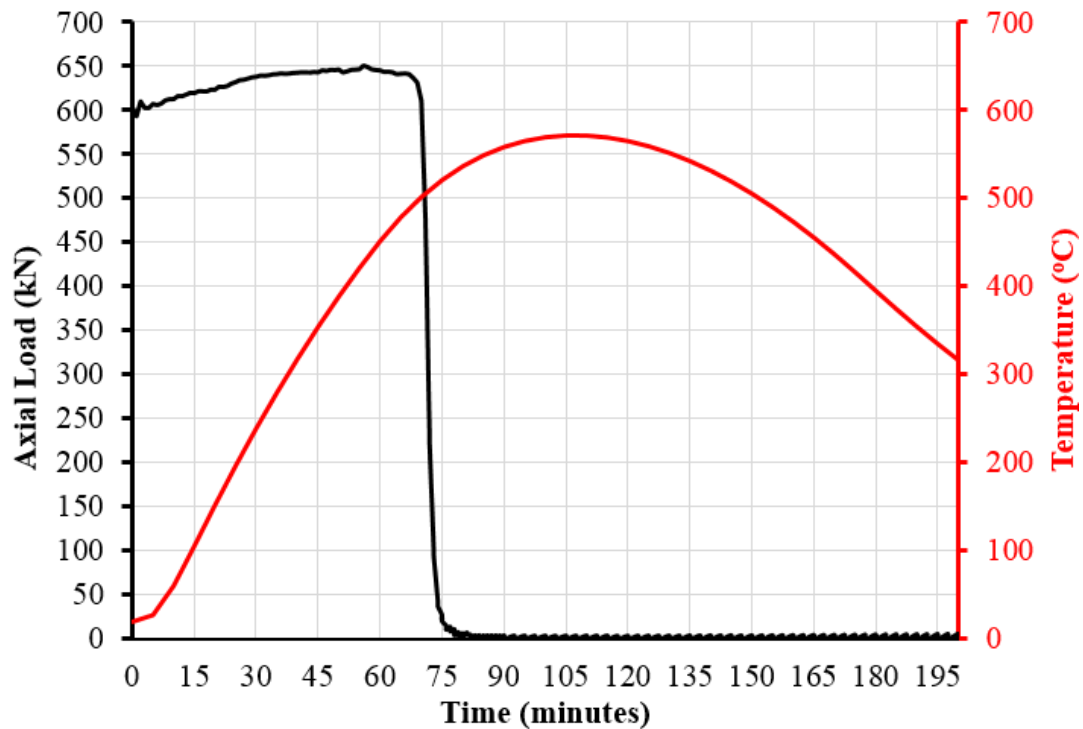
Figure 6.20 Response of Chicago building exposed to 5th story interior compartment Fire 3-1
 (a) rendering of interior gravity columns resulting in system collapse
 (b) vertical deflection and temperature versus time for the failed interior gravity columns

Table 6.1 Results of IFA analyses for non-fractured Chicago building at the 5th story

Fire #	Fire Location	0.75 * Max Fire Temp			1.0 * Max Fire Temp			1.5 (Fire 1,2) or 1.25 (Fire 3)* Max Fire Temp		
		Failure Type	Max vertical deflection (mm)	Time of failure (min)	Failure Type	Max vertical deflection (mm)	Time of failure (min)	Failure Type	Max vertical deflection (mm)	Time of failure (min)
1	5A	-	208	-	Column	1370	95	Column	1821	50
1	5B	-	214	-	Bay	2054	98	Bay	2226	50
1	5C	-	242	-	System	Collapse	91	System	Collapse	50
1	FULL	-	-	-	System	Collapse	100	System	Collapse	51
2	5A	-	169	-	-	235	-	Compartment	471	46
2	5B	-	159	-	-	219	-	Compartment	442	51
2	5C	-	187	-	-	288	-	Compartment	542	55
2	FULL	-	-	-	-	188	-	Compartment	465	46
3	5A	-	228	-	Column	1466	100	Column	1445	77
3	5B	-	-	-	Bay	1986	100	Bay	2122	76
3	5C	-	259	-	System	Collapse	100	System	Collapse	75
3	FULL	-	-	-	System	Collapse	103	System	Collapse	77

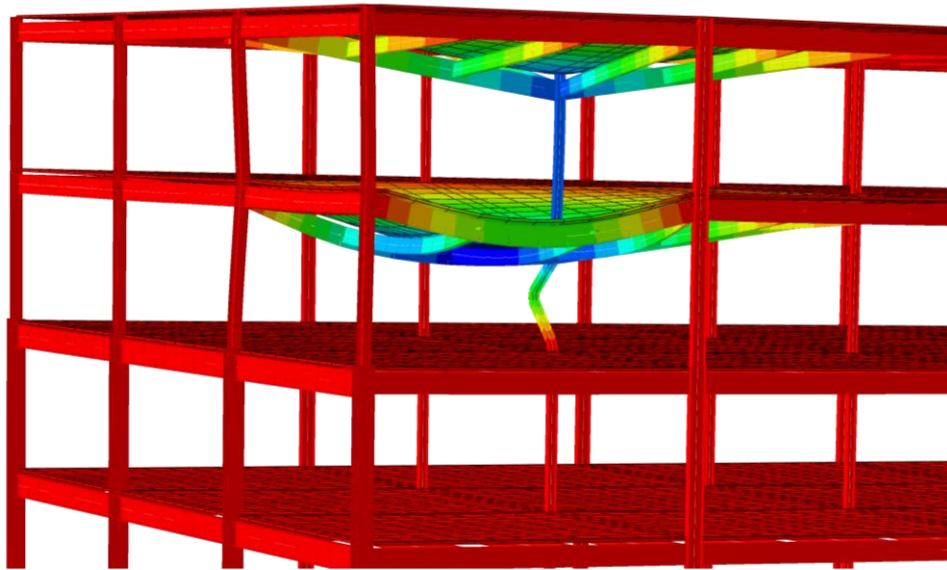


(a)

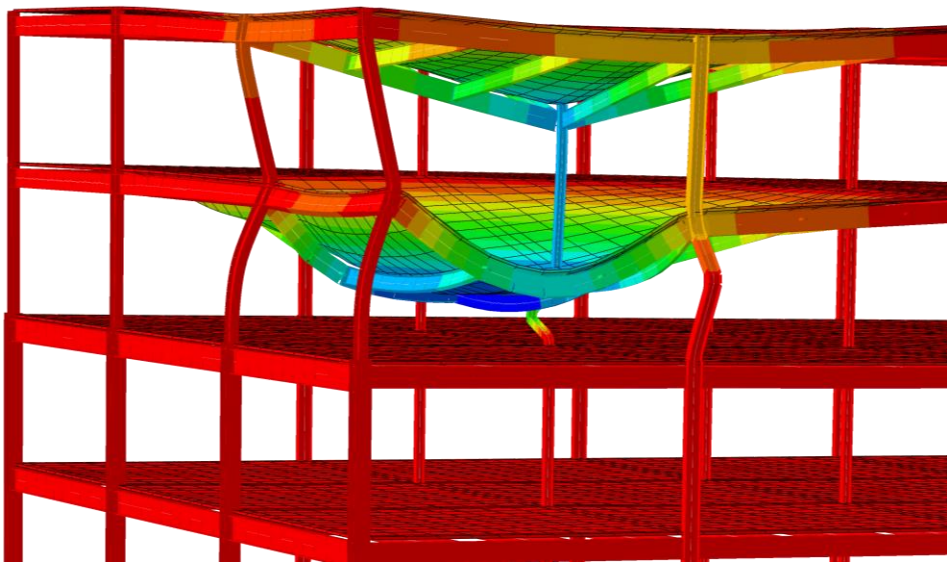


(b)

Figure 6.21 Response of Chicago building exposed to 9th story corner compartment Fire 1-1
 (a) rendering of interior gravity column failure
 (b) axial load and temperature versus time for the failed interior gravity column

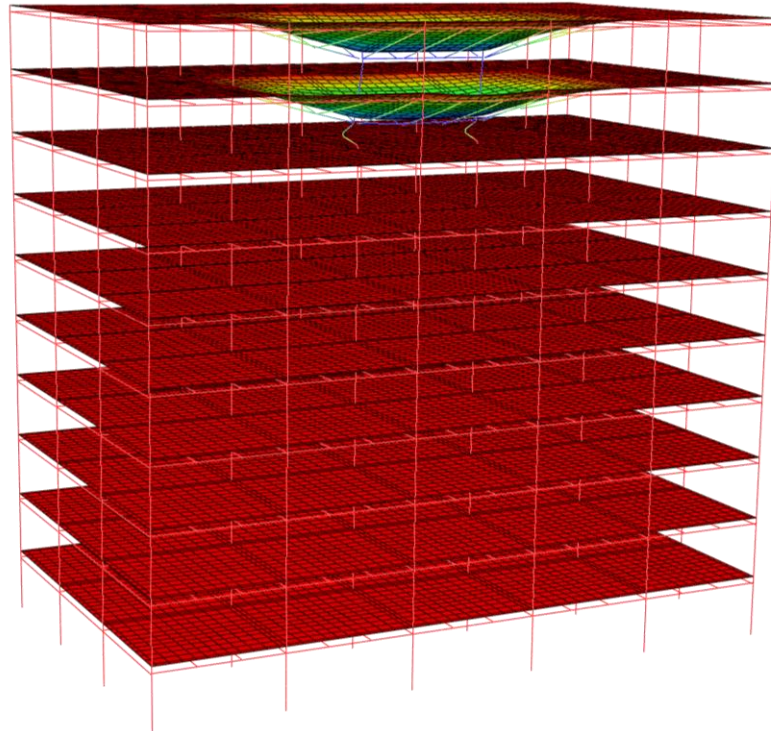


(a)

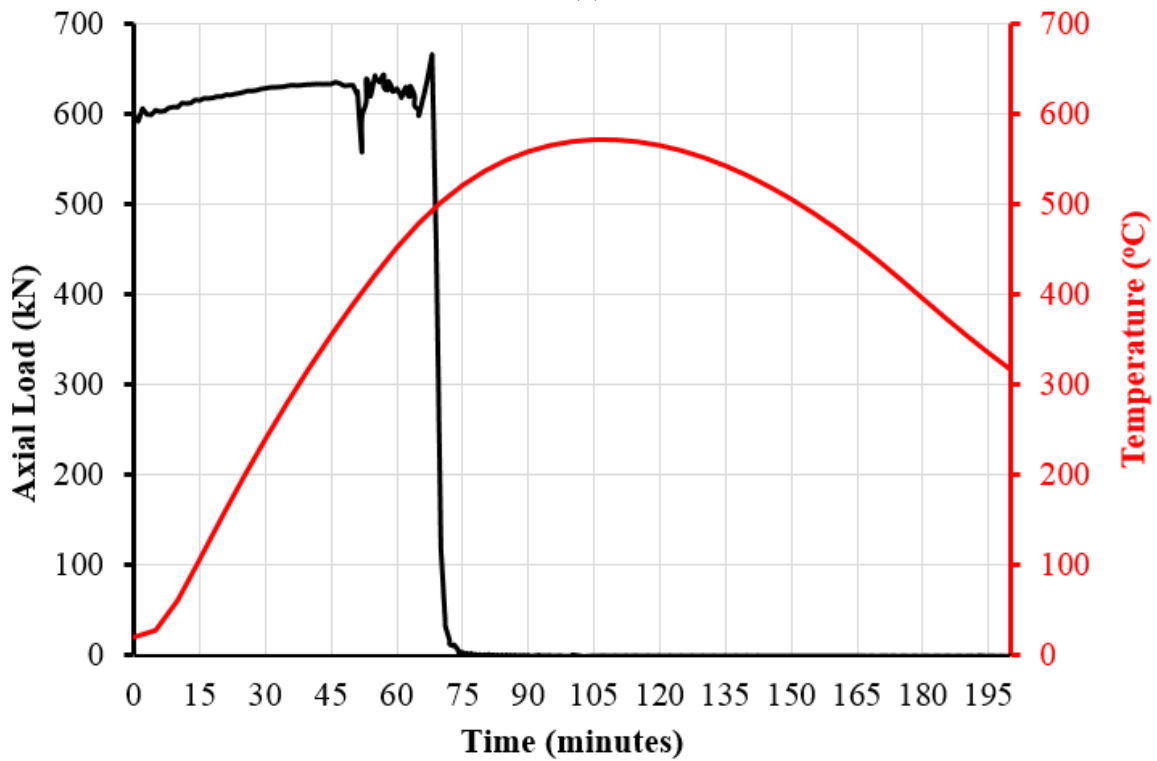


(b)

Figure 6.22 Response of Chicago building exposed to 9th story corner compartment Fire 1-1.5
(a) rendering of interior gravity column failure
(b) progressive collapse of adjacent moment frame columns



(a)



(b)

Figure 6.23 Response of Chicago building exposed to 9th story edge compartment Fire 1-1
 (a) rendering of interior gravity column failures
 (b) axial load and temperature versus time for the failed interior gravity columns

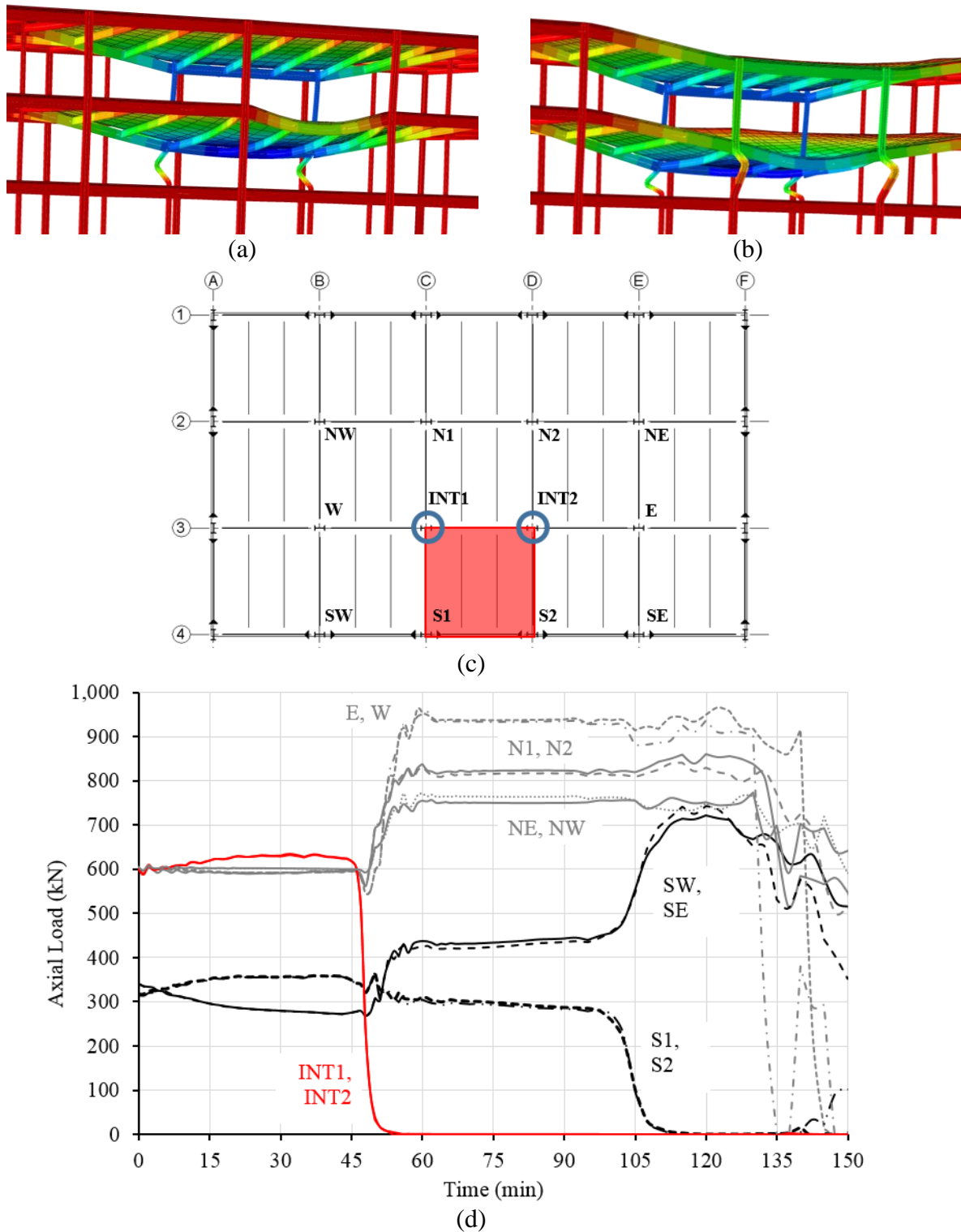
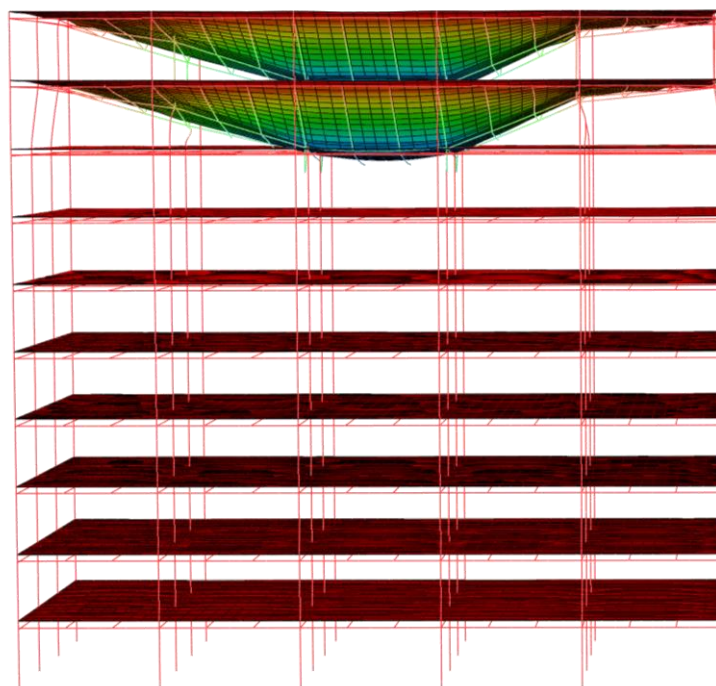
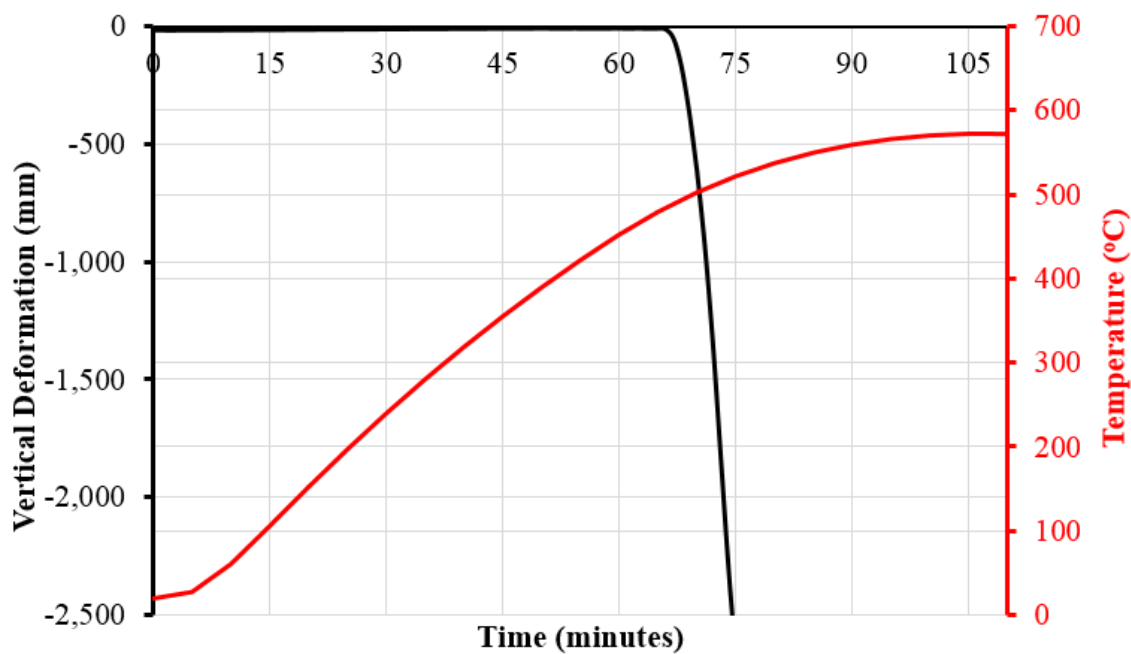


Figure 6.24 Response of Chicago building exposed to 9th story edge compartment Fire 1-1.5
 (a) rendering of interior gravity column failures, (b) rendering of collapse of adjacent moment frame columns, (c) column designations, (d) axial load versus time of columns adjacent to failed interior gravity columns, INT1-2



(a)



(b)

Figure 6.25 Response of Chicago building exposed to 9th story interior compartment Fire 1-1
 (a) rendering of interior gravity columns resulting in system collapse
 (b) vertical deflection and temperature versus time for the failed interior gravity columns

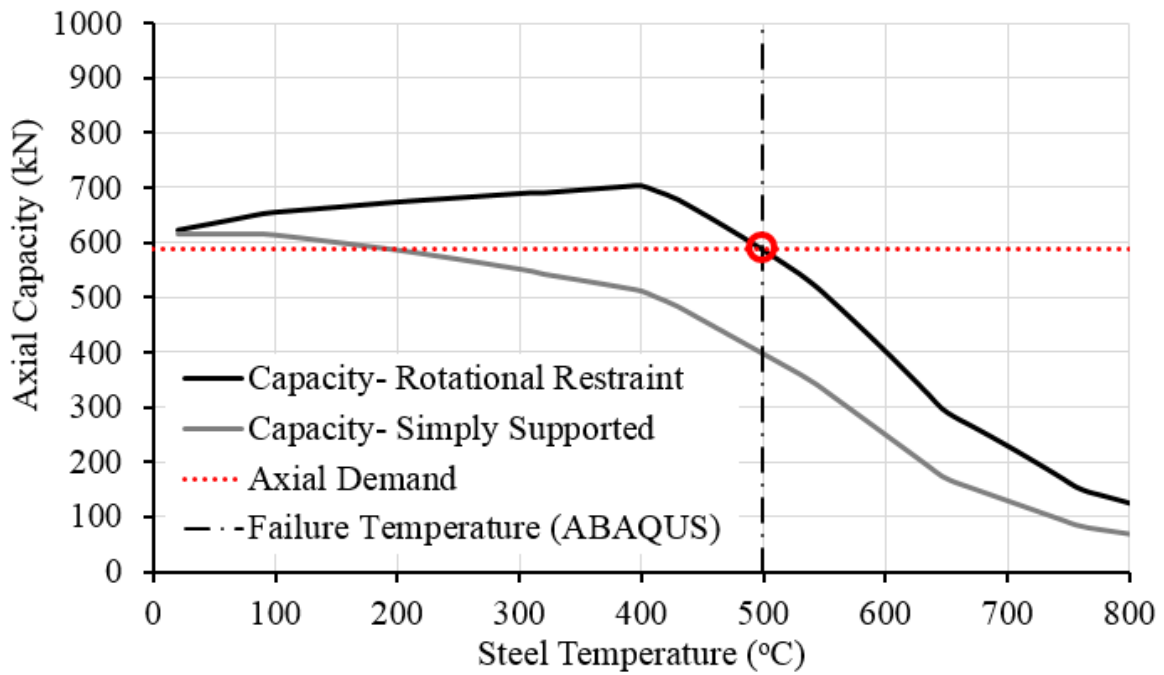
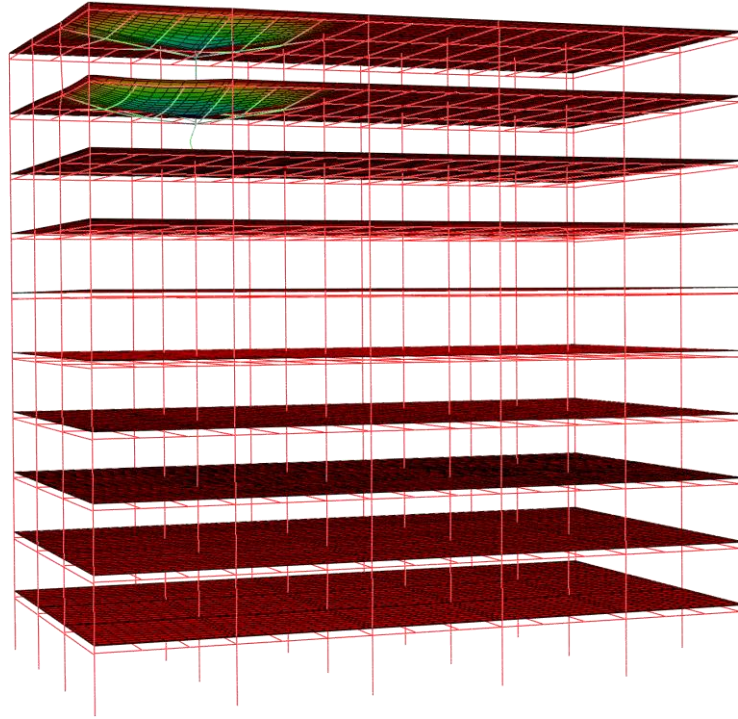
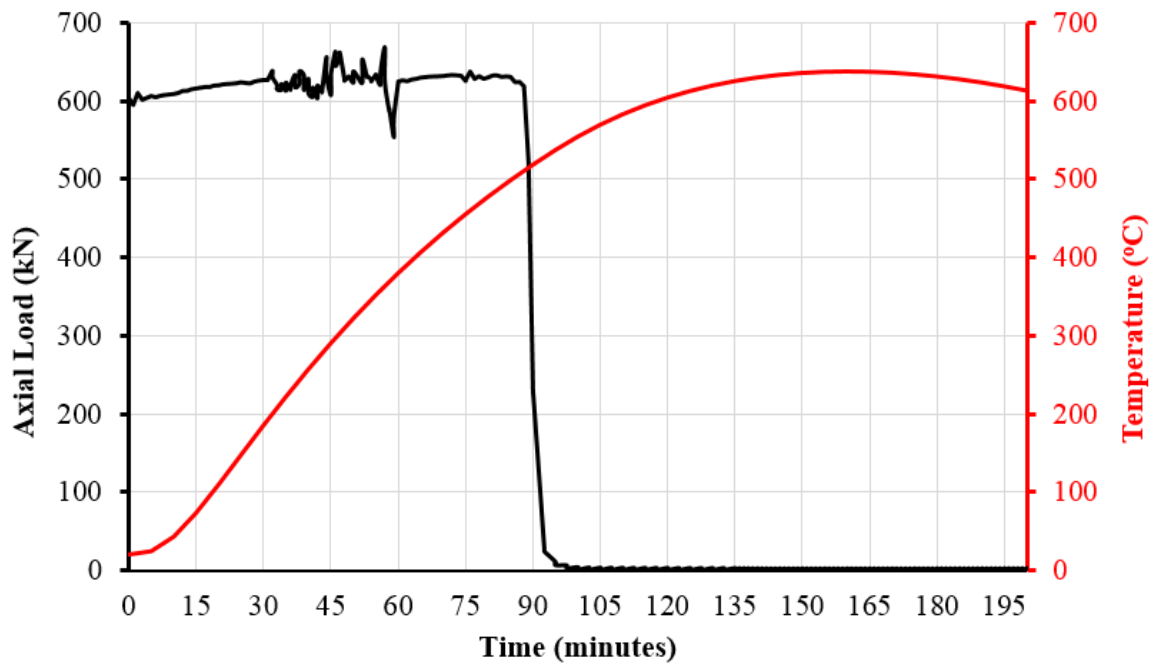


Figure 6.26 Ninth story W8x24 gravity column capacity versus temperature: comparison of ABAQUS results and calculated values

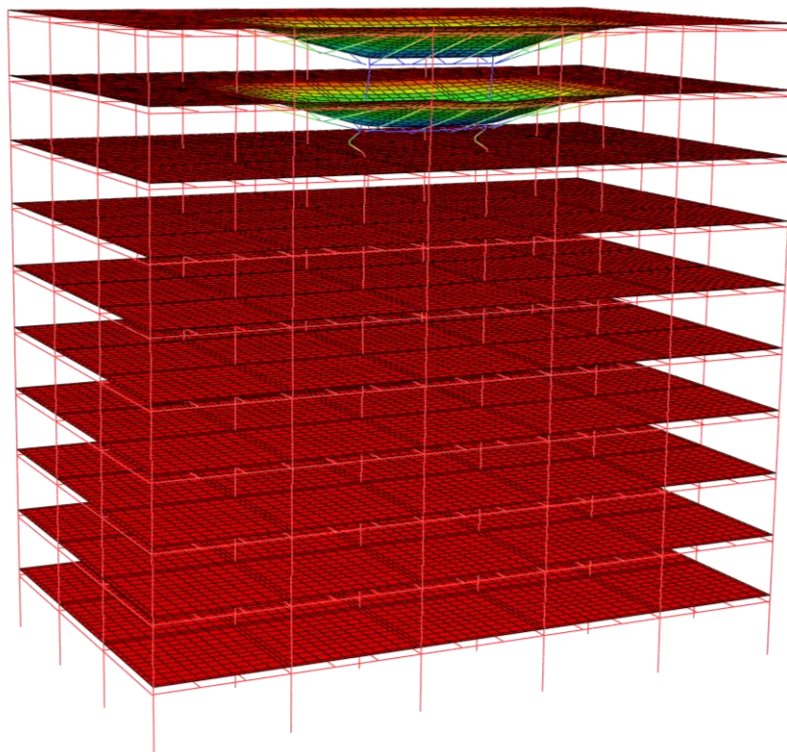


(a)

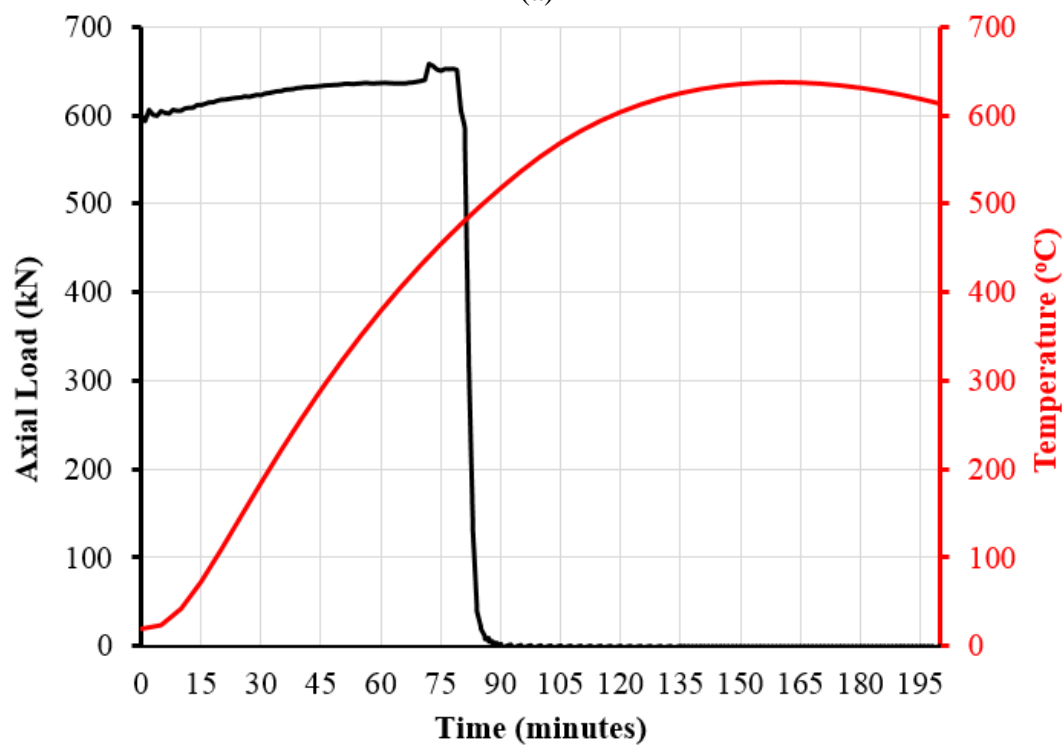


(b)

Figure 6.27 Response of Chicago building exposed to 9th story corner compartment Fire 3-1
 (a) rendering of interior gravity column failure
 (b) axial load and temperature versus time for the failed interior gravity column



(a)



(b)

Figure 6.28 Response of Chicago building exposed to 9th story edge compartment Fire 3-1

(a) rendering of interior gravity column failures

(b) axial load and temperature versus time for the failed interior gravity columns

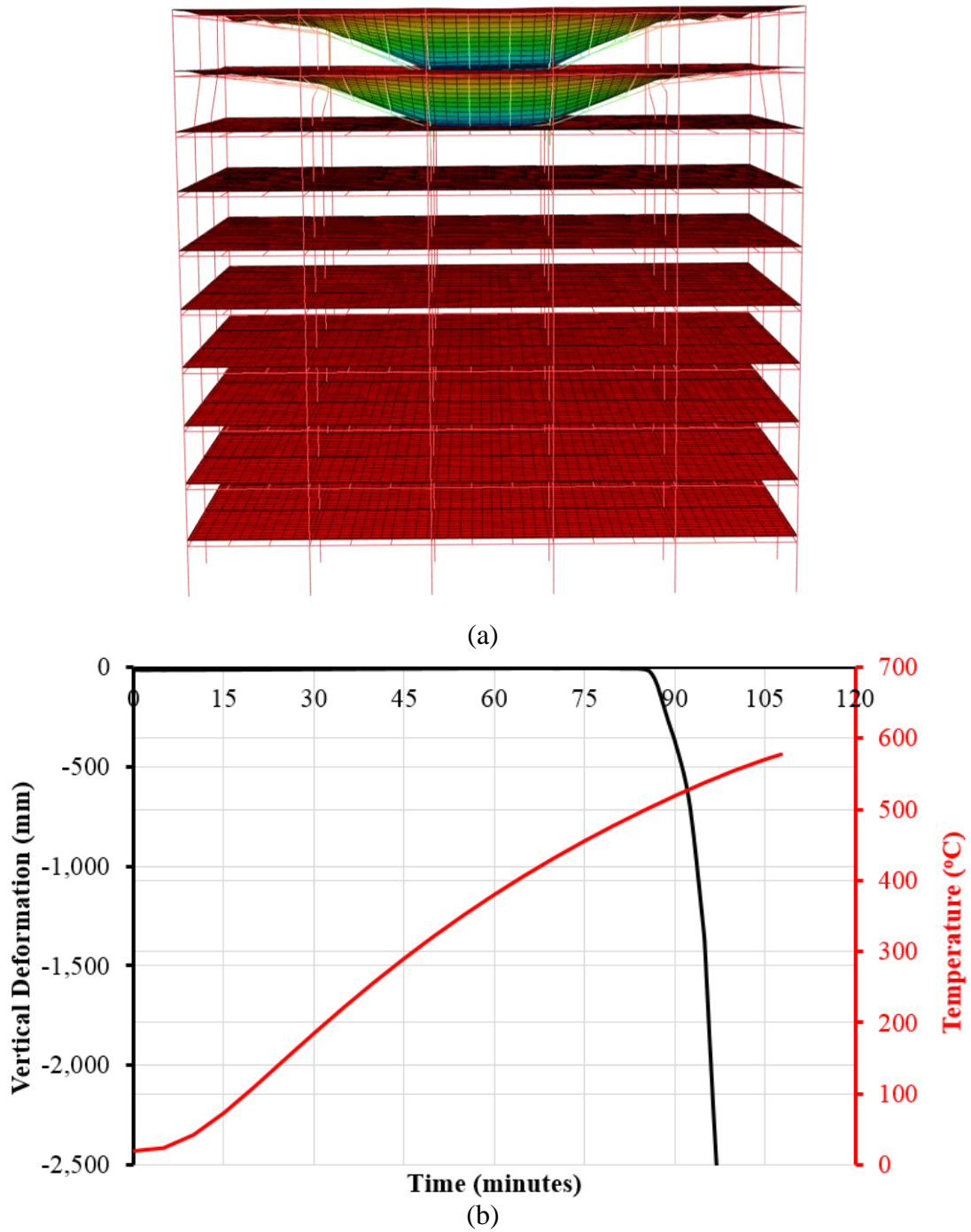
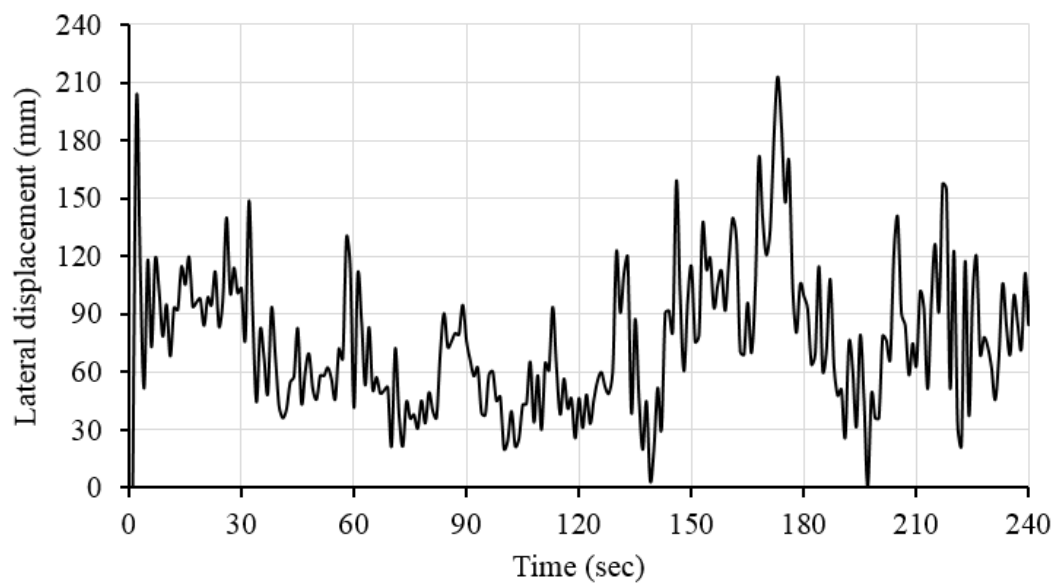


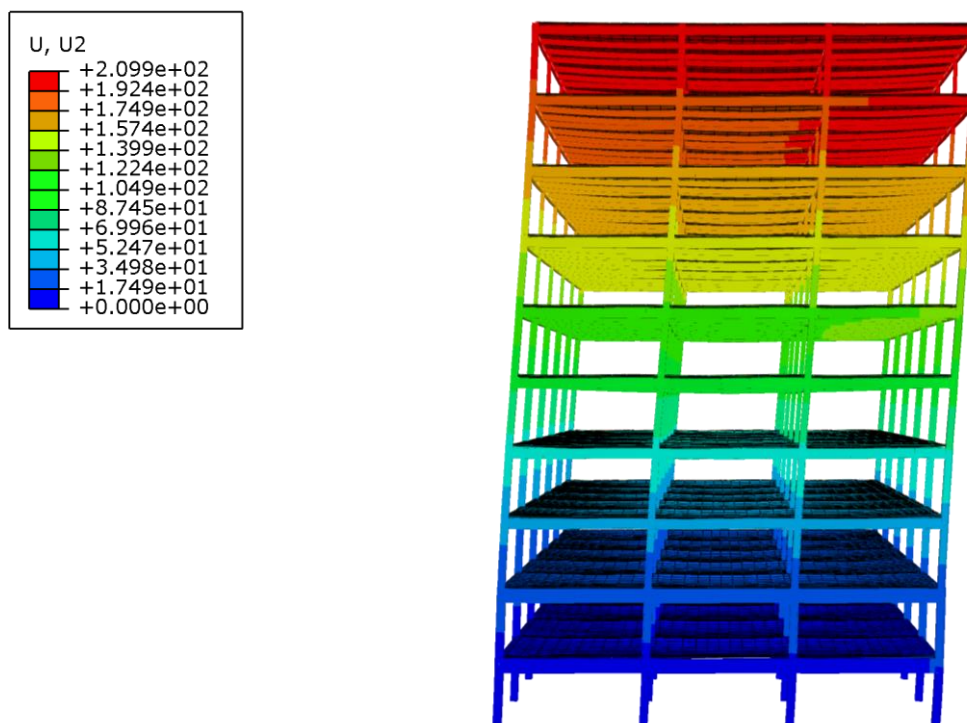
Figure 6.29 Response of Chicago building exposed to 9th story interior compartment Fire 3-1
 (a) rendering of interior gravity columns resulting in system collapse
 (b) vertical deflection and temperature versus time for the failed interior gravity columns

Table 6.2 Results of IFA analyses for non-fractured Chicago building at the 9th story

Fire #	Fire Location	0.75 * Max Fire Temp			1.0 * Max Fire Temp			1.5 (Fire 1,2) or 1.25 (Fire 3)* Max Fire Temp		
		Failure Type	Max vertical deflection (mm)	Time of failure (min)	Failure Type	Max vertical deflection (mm)	Time of failure (min)	Failure Type	Max vertical deflection (mm)	Time of failure (min)
1	9A	-	248	-	Column	1342	70	System	Collapse	46
1	9B	-	255	-	Bay	2144	69	System	Collapse	45
1	9C	-	247	-	System	Collapse	67	System	Collapse	45
1	FULL	-	-	-	System	Collapse	84	-	-	-
2	9A	-	208	-	-	275	-	Column	1297	37
2	FULL	-	-	-	-	213	-	System	Collapse	47
3	9A	-	254	-	Column	1420	88	System	Collapse	66
3	9B	-	249	-	Bay	1940	82	System	Collapse	66
3	9C	-	303	-	System	Collapse	85	System	Collapse	65
3	FULL	-	-	-	System	Collapse	100	-	-	-



(a)



(b)

Figure 6.30 Lateral response of Chicago building subjected to wind time history
 (a) Lateral displacement at roof versus time due to wind time history
 (b) Deflected shape (mm) at maximum deflection scaled by 10

CHAPTER 7. LOS ANGELES BUILDING SIMULATION RESULTS

Seismic, fire and wind simulations were conducted on the Los Angeles case study building. This chapter will present the results of these studies. These include finite element method modeling results from: (1) incremental dynamic analyses, (2) incremental fire analyses, and (3) wind hazard analyses.

7.1 Seismic Response

The Los Angeles building was subjected to ground motion time histories in order to assess seismic resilience. Modal analysis was first conducted to determine the fundamental period and mode shapes of the structure for determining the Rayleigh damping factors. The results of this analysis are given in Figure 7.1. Lateral translation in each direction are the first and second modes. Torsion is the third mode. The periods are 1.83 sec, 1.81 sec, and 1.11 sec, respectively. This building is stiffer than the Chicago building, but is still considered a flexible structure per ASCE 7 [5] criteria. The seven ground motions previously shown in Figure 4.11 and Figure 4.12 were applied to the base of the Los Angeles building as displacement time histories. Each ground motion was scaled per incremental dynamic analyses by the intensity measure, PGA. Ground motion intensities of 0.75, 1, and 1.25 times the PGA for each earthquake were studied. The designation EQ2-1 indicates earthquake ground motion 2 scaled by 1 times the PGA. Figure 7.2 shows the maximum story drift ratios that were recorded at each level for the seven different earthquakes scaled by different PGAs. The earthquake ground motions with 0.75 times PGA (Figure 7.2(a)) resulted in story drift ratios below 0.03, with many of the earthquake responses less than 0.015. The only earthquakes that resulted in drift ratios greater than 0.015 were ground motions 1, 4 and 7. This was to be expected, as the response spectrum in Figure 4.13 shows that at the fundamental period of the structure (1.83 sec), the spectral accelerations are highest for these three earthquakes. The largest drift ratio occurred at the first story due to earthquake 4. Earthquake 7 resulted in story drift ratios of approximately 0.02 at both story 1 and story 7. Earthquake 1 also experienced its highest story drift ratios at the first story.

Figure 7.2(b) shows the drift ratio response of the structure when subjected to 1 times the PGA of the design basis earthquake. Again, most drift ratios are below 0.015 with the exception of

earthquakes 1, 4, and 7. According to the Seismic Design Manual [11], special moment frame connections must be capable of withstanding 0.04 radians of interstory drift. Earthquake 7 surpasses this limit slightly.

The PGA for each ground motion was also increased by 25% and the response is shown in Figure 7.2(c). This earthquake level results in story drift behavior similar to, but somewhat increased, from the design basis earthquake case. Again, earthquakes 1, 4 and 7 experience the largest drifts at the first and second stories. The remainder of the earthquakes experience drift ratios at or less than 0.015.

Results have shown that earthquakes 1, 4 and 7 are strong ground motions that cause deflections beyond the acceptance criteria for special moment frame systems. On the other hand, the remaining four ground motions are relatively weak, not resulting in very much deformation or damage. Because seven ground motions have been used, ASCE 7 allows averaging the results instead of using the worst case scenario. However, more careful scaling of ground motions could have been conducted in order to scale all seven ground motions so that they more closely fit the response spectrum. The current scaled earthquakes were deemed acceptable because they cover a range of earthquake intensities.

As explained in Sections 5.2 and 5.3, the moment frame connections were modeled as fixed connectors which cannot fail. However, ductile damage was incorporated into the material models in order to simulate fracture at large interstory drift ratios. Whenever these interstory drifts exceeded this limit, fracture occurred. Unlike the Chicago building, which primarily experienced hinging and fracture in columns, the Los Angeles building was designed to comply with the strong column-weak beam approach and, thus, fracture occurs primarily in the moment frame beams within the protected zone. Figure 7.3 shows where fracture and plastic hinging have occurred in the perimeter moment frames for the instance of EQ1-1.25. The red circles indicated beam fracture, while the green circles indicate plastic hinging. Due to the larger drift ratios at the first and second stories in Figure 7.2(c), it is not surprising that fracture occurs at the lower level beam-to-column connections of the moment frames.

Table 7.1 summarizes where each of the beam fractures occur for each earthquake simulation with designations A, B and C. “A” represents the exterior connection of the exterior span of the moment frame. “B” represents the interior connection of the exterior span, and “C” indicates the connections within the interior span of the moment frame. N-S (North-South) indicates moment

frames along column lines A and F in Figure 4.5, and E-W (East-West) are moment frames along column lines 1 and 4. The numbers in the table indicate the story at which fracture has occurred. For instance, for EQ1-0.75, fracture only occurred at the first story of the structure. It fractured at all beam-to-column connections in the East-West direction and only at the exterior connection of the exterior span in the North-South direction. Fractures primarily occurred from earthquakes 1, 4, and 7. Fractures were also observed for earthquakes 2-1, 2-1.25, 3-1.25, and 6-1.25. In all cases except EQ7-0.75, fracture was limited to the lower three stories. No fracture is observed from earthquake 5.

The results of the incremental dynamic analyses is provided in Figure 7.4. This graph shows the peak ground acceleration versus the maximum story drift ratio observed for each ground motion. The markers indicate the results for the different scaled earthquakes: 0.75, 1, and 1.25. Lines with more than 3 markers means the earthquakes have been scaled beyond 1.25. In this instance, PGA is not a very effective intensity measure. As the graph shows, EQ 5 has the highest PGA values. From the ground motions provided in Figure 4.11 and Figure 4.12, the PGA for EQ5-1 is in excess of 1.5g. When looking at the response spectrum in Figure 4.13, it is clear that the peak ground acceleration affects stiff structures with low periods. At 1.83 sec, which is the fundamental period of the structure, the response of the structure subjected to this ground motion is very low. Thus, though the PGA is very high for this earthquake, its demand on the structure is relatively low. This is what creates the scatter of results in Figure 7.4. For these reasons, spectral acceleration (S_a) was chosen instead as the intensity measure (Figure 7.5). S_a is the maximum acceleration observed within the structure as it responds to the earthquake. This figure will be used to generate the fragility curve in Section 8.7.

The structure, exposed to the various earthquake intensities, was then exposed to compartment fires. The following sections explore the structural response of the building subjected to corner, edge, interior, and full story compartment fires at the fifth, ninth, and first stories.

7.2 Fifth Story Fires

The failure times and modes of failure for structures that have not experienced fracture are very similar to those described in Section 6.2 for the Chicago building. These findings will be summarized briefly below. Refer to Section 6.2 for more detailed descriptions of the building behavior.

A results summary of the fires subjected to the Los Angeles fifth story after earthquakes that did not cause fracture can be found in Table 7.2. The corner (5A), edge (5B), interior (5C) and full story compartments are subjected to Fires 1, 2, and 3 scaled by 0.75, 1, and 1.25 times the peak fire temperature. The failure modes for these scenarios are the same as those observed in the Chicago building. The deflections vary between the Chicago and Los Angeles simulations, but these differences are minor and do not ultimately affect the failure mode of the structure. In addition, the time of failure may vary by a few minutes but the failure modes are the same.

As with the Chicago building, the fires with 75% of the peak fire temperature did not result in any type of failure. For Fire 2, even 100% of the peak fire temperature did not result in failure, and it was not until the peak temperature was increased by 25% that compartment failures were observed. Fires 1 and 3 both resulted in column failures of the interior gravity columns for the corner compartments. The edge compartment also experienced interior gravity column failures, resulting in bay failure of the system. The interior compartment fires caused system collapse when the four interior gravity columns failed and their loads could not be redistributed to adjacent columns due to connection failures caused by the large deflections of the buckled columns. Fire 1 and Fire 3 varied in the time of failure, as the columns reached failure temperature at different times due to the varying heating rates of the two fires.

Table 7.1 showed that fracture was not typically observed at the fifth story, as it was mostly contained to the lower levels. For EQ7-0.75, however, fracture occurs at the fifth story. Fire 1-1 was exposed to compartment 5B2, which is where beam fracture had occurred. Due to the fracture, the moment frame girder (W27x94) is not supported at the beam ends. This causes significant deflection of the girder and slab in the compartment. The W27x94 girder reaches $L/20$ deflection (383 mm or 15 in) after 56 minutes of exposure to the fire. The interior gravity columns then collapse at 92 minutes. This results in bay failure with 2145 mm (84 in) of vertical deflection. Thus, the fracture initiates a compartment failure mode, but this eventually becomes a bay failure. The fracture only affects the column failure time by 6 minutes. More fire scenarios in beam-fractured compartments will be explained in Section 7.4.3 for first floor compartment fires.

7.3 Ninth Story Fires

As with the fifth story fires, the failure times and modes of failure for the Los Angeles building are very similar to those described in Section 6.3 for the Chicago building. Table 7.3 summarizes

the results of these findings for fires on the ninth story. Corner (9A), edge (9B), interior (9C) and full story compartment fires were examined for Fires 1, 2, and 3. Each of these fires were scaled at 0.75, 1 and 1.25 of the peak fire temperature. The failure modes are the same as the Chicago building for all cases except the four cases highlighted in gray. Refer to Section 6.3 on the Chicago fire results for a detailed description of the results of the non-highlighted scenarios. Note that between the Los Angeles and Chicago fire results, the deflections vary somewhat and the failure time may vary by a few minutes, but the failure mechanisms and times are essentially the same. Only the four unique cases highlighted in Table 7.3 will be explored more closely in the following sections.

7.3.1 Fire 1

The results of Fire 1-1.5 at the ninth story will be explained in the subsequent sections. Fire 1-0.75 and 1-1 caused the same results as the Chicago building and, thus, are not explained again. Refer to Section 6.3.1 for a detailed description of the results for these fire intensities.

7.3.1.1 Corner Compartment Fire

Figure 6.22 shows the response of the Chicago building when subjected to Fire 1-1.5 at the ninth story corner compartment. The fire caused failure of the interior gravity column at 46 minutes, which lead to subsequent failure of the moment frame columns within that compartment at 78 minutes. The gravity column is a W8x24 and the moment frame columns are W14x53 (N-S moment frame) and W12x45 (E-W moment frame). As would be expected, the W12x45 is the first moment frame column to buckle. The W12x45 column has a 0.16 utilization ratio, as shown in Table 8.6. This means that the demand on the column under ambient conditions is only 16% of the capacity of the column.

For the Los Angeles building, interior gravity column buckling occurs at 45 minutes (Figure 7.7(a)). The gravity column in this building is also a W8x24 and buckles when it reaches its failure temperature of 499°C. However, the moment frame columns remain stable throughout the fire and do not result in system collapse. The moment frame columns at this compartment are W14x176 (corner and E-W moment frame) and W14x283 (N-S moment frame). These columns have utilization ratios of 0.03 and 0.02, respectively, which shows that they are extremely overdesigned for gravity load combinations. Because of the excess capacity of the moment frame columns, only

gravity column failure occurs and system collapse is avoided. Seven minutes after the gravity column fails, the exterior W18x35 girder, circled in Figure 7.7(b), experiences connection failure and results in additional sag of the floor framing system at that location. The W18x35 is a gravity framing member with simple shear connections in order to avoid subjecting the corner moment frame column to biaxial bending.

7.3.1.2 Edge Compartment Fire

The ninth story edge compartment subjected to Fire 1-1.5 results in 1684 mm (66 in) of vertical deflection and bay failure at 46 minutes. The two interior gravity columns within the compartment collapse at 46 min upon reaching the failure temperature of 499°C. System collapse is avoided by redistributing the collapsed column loads to the adjacent columns. This is in contrast to the Chicago building scenario, which resulted in system collapse, as shown in Figure 6.24. As explained in the previous section, the moment frame columns in the Chicago building are lighter sections and have a higher utilization ratio than the more robust moment frame columns in the Los Angeles building. The Chicago moment frame columns eventually buckle due to the elevated temperature from Fire 1-1.5, causing system collapse but this does not happen in the Los Angeles building. In this instance, having a more robust moment frame system in the Los Angeles building has helped to prevent widespread system collapse.

7.3.2 Fire 3

The results of Fire 3-1.25 at the ninth story will be explained in the subsequent sections. Fire 3-0.75 and 3-1 caused the same results as the Chicago building and, thus, are not explained again. Refer to Section 6.3.3 for a detailed description of the results for these fire intensities.

7.3.2.1 Corner Compartment Fire

The failure modes of the Chicago and Los Angeles building are different for the ninth story corner compartment subjected to Fire 3-1.25. In the Chicago building, system collapse resulted. The interior gravity column failed at 66 min and after 52 additional minutes of fire, the three remaining columns in the compartment (W12x45 and W14x53 moment frame columns) buckled due to elevated temperatures.

The Los Angeles building only experienced column collapse. The interior gravity column failed at 63 minutes and the load from this column could be effectively redistributed to adjacent columns

in order to prevent system collapse. The moment frame columns in this compartment are W14x176 and W14x283, which have much more excess capacity than the moment frame columns in the Chicago building. As was the case with the ninth story corner compartment with Fire 1-1.5 in the Los Angeles building, the W18x35 exterior girder in the compartment experienced connection failure, which caused large deflections but not collapse similar to Figure 7.7(b).

It should be noted that the different failure modes of system collapse and column failure between the two buildings was not observed at the fifth story. This is because the moment frame columns at the Chicago building's fifth story were W14x99 and W14x109, which are much more robust than those at the ninth story.

7.3.2.2 *Edge Compartment Fire*

The ninth story edge compartment subjected to Fire 3-1.25 also resulted in different failure modes between the Chicago and Los Angeles buildings. The Chicago building experienced column collapse of the two interior gravity columns within the compartment at 66 minutes. As the fire continued, this caused eventual collapse of the remaining columns within the compartment.

In the Los Angeles building, the interior gravity columns also collapse at 66 minutes; however, the adjacent columns remain stable and only bay failure is observed. The maximum vertical deflection achieved is 2103 mm (83 in). Again, the robustness of the exterior moment frame benefits the system response in this instance, preventing system collapse and only resulting in bay failure, which is a much less dangerous and damaging failure mode.

7.4 First Story Fires

In the Chicago building, fires at only the fifth and ninth stories were studied. This was because damage tended to occur at upper levels; additionally, fire truck ladders cannot reach beyond 100 feet, so it is the upper levels of high rises, where firefighting is less accessible and efficient, that are the most dangerous. Throughout the IDA analyses for the Los Angeles, which was explained previously, fracture often occurred in the moment frame beams at the lower levels of the structure. It is for this reason that first story fires are being considered for this structure, in addition to the fifth and ninth stories. It is possible that fire mitigation techniques at the first story may be inhibited by seismic damage. For instance, water lines may have ruptures, preventing fire fighters from using hoses to extinguish a fire story fire that would have otherwise been easily extinguished.

There is also the potential for slow action from first responders due to various other dangers occurring at other sites or the possibility that access to the building could be hindered by other seismic damage. Ultimately, while first story fires would traditionally be easier to eradicate, the implications of the seismic event and its influence on fire responders and back up resources is unknown. For these reasons, a first story fire was considered as well.

The same fires used in the Chicago building, known as Fires 1 and 3 in Figure 4-18, were used to conduct IFA on the Los Angeles building. Both of these fires were scaled by 0.75, 1, and 1.25 or 1.5 times the peak fire temperature. The scalar factor of 1.5 was used for Fire 1 and 1.25 was for Fire 3. Fire 2 was not analyzed because of the previous studies that showed that failures were very unlikely with this fire.

Table 7.4 summarizes the failure modes, maximum vertical deflections, and times of failure for each of the fire scenarios. While the deflections and failure times vary from the fifth story compartment studies because of the different member sizes in the first and fifth compartments, the failure modes are the same at both levels. The fires scaled at 75% of the peak fire temperature did not produce any failures. The results of the other fire scenarios will be described in more detail below.

7.4.1 Fire 1

Fire 1-1 and Fire 1-1.5 are applied to the corner, edge, and interior compartments of the first story. The results described in this section are fire following earthquake scenarios where fracture did not occur during the earthquake. Section 7.4.3 will explore the building response to these fires in compartments where fracture has occurred.

7.4.1.1 Corner Compartment Fire

Fire 1-1 at the first story corner compartment produced column failure of the interior gravity column, which is the same failure mechanism observed for this fire at the fifth and ninth story corner compartments. Figure 7.8(a) is a rendering of the failure mode and final deflected shape. Figure 7.8(b) shows the interior gravity column axial load over time. The W14x90 gravity column loses load carrying capacity at 98 minutes, when it reaches its failure temperature of 524°C.

Fire 1-1.5 at the first story corner compartment also causes column failure. This, however, occurs at approximately 50 minutes, when the column reaches the failure temperature. Figure 7.9(a) shows the deflected shape of the system resulting from a column failure. Figure 7.9(b) graphs the axial load and temperature over time for the failed column subjected to Fire 1-1.5

7.4.1.2 Edge Compartment Fire

The edge compartment subjected to Fires 1-1 and 1-1.5 both experienced bay failures. The interior gravity columns within the fire-exposed compartment buckled due to elevated temperatures. Fire 1-1 resulted in 1748 mm (69 in) of total vertical deflection and column failure at 95 minutes. Fire 1-1.5 results in 1855 mm (73 in) of total vertical deflection and column failure at 50 minutes. Refer to Table 3.1 for a visual representation of bay failure.

7.4.1.3 Interior Compartment Fire

The interior compartment of the first story consists entirely of gravity framing members. When this compartment is subjected to Fires 1-1 and 1-1.5, all four gravity columns within the compartment fail. This causes an unsupported span of the gravity framing members of three bays. As was observed at all other interior compartments at the Chicago and Los Angeles fifth and ninth stories, the system is unable to stabilize itself after the failure of these gravity columns. This results in system collapse of the structure. System failure is initiated at 95 minutes for Fire 1-1 and 53 minutes for Fire 1-1.5. These are the times at which the gravity columns reach their failure temperature of 524°C.

7.4.1.4 Gravity Column Capacity Check

The utilization ratio for the W14x90 gravity columns at the first story is 0.60. This means that for the fire load combination of 1.2D+0.5L, the demand load at ambient conditions is 60% of the design capacity of the column. The design of the failed W14x90 gravity column was checked using the same procedure described in Section 6.2.1.5.

The axial capacity versus steel temperature relationship of the W14x90 gravity column is provided in Figure 7.10. The solid black line shows the column axial capacity when considering the rotational restraint of the story above. Note that in this scenario, because the column is located on the first floor, $n=2$ is used in Equation 6-4 when calculating the modified L/r factor. The column capacity using the traditional and more conservative simply supported column capacity equation

is drawn in gray. The axial demand on the column based on the load combination $1.2D+0.5L+A_T$ is 3092 kN (695 kips) as designated by a red dotted line. As mentioned previously, the column failed at 524°C in ABAQUS. The red circle in shows the intersection of demand and calculated capacity. This occurs at 504°C. Thus, as was the case with the fifth story and ninth story column design checks, the design equation closely predicts the failure temperature from ABAQUS but is slightly more conservative.

7.4.2 Fire 3

Fire 3-1 and Fire 3-1.25 are applied to the corner, edge, and interior compartments of the first story. The results described in this section are fire following earthquake scenarios where fracture did not occur during the earthquake. Section 7.4.3 will explore the building response to these fires in compartments where fracture has occurred.

7.4.2.1 Corner Compartment Fire

Fire 3-1 and 3-1.25 applied to the first story corner compartment has resulted in column failure of the interior gravity column. Figure 7.11 shows the axial load and temperature over time for the interior gravity column that failed after being subjected to Fire 3-1 for 103 minutes. Figure 7.12 shows the same relationship for that column, when subjected to Fire 3-1.25. The W14x90 interior gravity column fails at 76 minutes.

7.4.2.2 Edge Compartment Fire

As was the case with Fire 1-1, subjecting Fires 3-1 and 3-1.25 to the first story edge compartment resulted in bay failure. The two interior gravity columns buckled when they reached the failure temperature of 524°C. Fire 3-1 caused bay failure at 102 minutes with 1787 mm (70 in) of total vertical deflection. Fire 3-1.25 caused bay failure at 77 minutes with 1822 mm (72 in) of total vertical deflection. Because of the robustness of the moment frame columns within the fire compartment, these columns did not collapse and were able to carry some of the additional axial load from the failed columns, resulting in only bay failure and not system collapse.

7.4.2.3 Interior Compartment Fire

The interior compartment resulted in system collapse when the four interior gravity columns failed at 103 minutes (Fire 3-1) and 75 minutes (Fire 3-1.25). Despite having a very robust perimeter

moment frame system at the first story, the gravity framing system could not adequately transfer the loads to the moment frame system, resulting in progressive collapse of the adjacent gravity columns.

7.4.3 Fires in Structures with Beam Fracture

This section explains the results of Fires 1 and 3 applied to the first floor compartments of the Los Angeles when the structure has undergone beam fracture. Fire analyses were conducted for the structure after exposure to the earthquakes that caused first floor beam fracture as indicated in Table 7.1. In locations where beam fracture was observed at the moment frame beam ends, the welded connections were removed for the fire analyses, which is a conservative, simplified idealization of the actual scenario. An alternative, also conservative approach would be to remove the beam elements in the locations of fracture. Many of the compartment fires with beam fracture resulted in the same progression of failure: compartment failure, column collapse, and then connection failure resulting in significant framing deformations. A few different examples of this phenomenon are provided in more detail below.

Figure 7.13 shows the fire analysis results of Fire 1-1 in 1A (the first story corner compartment) applied to the structure that experienced EQ2-1.25. EQ2-1.25 had caused fracture of the N-S moment frame beam (W30x124) in that compartment. The lack of girder connections resulted in sag of the framing system, as shown in Figure 7.13(a). The composite slab essentially cantilevers from the adjacent W14x22 beam. The interior gravity column then fails at 95 mins (Figure 7.13(b)), which is only 3 min before the non-fractured Fire 1-1, 1A compartment scenario. In the non-fractured cases previously studied, this column failure leads to beam-to-column connection failures. These failures, however, did not compromise structural stability because the composite slab could effectively redistribute loads. In this scenario, however, the girder-to-column connections along the N-S moment frame have already been failed by the earthquake. Thus, when the beam-to-column connections framing into the gravity column fail, there is no support for the slab at the exterior column immediately adjacent to the failed interior column. For this reason, the framing floor system collapses (Figure 7.13(c)). The exterior column, a W14x398 becomes unbraced for two stories. A column capacity check, using the same procedure outlined in Section 6.2.1.5, reveals that for the maximum column axial load of 3928 kN, the column can withstand a critical (failure) temperature of 690°C. It should be noted that the maximum axial load in the

moment frame column is affected by column temperature and, thus, a high temperature of 690°C would actually result in a larger axial load; however, since the column only reaches 350°C from the Fire 1-1 scenario, it clearly has excess capacity and column collapse of the exterior framing system is avoided. If this were to occur at upper levels, it is feasible that the moment frame columns at the upper stories may not have enough excess capacity to withstand loading with a two story unbraced length.

The behavior of the structure that underwent EQ7-1 and Fire 1-1 at the corner compartment is shown in Figure 7.14. Figure 7.14(a) demonstrates the deflections in the framing system due to the fractured moment frame beams along the perimeter, as previously observed. Unlike the previous case, the exterior moment frame connections in the E-W moment frames were also fractured. When the interior gravity column failed after reaching its failure temperature at 95 min, the beam-to-column connections framing into the failed column also fail. This results in failure of the W18x35 exterior girder in the E-W moment frame and, thus, collapse of the corner of the framing system. The 2 bay by 2 bay portion of the first floor corner is unsupported and, thus, collapses.

This type of floor failure did not always occur, however. EQ1-0.75 caused fracture of only the exterior moment connection of the E-W moment frame. Figure 7.15 shows the resulting deflection of the system. The W30x124 beam behaves like a long cantilever beam which carries the floor framing system when the beam-to-column connections fail. Despite having a 25 foot cantilever, because of its reserve capacity, the deflection of the girder is relatively minimal compared to the deformations caused by column failure.

EQ3-1.25 caused beam fracture in the N-S moment frame beams. This caused sag of the framing system (Figure 7.16(a)), bay failure from column collapse (Figure 7.16(b)), and eventual collapse of the floor system at the fire compartment location and adjacent bays. Again, this was because the column collapses resulted in failed beam-to-column connections that, in turn, left the floor framing in this location completely unsupported. The same sequence of events is shown in Figure 7.17 for the structure subjected to EQ4-1 and then Fire 1-1 at compartment 1B.

The beam fractures, in many cases, may cause compartment failure from the sag of the composite slab as it attempts to span the loads between the bays. Though compartment failure occurs, these deflections are relatively minor compared to the deformations that occur once column failure. Figure 7.18 illustrates this principle, which shows plan views of the first story when the structure with EQ1-1.25 has been subjected to Fire 3-1 at 1B, the edge compartment. Sagging along the

entire perimeter of the building is observed in Figure 7.18(a) because of the beam fractures that the earthquake had caused. The maximum deflection of 467 mm (18 in) occurs at the compartment fire. When the gravity columns fail, resulting in bay failure (Figure 7.18(b)), the deformations are much more significant with a maximum deflection of 1897 mm (75 in).

Shear studs were removed when necessary to limit rigid body motion between the composite slab and the beam, but this still occurred as a limitation of the current modeling strategy. The shear stud connectors should be explored in more detail in future work to capture failure modes in the beam to slab interaction. The slab becomes the primary mechanism for transferring gravity loads, particularly when the moment frame girders are unsupported at both ends.

A summary of the findings for the Fire 1 scenarios that were studied are provided in Table 7.5, where the failure mechanisms (compartment, column and connection failure) are indicated as relevant (Y for yes) or not relevant (N for no) in the tables. It also provides the failure time, which is the time of column collapse. Again, in many instances compartment failure may first occur, but this is relatively insignificant compared to the column failure that follows and, thus, the column failure time is the noted value in the table. As mentioned previously, connection failures commonly occur due to column failure. The connection failure designations in these tables are meant to imply that the connection failures resulted in collapse of the slab and framing system. Table 7.6 summarizes the Fire 3 scenarios that were analyzed. The summaries show that interior column collapse occurs at approximately the same time as the non-fractured scenarios summarized in Table 7.4. System collapse does not occur for any of the studied scenarios. In most instances, compartment failure (slab sag) occurs, then column or bay failure, followed by connection failure which caused floor framing collapse. In cases where only one end of a moment frame beam is fractured, the beam effectively acts as a cantilever to carry slab loads and prevent floor framing collapse.

7.5 Wind Response

In order to capture dynamic effects of wind response, wind time histories were applied to each story of the building using the procedure explained in Section 5.8. Only one wind event was analyzed because the focus of this work is post-earthquake fires. Figure 7.19(a) shows the lateral roof displacement over time when subjected to a design-level wind event. This is the strength-level case and, when checking serviceability, these values can be reduced by a factor of 1.6. The

maximum deflection is 130 mm (5.1 in), which translates to 81 mm (3.2 in) for serviceability level loads. This is only approximately a 0.2% drift ratio, which is below the suggested $L/400$ limit, where L is the building height. Figure 7.19(b) portrays the deflected shape of the structure at the time of maximum deflection, with the deflections scaled by 10 in order to make it more visible.

The structure was able to withstand the wind event, remaining elastic and returning to its original, undeflected shape. Fire studies from the Chicago and Los Angeles buildings have shown that fire resilience is most vulnerable to the gravity framing system of the structure and that moment frame damage rarely controls as the failure mechanism of the structure subjected to fire. Thus, for a structure that is designed to remain elastic in a wind event, it can be presumed that the fire resilience of the structure after the wind event would be the same as the fire resilience of the structure if a wind event had never occurred. There is the potential of extreme wind loads, such as tornados, which could cause more extreme damage to the structure, but this type of hazard is outside the scope of this work.

7.6 Summary and Conclusions

In this chapter, the Los Angeles building was subjected to earthquakes, compartment fires at the first, fifth and ninth stories, and wind. The seven earthquakes were scaled by 0.75, 1 and 1.25 of the PGA. Earthquakes 1, 4, and 7 were found to be the most damaging, sometimes causing story drift ratios at the first story in excess of 0.04 radians. For story drift ratios beyond 0.02 radians, fracture would likely occur at the ends of the moment frame beams. This occurred primarily at the fifth story.

Fires 1, 2, and 3 were applied to corner, exterior and interior compartments at the fifth, ninth, and first stories. These fires were scaled by 0.75, 1, and 1.25 or 1.5 of the peak fire temperature. For structures that did not experience fracture during the earthquake, the fire following earthquake failure modes were the same as those observed in the Chicago building. The fires at 0.75 of the peak fire temperature did not cause failure. For fires at 1, 1.25 or 1.5 times the peak fire temperature, gravity column collapse occurs when the columns reach their critical, failure temperature. Corner compartment fires result in column failure, edge compartment fires result in bay failure, and interior compartment fires result in system collapse. The only difference between the Chicago and Los Angeles building results occurs at the ninth story for Fires 1-1.5 and 3-1.25. The Chicago building had resulted in system collapse because the moment frame columns within

the fire compartment experienced buckling after the interior gravity column failures. Because of the more robust moment frame system in the Los Angeles building, system collapse is avoided for these fires.

The first story was also analyzed for fire resilience because of the presence of beam fractures at this story. When fracture did not occur within the analyzed compartment, the fires resulted in the same failure modes as the fifth and ninth story cases. However, when beam fracture was present, compartment failure tended to occur, followed by gravity column failure and then failure of the beam-to-column connections to the failed column. This would usually lead to collapse of the floor framing system. Despite the exterior moment frame columns within the compartment becoming unbraced for two stories, the moment frame columns had enough excess capacity to prevent collapse.

When considering wind on the structure, a design wind time history was applied at each story. The structure remained elastic after this loading and, thus, had no impact on the fire resilience of the structure in a fire following wind scenario.

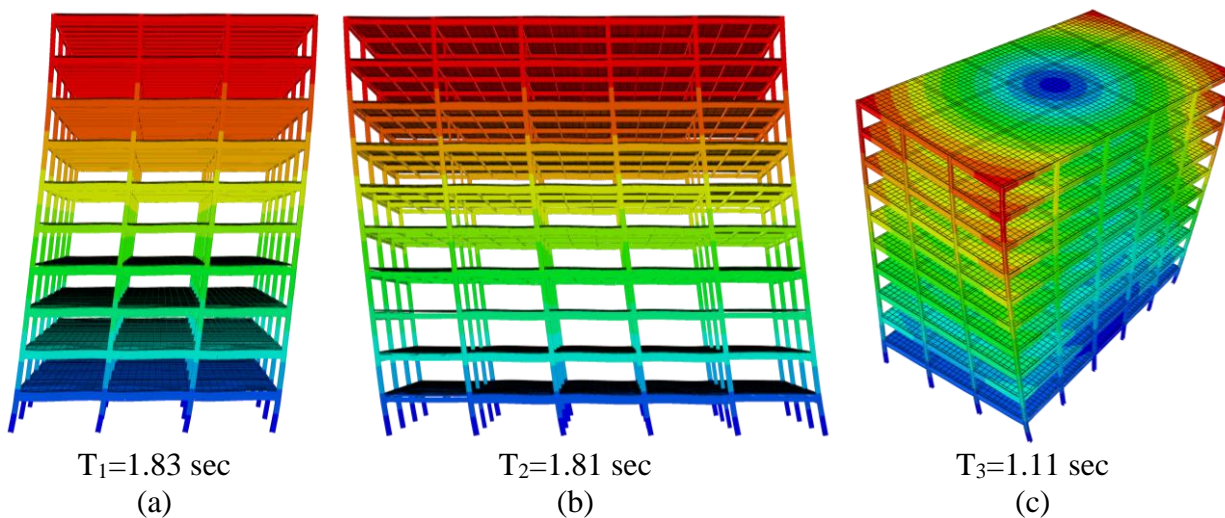


Figure 7.1 Modal shapes and periods for Los Angeles building
(a) first, (b) second, and (c) third modes

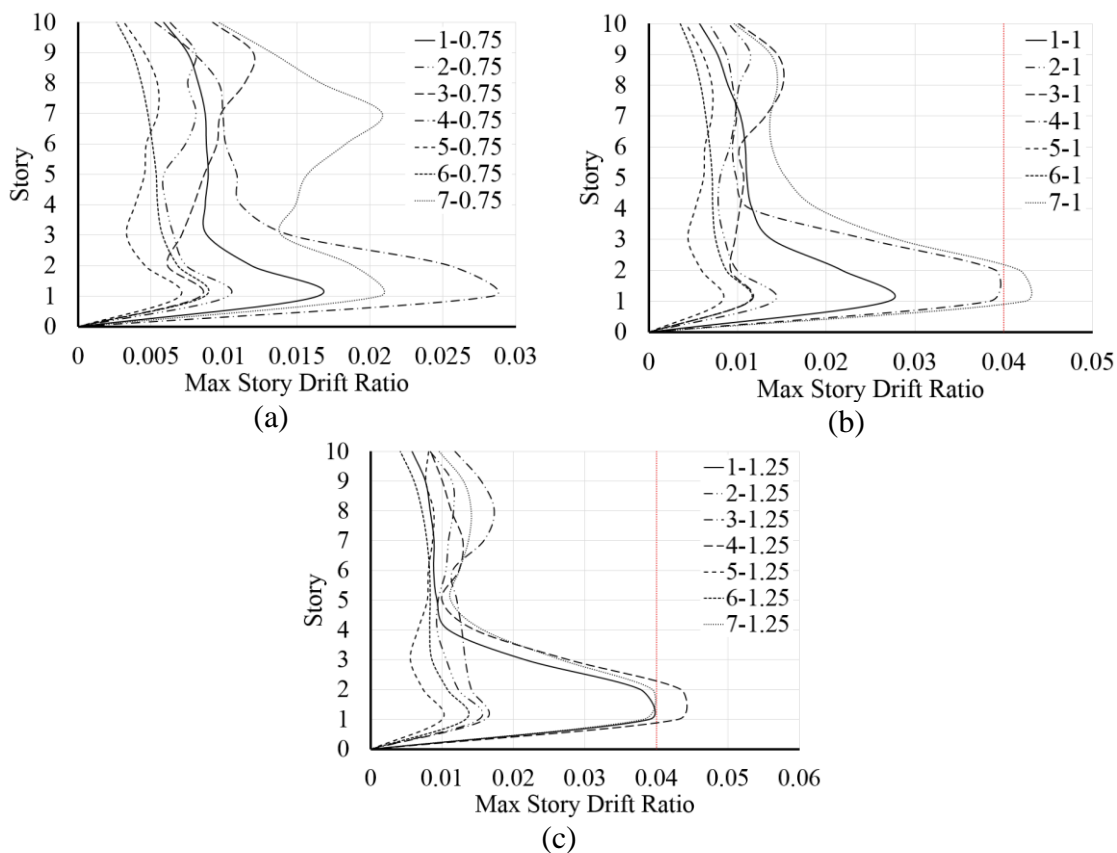


Figure 7.2 Maximum Story Drift Ratios for Los Angeles building
(a) 0.75*PGA (b) 1*PGA (c) 1.25*PGA

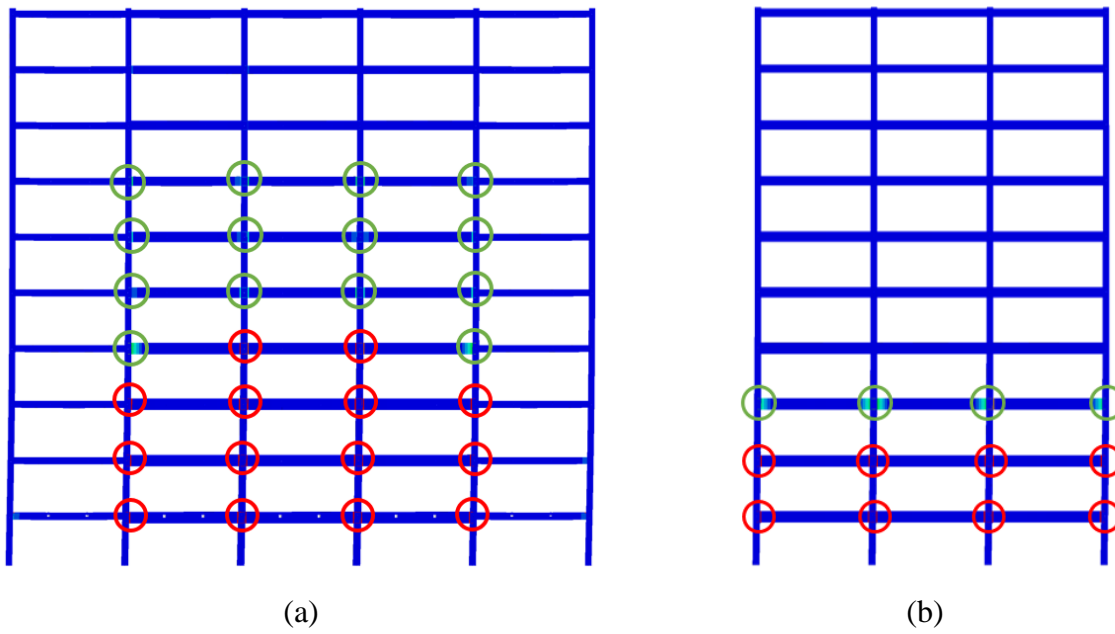
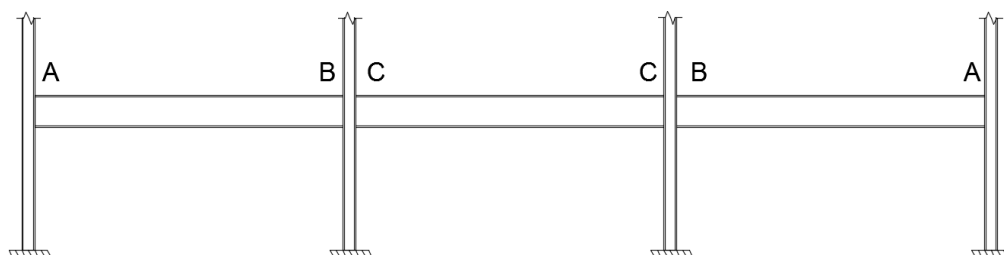


Figure 7.3 Fracture locations observed in Los Angeles building due to EQ1-1.25
(a) East-West moment frames, (b) North-South moment frames

Table 7.1 Beam fracture locations in Los Angeles building designated by story level

EQ	BEAM FRACTURE LOCATIONS AND STORIES					
	A		B		C	
	N-S	E-W	N-S	E-W	N-S	E-W
1-0.75	1	1	-	1	-	1
1-1	1	1-2	1	1-2	1	1-2
1-1.25	1-2	1-3	1-2	1-3	1-2	1-3
2-0.75	-	-	-	-	-	-
2-1	1	-	-	-	-	-
2-1.25	1	1	1	-	1	-
3-0.75	-	-	-	-	-	-
3-1	-	-	-	-	-	-
3-1.25	1	-	1	-	1	-
4-0.75	-	1-2	-	1-2	-	1
4-1	-	1-2	-	1-3	-	1-3
4-1.25	-	1-2	-	1-3	-	1-3
5-0.75	-	-	-	-	-	-
5-1	-	-	-	-	-	-
5-1.25	-	-	-	-	-	-
6-0.75	-	-	-	-	-	-
6-1	-	-	-	-	-	-
6-1.25	-	1	-	-	-	-
7-0.75	-	1-2, 6-7	-	1-2, 5-7	-	1-2, 5-7
7-1	1	1-3	1	1-3	1	1-3
7-1.25	1-2	1-3	1	1-3	1	1-3, 8



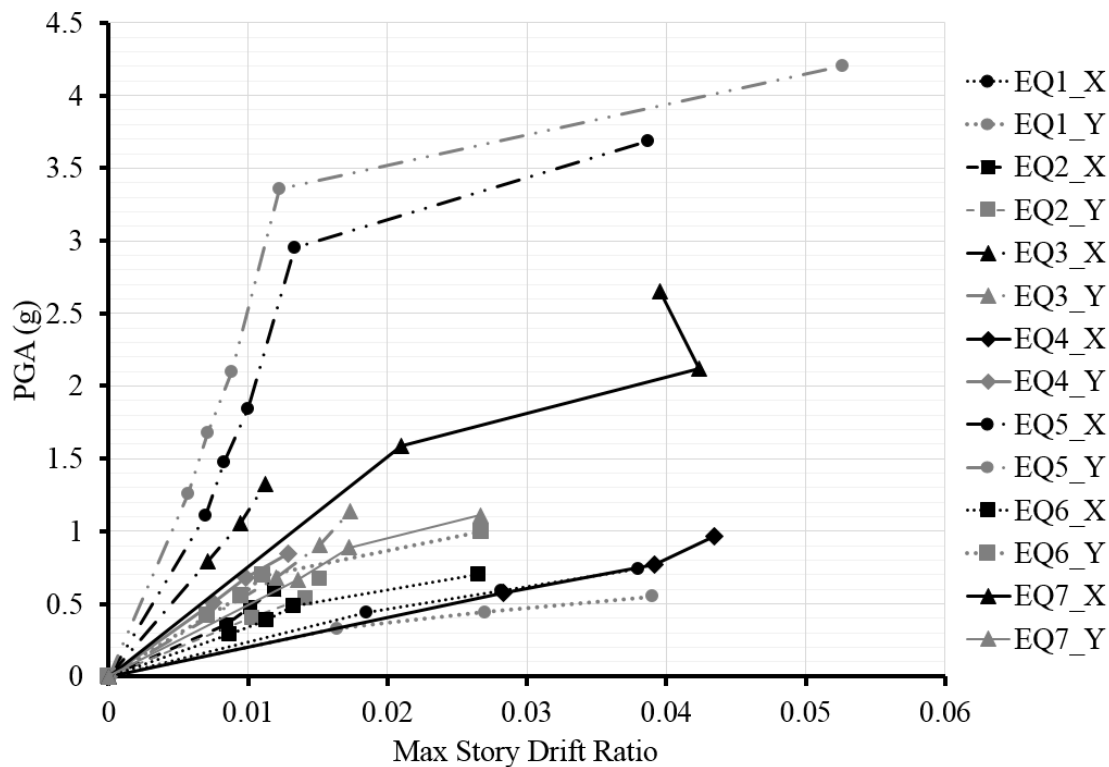


Figure 7.4 Results of IDA for Los Angeles building: PGA vs. maximum story drift ratio

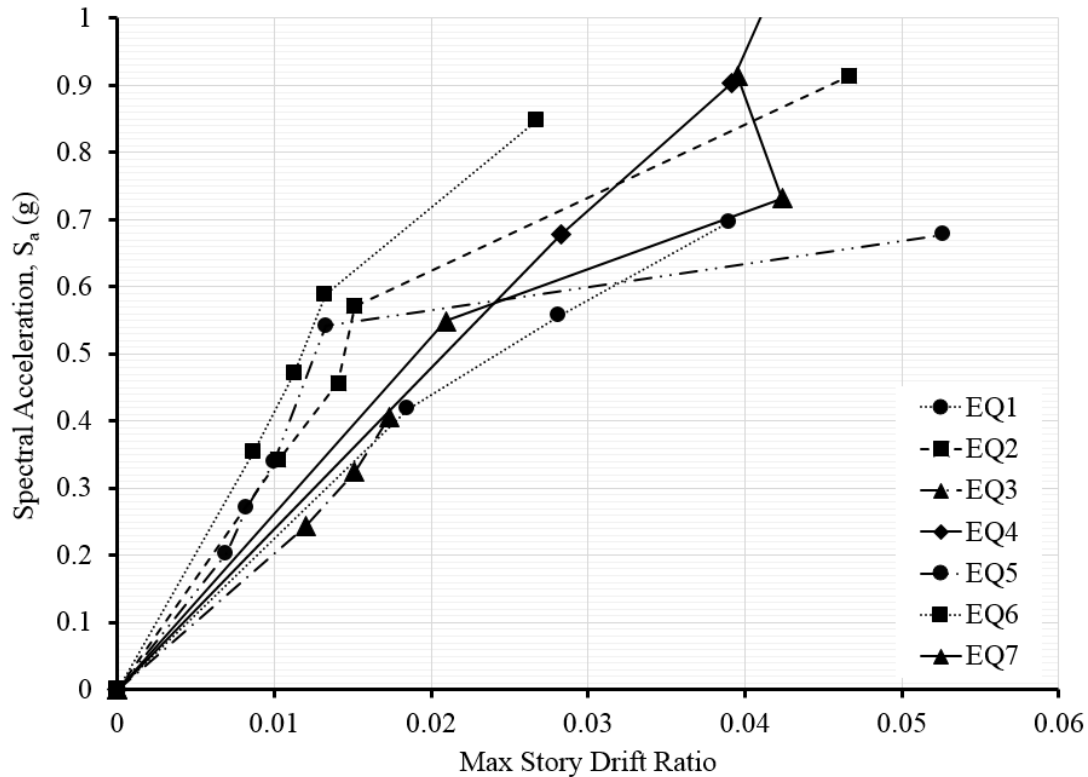
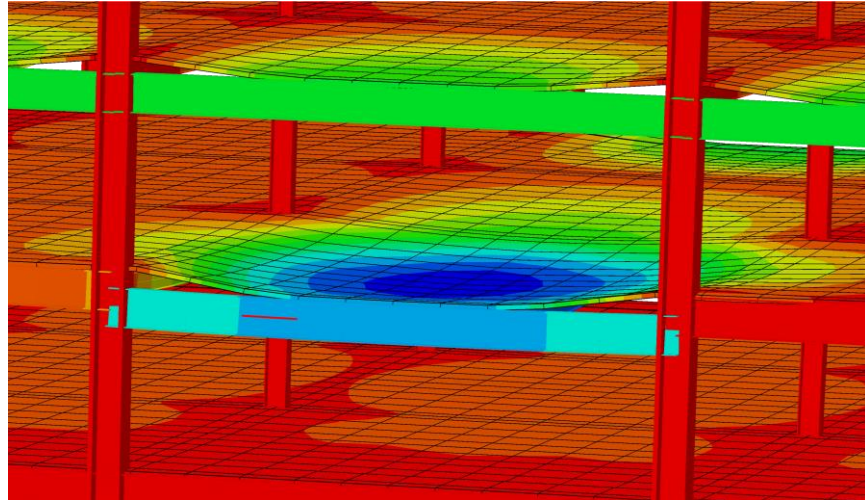


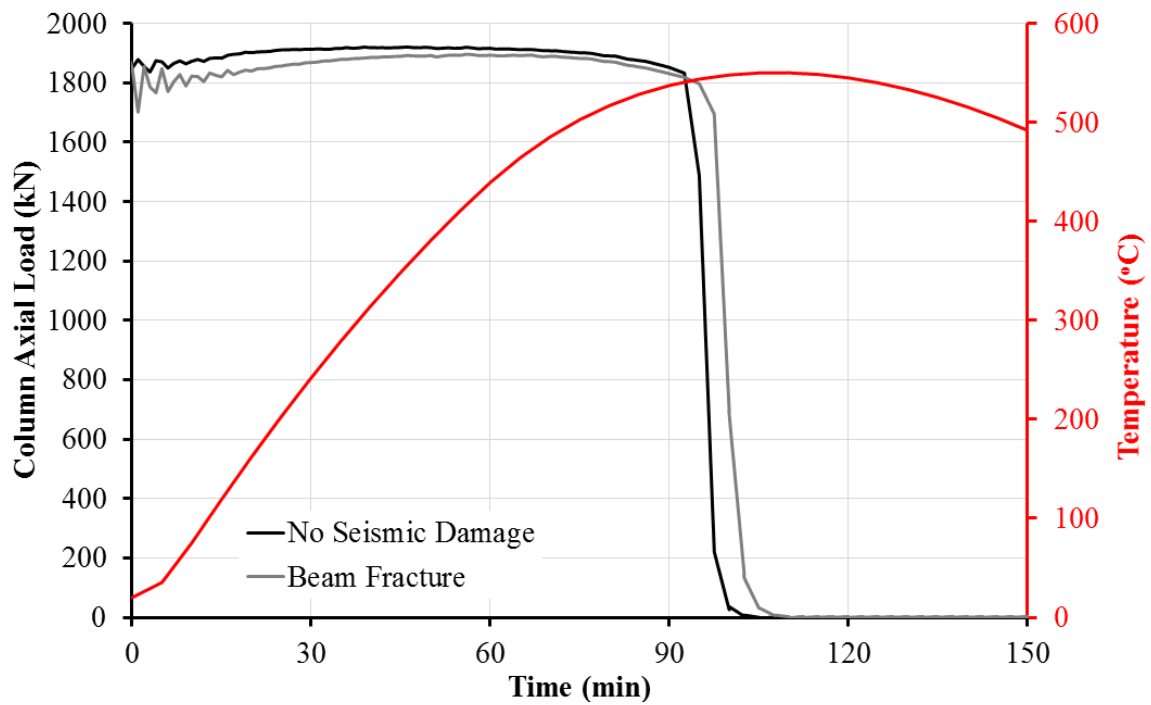
Figure 7.5 Results of IDA for Los Angeles building: S_a vs. maximum story drift ratio

Table 7.2 Results of IFA analyses for non-fractured Los Angeles building at the 5th story

Fire #	Fire Location	0.75 * Max Fire Temp			1.0 * Max Fire Temp			1.5 (Fire 1,2) or 1.25 (Fire 3)* Max Fire Temp		
		Failure Type	Max vertical deflection (mm)	Time of failure (min)	Failure Type	Max vertical deflection (mm)	Time of failure (min)	Failure Type	Max vertical deflection (mm)	Time of failure (min)
1	5A	-	262	-	Column	1957	98	Column	2020	52
1	5B	-	-	-	Bay	2150	98	Bay	1968	52
1	5C	-	-	-	System	Collapse	98	System	Collapse	52
1	FULL	-	-	-	System	Collapse	103	System	Collapse	52
2	5A	-	226	-	-	285	-	Compartment	615	55
2	5B	-	-	-	-	250	-	Compartment	481	60
2	5C	-	-	-	-	287	-	Compartment	550	60
2	FULL	-	-	-	-	226	-	Compartment	446	55
3	5A	-	266	-	Column	1270	103	Column	1660	76
3	5B	-	-	-	Bay	1895	105	Bay	1731	77
3	5C	-	-	-	System	Collapse	103	System	Collapse	77
3	FULL	-	-	-	System	Collapse	105	System	Collapse	78



(a)



(b)

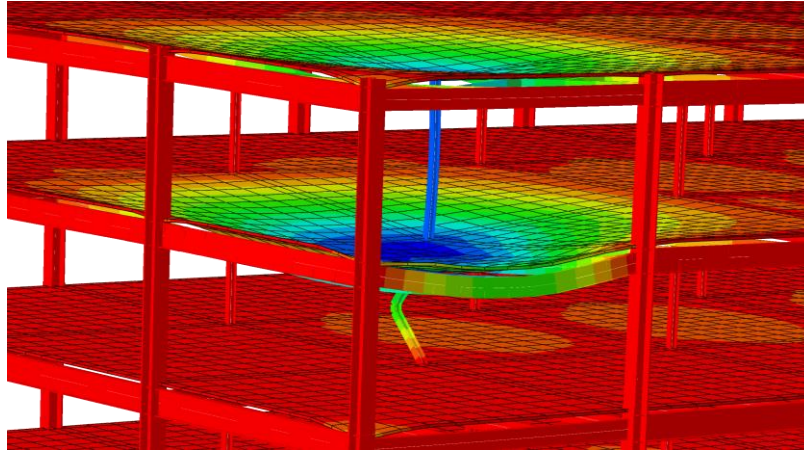
Figure 7.6 Response of Los Angeles building exposed to 5th story edge compartment Fire 1-1 after EQ7-0.75

(a) rendering of framing system sag

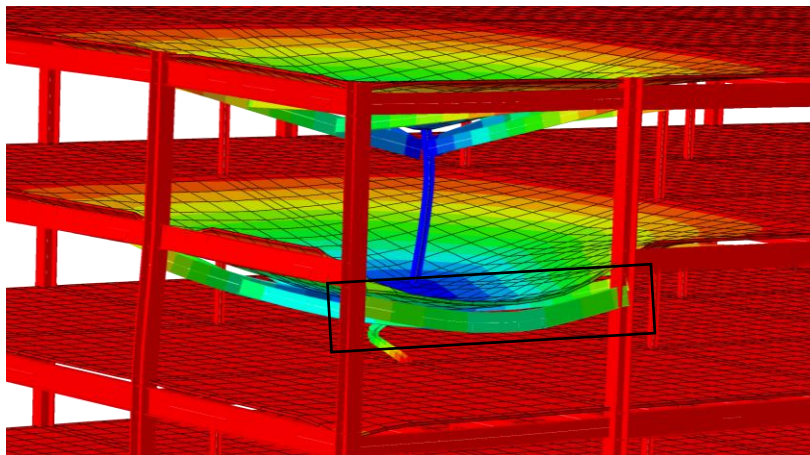
(b) axial load and temperature versus time for the failed interior gravity column

Table 7.3 Results of IFA analyses for non-fractured Los Angeles building at the 9th story

Fire #	Fire Location	0.75 * Max Fire Temp			1.0 * Max Fire Temp			1.5 (Fire 1,2) or 1.25 (Fire 3)* Max Fire Temp		
		Failure Type	Max vertical deflection (mm)	Time of failure (min)	Failure Type	Max vertical deflection (mm)	Time of failure (min)	Failure Type	Max vertical deflection (mm)	Time of failure (min)
1	9A	-	235	-	Column	1670	70	Column	2089	45
1	9B	-	-	-	Bay	2102	71	Bay	1684	46
1	9C	-	-	-	System	Collapse	80	System	Collapse	46
1	FULL	-	-	-	System	Collapse	82	System	Collapse	49
2	9A	-	194	-	-	261	-	Column	1612	37
2	FULL	-	-	-	-	220	-	System	Collapse	41
3	9A	-	243	-	Column	1958	85	Column	2162	63
3	9B	-	-	-	Bay	2095	86	Bay	2103	66
3	9C	-	-	-	System	Collapse	87	System	Collapse	65
3	FULL	-	-	-	System	Collapse	100	System	Collapse	73



(a)



(b)

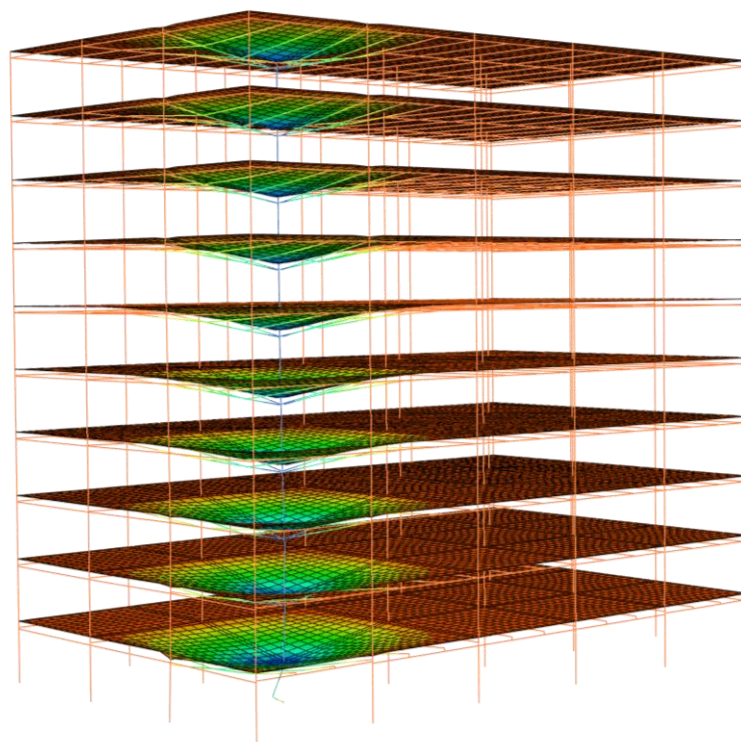
Figure 7.7 Response of Los Angeles building exposed to 9th story corner compartment Fire 1-1.5

(a) rendering of interior gravity column failure (45 min)

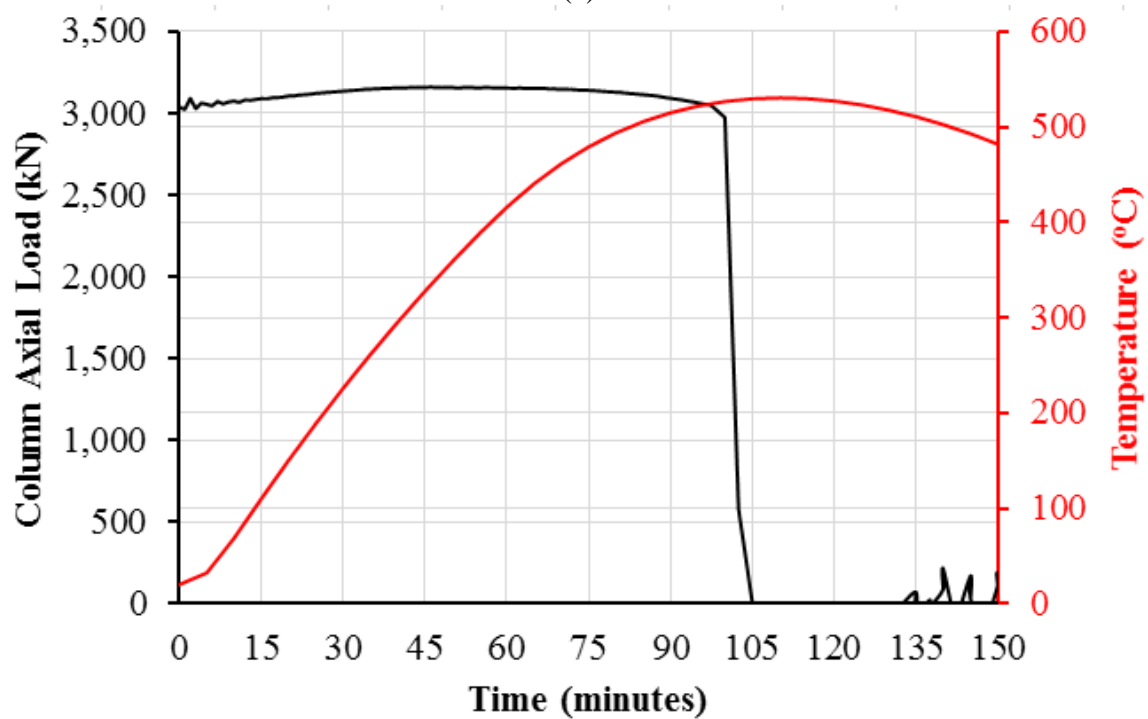
(b) W18x35 connection failure (52 min)

Table 7.4 Results of IFA analyses for non-fractured Los Angeles building at the 1st story

Fire #	Fire Location	0.75 * Max Fire Temp			1.0 * Max Fire Temp			1.5 (Fire 1) or 1.25 (Fire 3)* Max Fire Temp		
		Failure Type	Max vertical deflection (mm)	Time of failure (min)	Failure Type	Max vertical deflection (mm)	Time of failure (min)	Failure Type	Max vertical deflection (mm)	Time of failure (min)
1	1A	-	206	-	Column	1547	98	Column	1618	50
1	1B	-	150	-	Bay	1748	95	Bay	1855	50
1	1C	-	218	-	System	Collapse	95	System	Collapse	53
3	1A	-	171	-	Column	1547	103	Column	1529	76
3	1B	-	195	-	Bay	1787	102	Bay	1822	77
3	1C	-	244	-	System	Collapse	103	System	Collapse	75

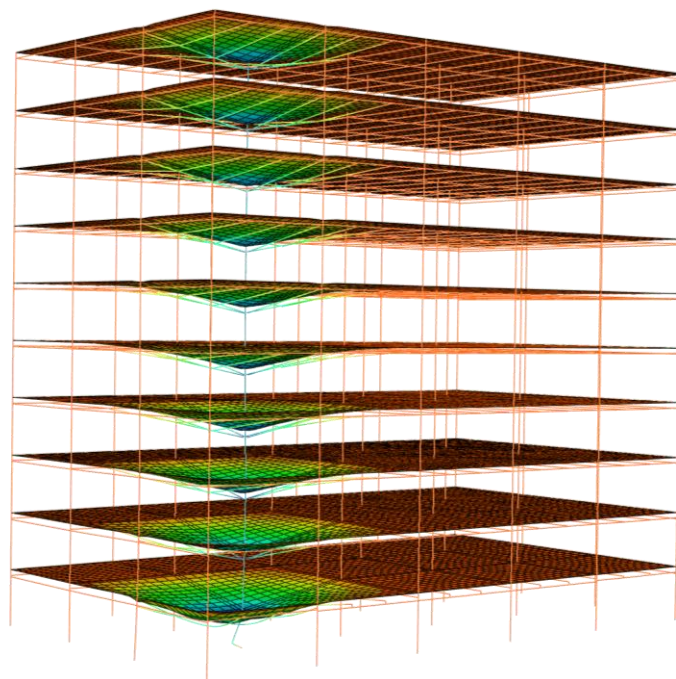


(a)

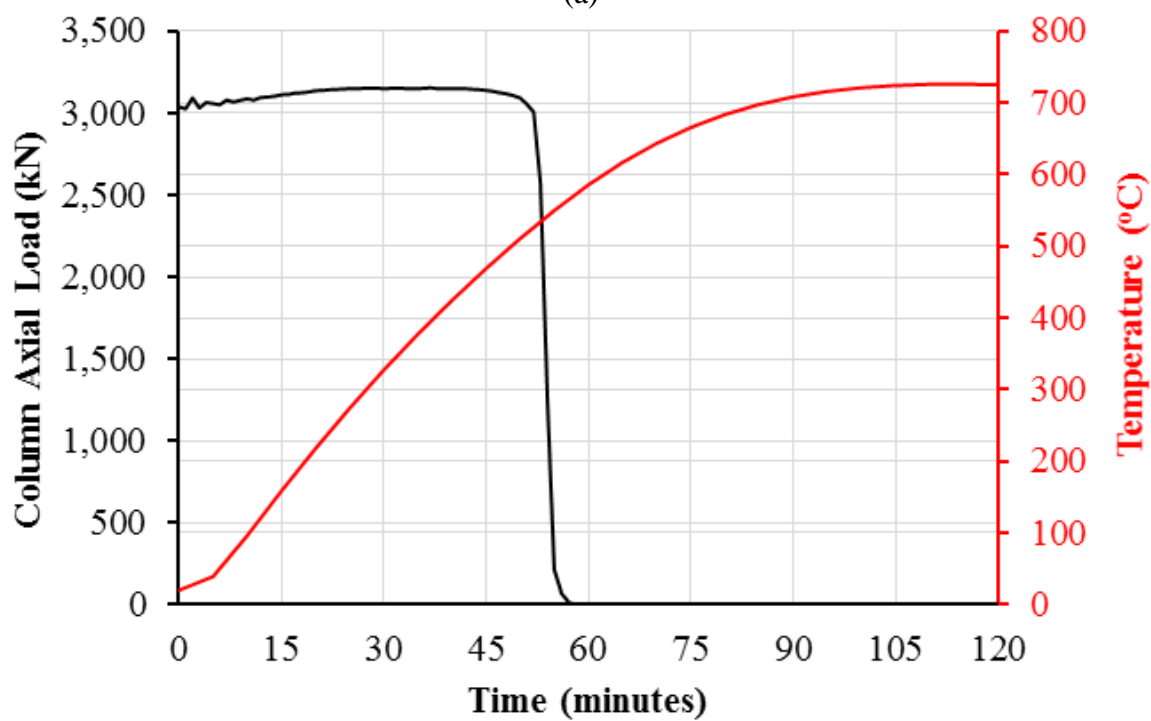


(b)

Figure 7.8 Response of Los Angeles building exposed to 1st story corner compartment Fire 1-1
 (a) rendering of interior gravity column failure
 (b) axial load and temperature versus time for the failed interior gravity column



(a)



(b)

Figure 7.9 Response of Los Angeles building exposed to 1st story corner compartment Fire 1-1.5

(a) rendering of interior gravity column failure

(b) axial load and temperature versus time for the failed interior gravity column

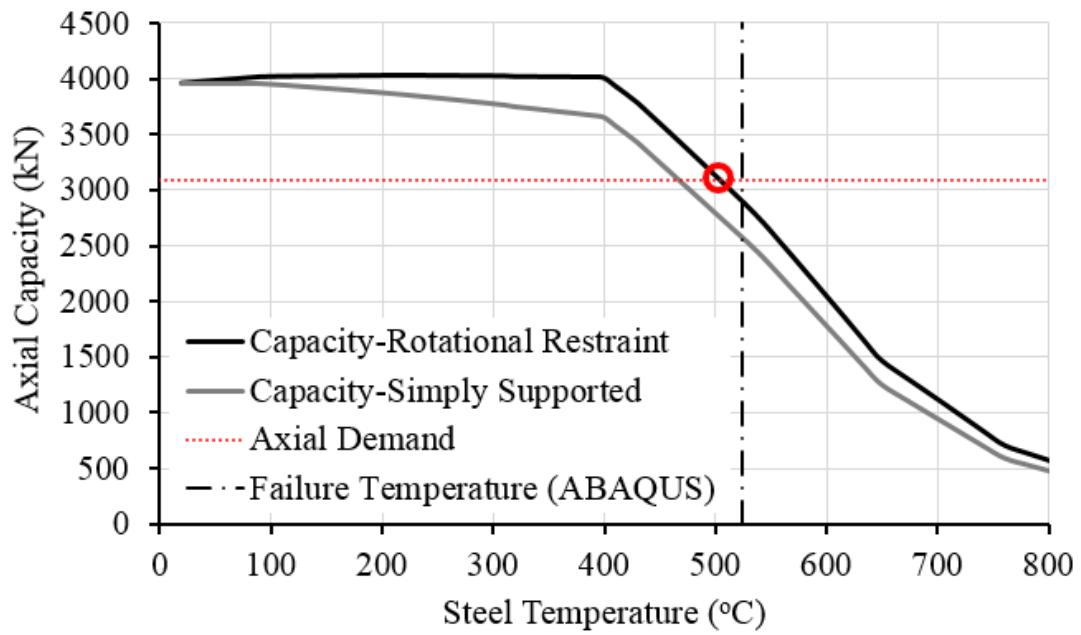


Figure 7.10 First story W14x90 gravity column capacity versus temperature: comparison of ABAQUS results and calculated values

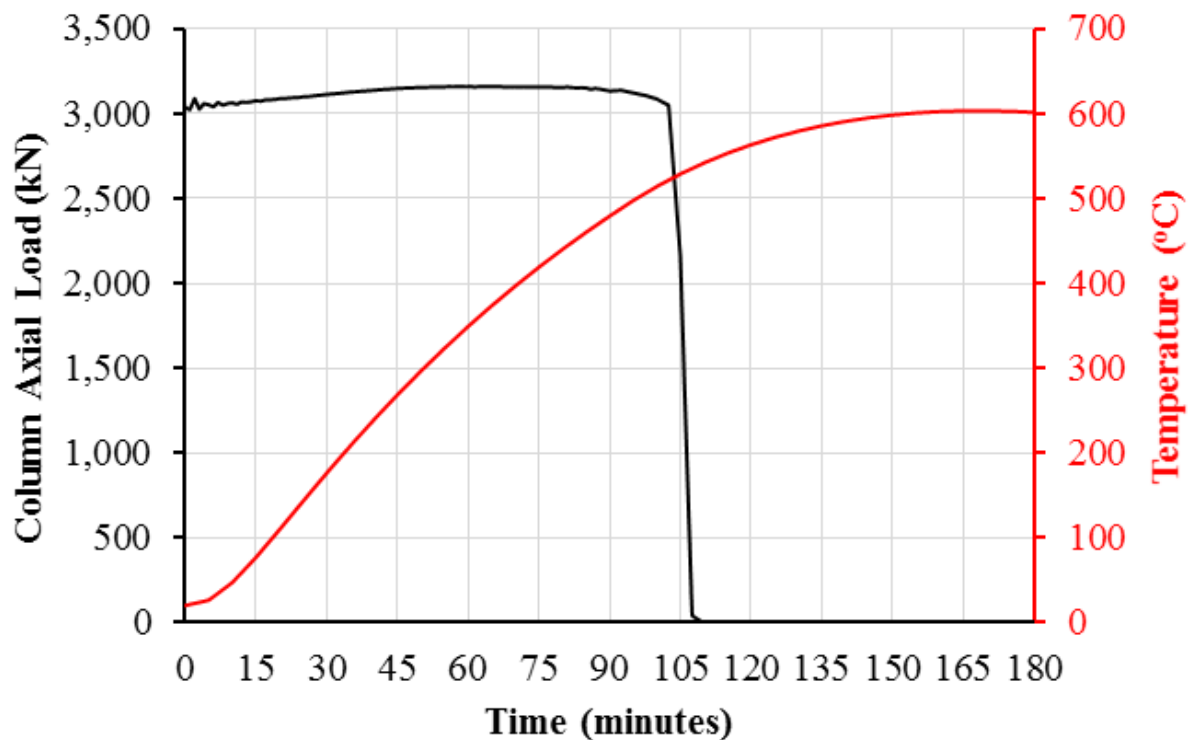


Figure 7.11 Axial load and temperature versus time for the failed interior gravity column in Los Angeles building exposed to 1st story corner compartment Fire 3-1

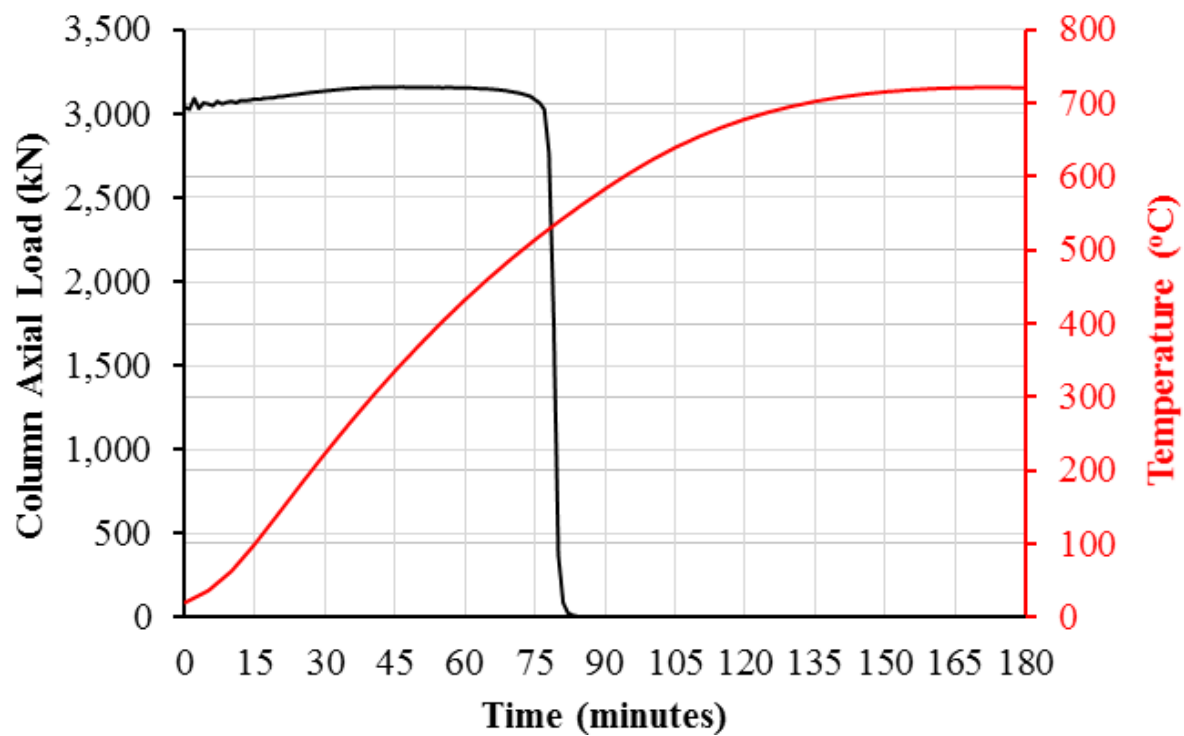


Figure 7.12 Axial load and temperature versus time for the failed interior gravity column in Los Angeles building exposed to 1st story corner compartment Fire 3-1.25

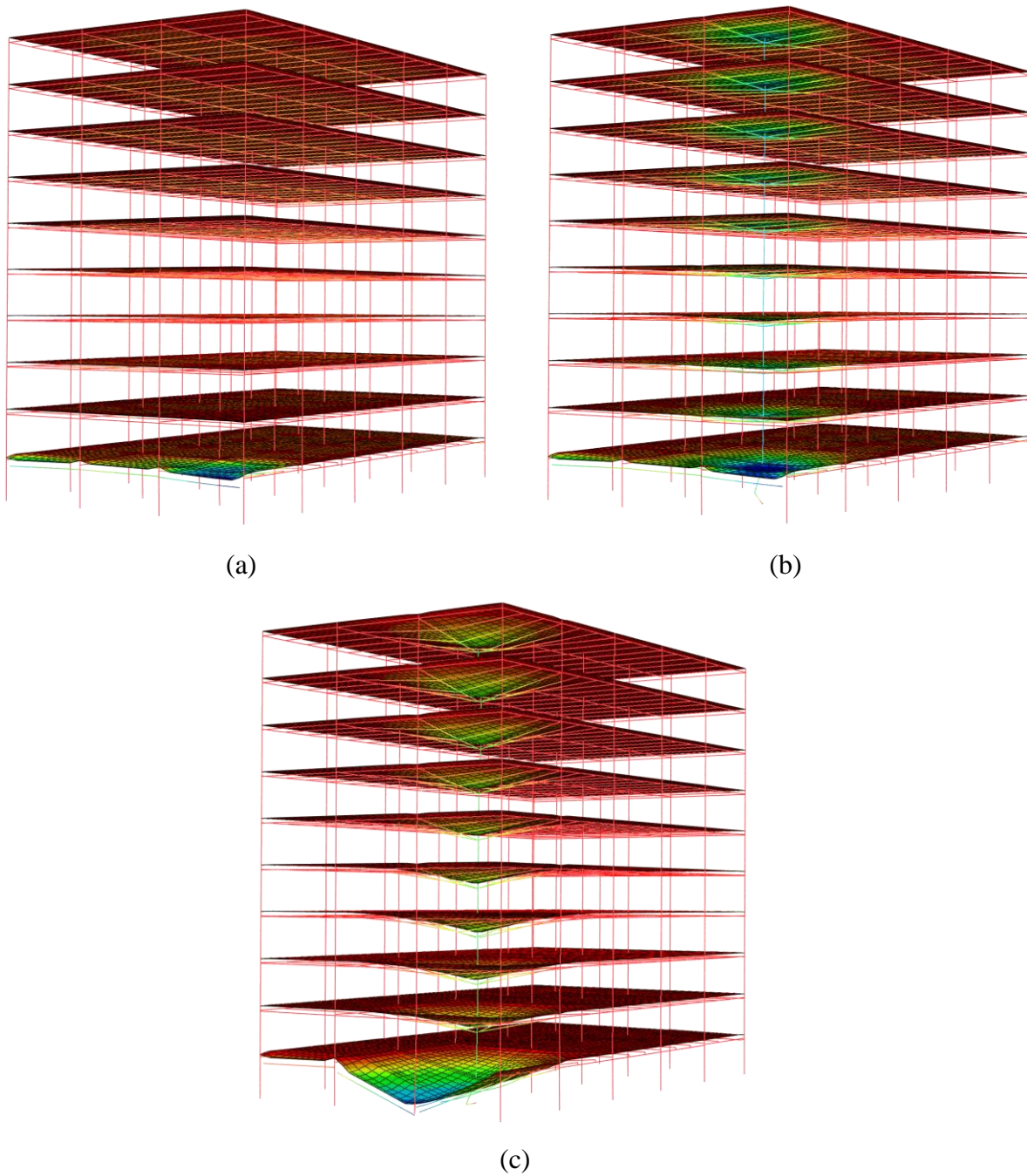


Figure 7.13 Progression of failure for 1st story corner compartment fire with fractured moment frame beams in Los Angeles building (EQ2-1.25 and Fire 1-1A)

(a) Moment frame beam-to-column connection failure

(b) Interior gravity column failure

(c) Gravity frame girder connection failure

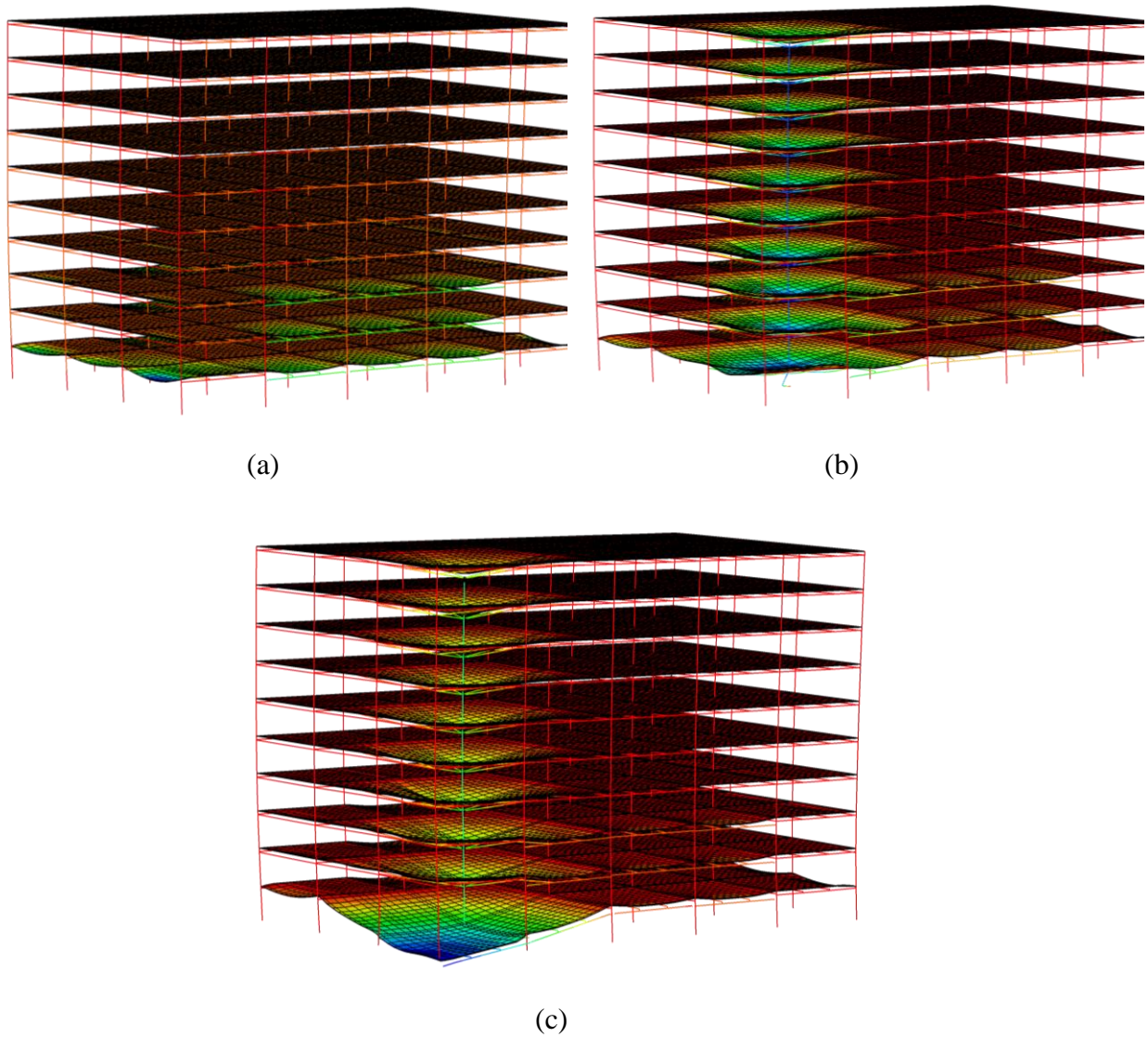


Figure 7.14 Progression of failure for 1st story corner compartment fire with fractured moment frame beams in Los Angeles building (EQ7-1 and Fire 1-1A)

- (a) Moment frame beam-to-column connection failure
- (b) Interior gravity column failure
- (c) Gravity frame girder connection failure

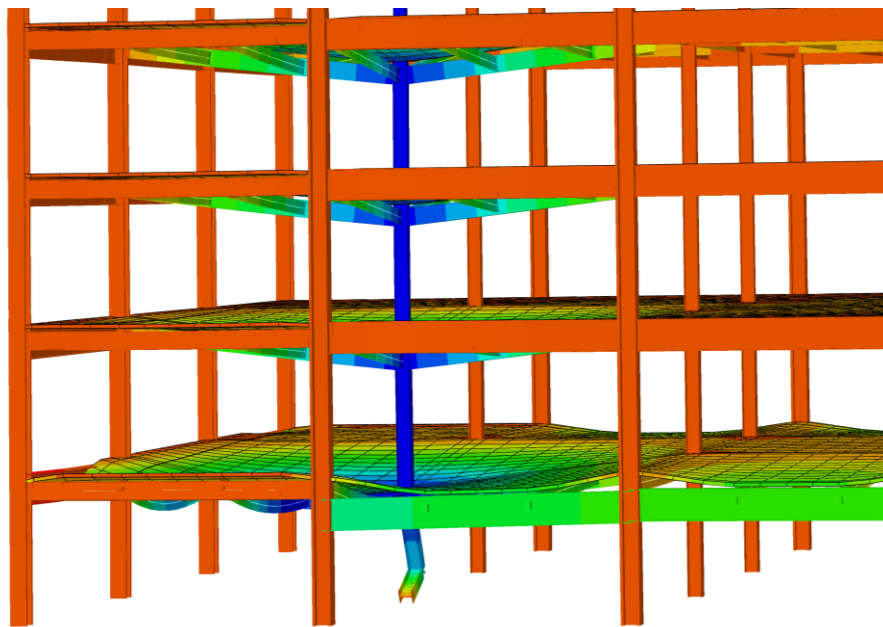


Figure 7.15 Progression of failure for 1st story corner compartment fire with fractured moment frame beams in Los Angeles building (EQ1-0.75 and Fire 3-1A)

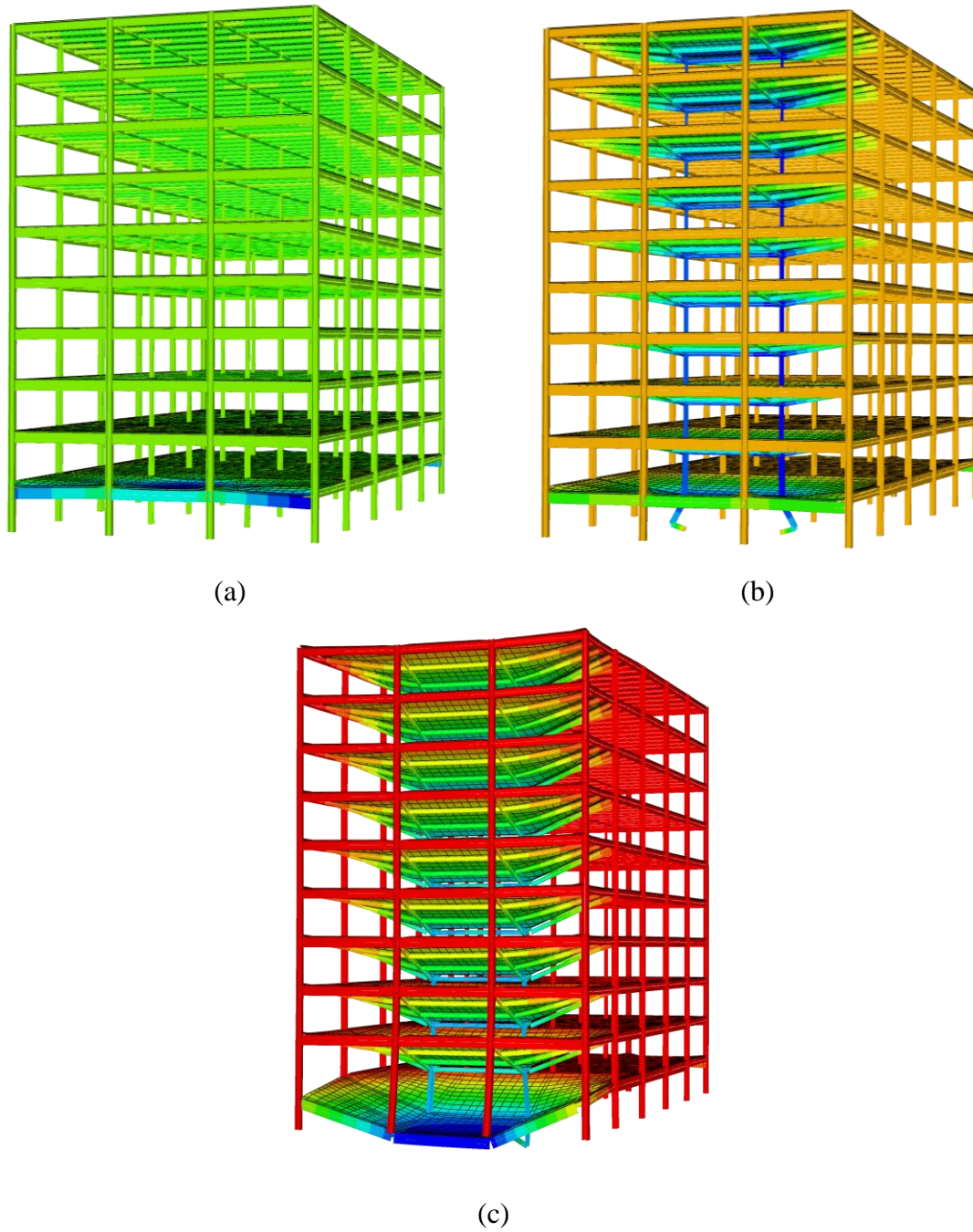


Figure 7.16 Progression of failure for 1st story edge compartment fire with fractured moment frame beams in Los Angeles building (EQ3-1.25 and Fire 3-1B2)

- (a) Moment frame beam-to-column connection failure
- (b) Interior gravity column failure
- (c) Gravity frame girder connection failure

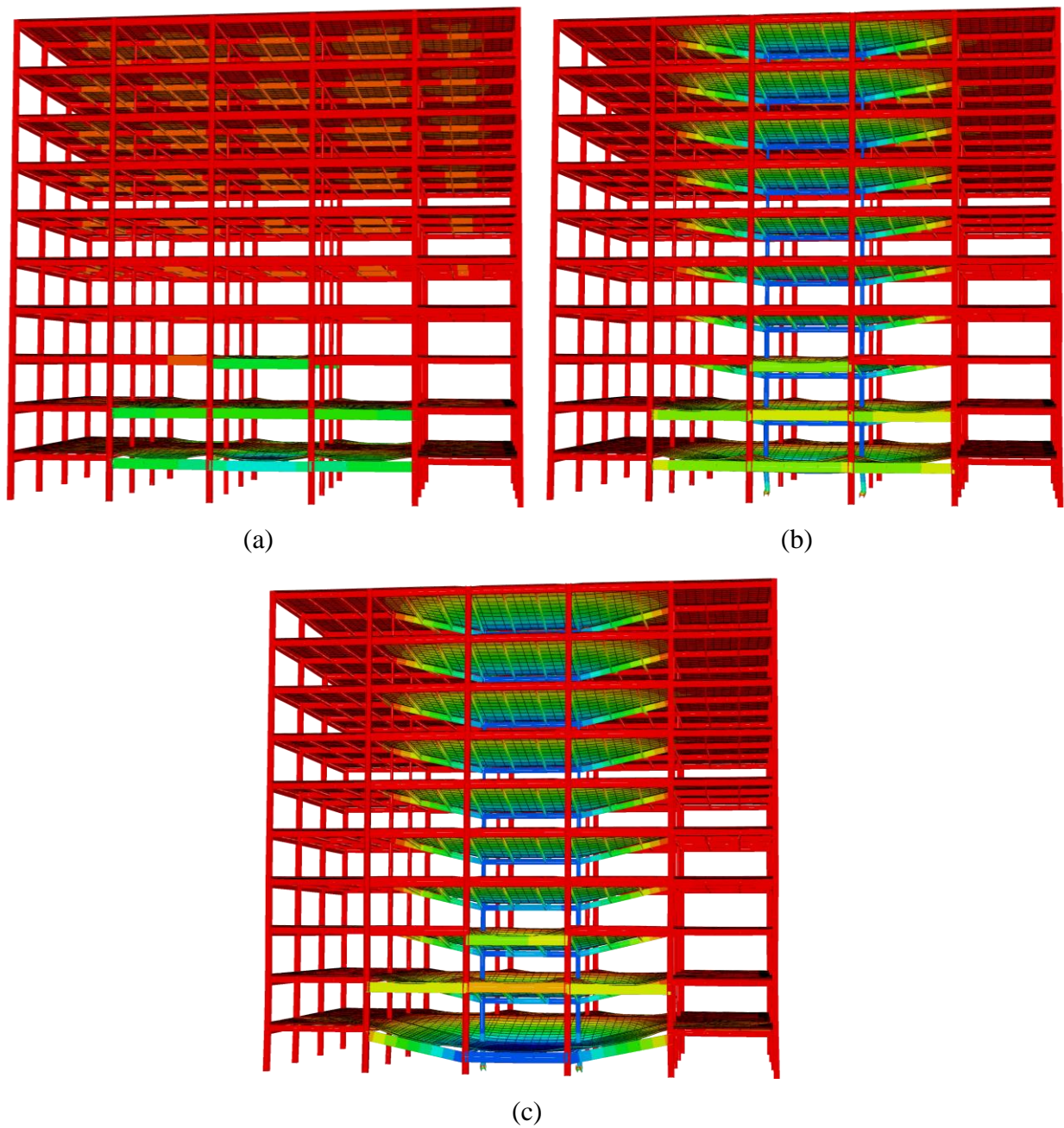


Figure 7.17 Progression of failure for 1st story edge compartment fire with fractured moment frame beams in Los Angeles building (EQ4-1 and Fire 1-1B)

- (a) Moment frame beam-to-column connection failure
- (b) Interior gravity column failure
- (c) Gravity frame girder connection failure

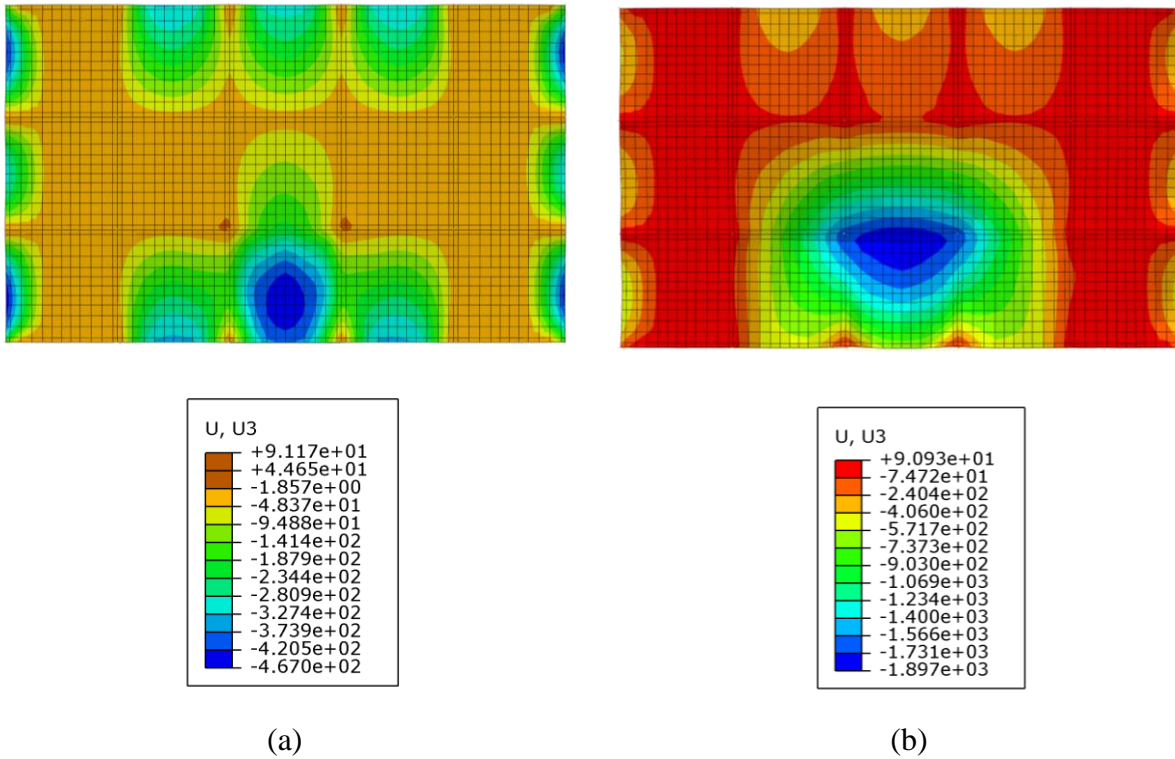


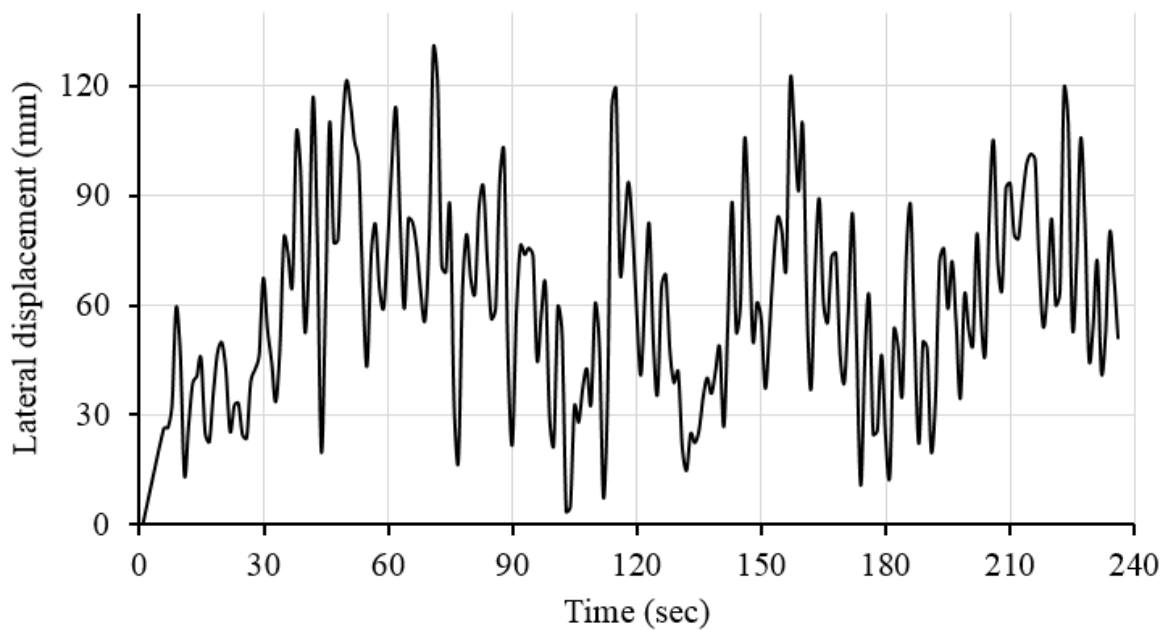
Figure 7.18 Plan view of vertical deformations (mm) in the Los Angeles building subjected to EQ1-1.25 and Fire 3-1B
 (a) Moment frame beam-to-column connection failure
 (b) Interior gravity column failures

Table 7.5 First story fire results for compartments with beam fracture: failure modes and times for Fire 1

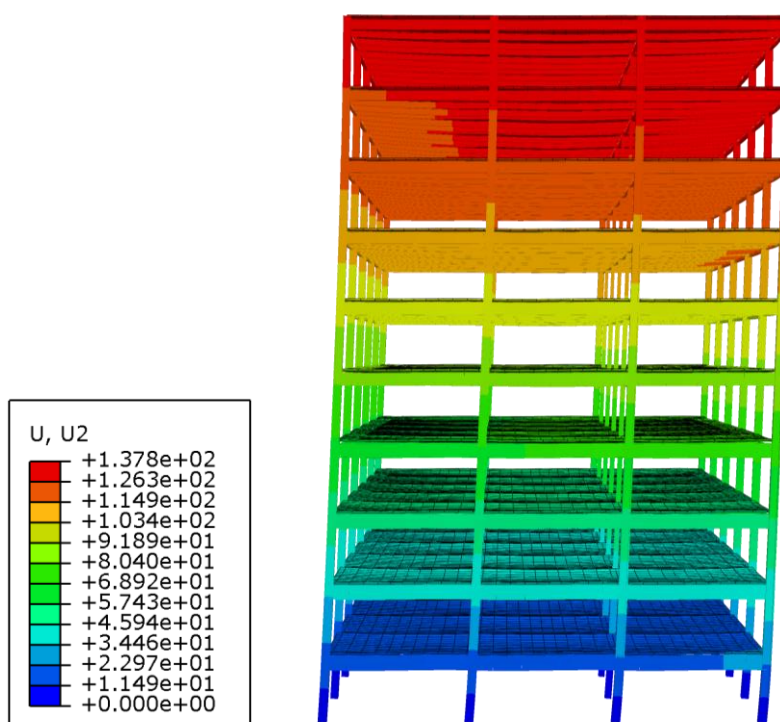
Fire 1-1_1A		Compartment Failure	Column Failure	Connection Failure	Failure time (min)
Earthquake	1-0.75	Y	Y	N	95
	1-1	Y	Y	Y	95
	1-1.25	Y	Y	Y	95
	2-1.25	Y	Y	Y	95
	3-1.25	Y	Y	Y	100
	4-0.75	Y	Y	N	98
	4-1	N	Y	N	98
	4-1.25	Y	Y	N	95
	7-0.75	N	Y	N	95
7-1	Y	Y	Y	95	
Fire 1-1_1B		Compartment Failure	Column/Bay Failure	Connection Failure	Failure time (min)
Earthquake	1-0.75	Y	Y	N	93
	1-1	N	Y	N	93
	1-1.25	N	Y	N	93
	2-1	Y	Y	N	95
	2-1.25	Y	Y	Y	98
	3-1.25	Y	Y	Y	95
	4-0.75	Y	Y	N	100
	4-1	Y	Y	Y	95
	4-1.25	Y	Y	N	95
	6-1.25	N	Y	N	95
	7-0.75	N	Y	N	95
7-1	Y	Y	Y	95	
Fire 1-1.5_1A		Compartment Failure	Column Failure	Connection Failure	Failure time (min)
EQ	7-1	Y	Y	Y	52
Fire 1-1_1.5B		Compartment Failure	Column/Bay Failure	Connection Failure	Time of Failure (min)
Earthquake	4-1	Y	Y	Y	95
	4-1.25	Y	Y	Y	95
	7-0.75	Y	Y	Y	95
	7-1	Y	Y	Y	95

Table 7.6 First story fire results for compartments with beam fracture: failure modes and times for Fire 3

Fire 3-1_1A		Compartment Failure	Column Failure	Connection Failure	Failure time (min)
Earthquake	1-0.75	N	Y	N	103
	1-1	Y	Y	Y	103
	1-1.25	N	Y	Y	100
	2-1	N	Y	N	100
	2-1.25	Y	Y	Y	100
	7-1	Y	Y	Y	103
Fire 3-1_1B		Compartment Failure	Column/Bay Failure	Connection Failure	Failure time (min)
Earthquake	1-1	Y	Y	Y	102
	2-1.25	N	Y	Y	100
	3-1.25	Y	Y	Y	105
	4-0.75	N	Y	N	105
	4-1	Y	Y	Y	105
	4-1.25	Y	Y	Y	105
	6-1.25	N	Y	N	105
	7-0.75	Y	Y	Y	105
	7-1	Y	Y	Y	102



(a)



(b)

Figure 7.19 Lateral response of Los Angeles building subjected to wind time history
 (a) Lateral displacement at roof versus time due to wind time history
 (b) Deflected shape (mm) at maximum deflection scaled by 10

CHAPTER 8. PILOT STUDY RESULTS

This chapter contains a number of different pilot studies that were implemented to examine how changes to individual aspects of the structural design will affect the post-earthquake fire resilience of the structure. These studies act as a starting point for potential future analyses. The studies include: implementing a 2 hr FRR for the gravity columns, using increased gravity column sizes, and implementing a mat of rebar in the composite slab. The influence of fireproofing damage on fire resilience is also explored. Horizontally travelling fires and aftershocks are applied to a select few of the fire scenarios. Finally, fragility curves of the seismic and post-earthquake fire analyses are developed and discussed.

8.1 Gravity Columns with 2 hr FRR

The incremental fire analyses conducted thus far have shown that, when all members are protected with the same fire resistance rating, the gravity columns are the vulnerable component regardless of seismic damage. There are a few exceptions to this. The first exception is when the fire is a short duration fire with a quick heating and cooling phase (such as Fire 2). This fire often results only in large deformations but not member failure. The other exception is when the structure has fractured during the earthquake and the damaged portion of the structure is subjected to the compartment fire. In this case, other failure modes may govern. Because of the prevalence of gravity column failures, studies were completed to understand the effect of increasing the fireproofing thickness on the gravity columns. The Chicago building was reanalyzed for fifth and ninth story corner compartment fires (5A and 9A) subjected to Fire 1-1, which is the fire that most closely follows the ASTM E119 and ISO 834 fire time-temperature curves.

8.1.1 Fifth Story Corner Compartment Fire

The fifth story interior gravity column is a W12x58. In all of the previous analyses, the fireproofing thickness on this column was 18 mm (3/4 in) in order to achieve a one hour fire resistance rating. In order to see the impact of fireproofing on the fire resilience, the compartment was subjected to the same Fire 1-1 but with a two hour fire rating on the W12x58 column. Design number X701 from Underwriters Laboratory [9] was used to specify 28 mm (1 1/8 in) of fireproofing thickness

required to achieve a two hour fire resistance rating. As Figure 8.1(a) shows, damage is limited to beam and slab deflections within the compartment. The additional fireproofing prevented the column from failing.

The gravity column did not fail because the fireproofing prevented the steel column from reaching its failure temperature. As Figure 6.17 showed, the gravity column was subjected to 1850 kN (416 kips) and could not support this load beyond an internal temperature of 544°C. Because the axial load in gravity columns is relatively unaffected by elevated temperatures, heat transfer analyses can be studied on the cross-section to determine if the internal steel temperatures surpass the failure temperature or not. This can provide a quick, simple method of predicting column failure and determining the required fireproofing to prevent failure. It does not, however, consider any other failure modes that could occur before column failure, or any other factors that could precipitate column failure through other means (such as a connection failure that would leave the column unbraced, or large deformations that could lead to a leaning column and a secondary effects failure).

Figure 8.2 compares the internal temperatures of the W12x58 cross-section with different fire resistance ratings: 1 hr (18 mm), 1.5 hr (22 mm) and 2 hr (28 mm). Note that the web and flange temperatures were very similar for this cross-sectional shape and that the larger temperature was used. Figure 8.2(a) illustrates the maximum steel temperatures versus time that the maximum temperature occurred for Fire 1. The graph considers Fires 1-1.5, 1-1, 1-0.75 and 1-0.5, which are distinguished by different geometric shapes. A steel temperature greater than the failure temperature indicates that the column will fail when subjected to that fire. According to the graph, column failure will occur for all Fire 1-1.5 cases regardless of whether 1, 1.5 or 2 hr FRR is used. As shown in the previous studies, a W12x58 column with a 1 hr FRR subjected to Fire 1-1 will fail at 103 minutes. By the prescriptive method, this is considered successful because the column has successfully carried load beyond the 1 hour that it was intended to. Adding only 4 mm of fireproofing to the 1 hr FRR (in order to achieve a 1.5 hr FRR) will prevent the column from ever reaching the failure temperature, when subjected to Fire 1-1. For all other Fire 1 cases with intensities less than 1, column failure will not occur. It is clear that adding fireproofing both decreases the steel temperature and increases the amount of time before maximum temperature is achieved. This helps to prolong the fire resilience of the system, allowing time for people to safely exit the building. In this case, a FRR of 1 hr reaches maximum temperature around 100 minutes.

Fire resistance ratings of 1.5 and 2 hrs reach maximum temperatures at 115 and 125 minutes, respectively. These times are all conservative with respect to their fire resistance ratings of 60, 90 and 120 minutes.

Figure 8.2(b) provides the same comparison of steel temperature versus time for Fire 2, which was a very hot, quick fire. Note that the time at which maximum temperature is reached is relatively short (50-60 minutes) but that the temperatures themselves are also relatively low. Because the fire heated quickly and then dissipated heat so quickly, the steel did not ever reach very high temperatures. Even with a Fire 2-1.5, no gravity column failures occur, regardless of a 1, 1.5, or 2 hr FRR.

Figure 8.2(c) compares the maximum internal temperature of the W12x58 column with the time it takes to reach the maximum temperature when subjected to Fire 3, a slower fire. The times at which maximum temperatures are reached vary from 150 to 195 minutes. Steel temperatures reach beyond failure temperature for all Fire 3-1.5 cases, and for Fire 3-1 with 1 and 1.5 hr FRRs. A 2 hr FRR for the column subjected to Fire 3-1 would prevent column failure. All other fire cases with lower intensities do not reach the failure temperature necessary to cause column failure.

8.1.2 Ninth Story Corner Compartment Fire

The same study was conducted at the ninth story using a compartment fire at the corner compartment (9A). Figure 8.1(b) shows the structural response when subjected to Fire 1-1 with all members assigned a 1 hr FRR except for the interior gravity column. This column is a W8x24 and was assigned a 2 hr FRR (41 mm per design number X772 in UL [9]). As was the case with the fifth story study, gravity column failure is prevented with increased fireproofing.

Figure 8.3 shows the internal temperatures of the W8x24 cross-section with different fire resistance ratings: 1 hr (21 mm), 1.5 hr (31 mm) and 2 hr (41 mm). It provides the maximum column temperature and the time at which that temperature was reached. These values are compared with the failure temperature of 499°C which was determined from previous analyses using ABAQUS. Though the temperatures and times vary slightly between the W8x24 cross-section and the W12x58 cross-section, the failures occur at nearly all the same fire intensity levels and fireproofing ratings. For Fire 1, shown in Figure 8.3(a), Fire 1-1.5 will cause column failure regardless of 1, 1.5 or 2 hr FRR. Fire 1-1 will cause a column failure, as observed in the previous

analyses, but adding additional fireproofing to achieve higher rating levels will prevent this. For intensities scaled at less than 1 times Fire 1, column failure will not occur.

The findings for Fire 2 are the same as the W12x58 column, except that, for Fire 2-1.5 with 1 hr FRR, column failure will occur. All other temperatures lie significantly below the failure temperature.

Fire 3 results in relatively high steel temperatures at times ranging from 150 to 220 minutes. A W8x24 column with 2 hr FRR will still fail when subjected to Fire 3-1.5. For Fire 3-1, a 2 hr FRR can prevent column collapse. For all lower-intensity fires, column failure will not occur.

8.1.3 Cost Comparison for Increased Fireproofing

These studies show that increasing fireproofing to vulnerable components can significantly affect the failure mode and time of failure of the structure. As previously discussed, column failure affects all of the stories above, which can cause widespread damage that will require significant repair or replacement. Fireproofing application, however, is a cost intensive procedure. A general rule of thumb is that fireproofing costs makes up 10-15% of the cost of the steel frame. A cost comparison of fireproofing costs for the structure with 1 hr and 2 hr fire resistance ratings is given in Table 8.1. These costs were calculated by interpolating and extrapolating values from RS Means [125]. These fireproofing costs represent the total cost for fireproofing all members within the building with all of the members having a 1 hr FRR and the gravity columns having either a 1 or 2 hr FRR. Cost was based on normal density sprayed cementitious fireproofing and included material, labor, and equipment costs. Material costs were interpolated based on costs provided for 1" of beam fireproofing and 1 1/8" and 2-3/16" of column fireproofing. Labor and equipment costs for less fireproofing were conservatively maintained using the greater thickness values, when interpolation was not possible. The Chicago building costs \$137,800 to fireproof the original design and \$139,800 to fireproof the new design with additional fireproofing on the gravity columns. The Los Angeles building costs less because the larger moment frame members do not require as much fireproofing. This building costs \$112,300 to fireproof all members with 1 hr FRR and \$116,400 to incorporate a 2 hr FRR on the gravity columns. The difference between total building fireproofing cost when the gravity columns have a 1 hr FRR versus a 2 hr FRR is approximately \$2,000. It is important to note that this value may be slightly greater when accounting for different labor costs. In addition, fireproofing adds an additional step to the

construction process that can prolong construction, which may be costly for the owner. However, fireproofing of the gravity columns only makes up 8% and 7% of the Chicago and Los Angeles building fireproofing costs, respectively, whereas the beams make up approximately 75% of the total fireproofing cost, so increasing beam fireproofing would be much more costly than increasing column fireproofing.

The prescriptive method has been proven to effectively withstand structural failures beyond the time thresholds prescribed in the method. It does not, however, ensure that collapse will not occur beyond that timeframe. The owner may decide it is worthwhile to spend the additional money to increase fireproofing thicknesses and, thereby, improve overall system resilience to fire by preventing column collapse. Increasing column fireproofing is a relatively cost effective solution for preventing system collapse and improving resilience.

8.2 Increased Gravity Column Sizes

As previously explained, this study has shown that gravity columns are vulnerable to collapse during compartment fires. In an effort to increase the fire resilience of the structure and as an alternative to increasing fireproofing thicknesses, gravity column sizes may choose to be increased. By choosing a heavier shape, the internal temperatures in the cross-section will be reduced and the capacity of the column increases. Note that only the column size is revised; the fireproofing thickness remains the same as what was required for the original column size.

Table 8.2 summarizes the original and revised gravity column sizes. The new shapes were chosen to be one to two sizes heavier than the original. All other structural members remain the same as those given in Chapter 4.

By increasing gravity column sizes, there is also the potential for reducing seismic drifts and, thus, damage. Studies have shown that the gravity columns contribute to the overall system stiffness more so than the gravity beams and shear connections [32]. However, when comparing seismic response of the case study buildings with the original and revised gravity column sizes, the increased column sizes reduce the maximum drift by less than 1% of the initial building's drift. This occurs for both the Chicago and Los Angeles and is essentially an insignificant change in response. It is presumed that this small change is due to the fact that gravity column sizes have only been increased by one to two sizes and that this does not affect the overall system

significantly. This was confirmed by a reduction in fundamental period of the Chicago building by only 0.02 seconds.

8.2.1 Fifth Story Corner Compartment Fire

Table 8.3 summarizes the failure types, times of failure and deflections that resulted from compartment fires at the fifth story corner compartment. This compartment originally had W12x58 interior gravity columns. Gravity columns at this story were increased to W12x72 for this study. Fires 1-1, 1-1.5 and 3-1 were simulated. Fire 2 was not analyzed, as it did not tend to produce failures. Each of these fires in the original building resulted in column failure of the interior gravity columns. The fifth story W12x58 column in the original building that was exposed to Fire 1-1 reached 560°C at 103 minutes but the new W12x72 exposed to the same fire reaches only 535°C at 107 minutes. While this is not a large change in demand, there is also the advantage of the increased column capacity. The original column collapsed at 95 minutes with a temperature of 544°C. By using a W12x72 column size, column failure is prevented and compartment failure results. The same is true for the column subjected to Fire 3-1. In the original building, column failure occurred at 100 minutes but with the increased column size, column failure is avoided. Instead, the beams reach a maximum relative deflection of 270 mm (11 in) and a total system deflection of 478 mm (19 in). For Fire 1-1.5, the increase in column size is not enough to prevent column failure. It does, however, increase the failure time from 50 minutes to 60 minutes, allowing for slightly more time for occupants to safely escape.

Table 8.4 and Table 8.5 summarize the utilization ratios for the original and revised gravity column sizes. The utilization ratio is calculated as the column demand (due to the fire load combination $1.2D+0.5L+A_T$) divided by the column capacity, ϕP_n at ambient conditions. The utilization ratio for the fifth story gravity columns was decreased from 0.64 to 0.48. This provides approximately 15% excess capacity in the column. For Fires 1 and 3, this change was enough to prevent collapse. For higher intensity fires such as Fire 1-1.5, this change may not prevent collapse.

8.2.2 Ninth Story Corner Compartment Fire

The lower portion of Table 8.3 provides the failure modes, times, and deflections for Fires 1-1, 1-1.5 and 3-1 at compartment 9A. W8x24 is the original gravity column size at the ninth level. The size was increased to W8x40 for this study. Fire 1-1 in compartment 9A of the original building

resulted in failure of the W8x24 70 minutes after the start of the fire. When analyzing with a W8x40, the column does not buckling. The system reaches a maximum vertical deflection of 434 mm (17 in) 85 minutes after post-flashover begins with the beams experiencing a relative maximum deflection of 293 mm (12 in), which does not cause compartment failure. The same behavior was observed for Fire 3-1. Column collapse at 88 minutes had been observed in the original building. Replacing the W8x24 columns with W8x40s prevented collapse of the column. Instead, only compartment failure occurred.

Fire 1-1.5 in the original building caused system collapse of the structure due to interior gravity column collapse and then eventual collapse of the remainder of columns within the compartment. The same progression of behavior and failure occurs with the revised building. The larger column size does, however, prolong the time before collapse. Collapse originally occurred after 46 minutes. It was lengthened to 66 minutes by using the W8x40 size.

From Table 8.4 and Table 8.5, the column utilization ratios are 0.73 and 0.35 for the W8x24 and W8x40 columns, respectively. As was the case at the fifth story, the reduced column utilization ratio appears to be beneficial for Fires 1-1 and 3-1, but not for a larger intensity fire such as Fire 1-1.5

8.2.3 Cost Comparison for Increased Gravity Column Sizes

Fire resilience of a conventional steel, moment frame mid-rise structure can be increased by using larger column sizes. There is, of course, a cost associated with this change. Table 8.8 summarizes the steel framing costs for all of the member steel in the Chicago and Los Angeles buildings. This cost includes material, labor, and equipment, and is based on RS Means cost estimates [125]. The steel for the original Chicago building costs \$1,810,400. When larger column sizes are used, it increases to \$1,838,200. This is an increase of nearly \$28,000 but only 1.55% of the steel building cost. The Los Angeles building is significantly more expensive because of the heavy moment frame sections. Its original steel cost is \$2,358,200. The modified cost due to the revised column sizes is \$ 2,383,600, which is a 1.12% cost increase. An increased gravity column size will increase the column capacity and lower the temperature demands on the member; this modification can prevent column, bay and system collapse, which are failures that may lead to demolition of the structure. An owner may choose to have an additional upfront cost in order to prevent the need to rebuild the building in the future.

8.3 Including Rebar Mat in Composite Slab

The floor diaphragms for the case study buildings in Chicago and Los Angeles are the same composite floor deck systems. The slab is a 3"-20 gauge metal deck with 2 ½" light weight concrete topping. Welded wire reinforcement of 152mmx152mm MW10 is embedded within the concrete topping slab. The composite slab serves multiple functions. It is used to transfer gravity loads from the slab to the building frame. It also functions as the floor diaphragm to transfer lateral loads from the slab to the lateral force resisting members. The diaphragm ensures that the frames are tied together and move laterally together when subjected to lateral loading. When a fire has occurred, the floor system often experiences large deflections and failure of members that cause large sags and deformations. In these instances, the diaphragm can also serve as a mechanism for catenary action within the floor system. The slab can redistribute gravity loads through membrane action, effectively bridging the failed floor system to avoid progressive collapse. In this study, the diaphragm strength and stiffness were increased by incorporating a rebar mat into the topping slab of the structure. Reinforcing bars of #5 at 12" on center in each orthogonal direction of the building were used in place of the welded wire fabric. This was done in order to evaluate the benefits of a rebar mat for increasing catenary action capacity.

Adding reinforcement within the slab can also potentially change diaphragm behavior by altering the stiffness of the slab and, thus, the distribution of lateral forces throughout the diaphragm. However, because most composite slabs without a rebar mat are already considered semi-rigid or rigid, the distribution of forces throughout the diaphragm is presumed to be similar for most regular diaphragms with or without additional steel reinforcement. There is, however, a notable difference in the diaphragm's performance in a fire event.

Results from the fire analyses conducted in Chapters 6 and 7 showed that the interior compartment (designated "C" in Figure 4.14) was prone to system collapses. For Fires 1-1, 1-1.5, 3-1 and 3-1.25, system failures were observed at the first, fifth and ninth story interior compartments. As explained previously, the four interior gravity columns within those compartments buckled due to elevated temperatures. This resulted in a floor system that needed to span three bays in order to redistribute loads and prevent collapse. This was not possible in the original building models which only modeled the topping slab, metal deck, and wire mesh.

The structure was reanalyzed at the fifth story interior compartment (5C) for Fires 1-1 and 3-1 using a rebar mat of #5 bars at 12" on center. The deflected shape of the structure exposed to Fire

3-1 is shown in Figure 8.4. Unlike the system failures observed in the interior compartment fires with the welded wire mesh, the structure is able to stabilize itself after the four interior columns fail at the fifth story. Instead of system collapse, it experiences bay failure. A vertical deflection of 2712 mm (106 in) was observed from Fire 3-1. Fire 1-1 caused a similar bay failure with 2708 mm (106 in) of maximum vertical deflection. When using more reinforcement of #5 at 6" on center, the maximum deflection when exposed to Fire 1-1 was reduced to 2420 mm (95 in). While this is still a very large deflection that would require significant repair, it prevents system collapse and, thus, increases the life safety for the occupants within the building.

It is important to note that while reinforcing bars are commonly used in select locations to minimize shrinkage and temperature cracks, or at the perimeter of the slab to transfer diaphragm forces, they are rarely used throughout the entire slab due to the high cost implications of additional material and labor. In addition, there is the potential for cracking and spalling of the concrete due to the minimal cover of the reinforcing bars. When reinforcing bars are being considered within the slab, thicker slabs should be used and consideration should be given to the seismic and fire response implications of a cracked slab.

8.4 Incorporating Fireproofing Damage

This pilot study explores whether fireproofing that is damaged during a seismic event will affect the post-earthquake fire performance of the structure. Because plastic hinging and fracture occur in different locations and to different members (columns as opposed to beams) for the Chicago and Los Angeles buildings, each building was analyzed separately to gauge the effect of incorporating fireproofing damage in different scenarios.

A limited number of experimental tests have been conducted to study the fireproofing damage through cyclic loading of gravity connections, moment connections, and columns. Keller and Pessiki [126] studied beam-column shear connection assemblies subjected to cyclic loading and observed cracking, spalling and debonding of the SFRM. Cracking was generally less than 8 mm (0.3 in) in width. Spalling of 70 mm by 90 mm (2.75 in x 3.5 in) sections were observed. For single plate shear connections, cracks occurred along the web connection plate. Braxtan and Pessiki [127] found that beam-to-column moment connections would experience SFRM debonding at the onset of yielding of the steel. Spalling of SFRM at beam flanges occurred at about 3% interstory drift. This included exposure of the steel for a 457 mm (18 in) long section of the bottom beam flange.

At locations of member buckling, debonding and deformation of the insulation also occurred. Wang et al. [128] conducted experimental tests of wide flange columns with SFRM. Again, debonding occurred at large deformations, which led to steel exposure of the column flange at the base of the column.

While these studies help to understand the potential failure modes of the SFRM as well as the frequency and extent of damage, it is still difficult to predict these failures for use in the building models. In the building model, temperatures are input at five integration points throughout the steel cross-section (Figure 5.7). Thus, instead of simulating cracks and debonding at beams, columns, and connections, fireproofing damage is expressed as a percentage of the total original fireproofing thickness. For instance, heat transfer of the steel cross-section is conducted using the full fireproofing thickness required per code, using no fireproofing, and various thicknesses in between. Additionally, SFRM damage is only applied to locations where the steel has reached yielding.

8.4.1 Chicago Building

Results of the incremental dynamic analyses showed that plastic hinging and fracture occurred primarily in the moment frame columns at the upper levels of the building. When fracture initiated in the columns, collapse occurred and, thus, SFRM damage was only explored in plastic hinge locations and not at fracture locations.

Heat transfer analyses were conducted for the columns that experienced plastic hinging by varying the thickness of fireproofing. Compartment 5A (the fifth story corner compartment) was subjected to Fire 1-1 after exposure to earthquake 4-3. EQ 4-3 is an earthquake that caused plastic hinging in the ninth story moment frame columns. Though yielding did not occur at compartment 5A, the impact of fireproofing damage was still studied at this level. The W14x99 moment frame column was reanalyzed with varying levels of fireproofing. Figure 8.5(a) shows the column axial load versus time relationship of the interior gravity column (W12x58) for two scenarios. The first is when the W14x99 does not have any fireproofing damage and, thus, the W12x58 is the first member to fail (shown by the solid, thick black line entitled “W12x58_No FP Damage”). The second scenario is when the W14x99 column has no fireproofing (100% damage) and, thus, the W14x99 column (denoted “W14x99_0mm” for 0mm of fireproofing) fails before the interior gravity column (denoted “W12x58”). The graph shows that the exterior column begins to lose load

carrying capacity at about 27 minutes and then the interior gravity column fails at 86 minutes. This is in contrast to the undamaged fireproofing scenario, for which failure is initiated by gravity column buckling at 98 minutes. Figure 8.5(b) shows the deflected shape of the system when the exterior moment frame column (W14x99, shown in yellow) buckles at its base. This deflected shape is similar to compartment failures but with additional sag at the failed column location, resulting in deflection in this location at the stories above. Figure 8.5(c) shows the deflected shape of the system when the interior gravity column has buckled. Column failure results and system collapse does not occur. Figure 8.5(a) also includes the temperature versus time relationship for the W14x99 column flanges for 0, 5 and 18 mm of fireproofing thickness. The W14x99 unprotected column fails at 27 minutes, which corresponds with a temperature of 680°C. This failure temperature can be achieved with 5 mm of fireproofing, which correlates to a loss in original fireproofing thickness (18 mm) of approximately 72%. This is a very substantial loss in thickness which seems unlikely based on the experimental tests previously conducted. The W14x99 column with more than 5 mm of fireproofing would not fail. Because of the low utilization ratio of the moment frame columns, there is reserve capacity that makes it unlikely that column failure due to fireproofing damage would occur prior to gravity column buckling.

Figure 8.6(a) shows the same relationship for Fire 1-1 exposed to compartment 9A (the ninth story corner compartment). It provides the column axial load versus time relationship for the W8x24 interior gravity column when no fireproofing damage is applied to any members. This scenario is shown as a thick black line denoted by “W8x24_No FP Damage.” In this scenario, failure occurs when the interior gravity column fails at 70 minutes. The same analysis is then conducted for the compartment fire with complete fireproofing damage to the exterior moment frame column, W12x45. The thick gray line shows the load versus time relationship for W12x45 without any fireproofing on it. Failure of this column occurs at approximately 30 minutes. This failure then triggers failure of the W8x24 interior gravity column at 65 minutes. The graph also shows the temperature versus time relationship of the perimeter moment frame W12x45 with 0, 5, 11 and 18 mm of fireproofing. The failure temperature of the W12x45 without fireproofing occurs at 30 minutes with a temperature of 745°C. This graph shows that the W12x45 would need to have less than 5 mm of fireproofing in order for the W12x45 to initiate failure. Again, it is unlikely that this level of fireproofing damage would occur throughout the member cross-section. Figure 8.6(b) is a rendering of the deflected shape at compartment 9A when the W12x45 moment frame column

buckles at the base of the column. This type of squashing or crumpling of the column causes it to lose load carrying capacity but does not result in extensive deformations in the framing system. This type of failure was observed in the Cardington fire tests [72]. The columns that were unprotected at the beam-to-column connections experienced this localized column buckling in the Cardington tests. Figure 8.6(c) shows the final deflected shape once the interior gravity column has buckled. This type of buckling causes much more significant deflections.

Fireproofing damage was also explored at the edge compartments, 5B and 9B. The results of the 9B fire simulation are shown in Figure 8.7. Figure 8.7(a) portrays the column axial load over time for the perimeter moment frame column (W12x45) and the interior gravity column (W8x24). The curves are similar to those described in Figure 8.6. However, the axial load increases more due to temperature because two moment frame connections are framing into the column at this location, as opposed to only one at compartment A, which results in greater constraint of the column against expansion. The W12x45 moment frame column buckles at approximately 30 minutes. This leads to only a slight sag of the exterior framing (less than the $L/20$ limit from the British Standard [105]) that should not hinder evacuation efforts of occupants. The interior column buckles at 59 minutes. This is only 6 minutes before the failure occurred in the seismically undamaged structure and only 11 minutes sooner than the structure with all members protected with 1 hr FRR. However, failure of the interior columns results in system collapse of the structure at 64 minutes. Because the moment frame columns have already failed, they were not able to carry the loads lost by the interior column collapses, and the crumpled exterior columns deform more significantly. This causes large deformations in the compartment and eventually leads to overloading of the other adjacent columns and, subsequently, failure of the system. This shows that significant fireproofing damage (in this case, less than 5 mm of remaining fireproofing) can change the failure mechanism from a bay failure, which is a relatively localized failure, to a system failure that is widespread and extremely dangerous.

Fire 1-1 at Compartment 5B was also studied. The column axial load and temperature versus time relationship is very similar to Figure 8.5. Figure 8.8(a) shows the relationship of the column axial loads over time. The gray line shows the exterior moment frame column (W14x99) with no fireproofing. As the temperatures in the compartment increase, the axial load increases from 960 kN to 1100 kN. At approximately 34 minutes, the column buckles (Figure 8.8(b)) and loses most of its load carrying capacity. It maintains approximately 100 kN of axial load. The remainder of

the load is transferred to adjacent columns, as can be seen in the increase of column axial load for the W12x58 interior gravity column (shown as a black dashed line in Figure 8.8(a)). This column eventually fails at 80 minutes, when there is a drop in the remainder of the axial load in the exterior column (gray line). Figure 8.8(c) shows the final deflected shape of the system. Collapse of the interior columns causes more deformation in the exterior moment frame columns, but the loads are able to redistribute to adjacent columns, causing only bay failure instead of system collapse. In this instance, having a more robust lateral system than the ninth story is ultimately a benefit, as system collapse is prevented.

Findings from this study show that severely damaged fireproofing (i.e. – 5 mm or less of fireproofing) at the moment frame columns can initiate column failure of the perimeter columns within the fire compartment. In general, the moment frame columns have enough excess capacity that, unless this type of unlikely severe damage occurs, gravity column failures will continue to be the controlling failure mechanism. These moment frame column failures experience crumpling of the column at either the column base or top, and do not experience the severe, global column buckling observed in the gravity columns. Ultimately, the gravity columns will still fail and failure of the perimeter columns speeds up this process. It may or may not cause system collapse, depending on the robustness of the moment frame at that level.

8.4.2 Los Angeles Building

As previously mentioned, the Los Angeles building primarily experienced plastic hinging and fracture in the moment frame beams in the beam-to-column connection protected zones. This is due to the strong column-weak beam philosophy which promotes energy dissipation in the beam protected zones as a means to prevent story collapse due to column hinging. Fireproofing was removed where beam plasticity occurred and two specific cases were studied for Fire 1-1.

The first study was exposing the first story compartment B2 (Figure 4.14) to Fire 1-1. In this compartment, the W30x124 moment frame beam experienced plasticity at the beam ends when subjected to EQ2-1. The locations (approximately 600 mm (24 in) from each end of the beam) were subjected to the fire without fireproofing protection. The beam experienced larger vertical deformations due to the lack of fireproofing, but this difference was too insignificant to cause a change in failure mechanism. Failure still occurred when the interior gravity columns failed, resulting in bay failure at the first story. Figure 8.9 shows the beam compressive load and midspan

vertical deflection over time for the W30x124 beam with and without fire protection damage at the beam ends. The W30x124 is a very stiff member which only carries a tributary width of 1270 mm (50 in); thus, its deflections are very low for both the fireproofing damage and no fireproofing damage cases. In fact, the deflections are less than 20 mm (~1") for both cases and deflections are increase only after the gravity columns fail at 100 minutes. The compressive forces in the beam vary depending on the fireproofing. As the beam with the fireproofing damage begins to sag, the compressive loads in the beam are reduced. Because these deflections are minimal, the beam never produces tensile forces. Despite these differences in deflection and forces, the failure mechanism of gravity column failure remains the same and the fireproofing damage to the beam does not affect the failure type or time of failure. This is not very surprising, as the W30x124 is very overdesigned for the fire load combination of 1.2D+0.5L.

The second study was conducted with Fire 1-1 at the fifth story edge compartment. This was conducted for the structure after being exposed to EQ1-1.25. The exterior girder is a W27x94 and experienced plastic hinging at the beam ends due to the earthquake. As with the previous study, the effect of fireproofing damage to the beam ends did not change the failure mechanism when the compartment was subjected to the fire. The structure still resulted in bay failure when the two interior gravity columns failed. Figure 8.10 shows a comparison of the exterior girder's compressive force and vertical midspan deflections over time. The gray lines represent the beam deflections and the black lines show the axial compressive load. The solid lines represent the beam with fireproofing damage (unprotected, exposed steel) at the beam ends. The dashed lines represent the girder fully protected along its length with fireproofing at a 1 hr FRR. The girder is very stiff, with the vertical deflection of the beam without fireproofing at the ends only reaching about 50 mm (2 in) when subjected to the fire. The axial force is also noticeably different when comparing the beam with and without fireproofing. The beam with the damaged fireproofing begins to lose axial compressive load as the beam begins to sag. Because the fireproofing damage is concentrated to a small region of the beam and because the beam is very overdesigned for the gravity load combination of 1.2D+0.5L, these differences in beam behavior are not enough to initiate a different failure mode.

One of the limitations of this modeling method is that the beam elements cannot capture local buckling. Bottom flange local buckling of the beams was observed in the Cardington fire tests [72]. This occurred when the beams tried to expand and were prevented by the columns and, thus,

the beams crumpled at the beam ends. It is possible that this same type of failure would occur in this scenario with no fireproofing at the beam ends, though it cannot be captured in these simulations.

It is also important to note that the connection of the beam to the slab using rigid connections may not be an accurate representation of the system behavior and a more detailed stud model should be explored to capture potential failure modes of the stud connectors. With rigid connectors, the studs can cause rigid body motion of the beam and slab together, causing unrealistic rigidity in the slab system. Implementing more detailed stud connectors in the model would require a number of rigid end offset due to the beam and shell elements (as explained previously in Section 5.2). This could potentially result in instabilities within the model and was outside the scope of this project. These connectors should be implemented as future work and the effect of fireproofing damage on the moment frame beams should be reevaluated.

Another consideration that should be looked at more closely is the beam-to-column connection strength. Studies by Yang [49] showed that moment frame connections can maintain their design strength up to 650°C with only a 25% stiffness reduction. This was the basis for using rigid connectors in the model to represent beam-to-column fixed connections. However, when considering damage to the moment frame beam, it is possible that the connections themselves may also experience fireproofing damage, likely resulting in connection temperatures greater than 650°C. Additional work is needed to determine the likelihood of this occurrence and how to capture this behavior in the building model. Tests by Braxtan and Pessiki [127] observed fireproofing damage primarily in the beam bottom flange and not directly in the connection region. Nevertheless, fireproofing damage at the beam-to-column connection interface should also be explored in more detail as future work.

These limited studies have shown that damaged fireproofing on moment frame beams does not affect the failure mode of the system. However, as discussed above, there are a number of limitations to the current modeling approach that must be studied more closely before definitive conclusions can be drawn about the impact of fireproofing damage on moment frame beam behavior.

8.5 Travelling Fires

In addition to compartment and full story fires, horizontally travelling fires were simulated. There is limited guidance on how to idealize moving fires without conducting computational fluid dynamics simulations. Jiang et al [76], however, provides a simplified method for fires moving across a floor. This approach assumes that the fuel is uniformly distributed across the entire floor, but recognizes that there is both near field and far field behavior of the fire. Near field is the area in which combustible fuels are burning. Far field are the areas yet to be subjected directly to flames. The constant burning time, t_b (sec), of the near field is calculated by:

$$t_b = \frac{q_f}{Q''} \quad \text{Equation 8-1}$$

q_f , as previously defined, is the fire load density (MJ/m^2), which depends on the function of the space. Q'' is the heat release rate per unit area (kW/m^2), which accounts for the mass burning rate and the heat of combustion of the fuels in the compartment. Q'' was presumed to be $480 \text{ kW}/\text{m}^2$. q_f varied based on the time-temperature curve being simulated. For Fire 1, $q_f = 420 \text{ MJ}/\text{m}^2$ and t_b was calculated at 15 minutes. This means that the fire burns for 15 minutes in the first compartment before ignitions occur in the adjacent compartment. Figure 8.11 and Figure 8.12 show the two presumed paths for the travelling fires. In the first scenario (referred to as D_M1), the fire begins at compartment 1 along the left (west) exterior of the building and moves to the right (east) one bay every 15 minutes. In the second scenario (referred to as D_M2), the fire begins in the center, interior compartment and spreads outward to each adjacent compartment at 15 minute intervals. It was found that full story fire studies for these two buildings result in the same failure initiation mode as the individual compartment fires. This section explores if moving fires affect the failure mode and time of failure when compared to full story fires. Fischer [74] studied the two above mentioned moving fire scenarios in the Chicago building for different fire resistance ratings of the structural members. When comparing full story fires and these two moving fires, the full story fires resulted in similar deflections, failure types and failure times as the moving fire scenarios. Full story fires and moving fires will be compared again, to evaluate the influence of earthquake damage on the failure modes.

The Chicago building was analyzed at the ninth story for Fire 1-1 travelling as scenario D_M1. This was performed for the structure after exposure to EQ4-3, which caused plastic hinging in the ninth story moment frame columns. The full story fire (non-travelling) scenario had caused interior

gravity column collapses at 84 minutes, resulting in system collapse at that level. Moving fire scenario M_D1 resulted in very similar results. The only difference is that, instead of all of the gravity columns failing at the same time as was the case with the full story fire, the moving scenario resulted in collapse of the first bay gravity columns at 89 minutes, followed by subsequent collapse of the remainder of the gravity columns at approximately 5 minute intervals (93, 98 and 103 minutes). The column axial loads and temperature versus time relationships are shown in Figure 8.13. In this case, the full story is an appropriate conservative approach in place of travelling fire D_M1.

The next scenario that was studied was the Los Angeles building subjected to Fire 1-1 as moving fire D_M1 on the fifth story. This structure was first subjected to EQ7-0.75, which caused fracture of the moment frame beam ends at edge compartment 5B (see Table 7.1). The edge compartment fire study from Chapter 7 resulted in bay failure at 92 minutes. The moving fire results in column collapse at 105 minutes and collapse of the columns within the adjacent bays at approximately 5 minute intervals, resulting in progressive collapse. When the gravity columns in the first bay reach their critical temperature, the adjacent bay is already heated, causing less restraint in the column. As Figure 8.14(a) shows, the columns experience essentially no axial load increase due increasing steel temperatures. The lower axial load in the moving fire delays the failure time by 13 minutes. The progression of system collapse is displayed in Figure 8.14(b).

The final moving fire scenario was studied at the first story for the structure after exposure to EQ2-1. This story was subjected to both Fires 1-0.75 and 1-1 for both moving fire scenarios. Fire 1-0.75 did not cause failure for either moving scenario, D_M1 or D_M2. Fire 1-1 for travelling fire scenarios D_M1 and D_M2 did not experience column failure and, instead, only resulted in compartment failure. Because the seismic damage occurred at the exterior moment frame members, it was presumed unlikely that scenario D_M2, where the interior compartment is heated and then the fire spreads outward, would initiate a failure other than interior column collapse. It was surprising to find that the travelling fire scenarios did not result in gravity column failure at all, as was expected based on the compartment fire studies conducted in Chapter 7. Due to the heated adjacent bays, the gravity columns were not restrained against expansion and, thus, they experienced a slightly lower maximum compressive load than was determined from the individual compartment studies. From the individual compartment studies, the critical temperature was determined in Section 7.4.1 to be 524°C. In the moving fire scenario, the column reaches the

maximum temperature from the heat transfer, which is 530°C temperature. Thus, the slightly lower axial load prevented failure in this case only because the previously failed columns were extremely close to withstanding the fire (only a 6°C difference). Figure 8.15 shows the close relationship between the column axial loads for the moving fire and the individual compartment fire, as well as the peak steel temperature compared to the critical steel temperature. This shows that even just slight variations in gravity loading or heat transfer assumptions and properties could prevent system failure from occurring at all. This is one of the drawbacks of the deterministic approach used in this study. Future work can draw upon what was learned in terms of failure modes and building behavior in order to incorporate a more probabilistic approach to this study. This will be discussed in more detail in the Section 8.7 discussion of fragility curves.

Results of these studies show that full story fires can be used to conservatively predict the failure mode and time of failure instead of using traveling fires. In this case, the gravity columns continue to be the vulnerable component. This may not be the case if the fire resistance rating of the members is not all the same. Additional studies should be conducted when using a higher fire resistance rating on the gravity columns in order to see if the traveling fire (particularly D_M1) varies from the full story fire because of damage to the perimeter members, which are subjected to the fire before the interior compartments.

8.6 Aftershocks

Aftershocks are earthquakes that occur after the main earthquake event. They tend to be smaller earthquakes that occur in the vicinity of the ruptured fault of the initial earthquake. The frequency and timing of these aftershocks, as well as their intensities, varies greatly by earthquake and are very difficult to predict. Aftershocks are particularly dangerous because they occur after structures may have already been damaged by the initial earthquake. Aftershocks can be even more dangerous when considering post-earthquake fires because the structures have already been subjected to a seismic event, a fire, and then are subjected to ground motions again.

The modeling approach described in this work can be used to extensively study the effects of different post-earthquake fire and aftershock events. For now, only one example will be illustrated for each building to illustrate the potential detrimental effects of this type of phenomenon.

The Chicago building experienced plastic hinging but no fracture at the ninth story moment frame columns when subjected to EQ3-3. This building was then subjected to Fire 3-0.75 at the corner

(9A) compartment and the full story (9D). As previously indicated, these fires caused deflections of the framing members but did not result in failure. These fires caused changes in the structural response to aftershocks, particularly at the upper levels of the building. Table 8.9 provides the maximum story drift ratios recorded at the eighth, ninth and tenth stories. The initial earthquake caused 0.0163 radians of maximum drift ratio. When EQ3-3 was applied to the structure again as an aftershock, the maximum drift ratio was 0.0241. Fire 3-0.75 at compartment 9A resulted in a drift ratio of 0.0257. Finally, that same fire applied to the entire story caused a maximum story drift ratio of 0.0353. The extent of fire clearly plays a role in the seismic response of the structure after the fire has ended. The aftershock that included the 9A compartment fire seems to behave closely to the aftershock scenario without fire. Because the fire is contained to only one compartment, this finding is not surprising. Additional studies would need to be conducted to validate this finding, but it is likely that fires contained to only one compartment may not significantly affect the aftershock performance of the structure.

For the full story fire and aftershock scenario, however, the structural response is notably different. Two of the perimeter moment frame columns buckled at the base of the ninth story during the aftershock ground motion. The moment frame beams connected to those columns behaved as cantilevered members to carry the load from these failed columns and prevent system collapse. This occurred after 13 secs of the EQ3-3 ground motion and the resulting deflected shape is shown in Figure 8.16. Because the column crumpled in a localized manner instead of a global buckling failure, the maximum displacement is 191 mm (8 in). It is interesting to note that the fire caused plasticity in the columns at this level as well as the floor framing. This led to plastic hinging in the moment frame beams that was much more prevalent than the aftershock without the fire, which primarily experienced plastic hinging at the moment frame columns. It is possible that the hinging at the moment frame beams helped to prevent system collapse.

The other study on aftershocks was conducted on the fifth story of the Los Angeles building. This structure was initially subjected to earthquake 2-1, which caused some plastic hinging at the lower level moment frame beams. No damage was observed at the fifth story. Fire 1-1 was next applied to compartment 5A, which caused column failure of the W12x58 gravity column. Finally, an aftershock of EQ2-1 was applied for only the first 8 sec of the record. This was tested in order to see if the gravity column failure would play a noticeable role in the seismic response of the

structure and, in fact, it did not. The structure maintains its integrity when subjected to lateral loads.

This section aims to show that aftershocks are yet another multi-hazard scenario that can and should be considered for steel buildings already subjected to earthquakes and fire following earthquake scenarios. Further studies are needed to draw more definitive conclusions about system behavior under these different scenarios.

8.7 Fragility Curves

8.7.1 State of the Art

Fragility functions are commonly used to synthesize incremental dynamic analyses. These curves identify the probability of failure (or some other unwanted outcome) to occur at different hazard intensity measures. The equation of the curve is:

$$P(C|x) = \varphi\left(\frac{\ln\left(\frac{x}{\theta}\right)}{\beta}\right) \quad \text{Equation 8-2}$$

where $P(C|x)$ is the probability of collapse or failure at an intensity measure of x . $\varphi(\)$ indicates a normal cumulative distribution function, which is the industry-accepted function for structural response to earthquakes. θ is the mean of the fragility function and β is the standard deviation.

As indicated in the equation above, the curve will be computed using the lognormal cumulative distribution function determined through incremental dynamic analyses and/or incremental fire analyses. The curve determines the probability that the damage measure (some decided measure of collapse or failure) occurs given a corresponding engineering demand parameter. In seismic design, the damage measure is often based on exceeding story drift ratios and connection rotations that correspond with a specified performance group (i.e. – collapse prevention, life safety, etc.).

For fire, the damage measure and engineering demand parameter is less decisive, as this approach has only recently been applied to fire analyses. An initial goal of this work was to create a 3D surface plot which plots the seismic IDA on the y-z axis and the fire IFA on the x-z axis. This would provide a fragility surface that represents the fragility curves for different earthquake-fire combinations. As will be explained further in the subsequent section, this was not particularly useful for the case study buildings analyzed in this work.

Researchers [42, 44, 46] have generated fragility curves from IFA at an individual component level. However, much less is known about applying this methodology to an entire building structure. Gernay et al. [47] provided the first known attempt at generating fire fragility curves at a building level. The researchers developed fragility functions at the compartment level for different fire locations throughout the building, and then combined these results using an approach by Shinozuka et al. [129]. This approach combined individual fragility functions with conditional probabilities for each fire location. Only the heating phase of the fire was considered in these studies. Fire load was selected as the intensity measure and two different damage states were used. These damage states were beam failure (categorized by surpassing the flexural capacity of the member or vertical midspan deflections in excess of $1/10^{\text{th}}$ the span) and column failure. This work provides an effective methodology for conducting fire resilience assessments, but it does not consider post-earthquake fire hazards. This work had the benefit of referring to well documented case studies (actual, experimental, and computational) in order to make informed decisions about what IM factors and damage parameters to introduce in the analyses.

Another benefit of the work by Gernay et al. [47] is that they attempted to approach these analyses from a probabilistic nature. Many of the fire parameters are inherently deterministic (the fire model, steel material and geometric properties, etc.) but there are opportunities to incorporate probabilities to capture a wider range of behavior. In particular, the structural model's steel properties and loading can incorporate uncertainty and variation. This is a limitation of the current work in this dissertation, as it entails a deterministic approach to fire hazard selection, while proposing a probabilistic methodology.

8.7.2 Application to Case Study Buildings

Fire research has been studied much more extensively to date than post-earthquake fire hazards and the primary goal of this dissertation was to understand the failure mechanisms and vulnerabilities in steel MRF buildings subjected to post-earthquake fire hazards. Because no known work has been conducted to date that includes the full building model (including the gravity framing system) in post-earthquake fire analyses, steel building response to post-earthquake fires had been previously unknown. Thus, despite being limited by deterministic loading, this work is important to understand building behavior in order to later apply the findings to more probabilistic

and performance based studies; however, its application to fragility functions is less useful than originally proposed in the analysis methodology.

For the two case study buildings, the findings show that seismic and fire responses are decoupled from one another when all members are protected by the same fire resistance rating. There may still be an opportunity to incorporate 3D fragility curves that capture post-earthquake fire behavior as mentioned in the proposed methodology in Chapter 3; however, because gravity column failure continued to be the initiating failure mechanism regardless of seismic damage, this approach is not beneficial for these specific case studies. It is possible that using different fire resistance ratings for different components may vary the failure mechanisms and lead to a more coupled response between seismic and fire hazards.

Fragility curves were generated from the incremental dynamic analyses. Because of the computationally taxing nature of the building models, a limited number of scenarios were used and data was limited. Curves were generated for story drift ratios (SDR) of 0.015 and 0.02 for both the Chicago and Los Angeles buildings. The IDA curves generated in Figure 6.5 and Figure 7.5 were interpolated to determine the spectral accelerations at the selected SDRs above. Figure 8.17 shows the resulting fragility curve for the seismic response of the two structures. The Los Angeles building can withstand larger spectral accelerations at lower probabilities of failure than the Chicago building, which definitively fails the specified drift ratio criteria at approximately 0.4g. This is compared to 1g for the building in Los Angeles.

Generation of the fire fragility curve was less definitive. Peak fire temperature (PFT) had been used as the intensity measure for the analyses, but the results showed that high peak fire temperatures did not necessarily correlate with failures. Fire 2, which had a high peak fire temperature, did not result in failures because it was a quick burning fire that did not cause high temperatures within the structural members. Instead of using peak fire temperature, Ingberg's fire area was explored as the intensity measure. This parameter calculates the area under the fire time-temperature curves as a means to compare fire intensities. This factor holds no real significance but seems to be an effective measure for accounting for high temperature fires while also considering fire duration. A fragility curve was generated from IFA results. This fragility function is shown in Figure 8.18. It considers failure as the exceedance of the acceptance criteria, $L/20$, as explained in Section 3.2. The horizontal axis is the Ingberg's fire area divided by the area computed for Fire 1-1. This shows that there is a 70% probability of failure for Fire 1-1. However, this

intensity measure also has its pitfalls because it over-predicts the intensity of Fire 3, the long duration fire. In the simulations, Fire 3-0.75 did not cause failure and, yet, the curve shows a higher probability of collapse for that fire than Fire 1-1, which always resulted in column collapse. Fire load, the intensity measure suggested by Gernay et al. [47], could not be easily implemented because the scaled fire scenarios were scaled by peak temperature and, thus, do not represent standard Eurocode time-temperature curves. In addition, the curves used in this study, include a cooling phase that is not represented in the work by Gernay et al [47].

Because none of the above mentioned intensity measures can be used to generate realistic fragility curves, an alternative approach was used. The above-mentioned intensity measures also only consider the fire and do not consider the different fire resistance ratings that each member may be designed for, which affect the structural response. Thus, a fragility function was created to determine the probability of failure (buckling) of the gravity columns at the fifth and ninth stories for different internal steel temperatures. Figure 8.19 shows the probability of column collapse at different internal steel temperatures. Because gravity column loads remain relatively constant with increasing temperatures, these failure temperatures could be easily calculated using the AISC procedure described in Section 6.2.1.5. In addition, it decouples the structural analysis from heat transfer, limiting the number of structural analyses that needed to be performed in favor of much quicker 2D heat transfer analyses. The results of the heat transfer analyses shown in Figure 8.2 and Figure 8.3 were used to generate the fragility functions. The fragility function represents column failure when it occurs in the corner compartment. When it occurs in the edge or interior compartments, however, this function represents bay and system failures, respectively. There is a 50% probability of column failure of a W8x24 (with a 0.73 utilization ratio) when the column reaches 515°C. There is a 50% probability of failure of a W12x58 column (with a 0.64 utilization ratio) when the column reaches 550°C. The internal steel temperatures can be converted back into intensity measures that are representative of the characteristics of the fire. It is recommended that fuel load density be used as the intensity measure for future work.

A drawback of this approach is the assumption that a critical individual member failure is the initiating failure case. It does not consider any possible structural failures that could occur prior to member failure, such as connection failure or failures caused by the interaction of deformations from another member. More research is needed to evaluate and determine the suggested intensity measure that should be used for system level response to compartment fires and fire following

earthquake scenarios. This work helps to identify the opportunities and shortcomings of different factors for use in fragility functions for fire analyses.

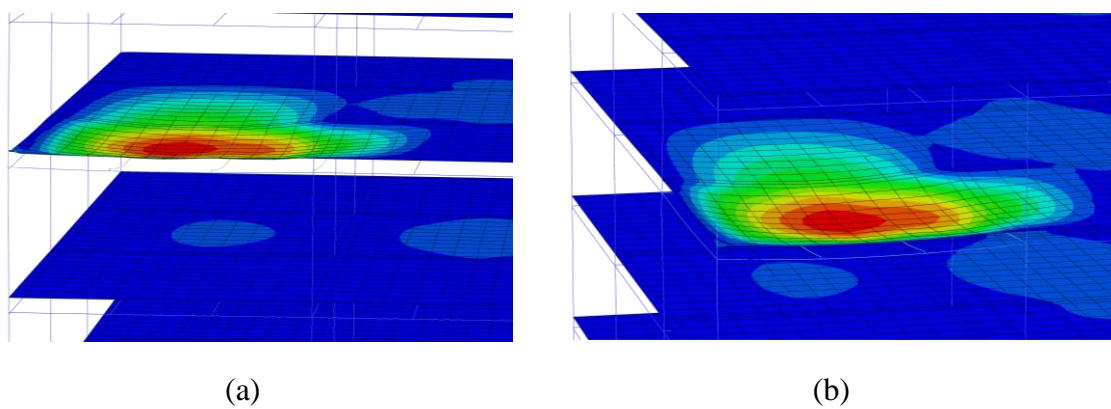
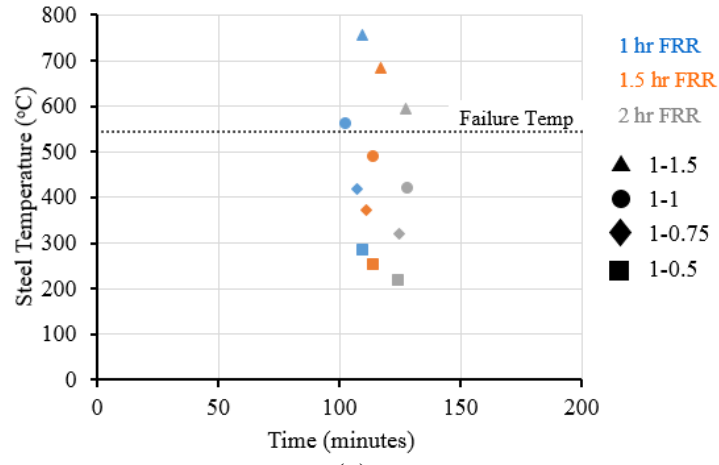


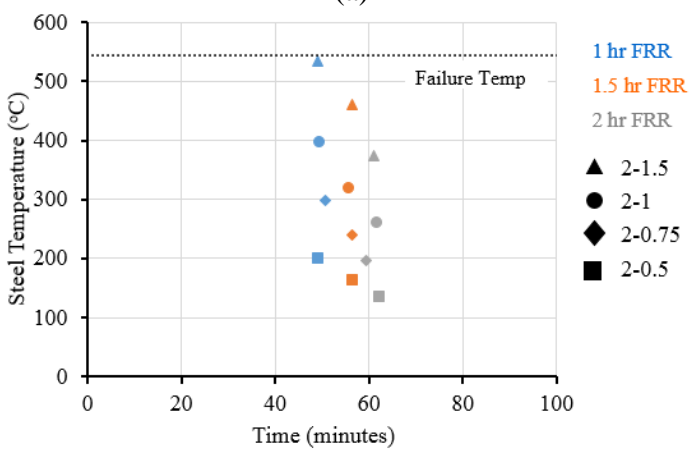
Figure 8.1 Compartment failures observed with 2 hr FRR on gravity columns

(a) Fire 1-1 at Compartment 5A

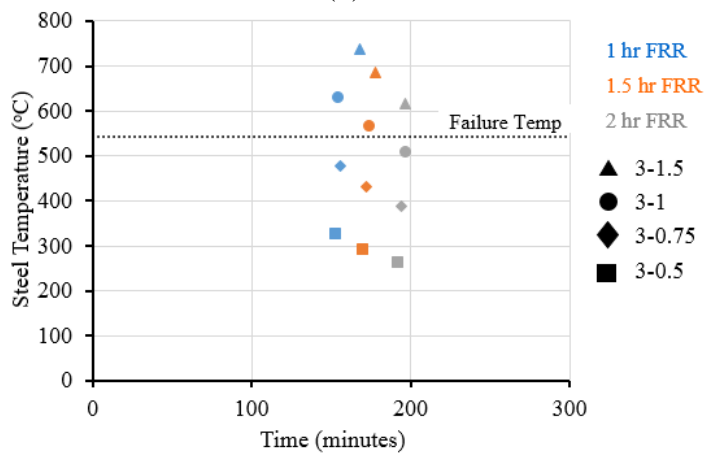
(b) Fire 1-1 at Compartment 9A



(a)

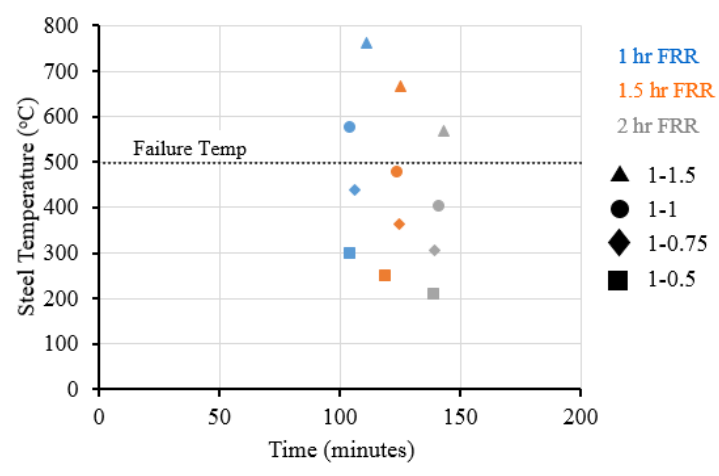


(b)

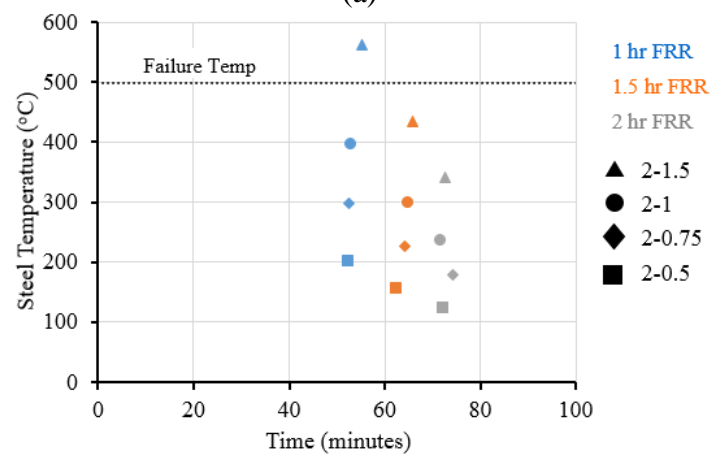


(c)

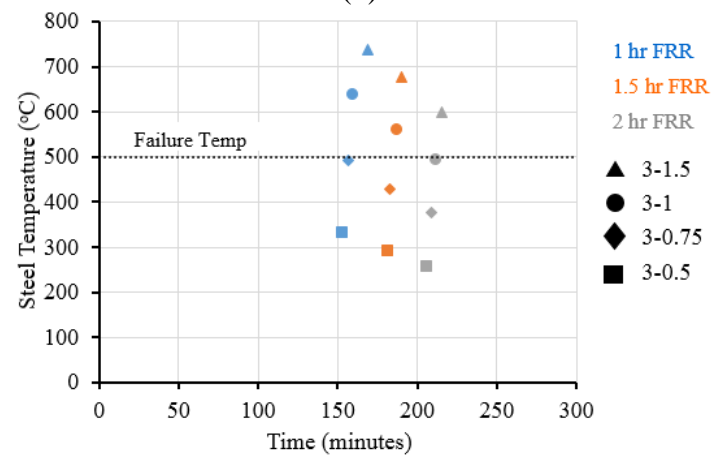
Figure 8.2 Peak steel temperature and time determined from heat transfer for W12x58 column (a) Fire 1, (b) Fire 2, (c) Fire 3



(a)



(b)



(c)

Figure 8.3 Peak steel temperature and time determined from heat transfer for W8x24 column
(a) Fire 1, (b) Fire 2, (c) Fire 3

Table 8.1 Cost comparison for structures with 1 hr FRR on all members versus 2 hr FRR on gravity columns and 1 hr FRR on all other members

	1 hr FRR	2 hr FRR	Cost increase (%)
Chicago Building	\$137,800	\$139,800	1.44%
Los Angeles Building	\$112,300	\$116,400	3.63%

Table 8.2 Original and revised gravity column sizes used in pilot study

Story	Original Gravity Column Size	Revised Gravity Column Size
9-10	W8x24	W8x40
7-8	W8x40	W8x58
5-6	W12x58	W12x72
3-4	W14x74	W14x90
1-2	W14x90	W14x109

Table 8.3 Failure type, time, and deflection for original versus revised gravity columns

Fire	Location	Original Failure Type	Original Failure Time	New Failure Type	Time of Max Deflection	Vertical Deflection	Time that Failure Initiates
1-1	5A	Column	95 min	Compartment	85 min	440 mm	63 min
1-1.5	5A	Column	50 min	Column	60 min	1726 mm	60 min
3-1	5A	Column	100 min	Compartment	146 min	478 mm	90 min
1-1	9A	Column	70 min	Compartment	86 min	434 mm	64 min
1-1.5	9A	System	46 min	System	66 min	-	66 min
3-1	9A	Column	88 min	Compartment	146 min	486 mm	87 min

Table 8.4 Utilization ratios for original gravity columns

Story	Column Size	$P_u, 1.2D+0.5L$ (kips)	ϕP_n (kips)	Utilization Ratio
10	W8x24	64	178	0.36
9	W8x24	129	178	0.73
8	W8x40	193	366	0.53
7	W8x40	258	366	0.70
6	W12x58	322	601	0.54
5	W12x58	386	601	0.64
4	W14x74	451	767	0.59
3	W14x74	515	767	0.67
2	W14x90	579	1067	0.54
1	W14x90	644	1067	0.60

Table 8.5 Utilization ratios for revised gravity columns

Story	Column Size	$P_u, 1.2D+0.5L$ (kips)	ϕP_n (kips)	Utilization Ratio
10	W8x40	64	366	0.18
9	W8x40	129	366	0.35
8	W8x58	193	546	0.35
7	W8x58	258	546	0.47
6	W12x72	322	806	0.40
5	W12x72	386	806	0.48
4	W14x90	451	1067	0.42
3	W14x90	515	1067	0.48
2	W14x109	579	1291	0.45
1	W14x109	644	1291	0.50

Table 8.6 Utilization ratios for Chicago moment frame columns

Story	Column Size	$P_u, 1.2D+0.5L$ (kips)	ϕP_n (kips)	Utilization Ratio
9	W12x45	64	396	0.16
9	W14x53	64	465	0.14
7	W14x53	129	465	0.28
7	W14x90	129	1067	0.12
5	W14x99	193	1173	0.16
5	W14x109	193	1291	0.15
3	W14x145	258	1746	0.15
3	W14x159	258	1912	0.13
1	W14x283	322	3436	0.09
1	W14x311	322	3774	0.09

Table 8.7 Utilization ratios for Los Angeles moment frame columns

Story	Column Size	$P_u, 1.2D+0.5L$ (kips)	ϕP_n (kips)	Utilization Ratio
9	W14x176	64	2122	0.03
9	W14x283	64	3436	0.02
7	W14x257	129	3113	0.04
7	W14x311	129	3774	0.03
5	W14x283	193	3436	0.06
5	W14x342	193	4177	0.05
3	W14x342	258	4177	0.06
3	W14x370	258	4514	0.06
1	W14x370	322	4514	0.07
1	W14x398	322	4852	0.07

Table 8.8 Cost comparison of steel framing for entire building using original column sizes and revised column sizes

	Original columns	Revised columns	Cost increase (%)
Chicago Building	\$1,810,400	\$1,838,200	1.55%
Los Angeles Building	\$2,358,200	\$2,383,600	1.12%

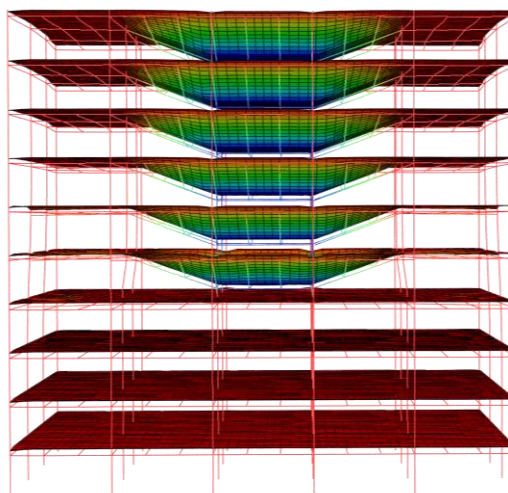
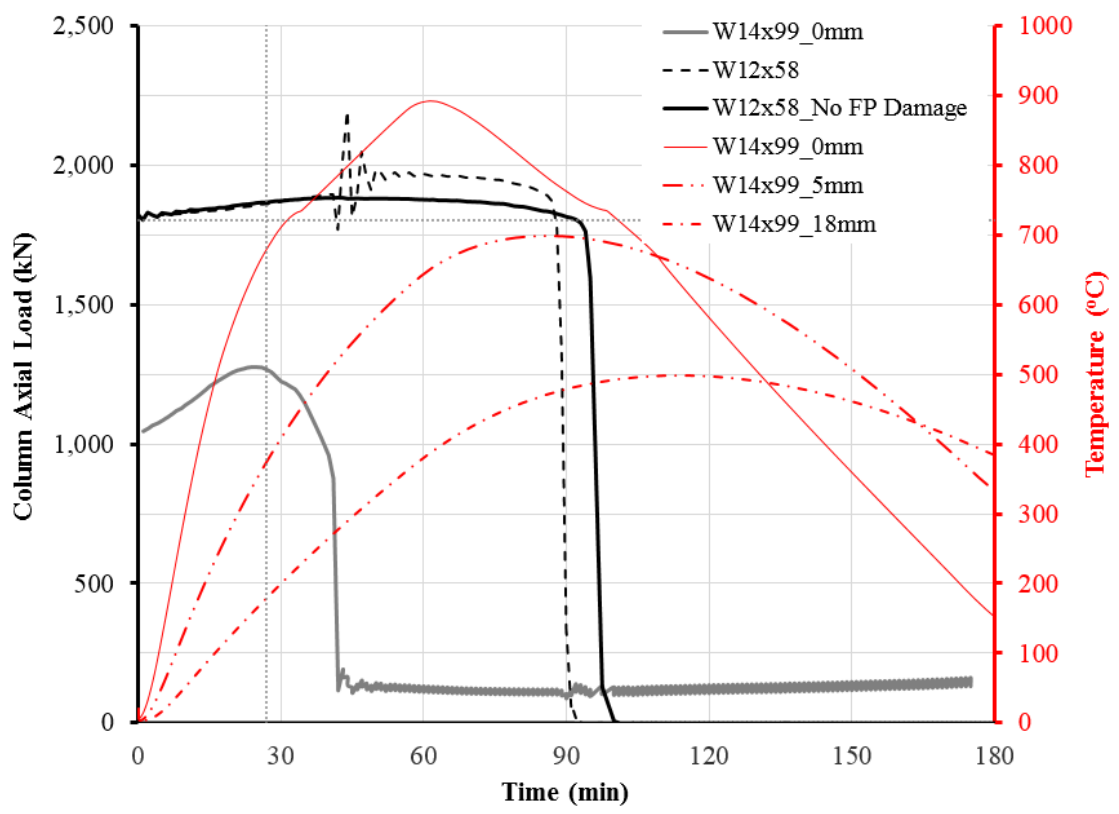
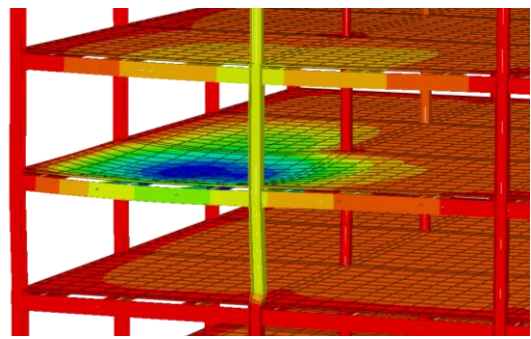


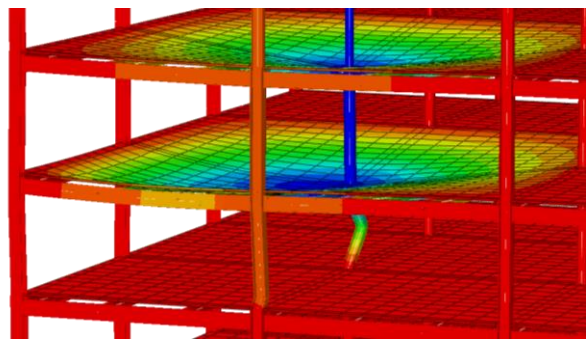
Figure 8.4 Bay failure for interior compartment Fire 3-1 using #5 @ 12" rebar mat



(a)

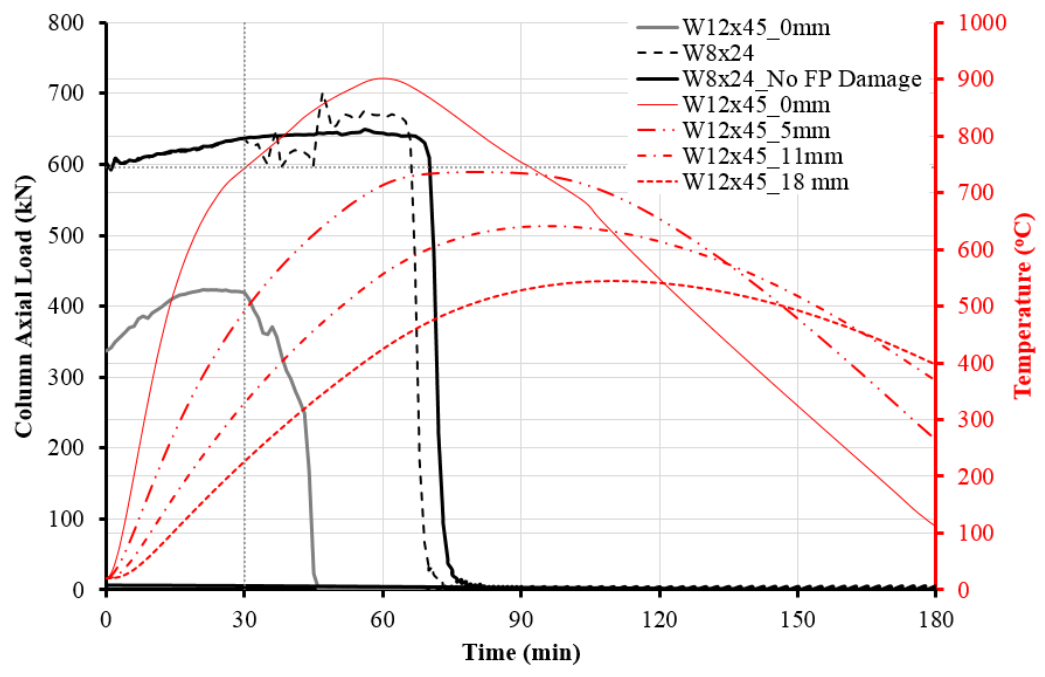


(b)

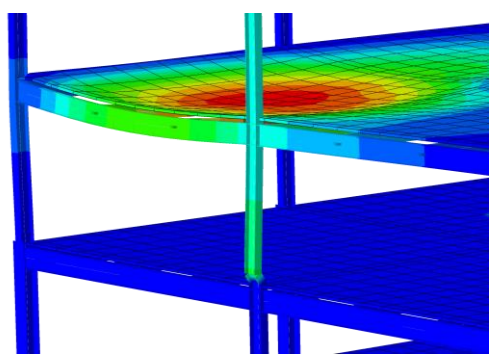


(c)

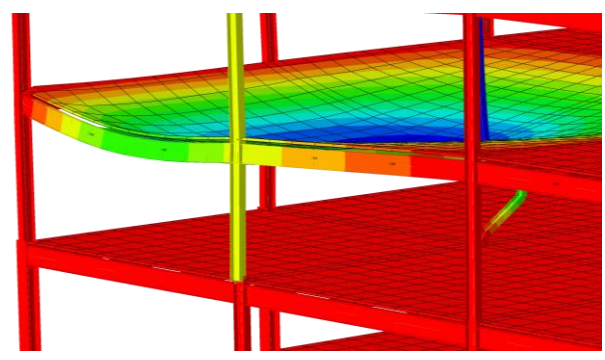
Figure 8.5 Influence of fireproofing damage on column axial load and temperature over time (Fire 1-1 in compartment 5A after EQ4-3)
(a) Column axial load and temperature versus time
(b) Exterior moment frame column buckling at 30 minutes
(c) Gravity column failure at 86 minutes



(a)



(b)



(c)

Figure 8.6 Influence of fireproofing damage on column axial load and temperature over time (Fire 1-1 in compartment 9A after EQ4-3)

- (a) Column axial load and temperature versus time
- (b) Exterior moment frame column buckling at 30 minutes
- (c) Gravity column failure at 65 minutes

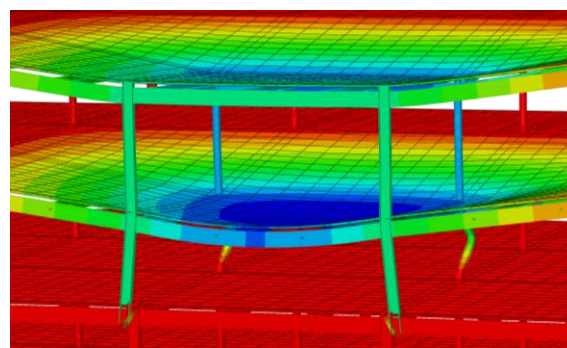
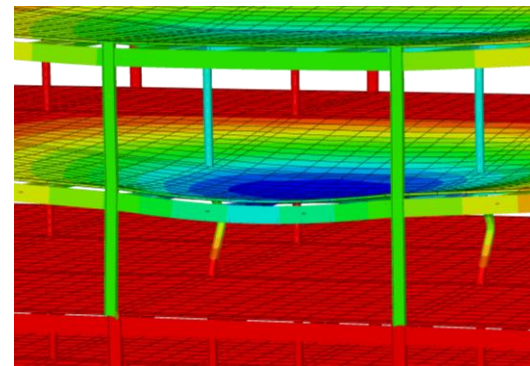
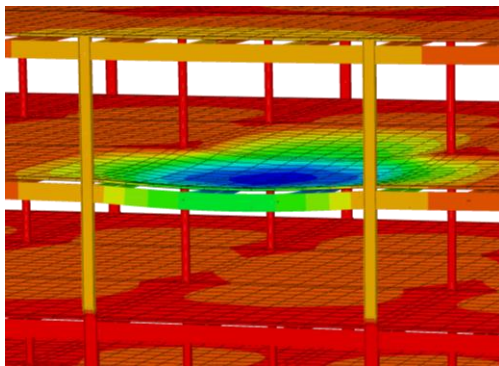
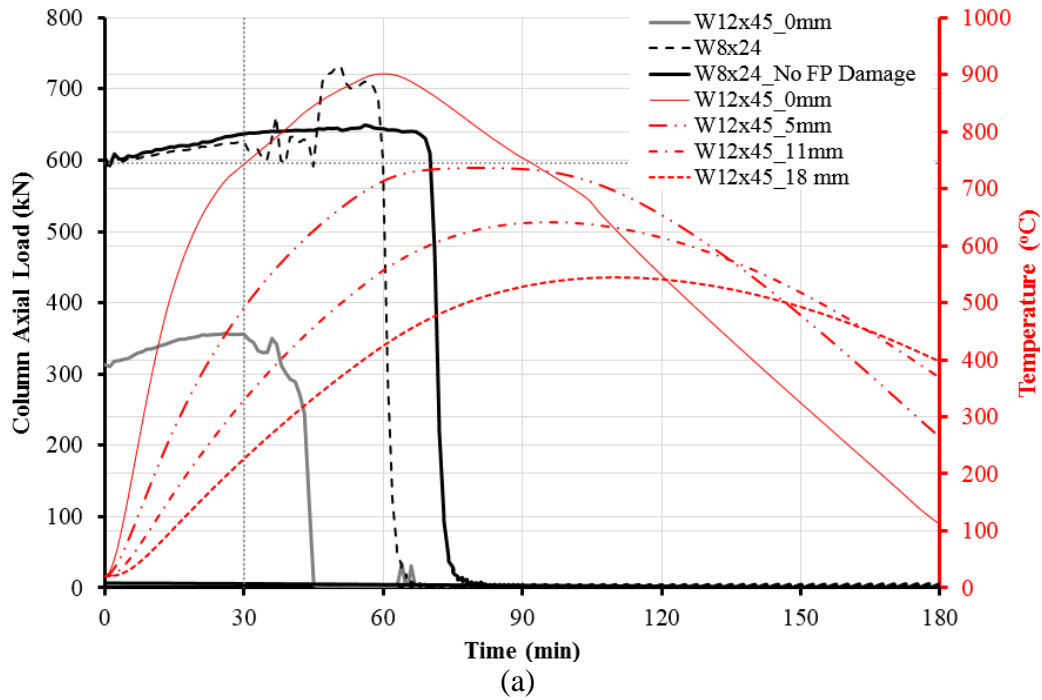
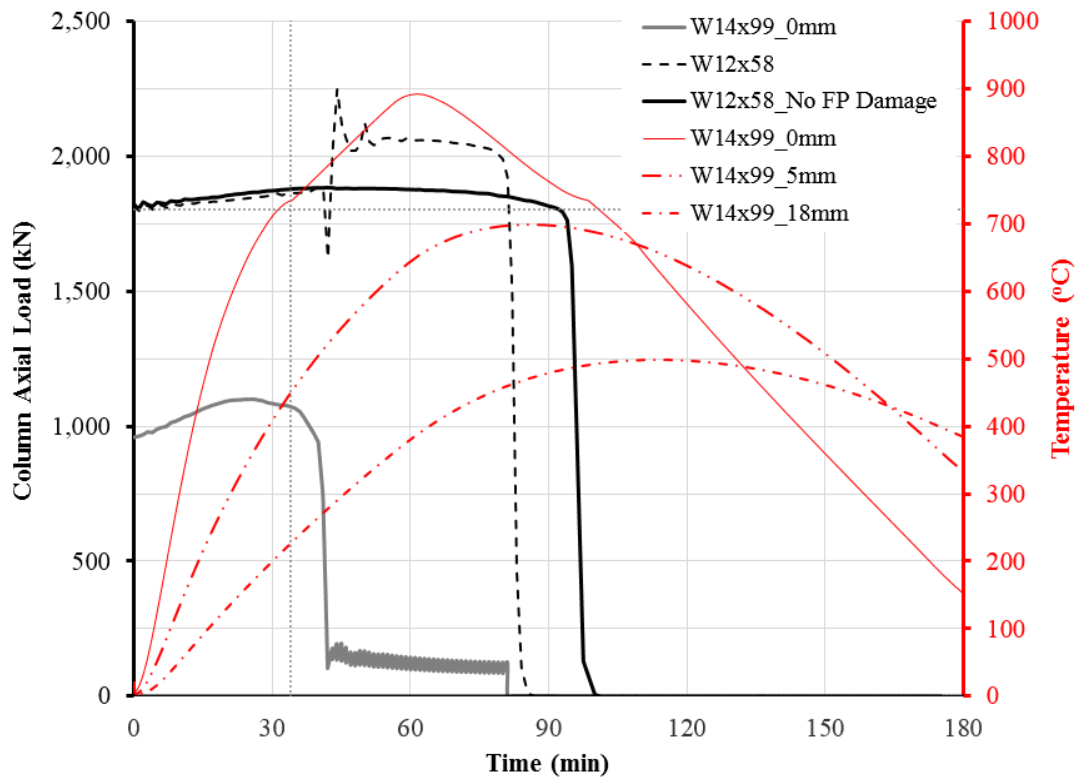
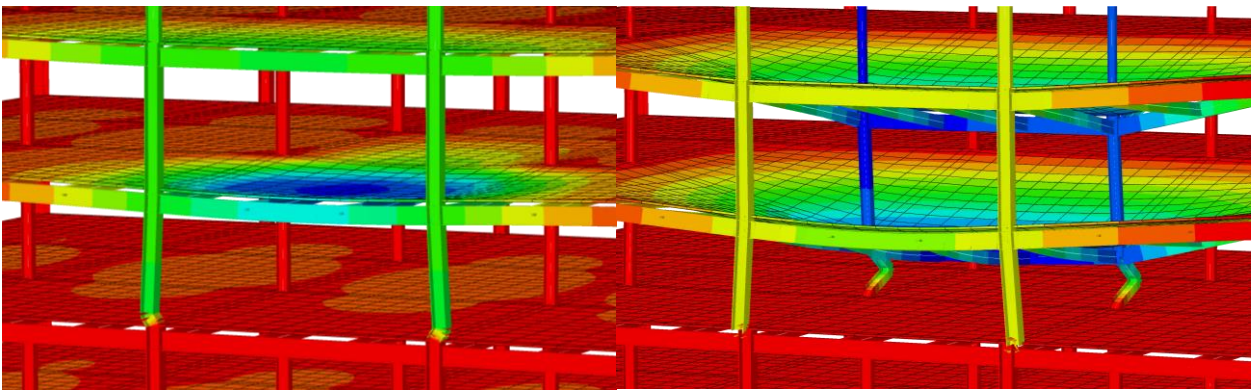


Figure 8.7 Influence of fireproofing damage on column axial load and temperature over time (Fire 1-1 in compartment 9B after EQ4-3)

- (a) Column axial load and temperature versus time, (b) Exterior moment frame column buckling at 30 minutes, (c) Gravity column failure at 59 minutes, (d) System collapse at 64 minutes



(a)



(b)

(c)

Figure 8.8 Influence of fireproofing damage on column axial load and temperature over time
(Fire 1-1 in compartment 5B after EQ4-3)

- (a) Column axial load and temperature versus time
- (b) Exterior moment frame column buckling at 34 minutes
- (c) Gravity column failure 80 minutes

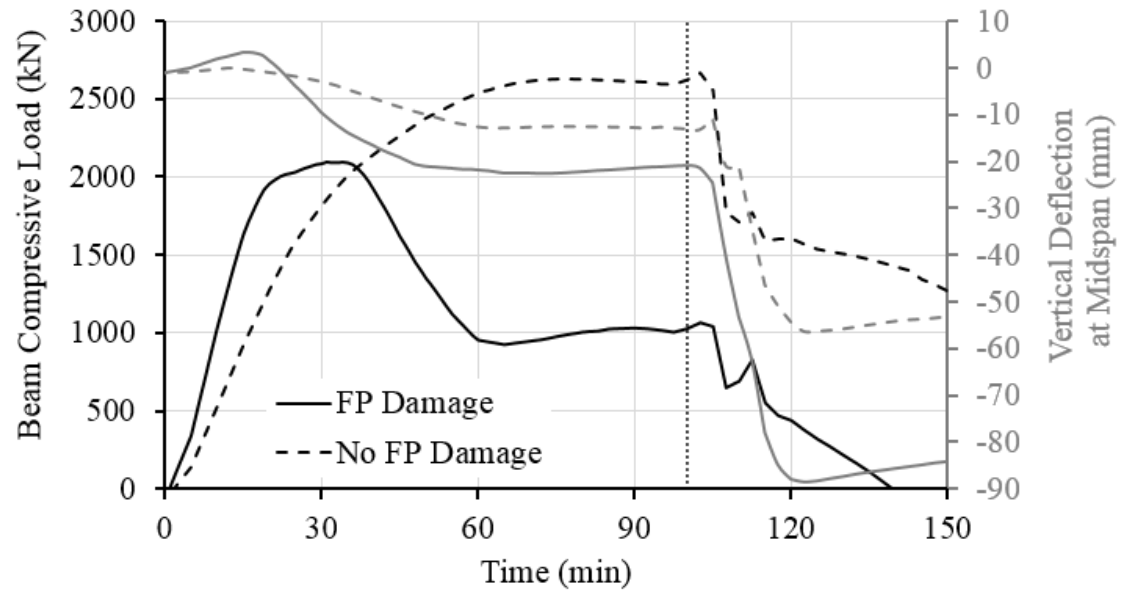


Figure 8.9 Comparison of beam compressive load and midspan vertical deflection of W30x124 subjected to Fire 1-1 in compartment 1B2, with and without fireproofing damage (EQ 2-1)

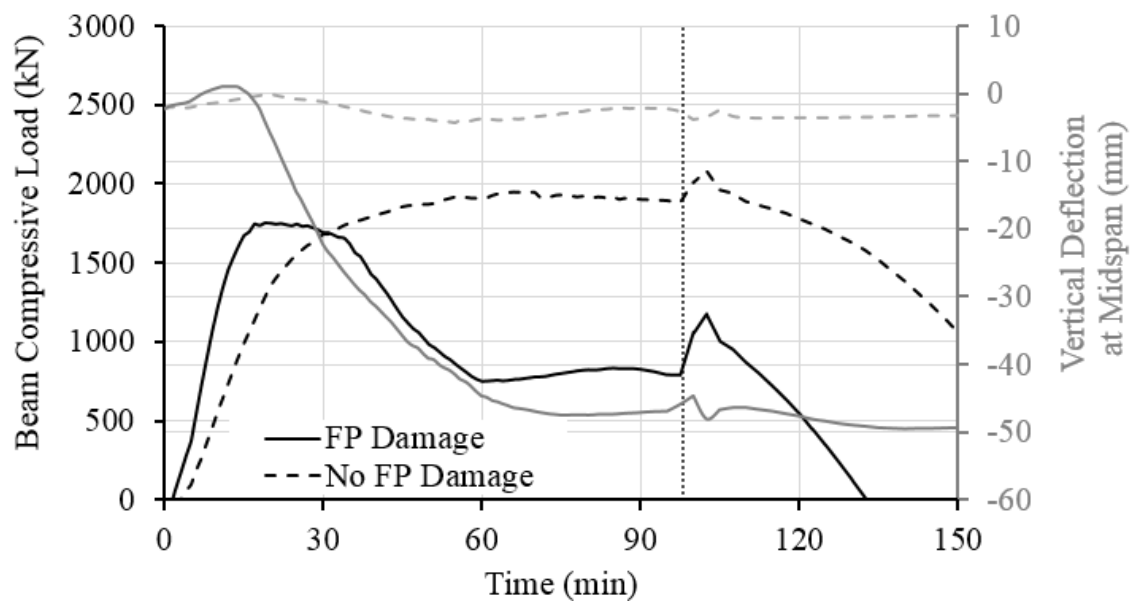


Figure 8.10 Comparison of beam compressive load and midspan vertical deflection of W27x94 subjected to Fire 1-1 in compartment 5B, with and without fireproofing damage (EQ1-1.25)

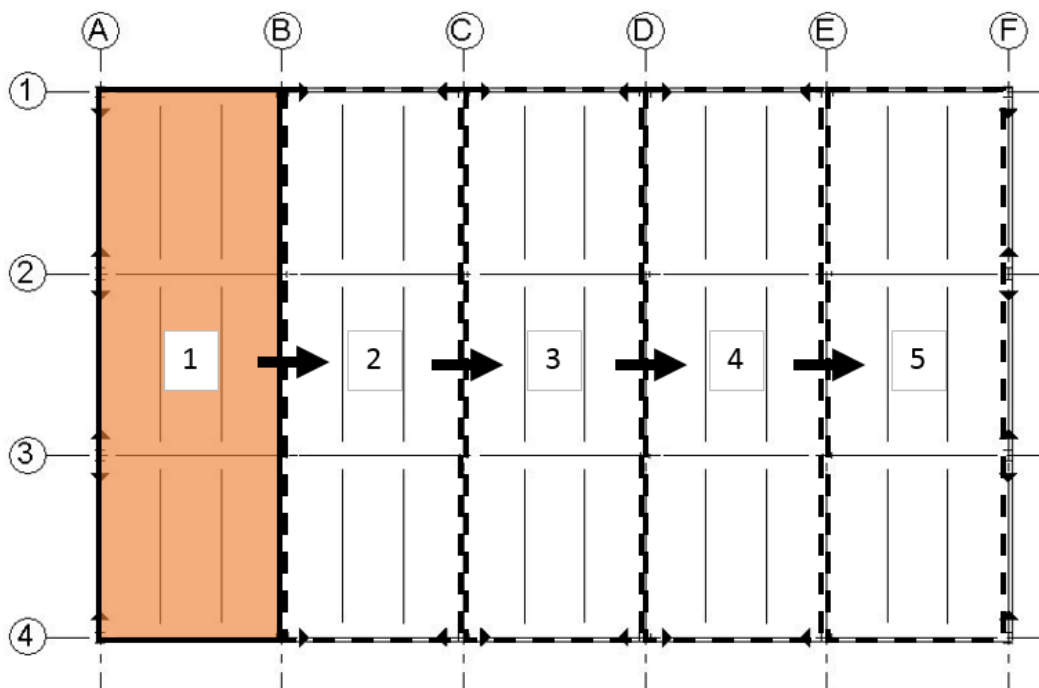


Figure 8.11 Moving fire: Scenario D_M1

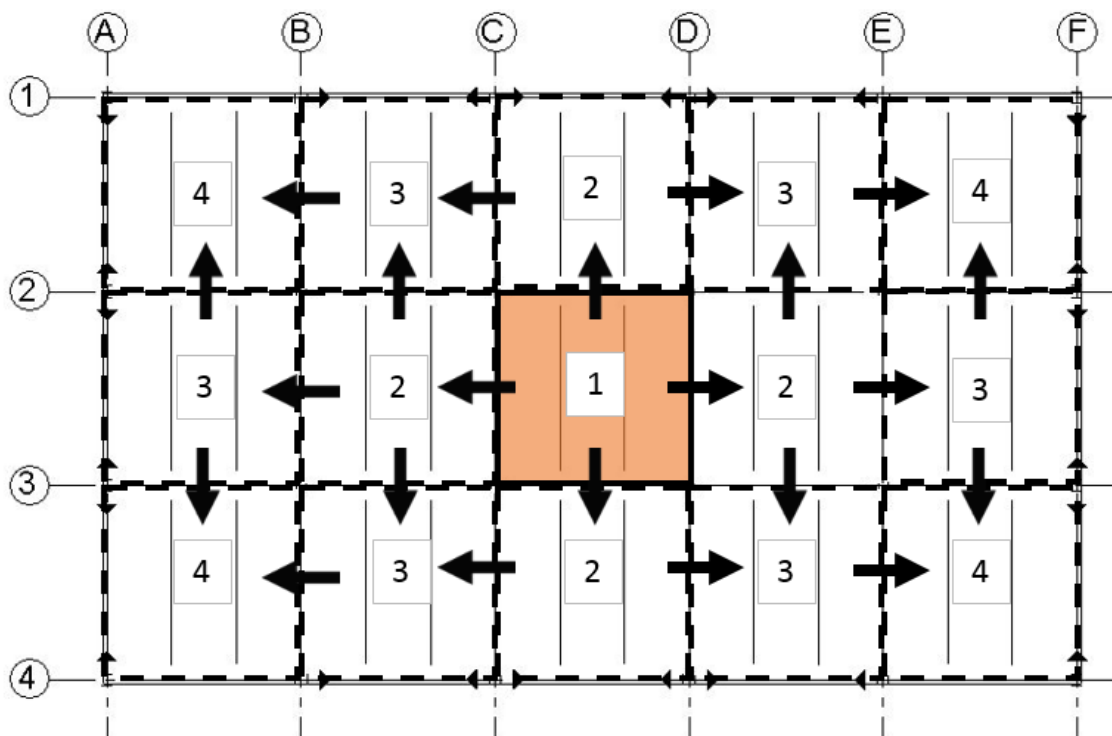


Figure 8.12 Moving fire: Scenario D_M2

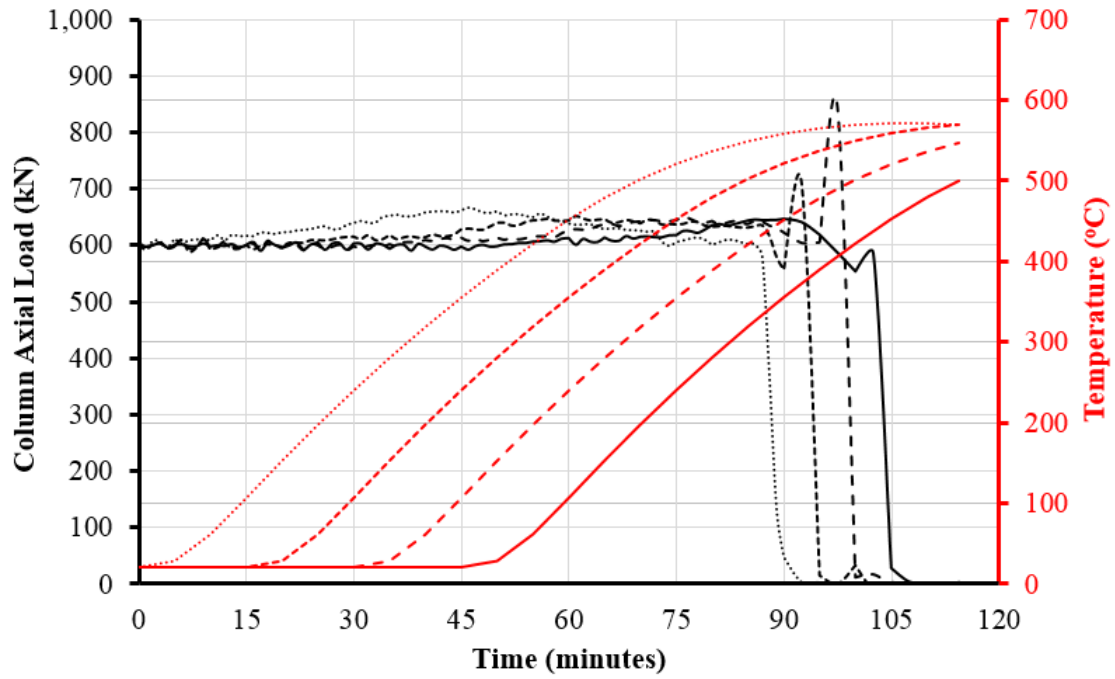
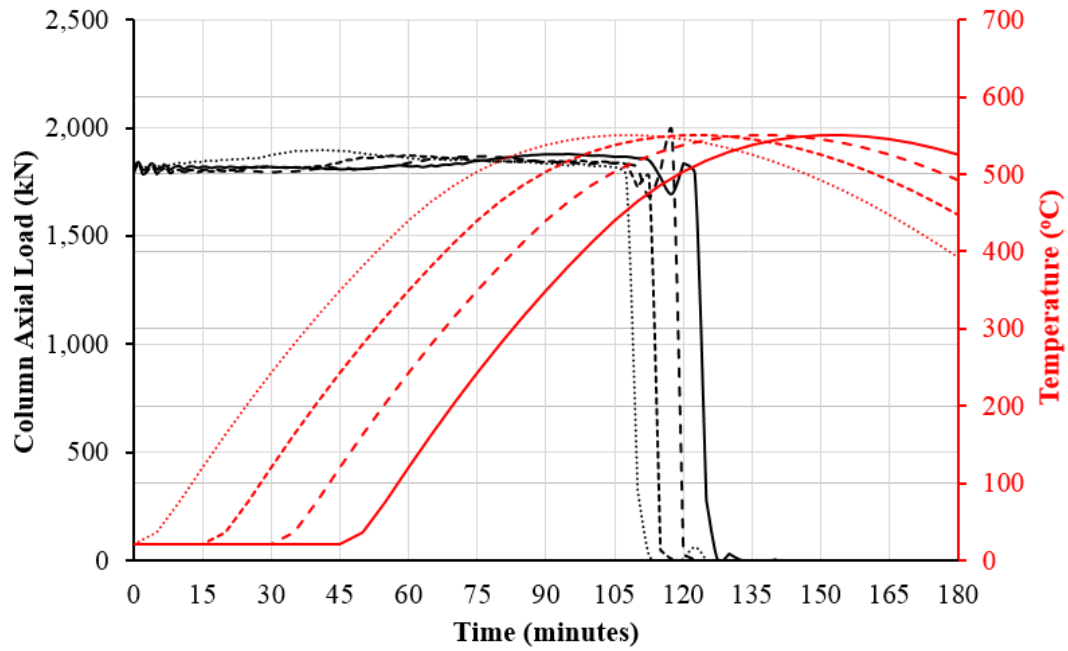
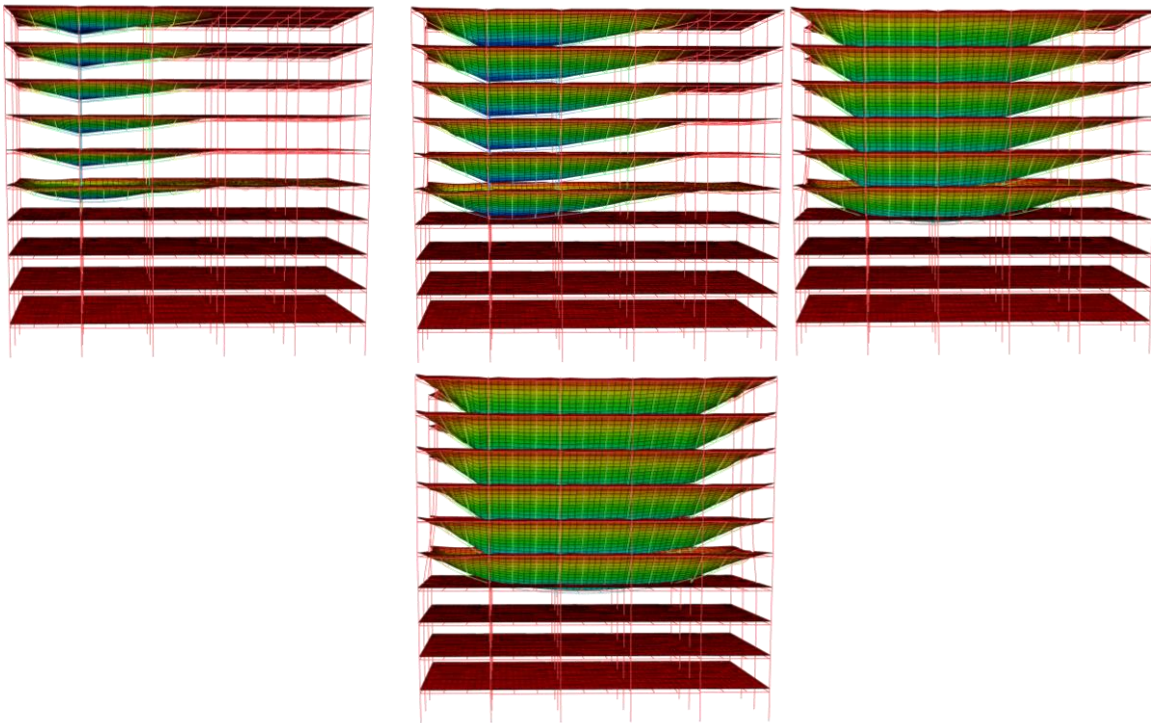


Figure 8.13 Column axial load and temperature versus time relationship for Chicago building (EQ4-3) with Fire 1-1 as travelling fire D_M1 at 9th story



(a)



(b)

Figure 8.14 Results of Fire 1-1 as travelling fire D_M1 at 5th story of Los Angeles building (EQ7-0.75)

- (a) Column axial load and temperature versus time relationship
 (b) Progression of column collapse

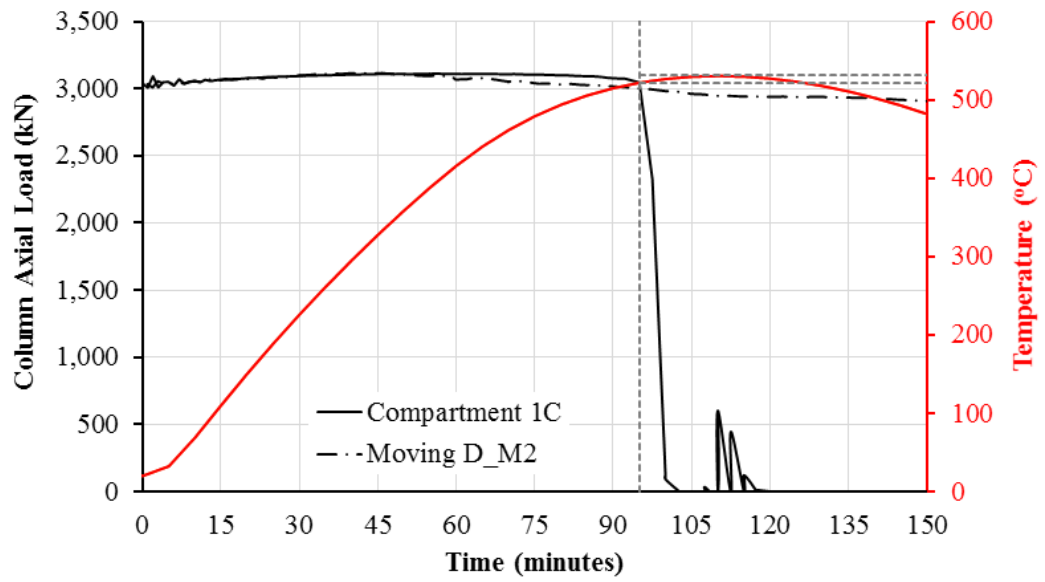


Figure 8.15 Column axial load and temperature versus time relationship for Los Angeles building (EQ4-3) with Fire 1-1 as travelling fire D_M2 at first story

Table 8.9 Story drift ratios of upper levels of Chicago building with aftershocks

Story	Main EQ3-3	EQ3-3 Aftershock (No fire)	EQ3-3 Aftershock (After Fire 3-0.75 at 9A)	EQ3-3 Aftershock (After Fire 3-0.75 at 9D)
10	0.0096	0.0226	0.0215	0.0353
9	0.0138	0.0241	0.0257	0.0219
8	0.0163	0.0168	0.0166	0.0147
MAX:	0.0163	0.0241	0.0257	0.0353

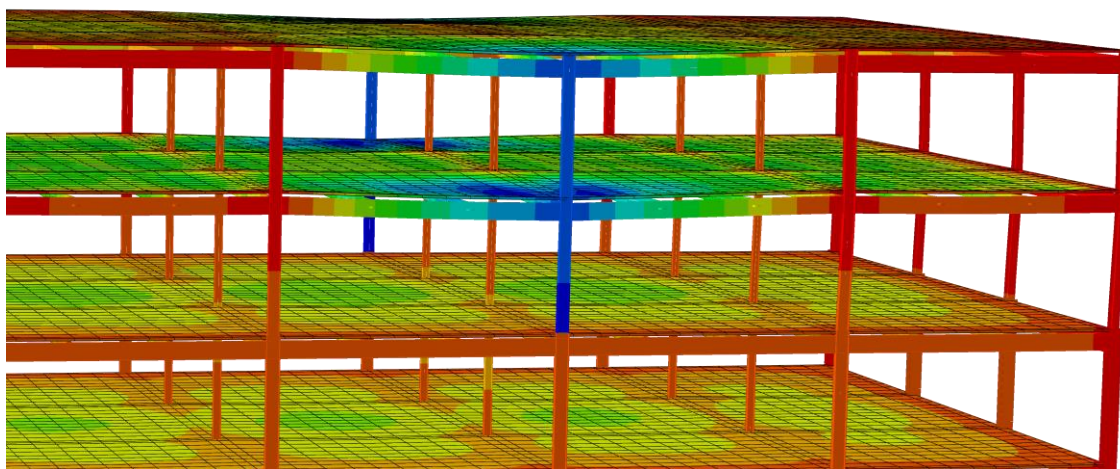


Figure 8.16 Deflected shape of Chicago building subjected to EQ3-3, Fire 6-0.75 at 9D and EQ3-3 aftershock

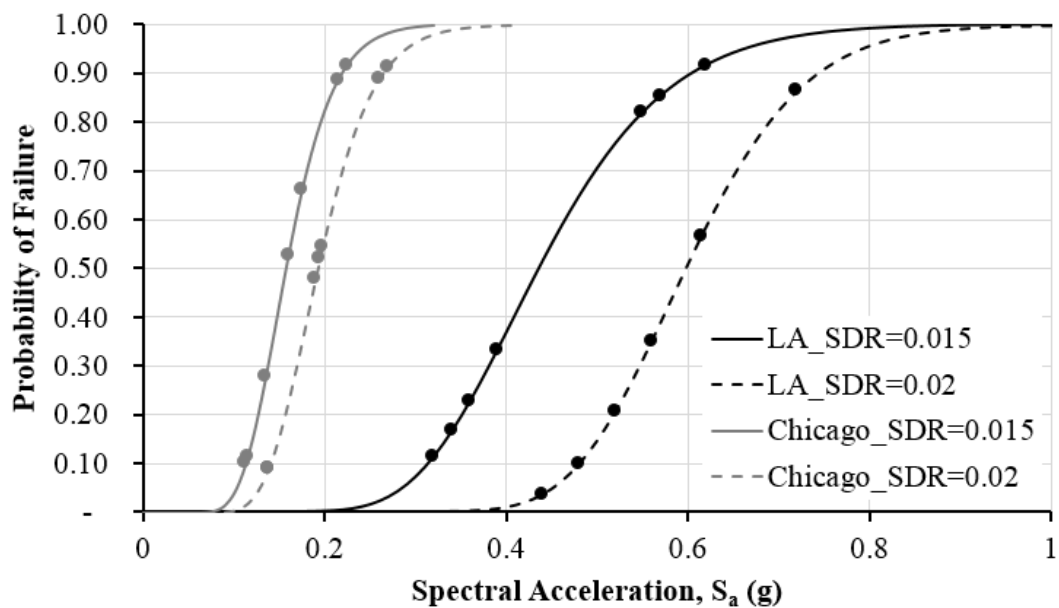


Figure 8.17 Seismic fragility curves for Chicago and Los Angeles buildings: Probability of exceeding specified story drift ratios (SDRs) vs. spectral accelerations

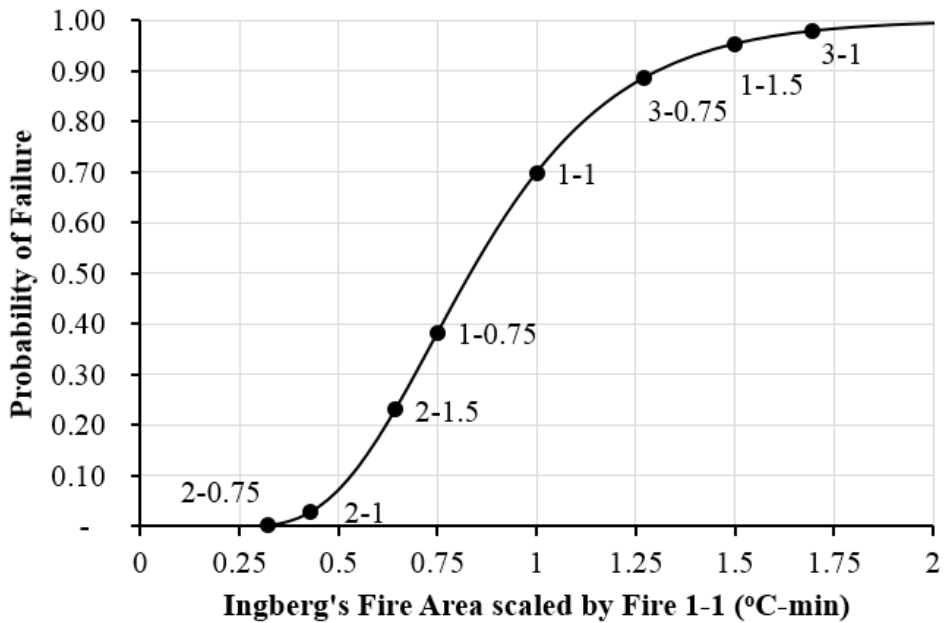


Figure 8.18 Fire fragility curve for Chicago and Los Angeles buildings: Probability of exceeding L/20 deflection vs. Ingberg's Fire Area

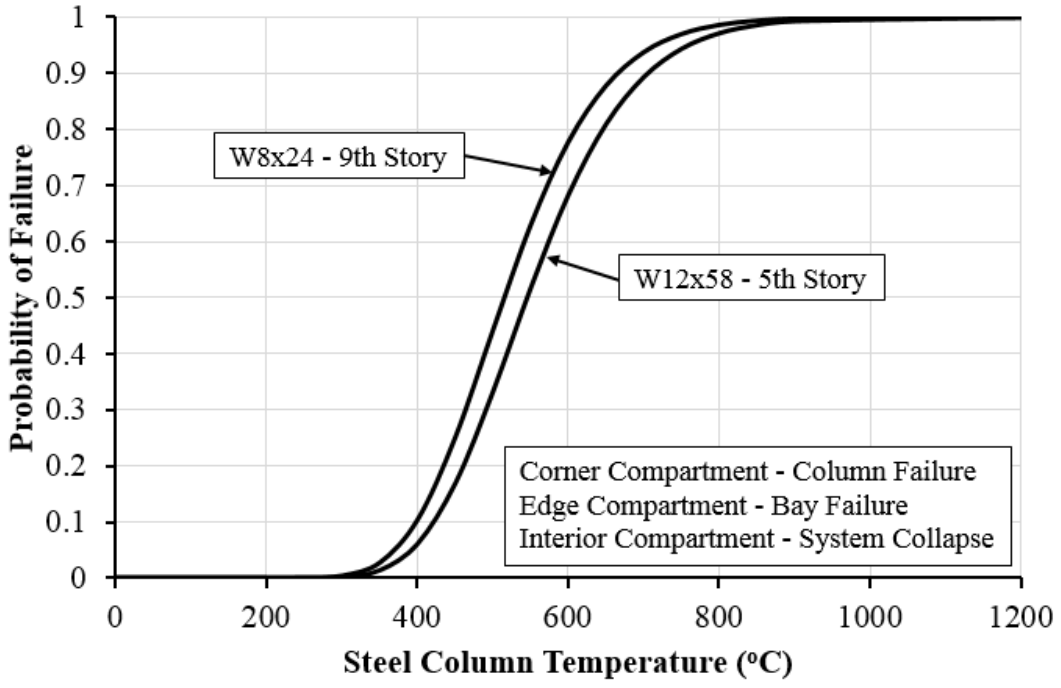


Figure 8.19 Fire fragility curve for Chicago and Los Angeles buildings: Probability of gravity column failure vs. gravity column internal temperature

CHAPTER 9. SUMMARY AND CONCLUSIONS

9.1 Research Summary

Building structures have traditionally been designed based on singular hazard events occurring independent of one another. This approach involves designing for wind, earthquake, fire, blast, and other hazards independently and then designing the system to withstand each hazard individually. It was not until recent years that a multi-hazard approach emerged where hazards were considered concurrently with one another, and structures were designed with a recognition that there are interrelationships between the optimal design for each hazard. These interrelationships may be synergistic or antagonistic but, ultimately, a multi-hazard design considers the overall building performance and resilience when subjected to a variety of hazards. Structural design for fire safety in the United States typically uses a prescriptive method to determine, based on furnace tests of components, the fireproofing thickness necessary to withstand a fire for a designated duration of time. This method has been proven effective for achieving the necessary fire resistance rating for members but it does not consider the level of damage that is caused, or the effect of the interrelationships of the structural elements. Thus, a performance based approach has emerged in order to understand the level of damage within a building subjected to fires by applying thermal loads to the structure.

This work explored development of a methodology for assessing multi-hazard resilience of steel buildings which included incremental dynamic analyses and incremental fire analyses. It focused primarily on post-earthquake fire hazards, while also briefly addressing wind hazards. This methodology was then implemented using two case study buildings.

Two ten-story office buildings were designed and analyzed. One was designed for hazard levels in Chicago, IL (low seismic area) and the other was designed for hazard levels in Los Angeles, CA (high seismic area). The buildings varied only in the design of the perimeter moment frame systems. After design of these buildings using conventional, linear static procedures, the structures were modeled as 3D building models using the finite element software, ABAQUS. This model used beam elements for the framing members and shell elements to model the slab. Rigid connectors were used to model the moment frame connections. Equivalent connectors that capture the axial force-axial displacement-moment-rotation-temperature relationship of the gravity shear

connections were used at beam-to-beam and beam-to-column connections of the gravity framing system. Material properties for the steel framing members and the concrete composite slab were taken from Eurocode [115].

Incremental dynamic analyses was used to assess seismic performance of each structure. Seven ground motions were generated for each structure and the intensities were scaled by the peak ground acceleration in order to cover a range of seismic intensities. Ground motions were applied as displacement time histories to the base of each structure and 5% Rayleigh damping was assumed. Results showed that the Chicago building required significant amplification of the ground motion (in the order of 3 times the PGA) in order to observe any type of inelasticity. Hinging occurred primarily in the moment frame columns. When fracture occurred in the columns, this initiated collapse of the structure. The Los Angeles building, however, primarily experienced plastic hinging and fracture in the protected zones of the moment frame beams. The lateral system of the LA building was controlled by seismic design and, thus, experienced inelasticity at 0.75 and 1 times the PGA. Story drift ratios were used as the damage parameter and, ultimately, spectral acceleration was chosen as the preferred intensity measure instead of PGA.

Incremental dynamic analyses were emulated in order to create a similar approach for fire assessment, known as incremental fire analyses. Seven compartment fire time-temperature curves generated from Eurocode [37] were initially selected. These curves were scaled by the peak fire temperature. The fires were reduced to only 3 when it was discovered that many of the scaled fires produced similar curves. Corner, edge and interior compartment fires were studied at the fifth and ninth stories of both buildings. The first story of the Los Angeles building was also studied because of the presence of seismic damage at this level. Full story and travelling fires were also analyzed. Heat transfer analyses were conducted on all of the structural members within the compartment. A 1 hr fire resistance rating was determined per IBC [7] as the minimum fire resistance rating requirement for these office buildings. The structural members were modeled with fireproofing at the thickness necessary to achieve the 1 hr FRR per the prescriptive method.

The compartment fires resulted in reoccurring failure modes: column failure, bay failure, compartment failure, connection failure and system failure, as summarized in Table 3.1. Acceptance criteria for these failures are also summarized in this table, based on deflection criteria of $L/20$ provided in BS 476-20 [105]. Column failure is when one column loses load carrying capacity but the loads can be redistributed to prevent progressive collapse. This was commonly

observed in the corner compartments for both buildings. Bay failure is when two columns within the fire compartment fail but, again, the system is able to restabilize and progressive collapse is prevented. This was common in edge compartment fires. Connection failures were most frequently observed after column failures and when compartments included fractured moment frame beams. System failure is when progressive collapse occurs. The findings from the incremental fire analyses showed that the gravity columns are the most vulnerable component of a steel building. The LA and Chicago buildings experience the same initial failure mode (column/bay failure). The perimeter moment frame only helps to prevent system collapse after column failure has occurred. This shows that seismic and fire are actually decoupled from one another when subjected to seismic events.

Wind time histories were also applied to the structures. Because structures are designed to remain elastic in wind events, fire following wind events result in the same structural performance as fire-only events. Wind can affect the cladding, which would in turn change the fire time-temperature curve.

Additional pilot studies were later conducted to understand how changes to specific building components affect the overall building resilience. Because the gravity columns were found to be the most vulnerable component, these columns were analyzed with a 2 hr FRR instead of the minimum requirement of 1 hr. Column collapse could be prevented for most fires by increasing fireproofing thickness. In a separate study, gravity column sizes at each level were also increased. This prevented column collapse and resulted in an increase of approximately 1-2% of the structural framing costs. Increasing fireproofing of the gravity columns was found to be less costly than increasing the gravity column sizes.

Fire analyses showed that the interior compartment fires tended to result in column collapses of the four columns within the compartment, causing system collapse because of the long span, unsupported framing system that resulted from the failed columns. By adding a rebar mat within the composite slab, system collapse could be prevented and only bay failure occurred.

During an earthquake, it is possible that the fireproofing on the structural members may detach and spall in areas where the steel has yielded; therefore, the effect of fireproofing damage on the fire resilience of the structure was studied for the Chicago and Los Angeles buildings. In the Chicago building, fireproofing damage was applied to the ends of the moment frame columns. Findings showed that these columns had so much excess capacity that, unless less than 5 mm of

fireproofing was left at these columns, gravity column failure would remain the initiating failure mode. Fireproofing damage within the Los Angeles building was applied to the protected zones of the moment frame beams. While the exposed steel caused an increase in deformation and a change in axial forces within the beam, these differences were not significant enough to change the failure mechanism of the system. Additional studies are needed to address the slab to beam stud connectors in order to ensure that the system is not over predicting the composite strength of the framing system.

Aftershocks were briefly studied to demonstrate that the fire location and extent of damage can play a role in the response of a structure subjected to an earthquake, followed by a fire, and then another earthquake. Preliminary findings seem to show that a fire exposed to only compartment does not change building behavior significantly in an aftershock event. When a full story fire has occurred, these differences are more evident.

9.2 Conclusions

Based on the results of the computational building models created to assess multi-hazard building resilience, the following conclusions are drawn:

- 1) Buildings in a low seismic region, not designed for strong column-weak beam, may be susceptible to moment frame column plastic hinging or fracture during high seismic events.
- 2) Seismic damage is very unlikely in the gravity frame members. Damage is concentrated at the moment frame members.
- 3) When exposed to fires and post-earthquake fires, gravity columns are the most vulnerable component in a steel moment frame system with all members protected at the same fire resistance rating. This finding was true at a lower, mid and upper level of a ten-story building, regardless of the perimeter moment frame robustness. It is also the case at corner, edge and interior compartments.
- 4) The column capacity equations provided in Appendix 4 of AISC 360 [48] can be used to closely predict column failure temperatures. The modified L/r factor for rotational restraint of the cooler columns above and below should be used for this calculation. The simply-supported L/r factor is too conservative.
- 5) The prescriptive method is a conservative approach for ensuring that fire resistance rating time is met. It does not, however, prevent failure beyond that time or provide any indication

of the extent of damage or likelihood of collapse. Structural resilience of the system can be assessed through performance based analysis methods.

- 6) Structural failure modes from compartment fires vary in the level of damage and likelihood of repair. Compartment failures are concentrated to only one framing bay. Column failures affect the four adjacent bays and the stories above. Bay failures affect the six adjacent bays and the stories above. System collapse varies in size but is the most detrimental and widespread. Compartment failures are the most resilient; in these causes, it is plausible to repair framing members within the compartment as the extent of damage is limited. The other failure modes (column and bay) could also be repaired, though it is likely not a cost-effective effort. These failures, where the system can effectively redistribute loads to prevent system collapse, are more resilient failure modes than progressive collapse failures.
- 7) Post-earthquake fire resilience for structures in high and low seismic areas are the same regardless of seismic damage, as long as moment frame connections have not fractured. Gravity columns typically fail first, causing column, bay or system failures. The failure of these columns is not influenced by the perimeter moment frame system because these gravity columns are much more vulnerable than the more robust moment frames. In high seismic areas, fractures within the moment frame system may lead to a subsequent failure mode (such as system collapse) after column failure, but studies have shown that gravity column failures consistently initiate the first failure mode.
- 8) For compartment fires where there is no seismic damage (no plastic hinging or fracture of members), the system responds the same as a fire-only scenario.
- 9) Seismic damage that has occurred in compartments other than the compartment subjected to the fire and its adjacent compartments does not affect the fire resilience of the structure.
- 10) The perimeter moment frames help to resist system collapse as long as their connections have not fractured when column failure occurs at the corner and edge compartments.
- 11) Short duration fires that heat and cool quickly are unlikely to cause a failure mode within the system when the member has fireproofing. This is because the fireproofing delays the heating process of the steel and the steel does not have time to reach high temperatures before the fire begins to cool.
- 12) Increasing gravity column sizes or the thickness of fireproofing at these columns can prevent the system from experiencing column failure. By preventing column collapse,

structural resilience is achieved. Increasing the fireproofing is likely a more cost-effective solution than increasing the steel sizes.

- 13) Incorporating reinforcing steel in the composite slab can prevent system collapse at the interior compartment by transferring large tensile forces through catenary action. Without this additional steel, a conventional composite slab cannot adequately transfer loads from failed gravity columns in order to prevent progressive collapse. A reinforcing mat in the composite slab can result in a more resilient structure.
- 14) Structural systems are designed to remain elastic in wind events and, thus, wind does not affect the fire resilience in a fire following wind scenario, as it does in a fire following earthquake scenario, where inelasticity occurs. Nonstructural wind damage, such as broken windows, can affect the time-temperature curve of the fire itself, as the breach would increase the opening factor of the compartment.
- 15) Traveling fires can be simulated conservatively using full story fires. The traveling fires that were studied produced the same failure modes and failure times as the full story fires. Travelling fires should be considered more closely for post-earthquake fire assessment when the controlling load case of the individual compartment fires is something other than gravity column failure.
- 16) Plastic hinging in moment frame columns can lead to debonding of fireproofing. These columns generally have enough reserve capacity that only severely damaged fireproofing (i.e. – less than 5mm thickness of SFRM remaining) would cause failure before the protected interior gravity columns. Damaged fireproofing does, however, affect when and if the perimeter moment frames fail after the gravity column failure occurs. This will affect whether only column or bay failures occur, or if system collapse occurs.

9.3 Future Work

This work established a methodology for multi-hazard analyses that can also be expanded to include other building types and sizes. Braced frame structures and high rise structures should be considered, as these may be very vulnerable to post-earthquake fire hazards. Aftershocks following post-earthquake fires should also be explored in more detail, as they have the potential of resulting in severe structural damage. As the industry continues to move towards a multi-hazard approach to assessing building resilience, other hazards should be incorporated into building models.

The work presented in this dissertation can be furthered through more detailed modeling of select components. In particular, the force-slip behavior of shear studs and the potential pullout failure modes of the stud connectors should be incorporated into the model. This will prevent rigid body motion of the slab and beams, and will ensure that the strength and stiffness of the framing members is not being overestimated. Moment frame connections are currently modeled as rigid connectors in the ABAQUS building model. Connections may be left unprotected due to fireproofing damage following a seismic event. For these instances, it would be beneficial to incorporate the force-displacement-moment-rotation-temperature behavior of the moment frame connections in order to capture a potential connection failure mode. Because gravity column failures were the initiating failure mode, the seismic and fire responses were decoupled from one another. By changing the fire resistance rating so that all components are not protected to the same level of fireproofing, more diverse response may be observed that couple the seismic and fire responses together.

Further research is needed to advance the understanding of steel building performance when subjected to post-earthquake fire hazards. Very few experimental tests have been conducted on steel components and assemblies subjected to post-earthquake fires [130, 131]. Instead, most work on PEF has been conducted computationally. Advancements in understanding of PEF behavior can be achieved through experimental testing of beam-to-column assemblies for both gravity and moment frames. In addition, experimental testing of the post-earthquake fire behavior of floor diaphragms should be conducted. Researchers can determine through computational modeling which other components or assemblies should be experimentally tested. These tests can in turn be used to verify and benchmark the computational models.

Throughout this work, resilience has been studied from a structural perspective. The work aimed to understand failure modes when subjected to different hazards, and to make improvements to select components that can improve overall system resilience. Efforts were made to limit the level and extent of structural damage as much as possible, while maintaining traditional construction practices. It must be acknowledged, however, that building resilience extends beyond merely structural resilience, including nonstructural components such as sprinklers systems, lighting/electrical/HVAC systems, interiors, and building contents. Integration of structural and nonstructural response to multi-hazard events is necessary to truly assess building resilience following an event. Focus on fire and fire following earthquake scenarios require improved

integration of structural and nonstructural systems in order to explore resilience at a community level. In particular, a more in depth understanding of how structural deformations and damage can affect nonstructural systems in a fire event is needed. This is an opportunity for future work.

REFERENCES

- [1] USGBC, “U.S. Green Building Council: LEED Pilot Credits,” [cited 2016 February 5]; Available from: <http://www.usgbc.org/credits/new-construction/v4/pilot-credits>, 2016.
- [2] USRC, “US Resiliency Council,” [cited 2016 February 5]; Available from: <http://www.usrc.org/>, 2016.
- [3] S. Mousavi, A. Bagchi, and V.K.R. Kodur, “Review of post-earthquake fire hazard to building structures,” *Canadian Journal of Civil Engineering*, 35(7): p. 689-698, 2008.
- [4] M.M. Ettouney and S. Alampalli, “Multihazard Considerations in Civil Infrastructure.” Boca Raton, FL: Taylor & Francis Group, LLC, 2017.
- [5] ASCE, *Minimum Design Loads for Buildings and Other Structures* (ASCE 7-10), American Society of Civil Engineers: Reston, VA, 2010.
- [6] FEMA, *Risk Assessment: A How-To Guide to Mitigate Potential Terrorist Attacks Against Buildings (FEMA 452): Risk Management Series*, Federal Emergency Management Agency (FEMA): Washington, D.C., 2005.
- [7] IBC, *International Building Code*. International Code Council, Inc.: Falls Church, VA, 2012.
- [8] ASTM, *ASTM E119-15: Standard Test Methods for Fire Tests of Building Construction and Materials*. American Society for Testing and Materials: West Conshohocken, PA, 2015.
- [9] UL, *UL Online Certifications Directory: Fire-Resistance Ratings - ANSI/UL263*. 2016; Available from: <http://database.ul.com/>.
- [10] J.L. Ruddy, J.P. Marlo, S.A. Loanneides, and F. Alfawakhiri, “AISC Design Guide 19 - Fire Resistance Of Structural Steel Framing,” American Institute of Steel Construction, Chicago, IL, 2003.
- [11] ANSI/AISC, *Seismic Provisions for Structural Steel Buildings* (AISC 341-10), American National Standards Institute/American Institute of Steel Construction: Chicago, IL, 2010.
- [12] M. Bruneau, C.M. Uang, and R. Sabelli, *Ductile Design of Steel Structures*. 2nd ed. New York: McGraw Hill, 2011.
- [13] Y.C. Lin, R. Sause, and J.M. Ricles, “Seismic Performance of Steel Self-Centering, Moment-Resisting Frame: Hybrid Simulations under Design Basis Earthquake.” *Journal of Structural Engineering*, 139(11): p. 1823-1832, 2013.

- [14] AISC, *Prequalified Connections for Special and Intermediate Steel Moment Frames for Seismic Applications* (ANSI/AISC 358-10), American Institute of Steel Construction: Chicago, IL, 2010.
- [15] A. Agarwal, “Stability Behavior of Steel Building Structures in Fire Conditions,” Doctor of Philosophy, School of Civil Engineering, Purdue University, West Lafayette, IN, 2011.
- [16] ASCE, *Seismic Evaluation and Retrofit of Existing Buildings* (ASCE/SEI 41-13), American Society of Civil Engineers: Reston, VA, 2013.
- [17] PEER, “PEER Ground Motion Database.” Available from: <http://ngawest2.berkeley.edu/>, Pacific Earthquake Engineering Research Center (PEER): Berkeley, CA, 2016.
- [18] COSMOS, “Strong-Motion Virtual Data Center (VDC).” Available from: <http://strongmotioncenter.org/vdc>, Consortium of Organizations for Strong Motion Observation Systems, 2016.
- [19] C.B. Haselton, “ATC Webinar on Recent Advances in Ground Motion Selection and Scaling.” 2015. 14 Oct 2015.
- [20] NIST, *Selecting and Scaling Earthquake Ground Motions for Performing Response-History Analyses*, in *NIST GCR 11-917-15*. National Institute of Standards and Technology: NEHRP Consultants Joint Venture, 2011.
- [21] FEMA, *Seismic Performance Assessment of Buildings (FEMA P-58-1)*. Vol. 1, Federal Emergency Management Agency (FEMA): Washington, D.C., 2012.
- [22] D. Vamvatsikos and C.A. Cornell, “Incremental dynamic analysis.” *Earthquake Engineering & Structural Dynamics*, 31(3): p. 491-514, 2002.
- [23] W.M. Chi, S. El-Tawil, G. Deierlein, and J.F. Abel, “Inelastic analyses of a 17-story steel framed building damaged during Northridge.” *Engineering Structures*, 20(4-6): p. 481-495, 1997.
- [24] D.A. Foutch and S.Y. Yun, “Modeling of steel moment frames for seismic loads.” *Journal of Constructional Steel Research*, 58: p. 529-564, 2002.
- [25] H. Krawinkler, *State of the Art Report on Systems Performance of Steel Moment Frames Subject to Earthquake Ground Shaking*, in *FEMA-355C*. Federal Emergency Management Agency: Washington, D.C., 2000.
- [26] D.G. Lignos and H. Krawinkler, “Development and Utilization of Structural Component Databases for Performance-Based Earthquake Engineering.” *Journal of Structural Engineering*, 139(8): p. 1382-1394, 2013.

- [27] PEER, *Tall Building Initiative: Guidelines for Performance-Based Seismic Design of Tall Buildings*, Pacific Earthquake Engineering Research Center (PEER): Berkeley, CA, 2010.
- [28] ATC, *Next-Generation Performance-Based Seismic Design Guidelines. Program Plan for New and Existing Buildings (FEMA 445)*. Applied Technology Council (ATC): Redwood City, CA, 2006.
- [29] LATBSDC, *An Alternative Procedure for Seismic Analysis and Design of Tall Buildings Located in the Los Angeles Region*. Los Angeles Tall Buildings Structural Design Council: Los Angeles, CA, 2014.
- [30] F.X. Flores, J.A. Jarrett, and F.A. Charney, "The Influence of Gravity-Only Framing on the Performance of Steel Moment Frames." in *15 World Conference on Earthquake Engineering*: Lisbon, Portugal, 2012.
- [31] J. Liu and A. Astaneh-Asl, "Cyclic Testing of Simple Connections Including Effects of Slab." *Journal of Structural Engineering*, 126: p. 32-39, 2000.
- [32] A. Gupta and H. Krawinkler, *Seismic Demands for Performance Evaluation of Steel Moment Resisting Frame Structures (SAC Task 5.4.3)*. The SAC Joint Venture, 1999.
- [33] J.P. Judd, F.A. Charney, and F.X. Flores, "The Influence of Gravity Framing on the Performance of Steel Buildings Subjected to Seismic Loads." in *Eighth International Workshop on Connections in Steel Structures*. Boston, MA: American Institute of Steel Construction, 2016.
- [34] NSF, "NEESR Planning: The Role of Gravity Framing in the Seismic Performance of Steel Buildings." Available from: https://www.nsf.gov/awardsearch/showAward?AWD_ID=1344592, 2013.
- [35] V.K.R. Kodur, M. Garlock, and N. Iwankiw, "Structures in Fire: State-of-the-Art, Research and Training Needs." *Fire Technology*, 48(4): p. 825-839, 2011.
- [36] ISO, *Fire Resistance Tests - Elements of building construction - Part 1: General Requirements (ISO 834-1:1999)*. International Organization for Standardization: Geneva, Switzerland, 2015.
- [37] EN, *Eurocode 1: Actions on structures, Part 1-2: General actions - Actions on structures exposed to fire (EN1991-1-2)*. European Committee for Standardization: Brussels, Belgium, 2002.
- [38] A.H. Buchanan, *Structural Design for Fire Safety*. Chichester, England: John Wiley & Sons, LTD, 2002.

- [39] J.M. Franssen and P. Vila Real, "Fire Design of Steel Structures. Eurocode 1: Actions on structures Part 1-2: Actions on structures exposed to fire. Eurocode 3: Design of steel structures Part 1-2: Structural fire design." ECCS Eurocode Design Manuals: 2012.
- [40] N.D. Pope, and C.G. Bailey, "Quantitative comparison of FDS and parametric fire curves with post-flashover compartment fire test data." *Fire Safety Journal*, 41(2): p. 99-110, 2006.
- [41] Y. Wang, I. Burgess, F. Wald, and M. Gillie, *Performance-Based Fire Engineering of Structures*. Boca Raton, FL: CRC Press, 2013.
- [42] D. Lange, S. Devaney, and A. Usmani, "An application of the PEER performance based earthquake engineering framework to structures in fire." *Engineering Structures*, 66: p. 100-115, 2014.
- [43] P. Moss, A. Abu, and R. Dhakal, "Incremental fire analysis (IFA) for probabilistic fire risk assessment." in *23rd Australasian Conference on the Mechanics of Structures and Materials (ACMSM23)*. Southern Cross University, Lismore, NSW, 2014.
- [44] S. Devaney, "*Development of Software for Reliability Based Design of Steel Framed Structures in Fire*." Doctor of Philosophy, The University of Edinburgh, Edinburgh, UK, 2014.
- [45] S.H. Ingberg, *Tests of the Severity of Building Fires*. National Fire Protection Assoc., 22(1): p. 43-61, 1928.
- [46] D. Rush, L. Bisby, I. Ioannou, and T. Rossetto, "Towards Fragility Analysis for Concrete Buildings in Fire: Residual Capacity of Concrete Columns." in *8th International Conference on Structures in Fire*. Shanghai, China, 2014.
- [47] T. Gernay, N.E. Khorasani, and M. Garlock, "Fire Fragility Curves for Steel Buildings in a Community Context: A methodology." *Engineering Structures*, 113: p. 259-276, 2016.
- [48] AISC, *Specification for Structural Steel Buildings (ANSI/AISC 360-10)*, American Institute of Steel Construction: Chicago, IL, 2010.
- [49] K.C. Yang, S.J. Chen, and M.C. Ho, "Behavior of beam-to-column moment connections under fire load." *Journal of Constructional Steel Research*, 65(7): p. 1520-1527, 2009.
- [50] H. Yu, I.W. Burgess, J.B. Davison, and R.J. Plank, "Experimental investigation of the behaviour of fin plate connections in fire." *Journal of Constructional Steel Research*, 65(3): p. 723-736, 2009.
- [51] M. Garlock, and S. Selamet, "Modeling and Behavior of Steel Plate Connections Subject to Various Fire Scenarios." *Journal of Structural Engineering*, July 2010: p. 897-906, 2010.

- [52] Y.C. Wang, X.H. Dai, and C.G. Bailey, "An experimental study of relative structural fire behaviour and robustness of different types of steel joint in restrained steel frames." *Journal of Constructional Steel Research*, 67(7): p. 1149-1163, 2011.
- [53] H. Mahmoud, B. Ellingwood, C. Turbert, M. Memari, "Response of Steel Reduced Beam Section Connections Exposed to Fire." *Journal of Structural Engineering*, 142(1): p. 04015076, 2016.
- [54] E.C. Fischer and A.H. Varma, "Fire resilience of composite beams with simple connections: Parametric studies and design." *Journal of Constructional Steel Research*, 128: p. 119-135, 2017.
- [55] K.S. Al-Jabri, A. Seibi, and A. Karrech, "Modelling of unstiffened flush end-plate bolted connections in fire." *Journal of Constructional Steel Research*, 62(1-2): p. 151-159, 2006.
- [56] G. Hu and M. Engelhardt, "Investigations on the Behavior of Steel Single Plate Beam End Framing Connections in Fire." *Journal of Structural Fire Engineering*, 2(3): p. 195-204, 2011.
- [57] P. Pakala, V. Kodur, S. Selamet, and M. Garlock, "Fire behavior of shear angle connections in a restrained steel frame." *Journal of Constructional Steel Research*, 77: p. 119-130, 2012.
- [58] Z.H. Qian, K.H. Tan, and I.W. Burgess, "Behavior of Steel Beam-to-Column Joints at Elevated Temperature: Experimental Investigation." *Journal of Structural Engineering*, 134(5): p. 713-726, 2008.
- [59] K.H. Tan and Z.F. Huang, "Structural Responses of Axially Restrained Steel Beams with Semirigid Moment Connection in Fire." *Journal of Structural Engineering*, 131(4): p. 541-551, 2005.
- [60] M.M.S. Dwaikat, V.K.R. Kodur, S.E. Quiel, M.E.M Garlock, "Experimental behavior of steel beam-columns subjected to fire-induced thermal gradients." *Journal of Constructional Steel Research*, 67(1): p. 30-38, 2011.
- [61] L. Choe, A.H. Varma, A. Agarwal, and A. Surovek, "Fundamental Behavior of Steel Beam-Columns and Columns under Fire Loading: Experimental Evaluation." *Journal of Structural Engineering*, 137(9): p. 954-966, 2011.
- [62] A. Agarwal, L. Choe, and A.H. Varma, "Fire design of steel columns: Effects of thermal gradients." *Journal of Constructional Steel Research*, 93: p. 107-118, 2014.
- [63] M.Z. Naser and V.K.R. Kodur, "Factors governing onset of local instabilities in fire exposed steel beams." *Thin-Walled Structures*, 98: p. 48-57, 2016.

- [64] B. Zhao and J. Kruppa, *Fire resistance of composite slabs with profiled steel sheet and of composite steel concrete beams, Part 2: Composite beams*. Luxembourg: European Commission, 1997.
- [65] K.L. Selden and A.H. Varma, "Composite beams under fire loading: numerical modeling of behavior." *Journal of Structural Fire Engineering*, 7(2): p. 142-157, 2016.
- [66] K.L. Selden, E.C. Fischer, and A.H. Varma, "Experimental Investigation of Composite Beams with Shear Connections Subjected to Fire Loading." *Journal of Structural Engineering*, 142(2), 2016.
- [67] V.K.R. Kodur, M. Naser, P. Pakala, and A. Varma, "Modeling the response of composite beam-slab assemblies exposed to fire." *Journal of Constructional Steel Research*, 80: p. 163-173, 2013.
- [68] S. Selamet and M.E. Garlock, "Predicting the maximum compressive beam axial force during fire considering local buckling." *Journal of Constructional Steel Research*, 71: p. 189-201, 2012.
- [69] J. Takagi and G.G. Deierlein, "Strength design criteria for steel members at elevated temperatures." *Journal of Constructional Steel Research*, 63(8): p. 1036-1050, 2007.
- [70] A. Agarwal and A.H. Varma, "Fire induced progressive collapse of steel building structures: The role of interior gravity columns." *Engineering Structures*, 58: p. 129-140, 2014.
- [71] EN, *Fire resistance tests - Part 1: General Requirements (EN1363-1)*. European Committee for Standardization: Brussels, Belgium, 2012.
- [72] STC, *The Behaviour of Multi-Storey Steel Framed Buildings in Fire*. British Steel plc, Swinden Technology Centre: South Yorkshire, UK, 1999.
- [73] C. Fang, B.A. Izzuddin, A.Y. Elghazouli, and D.A. Nethercot, "Robustness of steel-composite building structures subject to localised fire." *Fire Safety Journal*, 46(6): p. 348-363, 2011.
- [74] E.C. Fischer, "Fire Behavior of Simple (Shear) Connections in Steel-Frame Buildings," Doctor of Philosophy, Lyles School of Civil Engineering, Purdue University, West Lafayette, IN, 2015.
- [75] M. Memari and H. Mahmoud, "Performance of steel moment resisting frames with RBS connections under fire loading." *Engineering Structures*, 75: p. 126-138, 2014.
- [76] J. Jiang, G.Q. Li, and A. Usmani, "Progressive Collapse Mechanisms of Steel Frames Exposed to Fire." *Advances in Structural Engineering*, 17(3): p. 381-398, 2014.

- [77] R. Sun, Z. Huang, and I.W. Burgess, "Progressive collapse analysis of steel structures under fire conditions." *Engineering Structures*, 34: p. 400-413, 2012.
- [78] G. Flint, A. Usmani, S. Lamont, B. Lane, and J. Torero, "Structural Response of Tall Buildings to Multiple Floor Fires." *Journal of Structural Engineering*, 133(12): p. 1719-1732, 2007.
- [79] A.S. Usmani, Y.C. Chung, and J.L. Torero, "How did the WTC towers collapse: a new theory." *Fire Safety Journal*, 38(6): p. 501-533, 2003.
- [80] G. Flint, "Fire Induced Collapse of Tall Buildings," Doctor of Philosophy, The University of Edinburgh, Edinburgh, UK, 2005.
- [81] S.E. Quiel and M. Garlock, "Parameters for Modeling a High-Rise Steel Building Frame Subject to Fire." *Journal of Structural Fire Engineering*, 1(2): p. 115-134, 2010.
- [82] C. Röben, M. Gillie, and J. Torero, "Structural behaviour during a vertically travelling fire." *Journal of Constructional Steel Research*, 66(2): p. 191-197, 2010.
- [83] C.R. Scawthorn, "Fire Following Earthquake Aspects of the Southern San Andreas Fault Mw7.8 Earthquake Scenario." *Earthquake Spectra*, 27(2): p. 419-441, 2011.
- [84] C. Scawthorn, "Fires following the Northridge and Kobe Earthquakes," in *Thirteenth Meeting of the UJNR Panel on Fire Research and Safety*. NISTIR 6030. p. 325-335, 1996.
- [85] C. Scawthorn, J.M. Eidinger, and A.J. Schiff. "Fire Following Earthquake." in *Technical Council on Lifeline Earthquake Engineering, Monograph No. 26*, 2005.
- [86] R. Botting, "The Impact of Post-Earthquake Fire on the Urban Environment." in *Fire Engineering Research Report 98/1*. University of Canterbury, New Zealand, 1998.
- [87] J. Taylor, "Post Earthquake Fire in Tall Buildings and the New Zealand Building Code." *Fire Engineering Research Report 03/6*, 2003.
- [88] G. Della Corte, R. Landolfo, and F.M. Mazzolani, "Post-earthquake fire resistance of moment resisting steel frames." *Fire Safety Journal*, 38(7): p. 593-612, 2003.
- [89] D. Pantousa and E. Mistakidis. "Fire Resistance of a Steel Structure Under Different Fire-After-Earthquake Scenarios Considering Both Structural and Non-Structural Damage" in *8th Hellenic National Conference of Steel Structures*. Tripoli, Greece, 2014.
- [90] B. Behnam and H.R. Ronagh, "Behavior of moment-resisting tall steel structures exposed to a vertically traveling post-earthquake fire." *The Structural Design of Tall and Special Buildings*, 23(14): p. 1083-1096, 2014.

- [91] N.E. Khorasani, M.E.M. Garlock, and S.E. Quiel, "Modeling steel structures in OpenSees: Enhancements for fire and multi-hazard probabilistic analyses." *Computers & Structures*, 157: p. 218-231, 2015.
- [92] M. Memari, H. Mahmoud, and B. Ellingwood, "Post-earthquake fire performance of moment resisting frames with reduced beam section connections." *Journal of Constructional Steel Research*, 103: p. 215-229, 2014.
- [93] R. Zaharia and D. Pintea, "Fire after Earthquake Analysis of Steel Moment Resisting Frames." *International Journal of Steel Structures*, 9(4): p. 275-284, 2009.
- [94] B. Behnam and H.R. Ronagh, "An Engineering Solution to Improve Post-Earthquake Fire Resistance in Important Reinforced Concrete Structures." *Advances in Structural Engineering*, 17(7): p. 993-1009, 2014.
- [95] S.E. Quiel and S.M. Marjanishvili, "Fire Resistance of a Damaged Steel Building Frame Designed to Resist Progressive Collapse." *Journal of Performance of Constructed Facilities*, 26(4): p. 402-409, 2012.
- [96] N.L. Braxtan and S. Pessiki, "Bond performance of SFRM on steel plates subjected to tensile yielding." *Journal of Fire Protection Engineering*, 21(1): p. 37-55, 2011.
- [97] W.J. Keller and S. Pessiki, "Effect of earthquake-induced damage to spray-applied fire-resistive insulation on the response of steel moment-frame beam-column connections during fire exposure." *Journal of Fire Protection Engineering*, 22(4): p. 271-299, 2012.
- [98] S. Soroushian, A.E. Zaghi, E. Maragakis, A. Echevarria, Y. Tian, and A. Filiatrault, "Analytical Seismic Fragility Analyses of Fire Sprinkler Piping Systems with Threaded Joints." *Earthquake Spectra*, 31(2): p. 1125-1155, 2015.
- [99] A.E. Zaghi, E. Maragakis, A. Itani, and E. Goodwin, "Experimental and Analytical Studies of Hospital Piping Assemblies Subjected to Seismic Loading." *Earthquake Spectra*, 28(1): p. 367-384, 2012.
- [100] L.D. Carpenter, "High-rise building cladding drift accommodation." *The Structural Design of Tall and Special Buildings*, 13(5): p. 439-456, 2004.
- [101] T. Okazaki, M. Nakashima, K. Suita, and T. Matusmiya, "Interaction between cladding and structural frame observed in a full-scale steel building test." *Earthquake Engineering & Structural Dynamics*, 36(1): p. 35-53, 2007.
- [102] B. Faggiano and F.M. Mazzolani, "Fire after earthquake robustness evaluation and design: Application to steel structures." *Steel Construction*, 4(3): p. 183-187, 2011.
- [103] FEMA, *Prestandard and Commentary for the Seismic Rehabilitation of Buildings* (FEMA 356), Federal Emergency Management Agency (FEMA), Washington, D.C., 2000.

- [104] R.H.R. Tide, "Integrity of Structural Steel After Exposure to Fire." *Engineering Journal*, First Quarter, 1998.
- [105] BS, *Fire tests on building materials and structures. Method for determination of the fire resistance of elements of construction (general principles)* (BS 476-20), British Standards Institute, London, UK, 1987.
- [106] RAM Structural System, Bentley Systems, Inc., Exton, PA, 2013.
- [107] SeismoArtif, Seismosoft, Pavia, Italy, 2016.
- [108] B. Halldorsson and A.S. Papageorgious, "Calibration of the specific barrier model to earthquake of different tectonic regions." *Bulletin of the Seismological Society of America*, 95(4): p. 1276-1300, 2005.
- [109] D. Kwon and A. Kareem, "NatHaz on-line wind simulator (NOWS) : simulation of Gaussian multivariate wind fields." NatHaz Modeling Laboratory Report, University of Notre Dame, <http://windsim.ce.nd.edu/>, 2006.
- [110] E. Simiu and R.H. Scanlan, *Wind Effects on Structures*. Second Edition: A Wiley-Interscience Publication, New York, NY, 1986.
- [111] LACBC, *Los Angeles County Building Code*. American Publishing Corporation: Los Angeles, CA, 2011.
- [112] ABAQUS, Simulia - Dassault Systemes, Boston, MA, 2016.
- [113] M. Sarraj, "The Behaviour of Steel Fin Plate Connections in Fire," Doctor of Philosophy, Department of Civil and Structural Engineering, The University of Sheffield, Sheffield, UK, 2007.
- [114] EN, *Eurocode 3: Design of steel structures, Part 1-2: General rules - Structural fire design* (EN1993-1-2). European Committee for Standardization: Brussels, Belgium, 2005.
- [115] EN, *Eurocode 4: Design of composite steel and concrete structures, Part 1-2: General rules - Structural fire design* (EN1994-1-2). European Committee for Standardization: Brussels, Belgium, 2005.
- [116] A.K. Chopra, *Dynamics of Structures: Theory and Applications to Earthquake Engineering*. Fourth Edition. Prentice Hall: Upper Saddle River, NJ, 2012.
- [117] J.F. Hall, "Problems encountered from the use (or misuse) of Rayleigh damping." *Earthquake Engineering & Structural Dynamics*, 35(5): p. 525-545, 2006.

- [118] P. Hesam, A. Irfanoglu, and T. Hacker, "Effective Viscous Damping and Restoring Force in Reinforced Concrete Buildings," in *IMAC-XXXIV*. Orlando, FL, 2016.
- [119] E. Karamanci and D.G. Lignos, "Computational Approach for Collapse Assessment of Concentrically Braced Frames in Seismic Regions." *Journal of Structural Engineering*, 140(8): p. A4014019, 2014.
- [120] K. Le-Trung, K. Lee, J. Lee, and D.H. Lee, "Evaluation of seismic behaviour of steel special moment frame buildings with vertical irregularities." *The Structural Design of Tall and Special Buildings*, 21(3): p. 215-232, 2012.
- [121] K. Lee, "Performance Prediction and Evaluation of Steel Special Moment Frames for Seismic Loads," Doctor of Philosophy, University of Illinois at Urbana-Champaign, Champaign, IL, 2000.
- [122] X.M. Chen, J. Duan, H. Qi, and Y.G. Li, "Rayleigh Damping in Abaqus/Explicit Dynamic Analysis." *Applied Mechanics and Materials*, 627: p. 288-294, 2014.
- [123] S. Lee, "Nonlinear Dynamic Earthquake Analysis of Skyscrapers." in *CTBUH 8th World Congress*. Dubai, UAE, 2008.
- [124] FEMA, *Design Guide for Improving Critical Facility Safety from Flooding and High Winds* (FEMA 543), Federal Emergency Management Agency (FEMA), Washington, D.C., 2007.
- [125] R.S. Means, *R.S. Means Building Construction Cost Data*. RSMeans Construction Publishers and Consultants: Norwell, MA, 2015.
- [126] W.J. Keller and S. Pessiki, "Cyclic Load Tests of SFRM-Insulated Steel Gravity Frame Beam-Column Connection Assemblies." *Journal of Structural Engineering*, 141(10), 2015.
- [127] N.L. Braxtan and S.P. Pessiki, "Postearthquake Fire Performance of Sprayed Fire-Resistive Material on Steel Moment Frames." *Journal of Structural Engineering*, 137(9): p. 946-953, 2011.
- [128] W.Y. Wang, G.Q. Li, and V. Kodur, "Approach for Modeling Fire Insulation Damage in Steel Columns." *Journal of Structural Engineering*, 139(4): p. 491-503, 2013.
- [129] M. Shinozuka, M.Q. Feng, J. Lee, and T. Naganuma, "Statistical Analysis of Fragility Curves." *Journal of Engineering Mechanics*, 126(12): p. 1224-1231, 2000.
- [130] N.J.L. Braxtan, "Post-Earthquake Fire Performance of Steel Moment Frame Building Columns," Doctor of Philosophy, Lehigh University, Bethlehem, PA, 2010.

- [131] Y. Huang, W.J. Bevans, H. Xiao, Z. Zhou, and G. Chen, “Experimental validation of finite element model analysis of a steel frame in simulated post-earthquake fire environments.” in *Society of Photographic Instrumentation Engineering – Smart Structures and Materials & Nondestructive Evaluation and Health Monitoring*, San Diego, CA, 2012.

VITA

Rachel Chicchi was born and raised in East Brunswick, NJ. She received her Bachelor and Master degrees in Architectural Engineering from The Pennsylvania State University. Rachel then worked for four years as a structural engineer for Cannon Design in Buffalo, NY and became a licensed Structural Engineer in the state of Illinois.

Rachel is the recipient of the Purdue Doctoral Fellowship, Ellis Memorial Scholarship, Outstanding CE Graduate Student Service Award and the Magoon Award for Excellence in Teaching. She also completed the Graduate Instructional Development Certificate through The Purdue Teaching Academy Center for Instructional Excellence.

During her time at Purdue, she has served as president and vice-president of the Civil Engineering Graduate Student Advisory Council (CEGSAC), president and secretary of the Bowen Laboratory Student Advisory Council (BSAC), and secretary of the Purdue chapter of the Earthquake Engineering Research Institute (EERI). Rachel was also a member of the EERI Student Leadership Council, a select group of graduate student members nationwide which orchestrates the international Seismic Design Competition and Post-Earthquake Reconnaissance workshops.

In January 2018, she will join the University of Cincinnati as an Assistant Professor of structural engineering in the Department of Civil & Architectural Engineering & Construction Management.